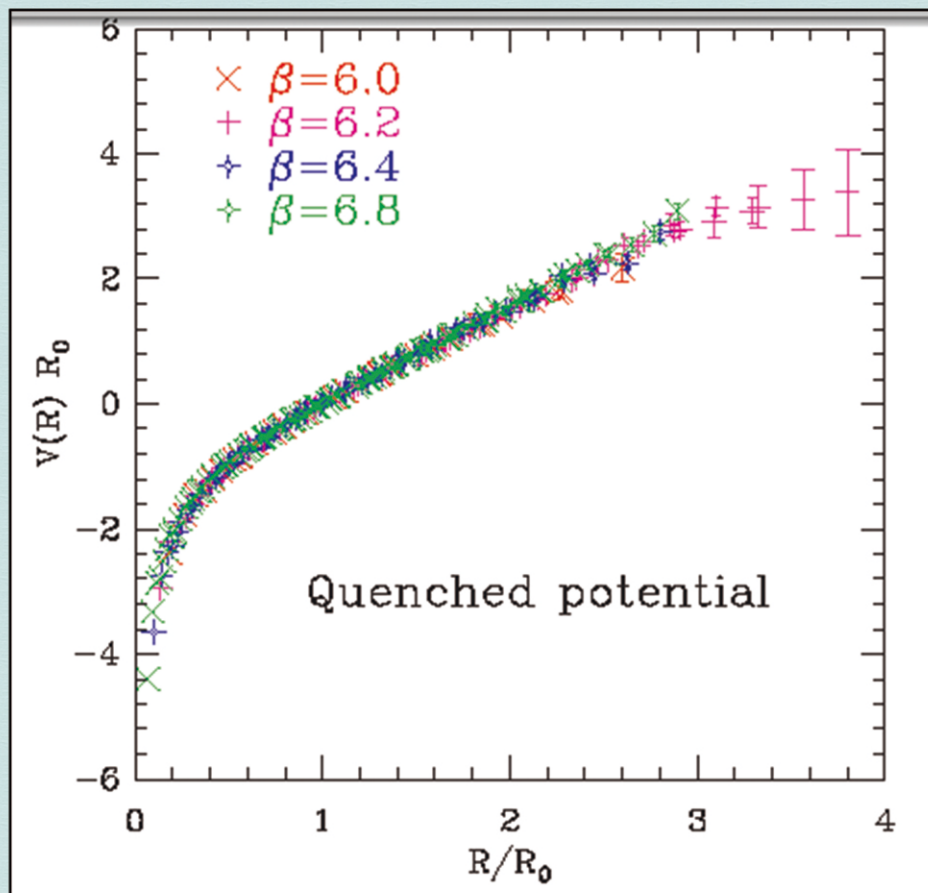


Journal of Modern Physics



ISSN: 2153-1196



Journal Editorial Board

ISSN: 2153-1196 (Print) ISSN: 2153-120X (Online)

<https://www.scirp.org/journal/jmp>

Editorial Board

Prof. Nikolai A. Sobolev	Universidade de Aveiro, Portugal
Prof. Mohamed Abu-Shady	Menoufia University, Egypt
Dr. Hamid Alemohammad	Advanced Test and Automation Inc., Canada
Prof. Emad K. Al-Shakarchi	Al-Nahrain University, Iraq
Dr. Francesco Bajardi	Scuola Superiore Meridionale, Italy
Prof. Antony J. Bourdillon	UHRL, USA
Dr. Swarniv Chandra	Government General Degree College, India
Prof. Tsao Chang	Fudan University, China
Prof. Wan Ki Chow	The Hong Kong Polytechnic University, China
Prof. Jean Cleymans	University of Cape Town, South Africa
Prof. Stephen Robert Cotanch	NC State University, USA
Prof. Claude Daviau	Ministry of National Education, France
Prof. Rami Ahmad El-Nabulsi	Chiang Mai University, Thailand
Prof. Peter Chin Wan Fung	The University of Hong Kong, China
Prof. Ju Gao	The University of Hong Kong, China
Prof. Robert Golub	North Carolina State University, USA
Dr. Sachin Goyal	University of California, USA
Dr. Wei Guo	Florida State University, USA
Prof. Karl Hess	University of Illinois, USA
Prof. Peter Otto Hess	Universidad Nacional Autónoma de México, Mexico
Prof. Ahmad A. Hujeirat	University of Heidelberg, Germany
Prof. Haikel Jelassi	National Center for Nuclear Science and Technology, Tunisia
Prof. Magd Elias Kahil	October University for Modern Sciences and Arts (MSA), Egypt
Prof. Santosh Kumar Karn	Dr. APJ Abdul Kalam Technical University, India
Prof. Guennadi A. Kouzaev	Norwegian University of Science and Technology, Norway
Prof. Sanjeev Kumar	Dr. Bhimrao Ambedkar University, India
Dr. Giuseppe Levi	Bologna University, Italy
Prof. Yu-Xian Li	Hebei Normal University, China
Prof. Anton A. Lipovka	Sonora University, Mexico
Prof. Wu-Ming Liu	Chinese Academy of Sciences, China
Dr. Ludi Miao	Cornell University, USA
Dr. Grégory Moreau	Paris-Saclay University, France
Prof. Christophe J. Muller	University of Provence, France
Dr. Rada Novakovic	National Research Council, Italy
Dr. Vasilis Oikonomou	Aristotle University of Thessaloniki, Greece
Prof. Vinod Prasad	Swami Sharddhanand College Delhi, India
Prof. Tongfei Qi	University of Kentucky, USA
Prof. Mohammad Mehdi Rashidi	University of Birmingham, UK
Prof. Haiduke Sarafian	The Pennsylvania State University, USA
Prof. Kunnat J. Sebastian	University of Massachusetts, USA
Dr. Ramesh C. Sharma	Ministry of Defense, India
Dr. Reinoud Jan Slagter	Astronomisch Fysisch Onderzoek Nederland, Netherlands
Dr. Giorgio Sonnino	Université Libre de Bruxelles, Belgium
Prof. Yogi Srivastava	Northeastern University, USA
Dr. Mitko Stoev	South-West University “Neofit Rilski”, Bulgaria
Dr. A. L. Roy Vellaisamy	City University of Hong Kong, China
Prof. Lev Zalman Vilenchik	Felicitex Therapeutics, USA
Prof. Anzhong Wang	Baylor University, USA
Prof. Cong Wang	Beihang University, China
Prof. Yuan Wang	University of California, Berkeley, USA
Prof. Peter H. Yoon	University of Maryland, USA
Prof. Meishan Zhao	University of Chicago, USA
Prof. Pavel Zhuravlev	University of Maryland at College Park, USA

Table of Contents

Volume 15 Number 1

January 2024

A Number Theoretic Analysis of the Enthalpy, Enthalpy Energy Density, Thermodynamic Volume, and the Equation of State of a Modified White Hole, and the Implications to the Quantum Vacuum Spacetime, Matter Creation and the Planck Frequency

M. Nardelli, A. S. Kubeka, A. Amani 1

Correspondence Principle for Empirical Equations in Terms of the Cosmic Microwave Background Temperature with Solid-State Ionics

T. Miyashita 51

Calculation of the Standard Model Parameters and Particles Based on a SU(4) Preon Model

J. Helm 64

The 111-Year-Old Cosmic Ray Puzzle Has Been Solved?

S. Dado, A. Dar 125

Calabi-Yau Topology of Primordial Fermions

E. E. Klingman 132

Journal of Modern Physics (JMP)

Journal Information

SUBSCRIPTIONS

The *Journal of Modern Physics* (Online at Scientific Research Publishing, <https://www.scirp.org/>) is published monthly by Scientific Research Publishing, Inc., USA.

Subscription rates:

Print: \$89 per issue.

To subscribe, please contact Journals Subscriptions Department, E-mail: sub@scirp.org

SERVICES

Advertisements

Advertisement Sales Department, E-mail: service@scirp.org

Reprints (minimum quantity 100 copies)

Reprints Co-ordinator, Scientific Research Publishing, Inc., USA.

E-mail: sub@scirp.org

COPYRIGHT

Copyright and reuse rights for the front matter of the journal:

Copyright © 2024 by Scientific Research Publishing Inc.

This work is licensed under the Creative Commons Attribution International License (CC BY).

<http://creativecommons.org/licenses/by/4.0/>

Copyright for individual papers of the journal:

Copyright © 2024 by author(s) and Scientific Research Publishing Inc.

Reuse rights for individual papers:

Note: At SCIRP authors can choose between CC BY and CC BY-NC. Please consult each paper for its reuse rights.

Disclaimer of liability

Statements and opinions expressed in the articles and communications are those of the individual contributors and not the statements and opinion of Scientific Research Publishing, Inc. We assume no responsibility or liability for any damage or injury to persons or property arising out of the use of any materials, instructions, methods or ideas contained herein. We expressly disclaim any implied warranties of merchantability or fitness for a particular purpose. If expert assistance is required, the services of a competent professional person should be sought.

PRODUCTION INFORMATION

For manuscripts that have been accepted for publication, please contact:

E-mail: jmp@scirp.org

A Number Theoretic Analysis of the Enthalpy, Enthalpy Energy Density, Thermodynamic Volume, and the Equation of State of a Modified White Hole, and the Implications to the Quantum Vacuum Spacetime, Matter Creation and the Planck Frequency

Michele Nardelli¹, Amos S. Kubeka^{2*}, Alizera Amani³

¹Dipartimento di Scienze della Terra, Università degli Studi di Napoli Federico II, Naples, Italy

²Department of Mathematical Sciences, University of South Africa, Unisa, South Africa

³Department of Physics, Ayatollah Amoli Branch, Islamic Azad University, Amol, Iran

Email: *kubekas@unisa.ac.za

How to cite this paper: Nardelli, M., Kubeka, A.S. and Amani, A. (2024) A Number Theoretic Analysis of the Enthalpy, Enthalpy Energy Density, Thermodynamic Volume, and the Equation of State of a Modified White Hole, and the Implications to the Quantum Vacuum Spacetime, Matter Creation and the Planck Frequency. *Journal of Modern Physics*, 15, 1-50.
<https://doi.org/10.4236/jmp.2024.151001>

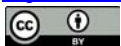
Received: November 18, 2023

Accepted: January 15, 2024

Published: January 18, 2024

Copyright © 2024 by author(s) and Scientific Research Publishing Inc. This work is licensed under the Creative Commons Attribution International License (CC BY 4.0).

<http://creativecommons.org/licenses/by/4.0/>



Open Access

Abstract

In this paper, we analyze the enthalpy, enthalpy energy density, thermodynamic volume, and the equation of state of a modified white hole. We obtain new possible mathematical connections with some sectors of Number Theory, Ramanujan Recurring Numbers, DN Constant and String Theory, that enable us to extract the quantum geometrical properties of these thermodynamic equations and the implication to the quantum vacuum spacetime geometry of our early universe as they act as the constraints to the nature of quantum gravity of the universe.

Keywords

Number Theory, Ramanujan Recurring Numbers, DN Constant, String Theory, Loop Quantum Gravity, Matter Creation, Enthalpy Energy Density, Thermodynamic Volume, Enthalpy

1. Introduction

The geometric structure of quantum gravity has been established to be discontinuous and other theories of quantum gravity like loop quantum gravity consider

the quantum geometry to be in the form of loops [1] while string theory considers quantum geometry to be in the form of strings [2]. We shall observe that the results of the analysis of this paper based on the work of thermodynamic constraints of a modified white hole [3] [4] encompass the form of quantum geometries as predicted by these two promising theories fundamental of physics. Precisely, it is shown that a full picture of complete quantum vacuum geometry is a combination of the two quantum geometries. A full connection of between the two quantum geometries is found through a number theoretic properties of the constraints of the thermodynamics of the modified white hole. The quantum vacuum geometry picture we found, indicates a clear depiction of the gauge bosons and the scalar bosons supergravity lattice and how they are related and arranged in relation to the graviton which through the analysis suggests that it may not be a gauge boson, but an independent quantum geometric force carrier as discussed by [5]. This then shows that in the final analysis, the quantum vacuum geometry that we derived, is fundamentally as it sheds some light of matter creations facilitated by the Higgs scalar boson from supersymmetric vacuum quantum geometry, through to symmetric breaking at the moment of big bang, and into the well know mechanism of matter formation moment after the big-bang

Our paper is structured as follows: Sections A and B, we analyse and list the number theoretic properties and the Ramanujan recurring number properties of the fundamental thermodynamic quantities of the modified white hole in the presence of a cosmological constant at extremely low entropy. Then in Section C, we apply these properties to quantum gravity and in the process we get a picture of the nature of the quantum geometry of the modified white whole in terms of octahedrons and a sphere, and we show that this quantum geometry has the properties of quantum strings and brane/Instanton. In Section D, we illustrate theoretic number connections to Planck multiple spectrum frequency and to the hypothetical Gluino mass.

SECTION A: Analysis the equations of the modified white hole enthalpy coupled to quantum Bose-Einstein condensate at extremely low entropy

The equations to be analysed in this section are from paper by [4]

2. Analysis of the Enthalpy of the Modified White Hole

The enthalpy of the modified white hole is given by

$$H(S) = \frac{2}{-\frac{S}{\pi} + b\left(\frac{S}{\pi}\right)^{1/2}} \left[1 - 2\pi a \ln\left(\frac{S}{\pi}\right)^{1/2} - ab\pi\left(\frac{\pi}{S}\right)^{1/2} \right]. \quad (1)$$

We analyze the number theoretic properties and the Ramanujan recurring number properties of the enthalpy Equation (1) as follows;

1) Exact result

The exact results of enthalpy Equation (1) is

$$\frac{2\left(\pi^{3/2}(-a)b\sqrt{\frac{1}{S}} - 2\pi a \log\left(\frac{\sqrt{S}}{\sqrt{\pi}}\right) + 1\right)}{\frac{b\sqrt{S}}{\sqrt{\pi}} - \frac{S}{\pi}}. \quad (2)$$

Which has the alternate forms;

$$\frac{2\pi\left(\pi^{3/2}ab\sqrt{\frac{1}{S}} + \pi a \log(S) - \pi a \log(\pi) - 1\right)}{\sqrt{\pi}b\sqrt{S} - S}, \quad (3)$$

$$\frac{2\pi\left(\pi a\left(\sqrt{\pi}b\sqrt{\frac{1}{S}} + \log\left(\frac{S}{\pi}\right)\right) - 1\right)}{\sqrt{s}\left(\sqrt{\pi}b - \sqrt{S}\right)}, \quad (4)$$

$$\frac{2\pi\left(\pi^{3/2}ab\sqrt{\frac{1}{S}} + 2\pi a \log\left(\frac{\sqrt{S}}{\sqrt{\pi}}\right) - 1\right)}{\sqrt{\pi}b\sqrt{S} - S}. \quad (5)$$

The alternative forms Equations (3), (4), and (5) has the following expanded form

$$\frac{2\pi^{3/2}ab\sqrt{\frac{1}{S}}}{\frac{b\sqrt{S}}{\sqrt{\pi}} - \frac{S}{\pi}} - \frac{4\pi a \log\left(\frac{\sqrt{S}}{\sqrt{\pi}}\right)}{\frac{b\sqrt{S}}{\sqrt{\pi}} - \frac{S}{\pi}} + \frac{2}{\frac{b\sqrt{S}}{\sqrt{\pi}} - \frac{S}{\pi}}. \quad (6)$$

Assuming a , b , and S are positive, the alternative forms are

$$\frac{2\pi\left(\pi^{3/2}ab + \pi a\sqrt{S} \log(S) - \pi a\sqrt{S} \log(\pi) - \sqrt{S}\right)}{\sqrt{\pi}bS - S^{3/2}}, \quad (7)$$

$$\frac{2\pi\left(\pi^{3/2}(-a)b + \pi a\sqrt{S} \log\left(\frac{\pi}{S}\right) + \sqrt{S}\right)}{\sqrt{\pi}bS - S^{3/2}}. \quad (8)$$

from which we obtain the expanded logarithmic form as

$$\frac{S^{-1/2} 2\pi}{b\sqrt{\pi} - \sqrt{S}} \pm \frac{2ab\pi^{5/2}}{(b\sqrt{\pi} - \sqrt{S})S} + \frac{S^{-1/2} 2a\pi^2 \log \pi}{b\sqrt{\pi} - \sqrt{S}} + \frac{S^{-1/2} (-2)a\pi^2 \log(S)}{b\sqrt{\pi} - \sqrt{S}}, \quad (9)$$

and assuming that $S > 0$, $\sqrt{S}/\sqrt{\pi} > 0$, and $S/\pi - (b\sqrt{S})/\sqrt{\pi} \neq 0$, then we get the alternate form

$$\frac{2\pi\left(-ab\pi^{3/2} + \sqrt{S} - 2a\pi\sqrt{S} \log\left(\frac{\sqrt{S}}{\sqrt{\pi}}\right)\right)}{(b\sqrt{\pi} - \sqrt{S})S}, \quad (10)$$

and the its derivative

$$\frac{\partial}{\partial a} \left(\frac{2 \left(1 - 2\pi a \log \left(\sqrt{\frac{S}{\pi}} \right) - ab\pi \sqrt{\frac{\pi}{S}} \right)}{-\frac{S}{\pi} + b\sqrt{\frac{S}{\pi}}} \right) = \frac{2\pi^2 \left(\sqrt{\pi}b\sqrt{\frac{1}{S}} + \log \left(\frac{S}{\pi} \right) \right)}{\sqrt{\pi}b\sqrt{S} - S} \tag{11}$$

2) Indefinite integral

Equation (11) has the following indefinite integral

$$\int \frac{2 \left(1 - ab\pi^{3/2} \sqrt{\frac{1}{S}} - 2a\pi \log \left(\frac{\sqrt{S}}{\sqrt{\pi}} \right) \right)}{\frac{b\sqrt{S}}{\sqrt{\pi}} - \frac{S}{\pi}} da = -\frac{2\pi \left(\frac{1}{2} \pi^{3/2} a^2 b \sqrt{\frac{1}{S}} + \pi a^2 \log \left(\frac{\sqrt{S}}{\sqrt{\pi}} \right) - a \right)}{\sqrt{\pi}b\sqrt{S} - S} + Constant \tag{12}$$

from which we obtain the alternate forms

$$\frac{\pi a \left(\pi^{3/2} (-a) b \sqrt{\frac{1}{S}} + \pi a (\log(\pi) - \log(S)) + 2 \right)}{\sqrt{\pi}b\sqrt{S} - S}, \tag{14}$$

$$-\frac{\pi a \left(\pi a \left(\sqrt{\pi}b\sqrt{\frac{1}{S}} + \log \left(\frac{S}{\pi} \right) \right) - 2 \right)}{\sqrt{S} (\sqrt{\pi}b - \sqrt{S})}, \tag{15}$$

$$\begin{aligned} & \frac{a^2 \sqrt{\frac{1}{S}} S^{3/2}}{b^4} - \frac{a^2}{b^4 \left(\frac{1}{S} \right)^{3/2} (\sqrt{\pi}b - \sqrt{S})} - \frac{\sqrt{\pi} a^2}{b^3 \sqrt{\frac{1}{S}}} - \frac{\pi a^2 \sqrt{\frac{1}{S}} \sqrt{S}}{b^2} \\ & - \frac{2\pi a^2 \log \left(\frac{\sqrt{S}}{\pi} \right)}{b^2} + \frac{2 \left(ab^2 \sqrt{S} - a^2 S^{3/2} \log \left(\frac{\sqrt{S}}{\sqrt{\pi}} \right) \right)}{b^4 (\sqrt{\pi}b - \sqrt{S})} - \frac{\pi^{3/2} a^2 \sqrt{\frac{1}{S}}}{b} \\ & - \frac{2\pi^{3/2} a^2 \log \left(\frac{\sqrt{S}}{\sqrt{\pi}} \right)}{b\sqrt{S}} - \frac{\pi^2 a^2 \sqrt{\frac{1}{S}}}{\sqrt{S}} + \frac{2a \left(b^2 - aS \log \left(\frac{\sqrt{S}}{\sqrt{\pi}} \right) \right)}{b^4} \\ & + \frac{2\sqrt{\pi} a \left(b^2 - aS \log \left(\frac{\sqrt{S}}{\sqrt{\pi}} \right) \right)}{b^3 \sqrt{S}} \end{aligned} \tag{16}$$

Assuming a , b , and S are positive, then the alternate forms are

$$\frac{\pi a \left(-\pi^{3/2} ab - \pi a \sqrt{S} \log(S) + \pi a \sqrt{S} \log(\pi) + 2\sqrt{S} \right)}{\sqrt{\pi}bS - S^{3/2}}, \tag{17}$$

$$\frac{\pi^{5/2} a^2 b}{\sqrt{S}(\sqrt{\pi b \sqrt{S}} - S)} - \frac{2\pi^2 a^2 \left(\frac{\log(S)}{2} - \frac{\log(\pi)}{2} \right)}{\sqrt{\pi b \sqrt{S}} - \sqrt{S}} + \frac{2\pi a}{\sqrt{\pi b \sqrt{S}} - \sqrt{S}} \quad (18)$$

$$\frac{\pi a \left(\pi^{3/2} (-a) b + \pi a \sqrt{S} \log\left(\frac{\pi}{S}\right) + 2\sqrt{S} \right)}{\sqrt{\pi b S} - S^{3/2}} \quad (19)$$

The expanded logarithmic form of the alternate forms Equation (17), (18), and (19) are then given by

$$\frac{2a\pi}{b\sqrt{\pi}\sqrt{S} - S} \pm \frac{a^2 b \pi^{5/2} \sqrt{\frac{1}{S}}}{b\sqrt{\pi}\sqrt{S} - S} + \frac{a^2 \pi^2 \log(\pi)}{b\sqrt{\pi}\sqrt{S} - S} \pm \frac{a^2 \pi^2 \log(S)}{b\sqrt{\pi}\sqrt{S} - S} \quad (20)$$

and assuming that $S > 0$, $\sqrt{S}/\sqrt{\pi} > 0$, and $\sqrt{\pi b \sqrt{S}} - S \neq 0$, then we get the alternate form

$$\frac{a\pi \left(-2 + ab\pi^{3/2} \sqrt{\frac{1}{S}} + 2a\pi \log\left(\frac{\sqrt{S}}{\sqrt{\pi}}\right) \right)}{b\sqrt{\pi}\sqrt{S} - S} \quad (21)$$

and then its derivative

$$\begin{aligned} & \frac{\partial}{\partial a} \left(\frac{2\pi \left(-a + \frac{1}{2} a^2 b \pi^{3/2} \sqrt{\frac{1}{S}} + a^2 \pi \log\left(\frac{\sqrt{S}}{\sqrt{\pi}}\right) \right)}{b\sqrt{\pi}\sqrt{S} - \sqrt{S}} \right) \\ &= - \frac{2\pi \left(\pi^{3/2} ab \sqrt{\frac{1}{S}} + 2\pi a \log\left(\frac{\sqrt{S}}{\sqrt{\pi}}\right) - 1 \right)}{\sqrt{\pi b \sqrt{S}} - S} \end{aligned} \quad (22)$$

3) Indefinite integral

We obtain the indefinite integral of the Equation (22) as

$$\begin{aligned} & \int - \frac{2\pi \left(-a + \frac{1}{2} a^2 b \pi^{3/2} \sqrt{\frac{1}{S}} + a^2 \pi \log\left(\frac{\sqrt{S}}{\sqrt{\pi}}\right) \right)}{b\sqrt{\pi}\sqrt{S} - S} da \\ &= - \frac{\pi a^2 \left(\pi^{3/2} ab \sqrt{\frac{1}{S}} + 2\pi a \log\left(\frac{\sqrt{S}}{\sqrt{\pi}}\right) - 3 \right)}{3(\sqrt{\pi b \sqrt{S}} - S)} + Constant \end{aligned} \quad (23)$$

which has the alternative forms

$$\frac{\pi a^2 \left(\pi^{3/2} (-a) b \sqrt{\frac{1}{S}} + \pi a (\log(\pi) - \log(S)) + 3 \right)}{3\sqrt{\pi b \sqrt{S}} - 3S}, \quad (24)$$

$$- \frac{\pi a^2 \left(\pi a \left(\sqrt{\pi b} \sqrt{\frac{1}{S}} + \log\left(\frac{S}{\pi}\right) \right) - 3 \right)}{3\sqrt{S}(\sqrt{\pi b} - \sqrt{S})}, \quad (25)$$

$$\begin{aligned}
 & \frac{a^3 \sqrt{\frac{1}{S}} S^{3/2}}{3b^4} - \frac{a^3}{3b^4 \left(\frac{1}{S}\right)^{3/2} (\sqrt{\pi}b - \sqrt{S})} - \frac{\sqrt{\pi}a^3}{3b^3 \sqrt{\frac{1}{S}}} - \frac{\pi a^3 \sqrt{\frac{1}{S}} \sqrt{S}}{3b^2} \\
 & \frac{2\pi a^3 \log\left(\frac{\sqrt{S}}{\sqrt{\pi}}\right)}{3b^2} - \frac{\pi^{3/2} a^3 \sqrt{\frac{1}{S}}}{3b} - \frac{2\pi^{3/2} a^3 \log\left(\frac{\sqrt{S}}{\sqrt{\pi}}\right)}{3b\sqrt{S}} - \frac{\pi^2 a^3 \sqrt{\frac{1}{S}}}{3\sqrt{S}} \\
 & \frac{a^2 \left(2aS \log\left(\frac{\sqrt{S}}{\sqrt{\pi}}\right) - 3b^2\right)}{3b^4} - \frac{\sqrt{\pi}a^2 \left(2aS \log\left(\frac{\sqrt{S}}{\sqrt{\pi}}\right) - 3b^3\right)}{3b^3 \sqrt{S}} \\
 & + \frac{3a^2 b^2 \sqrt{S} - 2a^3 S^{3/2} \log\left(\frac{\sqrt{S}}{\sqrt{\pi}}\right)}{3b^4 (\sqrt{\pi}b - \sqrt{S})}
 \end{aligned} \tag{26}$$

Equations (24), (25), and (26) has the expanded form

$$\frac{\pi^{5/2} a^3 b \sqrt{\frac{1}{S}}}{3(\sqrt{\pi}b\sqrt{S} - S)} - \frac{2\pi^2 a^3 \log\left(\frac{\sqrt{S}}{\sqrt{\pi}}\right)}{3(\sqrt{\pi}b\sqrt{S} - S)} + \frac{\pi a^2}{\sqrt{\pi}b\sqrt{S} - S} \tag{27}$$

and assuming $a, b,$ and S are positive, then we obtain the alternate form

$$\frac{\pi a^2 \left(-\pi^{3/2} ab - \pi a \sqrt{S} \log(S) + \pi a \sqrt{S} \log(\pi) + 3\sqrt{S}\right)}{3\sqrt{\pi}bS - 3S^{3/2}} \tag{28}$$

which has the expanded logarithmic form

$$\frac{3a^2 \pi}{3b\sqrt{\pi}\sqrt{S} - 3S} \pm \frac{a^3 b \pi^{5/2} \sqrt{\frac{1}{S}}}{3b\sqrt{\pi}\sqrt{S} - 3S} + \frac{a^3 \pi^2 \log(\pi)}{3b\sqrt{\pi}\sqrt{S} - 3S} \pm \frac{a^3 \pi^2 \log(S)}{3b\sqrt{\pi}\sqrt{S} - 3S}. \tag{29}$$

and assuming that $S > 0, \sqrt{S}/\sqrt{\pi} > 0,$ and $\sqrt{\pi}b\sqrt{S} - S \neq 0,$ then we get the alternate form

$$\frac{a^2 \pi \left(-3 + ab\pi^{3/2} \sqrt{\frac{1}{S}} + 2a\pi \log\left(\frac{\sqrt{S}}{\sqrt{\pi}}\right)\right)}{3(b\sqrt{\pi}\sqrt{S} - S)}, \tag{30}$$

which has the derivative

$$\begin{aligned}
 & \frac{\partial}{\partial a} \left(\frac{a^2 \pi \left(-3 + ab\pi^{3/2} \sqrt{\frac{1}{S}} + 2a\pi \log\left(\frac{\sqrt{S}}{\sqrt{\pi}}\right)\right)}{3(b\sqrt{\pi}\sqrt{S} - S)} \right) \\
 & = \frac{\pi a \left(\pi^{3/2} ab \sqrt{\frac{1}{S}} + 2\pi a \log\left(\frac{\sqrt{S}}{\sqrt{\pi}}\right) - 2\right)}{\sqrt{\pi}b\sqrt{S} - S}
 \end{aligned} \tag{31}$$

4) Indefinite integral

The indefinite integral of the Equation (31) is

$$\int -\frac{a^2 \pi \left(-3 + ab\pi^{3/2} \sqrt{\frac{1}{S}} + 2a\pi \log\left(\frac{\sqrt{S}}{\sqrt{\pi}}\right) \right)}{3(b\sqrt{\pi}\sqrt{S} - S)} da$$

$$= -\frac{\pi a^3 \left(\pi^{3/2} ab\sqrt{\frac{1}{S}} + 2\pi a \log\left(\frac{\sqrt{S}}{\sqrt{\pi}}\right) - 4 \right)}{4(3\sqrt{\pi}b\sqrt{S} - 2S)} + Constant \tag{32}$$

5) Volume analysis

Because of supersymmetry of space at extremely low entropy, then it is therefore possible to consider the vortices of the quantum vacuum schematized as cubes or octahedrons loops. We also assume that the quantum Van der Waals fluid [4] [6] are characterized by smooth spheres. In reality, the quantum vacuum will have n-dimensional hyperspheres in which the compactified dimensions “roll up” and octahedrons representing the “fluctuations”, containing vibrating quantum Van der Waals fluid particles.

Therefore, for $V = \frac{1}{3}\sqrt{2}a^3$ (octahedron volume) and $V = \frac{4}{3}\pi r^3$ (sphere volume), where $r = \frac{a}{2}$, we get the following;

a) Octahedron volume

From indefinite integral Equation (32) we obtain the following exact result

$$\frac{\pi a^6 \left(\pi a^{3/2} ab\sqrt{\frac{1}{S}} + 2\pi a \log\left(\frac{\sqrt{S}}{\sqrt{\pi}}\right) - 4 \right)}{6\sqrt{2}(3\sqrt{\pi}b\sqrt{S} - 3S)} \tag{33}$$

which has the alternative forms

$$\frac{\pi a^6 \left(\pi^{3/2} (-a)b\sqrt{\frac{1}{S}} + \pi a (\log(\pi) - \log(S)) + 4 \right)}{18(\sqrt{2\pi}b\sqrt{S} - \sqrt{2}S)}, \tag{34}$$

$$-\frac{\pi a^6 \left(\pi a \left(\sqrt{\pi}b\sqrt{\frac{1}{S}} + \log\left(\frac{S}{\pi}\right) \right) - 4 \right)}{18\sqrt{2}\sqrt{S}(\sqrt{\pi}b - \sqrt{S})}, \tag{35}$$

$$\frac{a^7 \sqrt{\frac{1}{S}} S^{3/2}}{18\sqrt{2}b^4} - \frac{a^7}{18\sqrt{2}b^4 \left(\frac{1}{S}\right)^{3/2} (\sqrt{\pi}b - \sqrt{S})} - \frac{\sqrt{\frac{\pi}{2}} a^7}{18b^3 \sqrt{\frac{1}{S}}} - \frac{\pi a^7 \sqrt{\frac{1}{S}} \sqrt{S}}{18\sqrt{2}b^2}$$

$$-\frac{\pi a^7 \log\left(\frac{\sqrt{S}}{\sqrt{\pi}}\right)}{9\sqrt{2}b^2} - \frac{\pi^{3/2} a^7 \sqrt{\frac{1}{S}}}{18\sqrt{2}b} - \frac{\pi^{3/2} a^7 \log\left(\frac{\sqrt{S}}{\sqrt{\pi}}\right)}{9\sqrt{2}b\sqrt{S}} - \frac{\pi^2 a^7 \sqrt{\frac{1}{S}}}{18\sqrt{2}\sqrt{S}} \tag{36}$$

$$\frac{a^6 \left(aS \log \left(\frac{\sqrt{S}}{\sqrt{\pi}} \right) - 2b^2 \right)}{9\sqrt{2}b^4} - \frac{\sqrt{\frac{\pi}{2}} a^6 \left(aS \log \left(\frac{\sqrt{S}}{\sqrt{\pi}} \right) - 2b^2 \right)}{9b^3\sqrt{S}}$$

$$- \frac{a^7 S^{3/2} \log \left(\frac{\sqrt{S}}{\sqrt{\pi}} \right) - 2a^6 b^2 \sqrt{S}}{9\sqrt{2}b^4 (\sqrt{\pi}b - \sqrt{S})}$$

The expanded form of Equations (34), (35), and (36) is

$$\frac{\pi^{5/2} a^7 b \sqrt{\frac{1}{S}}}{6\sqrt{2} (3\sqrt{\pi}b\sqrt{S} - 3S)} - \frac{\pi^2 a^7 \log \left(\frac{\sqrt{S}}{\sqrt{\pi}} \right)}{3\sqrt{2} (3\sqrt{\pi}b\sqrt{S} - 3S)} + \frac{\sqrt{2}\pi a^6}{3(3\sqrt{\pi}b\sqrt{S} - 3S)} \tag{37}$$

and assuming a , b , and S are positive, we obtain the alternate forms of Equation (37) as

$$\frac{\pi a^6 \left(\pi^{3/2} ab + \pi a \sqrt{S} \log(S) - \pi a \sqrt{S} \log(\pi) - 4\sqrt{S} \right)}{18\sqrt{2} (\sqrt{\pi}bS - S^{3/2})},$$

$$- \frac{\pi a^6 \left(\frac{\pi^{3/2} ab}{\sqrt{S}} + \pi a \log(S) - \pi a \log(\pi) - 4 \right)}{18(\sqrt{2\pi}b\sqrt{S} - \sqrt{2}S)}, \tag{38}$$

which has the expanded logarithmic form given by

$$\frac{\frac{1}{36} 4\sqrt{2} a^6 \pi}{b\sqrt{\pi}\sqrt{S} - S} + \frac{\frac{1}{36} (-1) \sqrt{\frac{2}{S}} a^7 b \pi^{5/2}}{b\sqrt{\pi}\sqrt{S} - S}$$

$$+ \frac{\frac{1}{36} \sqrt{2} a^7 \pi^2 \log(\pi)}{b\sqrt{\pi}\sqrt{S} - S} + \frac{\frac{1}{36} (-1) \sqrt{2} a^7 \pi^2 \log(S)}{b\sqrt{\pi}\sqrt{S} - S} \tag{39}$$

The alternate form of Equation (39) is

$$\frac{a^6 \pi \left(-4 + ab\pi^{3/2} \sqrt{\frac{1}{S}} + 2a\pi \log \left(\frac{\sqrt{S}}{\sqrt{\pi}} \right) \right)}{18\sqrt{2} (b\sqrt{\pi}\sqrt{S} - S)} \tag{40}$$

and its derivative is given by

$$\frac{\partial}{\partial a} \left(\frac{\left(a^3 \pi \left(-4 + ab\pi^{3/2} \sqrt{\frac{1}{S}} + 2a\pi \log \left(\frac{\sqrt{S}}{\sqrt{\pi}} \right) \right) \right) (\sqrt{2}a^3)}{3(4(3b\sqrt{\pi}\sqrt{S} - 3S))} \right)$$

$$= - \frac{\pi a^5 \left(7\pi^{3/2} ab \sqrt{\frac{1}{S}} + 7\pi a \log \left(\frac{S}{\pi} \right) - 24 \right)}{18(\sqrt{2\pi}b\sqrt{S} - \sqrt{2}S)} \tag{41}$$

The indefinite integral of Equation (41) is then given by

$$\int -\frac{a^6 \pi \left(-4 + ab\pi^{3/2} \sqrt{\frac{1}{S}} + 2a\pi \log\left(\frac{\sqrt{S}}{\sqrt{\pi}}\right) \right)}{6\sqrt{2} (3b\sqrt{\pi}\sqrt{S} - 3S)} da$$

$$= -\frac{\pi a^7 \left(7\pi^{3/2} ab\sqrt{\frac{1}{S}} + 7\pi a \log\left(\frac{S}{\pi}\right) - 32 \right)}{336\sqrt{2} (3\sqrt{\pi}b\sqrt{S} - 3S)} + constant \tag{42}$$

b) Sphere volume

From indefinite integral Equation (32) we obtain the exact result

$$\frac{\pi^2 a^6 \left(\pi^{3/2} ab\sqrt{\frac{1}{S}} + 2\pi a \log\left(\frac{\sqrt{S}}{\sqrt{\pi}}\right) - 4 \right)}{24(3\sqrt{\pi}b\sqrt{S} - 3S)} \tag{43}$$

which has the alternate forms

$$\frac{\pi^2 a^6 \left(\pi^{3/2} (-a)b\sqrt{\frac{1}{S}} + \pi a (\log(\pi) - \log(S)) + 4 \right)}{72(\sqrt{\pi}b\sqrt{S} - S)}, \tag{44}$$

$$\frac{\pi^2 a^6 \left(\pi a \left(\sqrt{\pi}b\sqrt{\frac{1}{S}} + \log\left(\frac{S}{\pi}\right) \right) - 4 \right)}{72\sqrt{S}(\sqrt{\pi}b - \sqrt{S})}, \tag{45}$$

$$\frac{a^7 \sqrt{\frac{1}{S}} S^{5/2}}{72b^6} - \frac{a^7}{72b^2 \left(\frac{1}{S}\right)^{5/2} (\sqrt{\pi}b - \sqrt{S})} - \frac{\sqrt{\pi}a^7}{72b^5 \left(\frac{1}{S}\right)^{3/2}} - \frac{\pi a^7 \sqrt{\frac{1}{S}} S^{3/2}}{72b^4}$$

$$- \frac{\pi^{3/2} a^7}{72b^3 \sqrt{\frac{1}{S}}} - \frac{\pi^2 a^7 \sqrt{\frac{1}{S}} \sqrt{S}}{72b^2} - \frac{\pi^2 a^7 \log\left(\frac{\sqrt{S}}{\sqrt{\pi}}\right)}{36b^2} - \frac{\pi^{5/2} a^7 \sqrt{\frac{1}{S}}}{72b}$$

$$\frac{\pi^{5/2} a^7 \log\left(\frac{\sqrt{S}}{\sqrt{\pi}}\right)}{36b\sqrt{S}} - \frac{\pi^3 a^7 \sqrt{\frac{1}{S}}}{72\sqrt{S}} - \frac{a^6 S \left(aS \log\left(\frac{\sqrt{S}}{\sqrt{\pi}}\right) - 2b^2 \right)}{36b^6} \tag{46}$$

$$\frac{\sqrt{\pi} a^6 \sqrt{S} \left(aS \log\left(\frac{\sqrt{S}}{\sqrt{\pi}}\right) - 2b^2 \right)}{36b^5} - \frac{\pi a^6 \left(aS \log\left(\frac{\sqrt{S}}{\sqrt{\pi}}\right) - 2b^2 \right)}{36b^4}$$

$$- \frac{\pi^{3/2} a^6 \left(aS \log\left(\frac{\sqrt{S}}{\sqrt{\pi}}\right) - 2b^2 \right)}{36b^3 \sqrt{S}} + \frac{2a^6 b^2 S^{3/2} - a^7 S^{5/2} \log\left(\frac{\sqrt{S}}{\sqrt{\pi}}\right)}{36b^6 (\sqrt{\pi}b - \sqrt{S})}$$

and the expanded forms of Equations (44), (45), and (46) are given by

$$\begin{aligned}
 &-\frac{\pi^{7/2} a^7 b \sqrt{\frac{1}{S}}}{72\sqrt{\pi b \sqrt{S}} - 72S} - \frac{\pi^3 a^7 \log(S)}{72\sqrt{\pi b \sqrt{S}} - 72S} + \frac{\pi^3 a^7 \log \pi}{72\sqrt{\pi b \sqrt{S}} - 72S} + \frac{\pi^2 a^6}{18(\sqrt{\pi b \sqrt{S}} - S)} \\
 &-\frac{\pi^{7/2} a^7 b \sqrt{\frac{1}{S}}}{24(3\sqrt{\pi b \sqrt{S}} - 3S)} - \frac{\pi^3 a^7 \log\left(\frac{\sqrt{S}}{\sqrt{\pi}}\right)}{12(3\sqrt{\pi b \sqrt{S}} - 3S)} + \frac{\pi^2 a^6}{6(3\sqrt{\pi b \sqrt{S}} - 3S)}
 \end{aligned} \tag{47}$$

Now assuming that a , b , and S are positive, then we obtain the alternate forms

$$\begin{aligned}
 &-\frac{\pi^2 a^6 \left(\pi^{3/2} ab + \pi a \sqrt{S} \log(S) - \pi a \sqrt{S} \log(\pi) - 4\sqrt{S} \right)}{72(\sqrt{\pi b S} - S^{3/2})} \\
 &-\frac{\pi^2 a^6 \left(\frac{\pi^{3/2} ab}{\sqrt{S}} + \pi a \log(S) - \pi a \log(\pi) - 4 \right)}{72(\sqrt{\pi b \sqrt{S}} - S)}
 \end{aligned} \tag{48}$$

with the expanded logarithmic form

$$\frac{\frac{1}{72} 4a^6 \pi^2}{b\sqrt{\pi \sqrt{S}} - S} + \frac{\frac{1}{72} (-1) a^7 b \pi^{7/2} \sqrt{\frac{1}{S}}}{b\sqrt{\pi \sqrt{S}} - S} + \frac{\frac{1}{72} a^7 \pi^3 \log(\pi)}{b\sqrt{\pi \sqrt{S}} - S} + \frac{\frac{1}{72} (-1) a^7 \pi^3 \log(S)}{b\sqrt{\pi \sqrt{S}} - S}. \tag{49}$$

The alternate form of Equation (49) is

$$-\frac{a^6 \pi^2 \left(-4 + ab\pi^{3/2} \sqrt{\frac{1}{S}} + 2a\pi \log\left(\frac{\sqrt{S}}{\sqrt{\pi}}\right) \right)}{72(b\sqrt{\pi \sqrt{S}} - S)}, \tag{50}$$

with the derivative

$$\begin{aligned}
 &\frac{\partial}{\partial a} \left(\frac{\left(a^3 \pi \left(-4 + ab\pi^{3/2} \sqrt{\frac{1}{S}} + 2a\pi \log\left(\frac{\sqrt{S}}{\sqrt{\pi}}\right) \right) \right) \left(4\pi \left(\frac{a}{2} \right)^3 \right)}{3(4(3b\sqrt{\pi \sqrt{S}} - 3S))} \right) \\
 &= \frac{\pi^2 a^5 \left(-7\pi^{3/2} ab \sqrt{\frac{1}{S}} - 7\pi a \log\left(\frac{S}{\pi}\right) + 24 \right)}{72(\sqrt{\pi b \sqrt{S}} - S)}
 \end{aligned} \tag{51}$$

and the indefinite integral

$$\begin{aligned}
 &\int -\frac{a^6 \pi^2 \left(-4 + ab\pi^{3/2} \sqrt{\frac{1}{S}} + 2a\pi \log\left(\frac{\sqrt{S}}{\sqrt{\pi}}\right) \right)}{24(3b\sqrt{\pi \sqrt{S}} - 3S)} da \\
 &= -\frac{\pi^2 a^7 \left(7\pi^{3/2} ab \sqrt{\frac{1}{S}} + 7\pi a \log\left(\frac{S}{\pi}\right) - 32 \right)}{4032(\sqrt{\pi b \sqrt{S}} - S)} + constant
 \end{aligned} \tag{52}$$

c) Number theoretic properties of the volume

i) DN Constant

Now dividing the two indefinite integral results for the octahedron and the sphere volumes; Equation (42) and Equation (52) respectively, we get

$$\int -\frac{a^6 \pi \left(-4 + ab\pi^{3/2} \sqrt{\frac{1}{S}} + 2a\pi \log\left(\frac{\sqrt{S}}{\sqrt{\pi}}\right) \right)}{6\sqrt{2}(3b\sqrt{\pi}\sqrt{S} - 3S)} da$$

$$= -\frac{\pi a^7 \left(7\pi^{3/2} ab \sqrt{\frac{1}{S}} + 7\pi a \log\left(\frac{S}{\pi}\right) - 32 \right)}{336\sqrt{2}(3\sqrt{\pi}b\sqrt{S} - 3S)} + constant \quad (53)$$

and

$$\int -\frac{a^6 \pi^2 \left(-4 + ab\pi^{3/2} \sqrt{\frac{1}{S}} + 2a\pi \log\left(\frac{\sqrt{S}}{\sqrt{\pi}}\right) \right)}{24(3b\sqrt{\pi}\sqrt{S} - 3S)} da$$

$$= -\frac{\pi^2 a^7 \left(7\pi^{3/2} ab \sqrt{\frac{1}{S}} + 7\pi a \log\left(\frac{S}{\pi}\right) - 32 \right)}{4032(\sqrt{\pi}b\sqrt{S} - S)} + constant \quad (54)$$

which simplifies to the exact result

$$\frac{6\sqrt{2}(\sqrt{\pi}b\sqrt{S} - S)}{\pi(3\sqrt{\pi}b\sqrt{S} - 3S)} \quad (55)$$

of which the expanded form is

$$\frac{6\sqrt{\frac{2}{\pi}}b\sqrt{S}}{3\sqrt{\pi}b\sqrt{S} - 3S} - \frac{6\sqrt{2}S}{\pi(3\sqrt{\pi}b\sqrt{S} - 3S)} \quad (56)$$

with the alternative form

$$\frac{2\sqrt{2}}{\pi} = 0.9003163161571\dots \quad (57)$$

which is a DN Constant.

ii) The property of the function

The function has an even parity

iii) Indefinite integral

$$\int \frac{6\sqrt{2}(b\sqrt{\pi}\sqrt{S} - S)}{\pi(3b\sqrt{\pi}\sqrt{S} - 3S)} db = \frac{2\sqrt{2}b}{\pi} + constant \quad (58)$$

iv) Global maximum

$$\max \left\{ \frac{\pi}{\left(\frac{(336\sqrt{2})(3\sqrt{\pi}(b\sqrt{S}) - 3S)}{\pi^2} \right)} \right\} = \frac{2\sqrt{2}}{\pi} \quad \text{at } (b, S) = \left(-\frac{12}{5}, -\frac{1}{2} \right) \quad (59)$$

v) Global minimum

$$\min \left\{ \frac{\pi}{\frac{\left((336\sqrt{2})(3\sqrt{\pi}(b\sqrt{S}) - 3S) \right)^2 \pi^2}{4032(\sqrt{\pi}b\sqrt{S} - S)}} \right\} = \frac{2\sqrt{2}}{\pi} \text{ at } (b, S) = \left(-\frac{12}{5}, -\frac{1}{2} \right) \quad (60)$$

vi) Limit

$$\lim_{b \rightarrow \pm\infty} \frac{6\sqrt{2}(b\sqrt{\pi}\sqrt{S} - S)}{\pi(3b\sqrt{\pi}\sqrt{S} - 3S)} = \frac{2\sqrt{2}}{\pi} \approx 0.900316 \quad (61)$$

$$\lim_{S \rightarrow \pm\infty} \frac{6\sqrt{2}(b\sqrt{\pi}\sqrt{S} - S)}{\pi(3b\sqrt{\pi}\sqrt{S} - 3S)} = \frac{2\sqrt{2}}{\pi} \approx 0.900316 \quad (62)$$

vii) Series representations

$$\frac{\pi}{\frac{\pi^2 \left((336\sqrt{2})(3\sqrt{\pi}(b\sqrt{S}) - 3S) \right)^2}{4032(\sqrt{\pi}b\sqrt{S} - S)}} = \frac{4}{\pi \sqrt{z_0} \sum_{k=0}^{\infty} \frac{(-1)^k \left(-\frac{1}{2} \right)_k (2 - z_0)^k z_0^{-k}}{k!}} \quad (63)$$

for (not $(z_0 \in \mathbb{R} \text{ and } -\infty < z_0 \leq 0)$)

$$\begin{aligned} & \frac{\pi}{\frac{\pi^2 \left((336\sqrt{2})(3\sqrt{\pi}(b\sqrt{S}) - 3S) \right)^2}{4032(\sqrt{\pi}b\sqrt{S} - S)}} \\ &= \frac{4}{\pi \exp\left(i\pi \left\lfloor \frac{\arg(2-x)}{2\pi} \right\rfloor \right) \sqrt{x} \sum_{k=0}^{\infty} \frac{(-1)^k (2-x)^k x^{-k} \left(-\frac{1}{2} \right)_k}{k!}} \end{aligned} \quad (64)$$

for $(x \in \mathbb{R} \text{ and } x < 0)$

$$\frac{\pi}{\frac{\pi^2 \left((336\sqrt{2})(3\sqrt{\pi}(b\sqrt{S}) - 3S) \right)^2}{4032(\sqrt{\pi}b\sqrt{S} - S)}} = \frac{4 \left(\frac{1}{z_0} \right)^{-1/2 \lfloor \arg(2-z_0)/(2\pi) \rfloor} z_0^{-1/2 \lfloor \arg(2-z_0)/(2\pi) \rfloor}}{\pi \sum_{k=0}^{\infty} \frac{(-1)^k \left(-\frac{1}{2} \right)_k (2 - z_0)^k z_0^{-k}}{k!}} \quad (65)$$

where $n!$ is the factorial function, $(a)_m$ is the Pochhammer symbol (rising factorial), \mathbb{R} is the set of real numbers, $\arg(z)$ is the complex argument, $\lfloor x \rfloor$ is the floor function, and i is the imaginary unit.

viii) Definite integral over a disk of radius R

$$\iint_{b^2+S^2 < R^2} \frac{6\sqrt{2}(\sqrt{\pi}b\sqrt{S} - S)}{\pi(3\sqrt{\pi}b\sqrt{S} - 3S)} dbdS = 2\sqrt{2}R^2 \quad (66)$$

Definite integral over a square of edge length $2L$

$$\int_{-L}^L \int_{-L}^L \frac{6\sqrt{2}(b\sqrt{\pi}\sqrt{S}-S)}{\pi(3b\sqrt{\pi}\sqrt{S}-3S)} dS db = \frac{8\sqrt{2}L^2}{\pi} \quad (67)$$

3. Analysis of the Thermodynamic Volume of the Modified White Hole

The thermodynamic volume of the modified white hole is given by

$$V = \frac{-5ab\left(\frac{\pi}{S}\right)^{1/2} + 2ab^2\left(\frac{\pi}{S}\right) + 2a - \frac{b}{(\pi S)^{1/2}} + \left(ab\left(\frac{\pi}{S}\right)^{1/2} - 2a\right)\ln\left(\frac{\pi}{S}\right) + \frac{2}{\pi}}{b\left(\frac{S}{\pi}\right)^{1/2} - \frac{S}{\pi}}. \quad (68)$$

The analysis gives the following number theoretic properties and the Ramanujan recurring number properties of the thermodynamic volume:

1) Alternate forms

The thermodynamic volume Equation (68) has the following alternate forms

$$a\left(\frac{2\pi b^2}{S} - 5\sqrt{\pi}b\sqrt{\frac{1}{S}} + 2\right) + a\left(\sqrt{\pi}b\sqrt{\frac{1}{S}} - 2\right)\log\left(\frac{S}{\pi}\right) + \frac{2 - \frac{\sqrt{\pi}b}{\sqrt{S}}}{\pi}, \quad (69)$$

$$\frac{\pi a \left(2\pi b^2 + \frac{\sqrt{\pi}b(\log(S) - 5 - \log(\pi))}{\sqrt{\frac{1}{S}}} - 2S(\log(S) - 1 - \log(\pi)) \right) - \sqrt{S}(\sqrt{\pi}b - 2\sqrt{S})}{\pi S}. \quad (70)$$

Assuming a , b , and S are positive, then the alternative forms Equations (69), and (70) becomes

$$\frac{(\sqrt{\pi}b - 2\sqrt{S})(2\pi^{3/2}ab + \pi a\sqrt{S}\log(S) - \pi a\sqrt{S}(1 + \log(\pi)) - \sqrt{S})}{\pi S} \quad (71)$$

and the derivative is

$$\begin{aligned} \frac{\partial}{\partial a} \left(-5ab\sqrt{\frac{\pi}{S}} + \frac{(2ab^2)\pi}{S} + 2a - \frac{b}{\sqrt{\pi S}} + \left(ab\sqrt{\frac{\pi}{S}} - 2a \right) \log\left(\frac{S}{\pi}\right) + \frac{2}{\pi} \right) \\ = \frac{2\pi b^2}{S} - 5\sqrt{\pi}b\sqrt{\frac{1}{S}} + \left(\sqrt{\pi}b\sqrt{\frac{1}{S}} - 2 \right) \log\left(\frac{S}{\pi}\right) + 2 \end{aligned} \quad (72)$$

The indefinite integral is then given by

$$\begin{aligned} \int \left(-5ab\sqrt{\frac{\pi}{S}} + \frac{(2ab^2)\pi}{S} + 2a - \frac{b}{\sqrt{\pi S}} + \left(ab\sqrt{\frac{\pi}{S}} - 2a \right) \log\left(\frac{S}{\pi}\right) + \frac{2}{\pi} \right) da \\ = \frac{\pi a^2 b^2}{S} - \frac{5}{2} \sqrt{\pi} a^2 b \sqrt{\frac{1}{S}} + \frac{1}{2} a^2 \left(\sqrt{\pi} b \sqrt{\frac{1}{S}} - 2 \right) \log\left(\frac{S}{\pi}\right) \\ + a^2 + \frac{a \left(2 - \frac{\sqrt{\pi}b}{\sqrt{S}} \right)}{\pi} + \text{constant} \end{aligned} \quad (73)$$

Dividing the alternate form Equation (69) by

$$b\sqrt{\frac{S}{\pi}} - \frac{S}{\pi} \tag{74}$$

we obtain the exact result

$$\frac{a\left(\frac{2\pi b^2}{S} - 5\sqrt{\pi}b\sqrt{\frac{1}{S}} + 2\right) + a\left(\sqrt{\pi}b\sqrt{\frac{1}{S}} - 2\right)\log\left(\frac{S}{\pi}\right) + \frac{2 - \frac{\sqrt{\pi}b}{\sqrt{S}}}{\pi}}{b\sqrt{\frac{S}{\pi}} - \frac{S}{\pi}} \tag{75}$$

2) Volume analysis

From the exact result Equation (75), and with $V = \frac{1}{3}\sqrt{2}a^3$ (octahedron volume) and $V = \frac{4}{3}\pi r^3$ (sphere volume), where $r = \frac{a}{2}$, we obtain respectively;

a) Octahedron volume:

The exact result

$$\frac{\sqrt{2}a^3 \left(a\left(\frac{2\pi b^2}{S} - 5\sqrt{\pi}b\sqrt{\frac{1}{S}} + 2\right) + a\left(\sqrt{\pi}b\sqrt{\frac{1}{S}} - 2\right)\log\left(\frac{S}{\pi}\right) + \frac{2 - \frac{\sqrt{\pi}b}{\sqrt{S}}}{\pi} \right)}{3\left(\frac{b\sqrt{S}}{\sqrt{\pi}} - \frac{S}{\pi}\right)} \tag{76}$$

b) Sphere volume:

The exact result

$$\frac{\pi a^3 \left(a\left(\frac{2\pi b^2}{S} - 5\sqrt{\pi}b\sqrt{\frac{1}{S}} + 2\right) + a\left(\sqrt{\pi}b\sqrt{\frac{1}{S}} - 2\right)\log\left(\frac{S}{\pi}\right) + \frac{2 - \frac{\sqrt{\pi}b}{\sqrt{S}}}{\pi} \right)}{6\left(\frac{b\sqrt{S}}{\sqrt{\pi}} - \frac{S}{\pi}\right)} \tag{77}$$

3) Number theoretic properties of the volume

By dividing the two exact results Equations (76), and (77), and simplifying by making the input $\frac{\sqrt{2}}{3} \times \frac{1}{\frac{\pi}{6}}$, we get the results

$$\frac{2\sqrt{2}}{\pi} \tag{78}$$

With the decimal approximation

$$0.9003163161571060695551991910067405826645741499552206255714374712\dots = \frac{2\sqrt{2}}{\pi}$$

which is a DN Constant, and also $\frac{2\sqrt{2}}{\pi}$ it has property that it is a transcendental number. The transcendental numbers have important properties in physics and in particular in astrophysics, particle physics, cosmology because they allow us to reformulate and resolve unresolved problems, and in our case, the geometry of quantum gravity of the very early universe [7].

The series representation of Equation (78) is

$$\frac{\frac{\sqrt{2}}{3\pi}}{6} = \frac{2\sqrt{z_0} \sum_{k=0}^{\infty} \frac{(-1)^k \left(-\frac{1}{2}\right)_k (2-z_0)^k z_0^{-k}}{k!}}{\pi} \tag{79}$$

for (not $(z_0 \in \mathbb{R}$ and $-\infty < z_0 \leq 0)$)

$$\frac{\frac{\sqrt{2}}{3\pi}}{6} = \frac{2 \exp\left(i\pi \left\lfloor \frac{\arg(2-x)}{2\pi} \right\rfloor\right) \sqrt{x} \sum_{k=0}^{\infty} \frac{(-1)^k (2-x)^k x^{-k} \left(-\frac{1}{2}\right)_k}{k!}}{\pi} \tag{80}$$

for $(x \in \mathbb{R}$ and $x < 0)$

$$\frac{\frac{\sqrt{2}}{3\pi}}{6} = \frac{2 \left(\frac{1}{z_0}\right)^{1/2 \lfloor \arg(2-z_0)/(2\pi) \rfloor} z_0^{1/2(1+\lfloor \arg(2-z_0)/(2\pi) \rfloor)} \sum_{k=0}^{\infty} \frac{(-1)^k \left(-\frac{1}{2}\right)_k (2-z_0)^k z_0^{-k}}{k!}}{\pi} \tag{81}$$

4. Analysis of the Enthalpy Energy Density of the Modified White Hole

The enthalpy energy density of the modified white hole is given by

$$\rho_{ent} = \frac{H(S)}{V} \tag{82}$$

and dividing the exact result Equation (2) by the alternative form Equation (69), we obtain

$$\frac{\frac{2}{-\frac{S}{\pi} + b\sqrt{\frac{S}{\pi}}} \left(1 - 2\pi a \log\left(\sqrt{\frac{S}{\pi}}\right) - ab\pi \sqrt{\frac{\pi}{S}}\right)}{a \left(2 - 5b\sqrt{\pi} \sqrt{\frac{1}{S}} + \frac{2b^2\pi}{S}\right) + \frac{2 - \frac{b\sqrt{\pi}}{\sqrt{S}}}{\pi} + a \left(-2 + b\sqrt{\pi} \sqrt{\frac{1}{S}}\right) \log\left(\frac{S}{\pi}\right)} \cdot \frac{b\sqrt{\frac{S}{\pi}} - \frac{S}{\pi}}{\pi} \tag{83}$$

Then the analysis gives the following number theoretic properties and the Ramanujan recurring number properties of the enthalpy energy density. The exact result is

$$\frac{2\left(\pi^{3/2}(-a)b\sqrt{\frac{1}{S}} - 2\pi a \log\left(\frac{\sqrt{S}}{\sqrt{\pi}}\right) + 1\right)}{a\left(\frac{2\pi b^2}{S} - 5\sqrt{\pi}b\sqrt{\frac{1}{S}} + 2\right) + a\left(\sqrt{\pi}b\sqrt{\frac{1}{S}} - 2\right)\log\left(\frac{S}{\pi}\right) + \frac{2 - \frac{\sqrt{\pi}b}{\sqrt{S}}}{\pi}}, \quad (84)$$

and for $S = 12.566\dots = 4\pi$, we obtain

$$\frac{2\left(-\frac{\pi ab}{2} - 2\pi a \log(2) + 1\right)}{a\left(\frac{b^2}{2} - \frac{5b}{2} + 2\right) + \log(4)a\left(\frac{b}{2} - 2\right) + \frac{2 - \frac{b}{2}}{\pi}}, \quad (85)$$

which has the alternate forms

$$\frac{2\pi(\pi a(b + \log(16)) - 2)}{2\pi a\left(\frac{1}{2}(b - 4)(b - 1)\right) + \pi \log(16)a\left(\frac{b}{2} - 2\right) - b + 4} \quad (86)$$

$$\frac{2\pi(\pi a(b + \log(16)) - 2)}{2\pi a\left(\frac{1}{2}(b^2 - 5b + 4)\right) + \pi \log(16)a\left(\frac{b}{2} - 2\right) - b + 4} \quad (87)$$

$$\frac{2\pi(\pi ab + 4\pi a \log(2) - 2)}{2\pi a\left(\frac{b^2}{2} - \frac{5b}{2} + 2\right) + 2\pi \log(4)a\left(\frac{b}{2} - 2\right) - b + 4} \quad (88)$$

The alternate forms Equations (86), (87), and (88) have the expanded forms

$$\begin{aligned} & \frac{4\pi a \log(2)}{a\left(\frac{b^2}{2} - \frac{5b}{2} + 2\right) + 2\log(2)a\left(\frac{b}{2} - 2\right) - \frac{b}{2\pi} + \frac{2}{\pi}} - \frac{\pi ab}{a\left(\frac{b^2}{2} - \frac{5b}{2} + 2\right) + 2\log(2)a\left(\frac{b}{2} - 2\right) - \frac{b}{2\pi} + \frac{2}{\pi}} \\ & + \frac{2}{a\left(\frac{b^2}{2} - \frac{5b}{2} + 2\right) + 2\log(2)a\left(\frac{b}{2} - 2\right) - \frac{b}{2\pi} + \frac{2}{\pi}} - \frac{4\pi a \log(2)}{a\left(\frac{b^2}{2} - \frac{5b}{2} + 2\right) + 2\log(2)a\left(\frac{b}{2} - 2\right) - \frac{b}{2\pi} + \frac{2}{\pi}} \quad (89) \\ & - \frac{\pi ab}{a\left(\frac{b^2}{2} - \frac{5b}{2} + 2\right) + 2\log(2)a\left(\frac{b}{2} - 2\right) - \frac{b}{2\pi} + \frac{2}{\pi}} + \frac{2}{a\left(\frac{b^2}{2} - \frac{5b}{2} + 2\right) + 2\log(2)a\left(\frac{b}{2} - 2\right) - \frac{b}{2\pi} + \frac{2}{\pi}} \end{aligned}$$

with the expanded logarithmic form

$$\begin{aligned} & \frac{4\pi}{4 - b + 2\pi a\left(\frac{1}{2}(4 - 5b + b^2)\right) + 4\pi a\left(\frac{1}{2}(-4 + b)\right)\log(2)} \\ & - \frac{2ab\pi^2}{4 - b + 2\pi a\left(\frac{1}{2}(4 - 5b + b^2)\right) + 4\pi a\left(\frac{1}{2}(-4 + b)\right)\log(2)} \quad (90) \\ & - \frac{8ab\pi^2 \log(2)}{4 - b + 2\pi a\left(\frac{1}{2}(4 - 5b + b^2)\right) + 4\pi a\left(\frac{1}{2}(-4 + b)\right)\log(2)} \end{aligned}$$

which has the alternate form

$$\frac{2\pi(2 - ab\pi - 4a\pi \log(2))}{4 - b + 2\pi a \left(\frac{1}{2}(-4 + b)(-1 + b) \right) + 2\pi a \left(\frac{1}{2}(-4 + b) \right) \log(4)}. \quad (91)$$

The root for the variable b is

$$b = \frac{2 - \pi a \log(16)}{\pi a}. \quad (92)$$

1) Indefinite integral

The indefinite integral for the alternative form Equation (91) is

$$\begin{aligned} & \int \frac{2 \left(1 - \frac{ab\pi}{2} - 2a\pi \log(2) \right)}{\frac{2-b}{\pi} + a \left(2 - \frac{5b}{2} + \frac{b^2}{2} \right) + a \left(-2 + \frac{b}{2} \right) \log(4)} da \\ &= - \frac{2\pi \left(\frac{1}{2} \pi a^2 (b + \log(16)) - 2a \right)}{2\pi a \left(\frac{1}{2} (b^2 - 5b + 4) \right) + \pi \log(16) a \left(\frac{b}{2} - 2 \right) - b + 4} + \text{constant} \end{aligned} \quad (93)$$

from which we obtain the alternate forms

$$\frac{\pi(-1)a(\pi ab + 4\pi a \log(2) - 4)}{\pi ab^2 - 5\pi ab + 2\pi ab \log(2) + 4\pi a - 8\pi a \log(2) - b + 4}, \quad (94)$$

$$- \frac{\pi a (\pi a (b + \log(16)) - 4)}{(b - 4) (\pi a (b - 1 + \log(4)) - 1)}, \quad (95)$$

$$- \frac{2\pi a (\pi a (b + \log(16)) - 4)}{(b - 4) (\pi a (2b - 2 + \log(16)) - 2)}. \quad (96)$$

The expanded form of Equations (93), (94) and (95) is

$$\begin{aligned} & - \frac{\pi^2 a^2 \log(16)}{\pi a (b^2 - 5b + 4) + \pi a \left(\frac{b}{2} - 2 \right) \log(16) - b + 4} \\ & - \frac{\pi^2 a^2 b}{a (b^2 - 5b + 4) + \pi a \left(\frac{b}{2} - 2 \right) \log(16) - b + 4} \\ & + \frac{4\pi a}{a (b^2 - 5b + 4) + \pi a \left(\frac{b}{2} - 2 \right) \log(16) - b + 4} \end{aligned} \quad (97)$$

Assuming a , b , and S are positive, then we have the alternative form

$$\begin{aligned} & \frac{4\pi a}{\pi a (b^2 - 5b + 4) + 4\pi a \left(\frac{b}{2} - 2 \right) \log(2) - b + 4} \\ & - \frac{\pi^2 a^2 (b + 4 \log(2))}{\pi a (b^2 - 5b + 4) + 4\pi a \left(\frac{b}{2} - 2 \right) \log(2) - b + 4} \end{aligned} \quad (98)$$

From which the expanded logarithmic form is

$$\frac{4a\pi}{4-b+4a\pi-5ab\pi+ab^2\pi-8a\pi\log(2)+2ab\pi\log(2)} - \frac{a^2b\pi^2}{4-b+4a\pi-5ab\pi+ab^2\pi-8a\pi\log(2)+2ab\pi\log(2)} - \frac{4a^2\pi^2\log\log(2)}{4-b+4a\pi-5ab\pi+ab^2\pi-8a\pi\log(2)+2ab\pi\log(2)} \tag{99}$$

The alternate form of the Equation (99) is

$$-\frac{2a\pi(-4+ab\pi+a\pi\log(16))}{8-2b+8a\pi-10ab\pi+2ab^2\pi-4a\pi\log(16)+ab\pi\log(16)}, \tag{100}$$

with the roots are

$$a = 0, b - 4 \neq 0, \\ a \neq 0, b = \frac{4 - 4\pi a \log(2)}{\pi a}, \\ 8\pi^2 a^2 + 16\pi^2 a^2 \log(2)^2 + 24\pi^2 a^2 \log(2) - 32\pi a - 40\pi a \log(2) + 24 \neq 0 \\ b = \frac{4 - \pi a \log(16)}{\pi a} \tag{101}$$

2) Series expansion

The Taylor series expansion about $a = 0$ is

$$\frac{4\pi a}{b-4} - \frac{\pi^2 a^2 (3b-4+\log(16))}{b-4} - \frac{a^3 \left(\pi^2 (6b^2 + b(5\log(16)-14) + 8 + \log(16)^2 - 6\log(16)) \right)}{2(b-4)} - \frac{a^4 \left(\pi^3 (2b-2+\log(16))^2 (3b-4+\log(16)) \right)}{4(b-4)} - \frac{a^5 \left(\pi^5 (2b-2+\log(16))^3 (3b-4+\log(16)) \right)}{8(b-4)} + o(a^6) \tag{102}$$

and the Laurent series expansion about $a = 0$ is

$$-\frac{2a(\pi(b+\log(16)))}{(b-4)(2b-2+\log(16))} + \frac{4(3b-4+\log(16))}{(b-4)(2b-2+\log(16))^2} + \frac{8(3b-4+\log(16))}{\pi a(b-4)(2b-2+\log(16))^3} + \frac{16(3b-4+\log(16))}{\pi^2 a^2(b-4)(2b-2+\log(16))^4} + o\left(\left(\frac{1}{a}\right)^3\right) \tag{103}$$

The derivative of the alternative form, Equation (100) is

$$\frac{\partial}{\partial a} \left(\frac{2\pi \left(-2a + \frac{1}{2} a^2 \pi (b + \log(16)) \right)}{4 - b + \frac{2}{2} \pi (a(4 - 5b + b^2)) + \pi \left(a \left(-2 + \frac{b}{2} \right) \right) \log(16)} \right) \quad (104)$$

$$= - \frac{2\pi \left(\pi^2 a^2 (2b^2 + b(\log(16) - 2) \log(16)) - 4\pi a (b + \log(16)) - 8 \right)}{(b - 4) \left(\pi a (2b - 2 + \log(16)) - 2 \right)^2}$$

With the indefinite integral given by

$$\int - \frac{2\pi \left(-2a + \frac{1}{2} a^2 \pi (b + \log(16)) \right)}{4 - b + a(4 - 5b + b^2) \pi + a \left(-2 + \frac{b}{2} \right) \pi \log(16)} da$$

$$= - \frac{\pi}{(b - 4) (2b - 2 + \log(16))^3} \left(a^2 (b + \log(16)) (2b - 2 + \log(16))^2 \right) \quad (105)$$

$$- \frac{4a(3b - 4 + \log(16))(2b - 2 + \log(16))}{\pi}$$

$$- \frac{8(3b - 4 + \log(16)) \log(2 - \pi a (2b - 2 + \log(16)))}{\pi^2} \Bigg) + constant$$

Taking the limit of alternative form, Equation (100) as $b \rightarrow \pm\infty$, we get

$$\lim_{b \rightarrow \pm\infty} - \frac{2\pi \left(-2a + \frac{1}{2} a^2 \pi (b + \log(16)) \right)}{4 - b + a(4 - 5b + b^2) \pi + a \left(-2 + \frac{b}{2} \right) \pi \log(16)} = 0, \quad (106)$$

and for $V = \frac{1}{3} \sqrt{2} a^3$ (octahedron volume) and $V = \frac{4}{3} \pi r^3$ (sphere volume),

where $r = \frac{a}{2}$, we obtain the following respectively;

a) Octahedron volume

For the octahedron volume we have

$$\frac{2\sqrt{2}\pi a^3 \left(\frac{1}{2} \pi a^2 (b + \log(16)) - 2a \right)}{3 \left(\pi a (b^2 - 5b + 4) + \pi a \left(\frac{b}{2} - 2 \right) \log(16) - b + 4 \right)}, \quad (107)$$

and plotting this result, we obtain the following 3D and the contour plots that can be related to a D-brane/Instanton.

The key observation from **Figure 1** and **Figure 2** and as confirmed by [4], is that at $a = 1$, which is taken as the energy density of the universe at the Big bang, with $b = 0$ the zero spacetime volume, the vacuum geometry brakes/or there is symmetry breaking on the vacuum quantum geometry. We see from the plots as the vacuum spacetime break/tear apart. Continuing further, we obtained the following properties of the Equation (107), that the alternate forms are

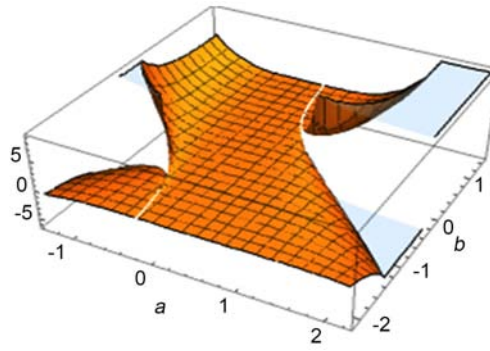


Figure 1. 3D plot.

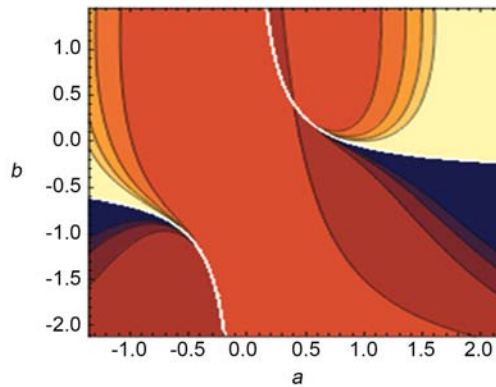


Figure 2. Contour plot.

$$\frac{\sqrt{2}\pi(-1)a^4(\pi ab + 4\pi a \log(2) - 4)}{3(\pi ab^2 - 5\pi ab + 2\pi ab \log(2) + 4\pi a - 8\pi a \log(2) - b + 4)}, \tag{108}$$

$$\frac{\sqrt{2}\pi a^4(\pi a(b + \log(16)) - 4)}{3(b - 4)(\pi a(b - 1 + \log(4)) - 1)}, \tag{109}$$

$$\frac{2\sqrt{2}\pi a^4(\pi a(b + \log(16)) - 4)}{3(b - 4)(\pi a(2b - 2 + \log(16)) - 2)}. \tag{110}$$

The expanded forms of Equations (108), (109), and (110) are

$$\begin{aligned} & \frac{\sqrt{2}\pi^2 a^5 \log(16)}{3\left(\pi a(b^2 - 5b + 4) + \pi a\left(\frac{b}{2} - 2\right)\log(16) - b + 4\right)} \\ & - \frac{\sqrt{2}\pi^2 a^5 b}{3\left(\pi a(b^2 - 5b + 4) + \pi a\left(\frac{b}{2} - 2\right)\log(16) - b + 4\right)} \\ & + \frac{4\sqrt{2}\pi a^4}{3\left(\pi a(b^2 - 5b + 4) + \pi a\left(\frac{b}{2} - 2\right)\log(16) - b + 4\right)} \\ & + \frac{-2\sqrt{2}\pi^2 a^5 b - 2\sqrt{2}\pi^2 a^5 \log(16) + 8\sqrt{2}\pi a^4}{6\pi ab^2 - 30\pi ab + 3\pi ab \log(16) + 24\pi a - 12\pi a \log(16) - 6b + 24} \end{aligned} \tag{111}$$

and assuming a , b , and S are positive, then we have the alternative form

$$\frac{4\sqrt{2}\pi a^4}{3\left(\pi a(b^2 - 5b + 4) + 4\pi a\left(\frac{b}{2} - 2\right)\log(2) - b + 4\right)} \frac{\sqrt{2}\pi^2 a^5 (b + 4\log(2))}{3\left(\pi a(b^2 - 5b + 4) + 4\pi a\left(\frac{b}{2} - 2\right)\log(2) - b + 4\right)} \quad (112)$$

from which the expanded logarithmic form is

$$\frac{4\sqrt{2}a^4\pi}{12 - 3b + 12a\pi - 15ab\pi + 3ab^2\pi - 24a\pi\log(2) + 6ab\pi\log(2)} - \frac{\sqrt{2}a^5b\pi^2}{12 - 3b + 12a\pi - 15ab\pi + 3ab^2\pi - 24a\pi\log(2) + 6ab\pi\log(2)} + \frac{4\sqrt{2}a^5\pi^2\log\log(2)}{12 - 3b + 12a\pi - 15ab\pi + 3ab^2\pi - 24a\pi\log(2) + 6ab\pi\log(2)} \quad (113)$$

with the alternate form

$$\frac{2\sqrt{2}a^4\pi(-4 + ab\pi + a\pi\log(16))}{3(8 - 2b + 8a\pi - 10ab\pi + 2ab^2\pi - 4a\pi\log(16) + ab\pi\log(16))} \quad (114)$$

The roots of the alternate form Equation (114) are

$$a = 0, \quad b - 4 \neq 0,$$

$$a \neq 0, \quad b = \frac{4 - 4\pi a \log(2)}{\pi a},$$

$$8\pi^2 a^2 + 16\pi^2 a^2 \log(2)^2 + 24\pi^2 a^2 \log(2) - 32\pi a - 40\pi a \log(2) + 24 \neq 0,$$

$$b = \frac{4 - \pi a \log(16)}{\pi a} \quad (115)$$

Furthermore, the Taylor series expansion about $a = 0$ is

$$\frac{4(\sqrt{2}\pi)a^4}{3(b-4)} - \frac{a^5(\sqrt{2}\pi^2(3b-4+\log(16)))}{3(b-4)} - \frac{a^6\left(\pi^3(6b^2+b(5\log(16)-14)+8+\log(16)^2-6\log(16))\right)}{3(\sqrt{2}(b-4))} - \frac{a^7\left(\pi^4(2b-2+\log(16))^2(3b-4+\log(16))\right)}{6(\sqrt{2}(b-4))} - \frac{a^8\left(\pi^5(2b-2+\log(16))^3(3b-4+\log(16))\right)}{12(\sqrt{2}(b-4))} + O(a^9) \quad (116)$$

and about $a = \infty$ is

$$\begin{aligned} & \frac{2a^4(\sqrt{2}\pi(b+\log(16)))}{3((b-4)(2b-2+\log(16)))} + \frac{4\sqrt{2}a^3(3b-4+\log(16))}{3(b-4)(2b-2+\log(16))^2} \\ & + \frac{8\sqrt{2}a^2(3b-4+\log(16))}{3\pi(b-4)(2b-2+\log(16))^3} + \frac{16\sqrt{2}a(3b-4+\log(16))}{3\pi^2(b-4)(2b-2+\log(16))^4} \\ & + \frac{32\sqrt{2}(3b-4+\log(16))}{3\pi^3(b-4)(2b-2+\log(16))^5} + O\left(\left(\frac{1}{a}\right)^1\right) \end{aligned} \tag{117}$$

The derivative of the alternate form Equation (113) is

$$\begin{aligned} & \frac{\partial}{\partial a} \left(\frac{\left(2\pi \left(-2a + \frac{1}{2}a^2\pi(b+\log(16)) \right) \right) (\sqrt{2}a^3)}{3 \left(4-b+a(4-5b+b^2)\pi + a \left(-2 + \frac{b}{2} \right) \pi \log(16) \right)} \right) \\ & = \left(4\sqrt{2}\pi a^3 \left(2\pi^2 a^2 (2b^2 + b(\log(4096) - 2) + (\log(16) - 2)\log(16)) \right. \right. \\ & \quad \left. \left. + \pi a(-17b + 12 - 11\log(16) + 16) \right) \right) / \left(3(b-4)(\pi a(2b-2+\log(16)) - 2)^2 \right) \end{aligned} \tag{118}$$

and the indefinite integral is

$$\begin{aligned} & \int - \frac{2\sqrt{2}a^3\pi \left(-2a + \frac{1}{2}a^2\pi(b+\log(16)) \right)}{3 \left(4-b+a(4-5b+b^2)\pi + a \left(-2 + \frac{b}{2} \right) \pi \log(16) \right)} da \\ & = \sqrt{2}\pi \left(-6a^5(b+\log(16))(2b-2+\log(16))^5 + \frac{15a^4(3b-4+\log(16))(2b-2+\log(16))^4}{\pi} \right. \\ & \quad + \frac{40a^3(3b-4+\log(16))(2b-2+\log(16))^3}{\pi^2} + \frac{120a^2(3b-4+\log(16))(2b-2+\log(16))^2}{\pi^3} \\ & \quad \left. + \frac{480a(3b-4+\log(16))(2b-2+\log(16))}{\pi^4} + \frac{960(3b-4+\log(16))\log(2-\pi a(2b-2+\log(16)))}{\pi^5} \right) \\ & \quad / \left(45(b-4)(2b-2+\log(16))^6 \right) + constant \end{aligned} \tag{119}$$

b) Sphere volume

For the octahedron volume we have

$$\frac{\pi^2 a^3 \left(\frac{1}{2} \pi a^2 (b + \log(16)) - 2a \right)}{3 \left(\pi a (b^2 - 5b + 4) + \pi a \left(\frac{b}{2} - 2 \right) \log(16) - b + 4 \right)}, \tag{120}$$

And similarly plotting this result, we obtain the following 3D and the contour plots that can be related to a D-brane/Instanton.

The observation in **Figure 3**, and **Figure 4**, is the same as in **Figure 1**, and **Figure 2**. Continuing further, we obtained the following properties of the Equation (120), that the alternate forms are

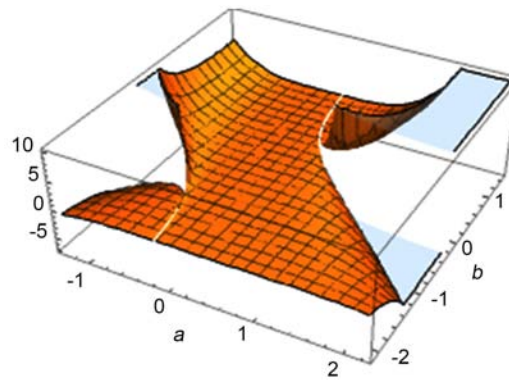


Figure 3. 3D plot.

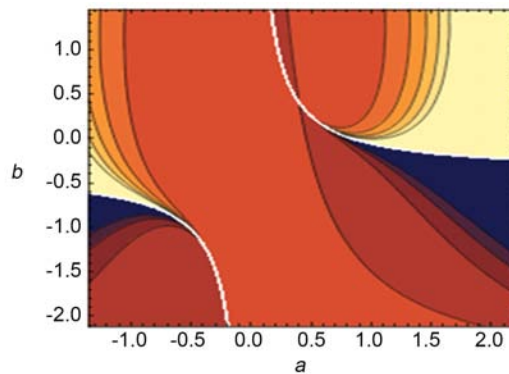


Figure 4. Contour plot.

$$\frac{\pi^2 a^4 (\pi ab + 4\pi a \log(2) - 4)}{3 \times 2 (\pi ab^2 - 5\pi ab + 2\pi ab \log(2) + 4\pi a - 8\pi a \log(2) - b + 4)}, \quad (121)$$

$$\frac{\pi^2 a^4 (\pi a (b + \log(16)) - 4)}{6(b - 4) (\pi a (b - 1 + \log(4)) - 1)}, \quad (122)$$

$$\frac{\pi^2 a^4 (\pi a (b + \log(16)) - 4)}{3(b - 4) (\pi a (2b - 2 + \log(16)) - 2)} \quad (123)$$

from which the expanded forms are

$$\begin{aligned} & \frac{\pi^3 a^5 \log(16)}{6 \left(\pi a (b^2 - 5b + 4) + \pi a \left(\frac{b}{2} - 2 \right) \log(16) - b + 4 \right)} \\ & \frac{\pi^3 a^5 b}{6 \left(\pi a (b^2 - 5b + 4) + \pi a \left(\frac{b}{2} - 2 \right) \log(16) - b + 4 \right)} \\ & + \frac{2\pi^2 a^4}{6 \left(\pi a (b^2 - 5b + 4) + \pi a \left(\frac{b}{2} - 2 \right) \log(16) - b + 4 \right)} \\ & + \frac{-\pi^3 a^5 b - \pi^3 a^5 \log(16) + 4\pi^2 a^4}{6\pi ab^2 - 30\pi ab + 3\pi ab \log(16) + 24\pi a - 12\pi a \log(16) - 6b + 24} \end{aligned} \quad (124)$$

Assuming a , b , and S are positive, the alternative forms are

$$\frac{2\pi^2 a^4}{3\left(\pi a(b^2 - 5b + 4) + 4\pi a\left(\frac{b}{2} - 2\right)\log(2) - b + 4\right)} - \frac{\pi^3 a^5 (b + 4\log(2))}{6\left(\pi a(b^2 - 5b + 4) + 4\pi a\left(\frac{b}{2} - 2\right)\log(2) - b + 4\right)} \tag{125}$$

and thus the expanded form is

$$\frac{2a^4\pi^2}{12 - 3b + 12a\pi - 15ab\pi + 3ab^2\pi - 24a\pi\log(2) + 6ab\pi\log(2)} + \frac{-\frac{1}{2}a^5b\pi^3}{12 - 3b + 12a\pi - 15ab\pi + 3ab^2\pi - 24a\pi\log(2) + 6ab\pi\log(2)} + \frac{2a^5\pi^3\log\log(2)}{12 - 3b + 12a\pi - 15ab\pi + 3ab^2\pi - 24a\pi\log(2) + 6ab\pi\log(2)} \tag{126}$$

from which the alternate form is

$$\frac{a^4\pi^2(-4 + ab\pi + a\pi\log(16))}{3(8 - 2b + 8a\pi - 10ab\pi + 2ab^2\pi - 4a\pi\log(16) + ab\pi\log(16))} \tag{127}$$

with the roots

$$a = 0, \quad b - 4 \neq 0, \\ a \neq 0, \quad b = \frac{4 - 4\pi a\log(2)}{\pi a}, \\ 8\pi^2 a^2 + 16\pi^2 a^2 \log(2)^2 + 24\pi^2 a^2 \log(2) - 32\pi a - 40\pi \log(2) + 24 \neq 0, \\ b = \frac{4 - \pi a\log(16)}{\pi a}. \tag{128}$$

The Taylor series expansion about $a = 0$, is

$$\frac{2\pi^2 a^4}{3(b-4)} - \frac{a^5(\pi^3(3b-4+\log(16)))}{6(b-4)} - \frac{a^6(\pi^4(6b^2+b(5\log(16)-14)+8+\log(16)^2-6\log(16)))}{12(b-4)} - \frac{a^7(\pi^5(2b-2+\log(16))^2(3b-4+\log(16)))}{24(b-4)} - \frac{a^8(\pi^6(2b-2+\log(16))^3(3b-4+\log(16)))}{48(b-4)} + O(a^9) \tag{129}$$

and about $a = \infty$, is

$$\begin{aligned} & -\frac{a^4(\pi^2(b+\log(16)))}{3((b-4)(2b-2+\log(16)))} + \frac{2\pi a^3(3b-4+\log(16))}{3(b-4)(2b-2+\log(16))^2} \\ & + \frac{4a^2(3b-4+\log(16))}{3(b-4)(2b-2+\log(16))^3} + \frac{8a(3b-4+\log(16))}{3\pi(b-4)(2b-2+\log(16))^4} \\ & + \frac{16(3b-4+\log(16))}{3\pi^2(b-4)(2b-2+\log(16))^5} + O\left(\left(\frac{1}{a}\right)^1\right) \end{aligned} \tag{130}$$

The derivative of the alternate form Equation (127)

$$\begin{aligned} & \frac{\partial}{\partial a} \left[\frac{\left(2\pi\left(-2a + \frac{1}{2}a^2\pi(b+\log(16))\right)\right)\left(4\pi\left(\frac{a}{2}\right)^3\right)}{3 \times \left(4-b+a(4-5b+b^2)\pi + a\left(-2 + \frac{b}{2}\right)\pi \log(16)\right)} \right] \\ & = -\left(2\pi^2 a^3\left(2\pi^2 a^2(2b^2 + b(\log(4096) - 2) + (\log(16) - 2)\log(16))\right.\right. \\ & \left.\left. + \pi a(-17b + 12 - 11\log(16) + 16)\right)\right) / \left(3(b-4)(\pi a(2b-2+\log(16)) - 2)^2\right) \end{aligned} \tag{131}$$

and the indefinite integral is

$$\begin{aligned} & \int -\frac{a^3\pi^2\left(-2a + \frac{1}{2}a^2\pi(b+\log(16))\right)}{3\left(4-b+a(4-5b+b^2)\pi + a\left(-2 + \frac{b}{2}\right)\pi \log(16)\right)} da \\ & = \pi^2 \left(-6a^5(b+\log(16))(2b-2+\log(16))^5 + \frac{15a^4(3b-4+\log(16))(2b-2+\log(16))^4}{\pi} \right. \\ & \left. + \frac{40a^3(3b-4+\log(16))(2b-2+\log(16))^3}{\pi^2} + \frac{120a^2(3b-4+\log(16))(2b-2+\log(16))^2}{\pi^3} \right. \\ & \left. + \frac{480a(3b-4+\log(16))(2b-2+\log(16))}{\pi^4} + \frac{960(3b-4+\log(16))\log(2-\pi a(2b-2+\log(16)))}{\pi^5} \right) \\ & / \left(90(b-4)(2b-2+\log(16))^6\right) \end{aligned} \tag{132}$$

c) The ratio of the Octahedron volume to the sphere volume and its number theoretic properties

Taking the limit

$$\lim_{b \rightarrow \pm\infty} -\frac{a^3\pi^2\left(-2a + \frac{1}{2}a^2\pi(b+\log(16))\right)}{3\left(4-b+a(4-5b+b^2)\pi + a\left(-2 + \frac{b}{2}\right)\pi \log(16)\right)} = 0, \tag{133}$$

and thus, dividing Octahedron volume Equation (107) by the Sphere volume Equation (120), and simplifying by the factor

$$\frac{-2\sqrt{2}\pi}{-\pi^2} \tag{134}$$

we obtained

$$\frac{2^{3/2}}{\pi} \tag{135}$$

with decimal approximation

$$0.90031631615710606955519919100674058266457414995522206255714374712 = \frac{2\sqrt{2}}{\pi}$$

(which is DN Constant, and it is also a transcendental number as well). It has the following series representations

$$\frac{-2\sqrt{2}\pi}{-\pi^2} = \frac{2\sqrt{z_0} \sum_{k=0}^{\infty} \frac{(-1)^k \left(-\frac{1}{2}\right)_k (2-z_0)^k z_0^{-k}}{k!}}{\pi} \tag{136}$$

for (not $(z_0 \in \mathbb{R}$ and $-\infty < z_0 \leq 0)$)

$$\frac{-2\sqrt{2}\pi}{-\pi^2} = \frac{2 \exp\left(i\pi \left\lfloor \frac{\arg(2-x)}{2\pi} \right\rfloor\right) \sqrt{x} \sum_{k=0}^{\infty} \frac{(-1)^k (2-x)^k x^{-k} \left(-\frac{1}{2}\right)_k}{k!}}{\pi} \tag{137}$$

for $(x \in \mathbb{R}$ and $x < 0)$

$$\frac{-2\sqrt{2}\pi}{-\pi^2} = \frac{2 \left(\frac{1}{z_0}\right)^{1/2 \lfloor \arg(2-z_0)/(2\pi) \rfloor} z_0^{1/2(1+\lfloor \arg(2-z_0)/(2\pi) \rfloor)} \sum_{k=0}^{\infty} \frac{(-1)^k \left(-\frac{1}{2}\right)_k (2-z_0)^k z_0^{-k}}{k!}}{\pi} \tag{138}$$

5. Analysis of the Equation of State of the Modified White Hole

The equation of state of the modified white hole is given by

$$T(V,P) = -\left(1 - \frac{1}{4\pi}\right) \frac{1}{2\pi r^2} \left[\frac{V}{2\pi r^2 - r^2 + br} \left(1 - \frac{a \ln r}{2} - \frac{ab}{4r}\right) + \left(V - \frac{2\pi r^2}{1 - \frac{1}{4\pi}} \left(r - \frac{r}{2\pi} + \frac{b}{4\pi} \right) \right) P \right] + \frac{a}{8\pi r} - \frac{ab}{16\pi r} \tag{139}$$

The analysis gives the following number theoretic properties and the Ramanujan recurring number properties of the equations of state:

The exact result is

$$\frac{\left(1 - \frac{1}{4\pi}\right) \left(\frac{V \left(-\frac{ab}{4r} - \frac{1}{2} a \log(r) + 1 \right)}{br + 2\pi r^2 - r^2} + P \left(V - \frac{2\pi r^2 \left(\frac{b}{4\pi} - \frac{r}{2\pi} + r \right)}{1 - \frac{1}{4\pi}} \right) \right)}{2\pi r^2} - \frac{ab}{16\pi r} + \frac{a}{8\pi r} \tag{140}$$

and considering $S = 4\pi$, we obtain V to be

$$-5ab\sqrt{\frac{\pi}{4\pi}} + (2ab^2)\frac{\pi}{4\pi} + 2a - \frac{b}{\sqrt{\pi(4\pi)}} + \left(ab\sqrt{\frac{\pi}{4\pi}} - 2a\right)\log\left(\frac{4\pi}{\pi}\right) + \frac{2}{\pi}, \quad (141)$$

which then simplifies to

$$\frac{ab^2}{2} - \frac{5ab}{2} + \log(4)\left(\frac{ab}{2} - 2a\right) + 2a - \frac{b}{2\pi} + \frac{2}{\pi}, \quad (142)$$

which when we plot it, get the 3D and the contour plots below that can be related to a D-brane/Instanton,

From **Figure 5**, and **Figure 6**, we note that the gravitational potential is almost zero as the self vacuum perturbations have not started to take effects resulting in the flat quantum vacuum geometry. The alternate forms of Equation (142) are

$$\frac{(b-4)(\pi a(b-1+\log(4))-1)}{2\pi} \quad (143)$$

$$\frac{(b-4)(\pi ab - \pi a + \pi a \log(4) - 1)}{2\pi} \quad (144)$$

$$\frac{(b-4)(\pi ab - \pi a - 1)}{2\pi} + \frac{1}{2}a(b-4)\log(4) \quad (145)$$

which have the expanded logarithmic form

$$-\frac{5ab}{2} + \frac{ab^2}{2} + 2a - \frac{b}{\pi 2} - 4a \log(2) + ab \log(2) + \frac{2}{\pi} \quad (146)$$

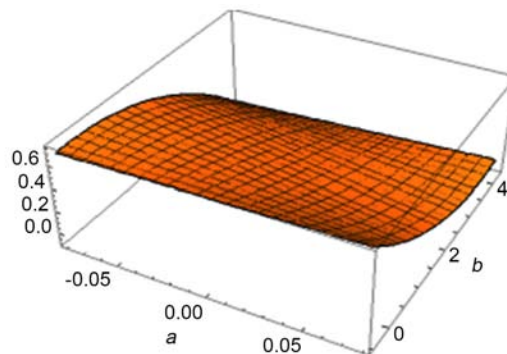


Figure 5. 3D plot.

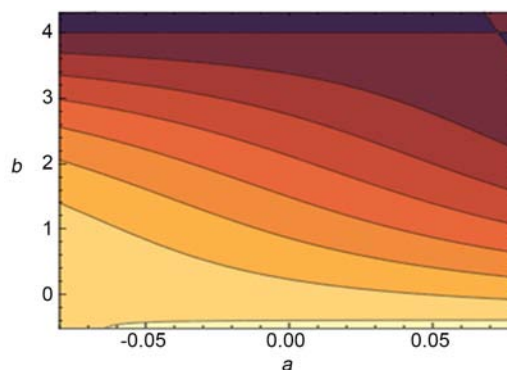


Figure 6. Contour plot.

1) number theoretic properties of the equation of state

a) Roots

From which the alternate form

$$\frac{4 - b + 4a\pi - 5ab\pi + ab^2\pi - 4a \log(4) + ab\pi \log(4)}{2\pi} \tag{147}$$

and the roots are

$$a \neq 0, b = \frac{\pi a - 2\pi a \log(2) + 1}{\pi a},$$

$$b = 4 \tag{148}$$

$$b = \frac{\pi a - \pi a \log(4) + 1}{\pi a} \tag{149}$$

The polynomial discriminant is

$$\Delta_b = \frac{9\pi^2 a^2 + \pi^2 a^2 \log(4)^2 + 6\pi^2 a^2 \log(4) - 6\pi a - 2\pi a \log(4) + 1}{4\pi^2}, \tag{150}$$

and the integer root are

$$a = 0, b = 4. \tag{151}$$

Thus the derivative of the alternative form Equation (147) is

$$\frac{\partial}{\partial a} \left(-5ab\sqrt{\frac{\pi}{4\pi}} + \frac{(2ab^2)\pi}{4\pi} + 2a - \frac{b}{\sqrt{\pi(4\pi)}} + \left(ab\sqrt{\frac{\pi}{4\pi}} - 2a \right) \log\left(\frac{4\pi}{\pi}\right) + \frac{2}{\pi} \right)$$

$$= \frac{1}{2}(b-4)(b-1+\log(4)) \tag{152}$$

b) Indefinite integral

The indefinite integral is

$$\int \left(2a - \frac{5ab}{2} + \frac{ab^2}{2} + \frac{2}{\pi} - \frac{b}{2\pi} + \left(-2a + \frac{ab}{2} \right) \log(4) \right) da$$

$$= \frac{(b-4) \left(\frac{1}{2} \pi a^2 (b-1+\log(4)) - a \right)}{2\pi} + constant \tag{153}$$

which when we plot it, get the 3D plot that can be related to a D-brane/Instanton, and we also plot its contour plot

From **Figure 7**, and **Figure 8**, we also observe that the vacuum quantum geometry starts to be uneven, meaning the seeds for the gravitational potential are starting to take effects due to the self-perturbations starting to take effect.

The alternate forms of indefinite integral Equation (153) is

$$\frac{a(b-4)(\pi ab - \pi a + 2\pi a \log(2) - 2)}{2\pi^2} \tag{154}$$

$$\frac{a(b-4)(\pi a(b-1+\log(4)) - 2)}{4\pi} \tag{155}$$

$$\frac{1}{4} a^2 (b-4) \log(4) + \frac{a(b-4)(\pi ab - \pi a - 2)}{4\pi} \tag{156}$$

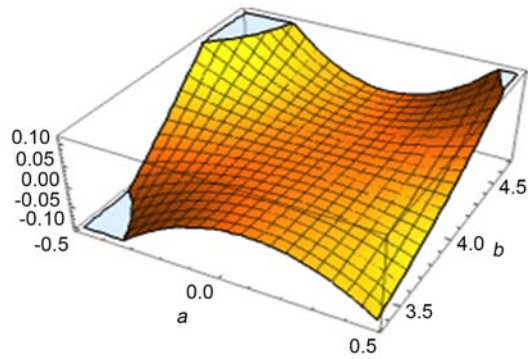


Figure 7. 3D plot.

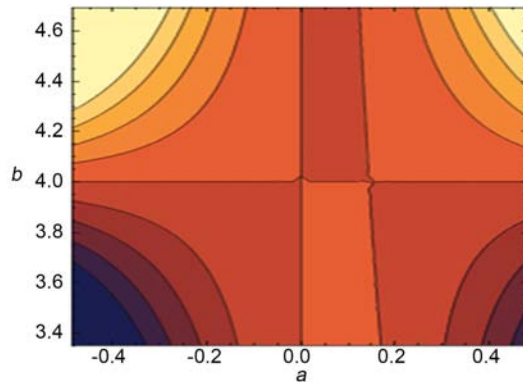


Figure 8. Contour plot.

and assuming a , b , and S are positive, then we have the alternative form

$$\frac{1}{4}a^2b(b-1+2\log(2))-a^2(b-1+2\log(2))-\frac{ab}{2\pi}+\frac{2a}{\pi}, \quad (157)$$

from which the expanded logarithmic form is

$$\frac{2a}{\pi}+a^2\pm\frac{5}{4}a^2b-2a^2\log(2)+\frac{-\frac{1}{2}ab}{\pi}+\frac{1}{4}a^2b^2+\frac{1}{2}a^2b\log(2). \quad (158)$$

From the expanded logarithmic form, Equation (158), the alternative form is

$$\frac{a(-4+b)(-2-a\pi+ab\pi+a\pi\log(4))}{4\pi} \quad (159)$$

With the root

$$\begin{aligned} a \neq 0, \quad b &= \frac{\pi a - 2\pi a \log(2) + 2}{\pi a}, \\ a &= 0, \quad b = 4, \\ b &= \frac{\pi a - \pi a \log(4) + 2}{\pi a} \end{aligned} \quad (160)$$

The polynomial discriminant is

$$\Delta_a = \frac{b^2 - 8b + 16}{4\pi^2} \quad (161)$$

and the derivative is

$$\frac{\partial}{\partial a} \left(\frac{(-4+b) \left(-a + \frac{1}{2} a^2 \pi (-1+b+\log(4)) \right)}{2\pi} \right) \tag{162}$$

$$= \frac{(-4+b) (\pi a (b-1+\log(4)) - 1)}{2\pi}$$

with the indefinite integral

$$\int \frac{(-4+b) \left(-a + \frac{1}{2} a^2 \pi (-1+b+\log(4)) \right)}{2\pi} da \tag{163}$$

$$= \frac{(b-4) \left(\frac{1}{3} \pi a^3 (b-1+\log(4)) - a^2 \right)}{4\pi} + Constant.$$

From the above indefinite integral, we have the following 3D and the contour plots that can be related to a D-brane/Instanton,

From **Figure 9**, and **Figure 10**, we also observe that the vacuum quantum geometry starts to be more uneven that that in **Figure 7** and **Figure 8**. That is, the gravitational potential of the quantum vacuum geometry is growing, as a result of the growth of the vacuum self-perturbations.

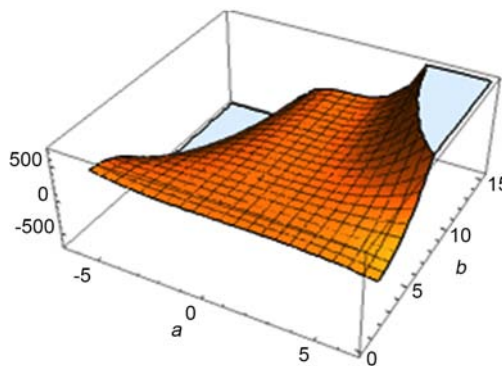


Figure 9. 3D plot.

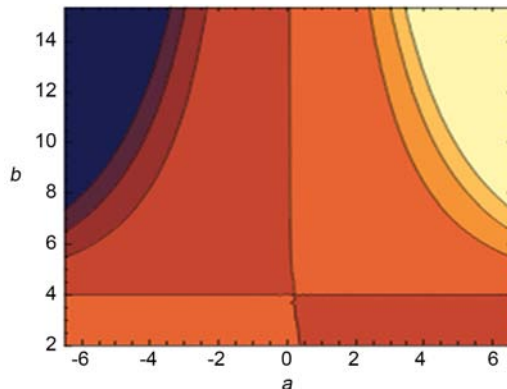


Figure 10. Contour plot.

The alternate forms of the indefinite integral Equation (163) are

$$\frac{a^2(b-4)(\pi ab - \pi a + 2\pi a \log(2) - 3)}{4\pi^3} \quad (164)$$

$$\frac{a^2(b-4)(\pi a(b-1 + \log(4)) - 3)}{12\pi} \quad (165)$$

$$\frac{1}{2}a^3(b-4)\log(4) + \frac{a^2(b-4)(\pi ab - \pi a - 3)}{12\pi} \quad (166)$$

and assuming a , b , and S are positive, then we have the alternative form

$$\frac{1}{12}a^3b(b-1 + 2\log(2)) - \frac{1}{2}a^3(b-1 + 2\log(2)) - \frac{a^2b}{4\pi} + \frac{a^2}{\pi}. \quad (167)$$

The expanded logarithmic form of Equation (167) is

$$\frac{a^2}{\pi} + \frac{1}{3}a^3 \pm \frac{5}{12}a^3b \pm \frac{2}{3}a^3\log(2) + \frac{-\frac{1}{4}a^2b}{\pi} + \frac{1}{12}a^3b^2 + \frac{1}{6}a^3b\log(2) \quad (168)$$

and the alternate form is

$$\frac{a^2(-4+b)(-3 - a\pi + ab\pi + a\pi\log(4))}{12\pi}, \quad (169)$$

with the root

$$\begin{aligned} a \neq 0, \quad b &= \frac{\pi a - 2\pi a \log(2) + 3}{\pi a}, \\ a \neq 0, \quad b &= 4, \\ b &= \frac{\pi a - \pi a \log(4) + 3}{\pi a}. \end{aligned} \quad (170)$$

The polynomial discriminant is $\Delta = 0$, and the derivative of the alternate form Equation (169) is

$$\begin{aligned} \frac{\partial}{\partial a} \left(\frac{(-4+b) \left(-a^2 + \frac{1}{3}a^3\pi(-1+b+\log(4)) \right)}{4\pi} \right) \\ = \frac{a(-4+b)(\pi a(b-1+\log(4)) - 2)}{4\pi} \end{aligned} \quad (171)$$

and the indefinite integral is

$$\begin{aligned} \int \frac{(-4+b) \left(-a^2 + \frac{1}{3}a^3\pi(-1+b+\log(4)) \right)}{4\pi} da \\ = \frac{(b-4) \left(\frac{1}{4}\pi a^4(b-1+\log(4)) - a^3 \right)}{12\pi} + Constant. \end{aligned} \quad (172)$$

The local minimum is

$$\min \left\{ \frac{(-4+b) \left(-a^2 + \frac{1}{3} a^3 \pi (-1+b+\log(4)) \right)}{4\pi} \right\} = -\frac{1}{12\pi^3 (3+\log(4))}$$

at

$$(a, b) = \left(\frac{1}{\pi(3+2\log(2))}, 7+2\log(2) \right) \tag{173}$$

In conclusion, the indefinite integral result Equation (172), and for $V = \frac{1}{3}\sqrt{2}a^3$ (octahedron volume) and $V = \frac{4}{3}\pi r^3$ (sphere volume), where $r = \frac{a}{2}$, we obtain:

1) Octahedron volume

For the octahedron we have

$$\frac{a^3(b-4) \left(\frac{1}{4}\pi a^4(b-1+\log(4)) - a^3 \right)}{18\sqrt{2}\pi} \tag{174}$$

which when we plot it, get the 3D and the contour plots that can be related to a D-brane/Instanton

From **Figure 11**, and **Figure 12**, we now observe that the vacuum gravitational potential has grown exponentially and infinitely high as a results of the exponentially grown and infinitely high growth vacuum self-perturbations near $a = 1$, *i.e.* the energy density of the universe at the big bang.

The alternate forms were found to be

$$\frac{\sqrt{2}a^6(b-4)(\pi ab - \pi a + 2\pi a \log(2) - 4)}{4 \times 12\pi^3} \tag{175}$$

$$a^6 \left(a \left(\frac{1}{18\sqrt{2}} - \frac{\log(4)}{18\sqrt{2}} \right) + \frac{\sqrt{2}}{9\pi} \right) + b \left(\frac{a^7 b}{72\sqrt{2}} + a^6 \left(a \left(\frac{\log(4)}{72\sqrt{2}} - \frac{5}{72\sqrt{2}} \right) - \frac{1}{18\sqrt{2}\pi} \right) \right) \tag{176}$$

$$\frac{a^6(b-4)(\pi a(b-1+\log(4)) - 4)}{72\sqrt{2}\pi} \tag{177}$$

and the expanded form is

$$\frac{a^3(b-4) \left(\frac{1}{4}\pi a^4 b - \frac{\pi a^4}{4} + \frac{1}{2}\pi a^4 \log(2) - a^3 \right)}{18\sqrt{2}\pi} \tag{178}$$

with the expanded logarithmic form

$$\begin{aligned} & \frac{1}{36} \times 4\sqrt{2}a^6 + \frac{1}{36}(-1)\sqrt{2}a^6 b + \frac{\sqrt{2}a^7}{36} - \frac{a^7 b \sqrt{2}}{36 \times 2 \times 2} + \frac{1}{36}\sqrt{2}a^7(-1)b \\ & + \frac{a^7 b^2 \sqrt{2}}{36 \times 2 \times 2} - \frac{1}{18}\sqrt{2}a^7 \log(2) + \frac{a^7 b \log(2)\sqrt{2}}{36 \times 2} \end{aligned} \tag{179}$$

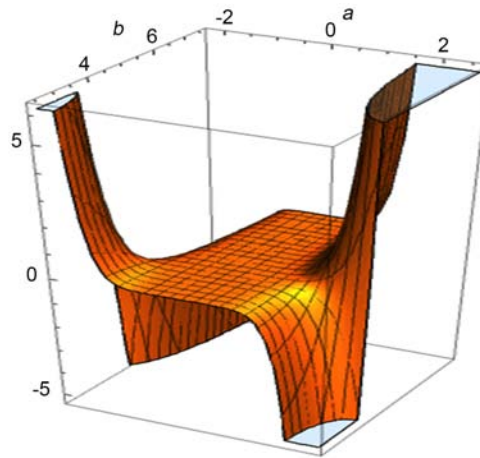


Figure 11. 3D plot.

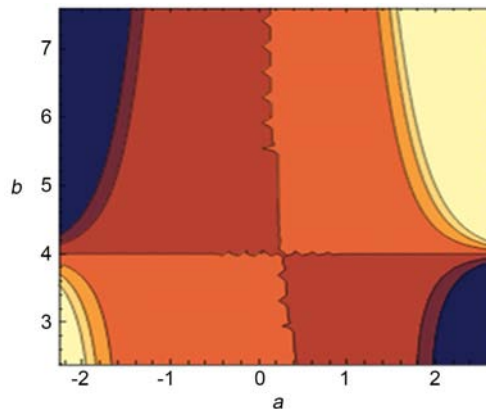


Figure 12. Contour plot.

The alternate form of Equation (179) is

$$\frac{a^6(-4+b)(-4-a\pi+ab\pi+a\pi\log(4))}{72\sqrt{2}\pi} \tag{180}$$

With the root

$$\begin{aligned} a \neq 0, \quad b &= \frac{\pi a - 2\pi a \log(2) + 4}{\pi a}, \\ a = 0, \quad b &= 4, \\ b &= \frac{\pi a - \pi a \log(2) + 4}{\pi a}. \end{aligned} \tag{181}$$

The polynomial discriminant is $\Delta = 0$, and the derivative is

$$\begin{aligned} &\frac{\partial}{\partial a} \left(\frac{\left((-4+b) \left(-a^3 + \frac{1}{4} a^4 \pi (-1+b+\log(4)) \right) \right) (\sqrt{2} a^3)}{(12\pi) \times 3} \right) \\ &= \frac{a^5(-4+b)(7\pi a(b-1+\log(4))-24)}{72\sqrt{2}\pi} \end{aligned} \tag{182}$$

and the indefinite integral

$$\int \frac{a^3(-4+b)\left(-a^3 + \frac{1}{4}a^4\pi(-1+b+\log(4))\right)}{18\sqrt{2}\pi} da \tag{183}$$

$$= \frac{a^7(b-4)(7\pi a(b-1+\log(4))-32)}{4032\sqrt{2}\pi} + Constant$$

The local minimum is

$$\min \left\{ \frac{\left((-4+b)\left(-a^3 + \frac{1}{4}a^4\pi(-1+b+\log(4))\right) \right) (\sqrt{2}a^3)}{(12\pi)3} \right\}$$

$$= -\frac{3200000\sqrt{2}}{7411887\pi^7(3+\log(4))^5}$$

at

$$(a,b) = \left(\frac{20}{7\pi(3+2\log(2))}, \frac{23}{5}, \frac{2\log(2)}{5} \right) \tag{184}$$

2) sphere volume

For the sphere we have

$$\frac{1}{72}a^3(b-4)\left(\frac{1}{4}\pi a^4(b-1+\log(4))-a^3\right) \tag{185}$$

Which when we plot it, get the 3D plot that can be related to a D-brane/ Instanton, and we also plot its contour plot

As in **Figure 13**, and **Figure 14** in case of the octahedron, here, we also observe that the vacuum gravitational potential has grown exponentially and infinitely high as a results of the exponentially grown and infinitely high growth vacuum self-perturbations near $a = 1$, *i.e.* the energy density of the universe at the big bang.

The alternate forms of Equation (185) are

$$\frac{a^6(b-4)(\pi ab - \pi a + 2\pi a \log(2) - 4)}{2 \times 2 \times 2 \times 4 \times 3 \times 3} \tag{186}$$

$$a^6 \left(a \left(\frac{\pi}{72} - \frac{1}{72} \pi \log(4) \right) + \frac{1}{18} \right) \tag{187}$$

$$+ b \left(\frac{1}{288} \pi a^7 b + a^6 \left(a \left(\frac{1}{288} \pi \log(4) - \frac{5\pi}{288} \right) - \frac{1}{72} \right) \right)$$

$$a^6 \left(a \left(b \left(\frac{\pi b}{288} - \frac{5\pi}{288} + \frac{1}{288} \pi \log(4) \right) + \frac{\pi}{72} - \frac{1}{72} \pi \log(4) \right) - \frac{b}{72} + \frac{1}{18} \right) \tag{188}$$

and assuming a, b , and S are positive, then we have the alternative form

$$\frac{1}{288} \pi a^7 b (b-1+2\log(2)) - \frac{1}{72} \pi a^7 (b-1+2\log(2)) - \frac{a^6 b}{72} + \frac{a^6}{18}, \tag{189}$$

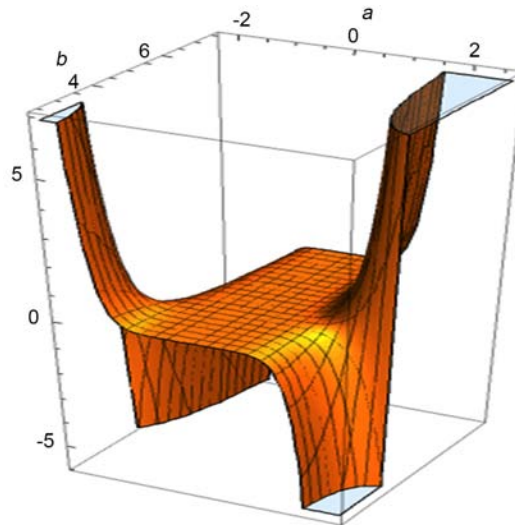


Figure 13. 3D plot.

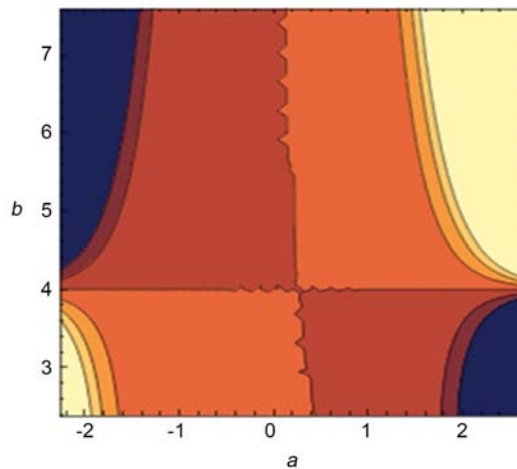


Figure 14. Contour plot.

from which the expanded logarithmic form is

$$\frac{a^6}{18} + \frac{1}{72}(-1)a^6b + \frac{1}{72}a^7\pi - \frac{5a^7b\pi}{72 \times 4} + \frac{a^7b^2\pi}{72 \times 4} - \frac{1}{36}a^7\pi \log(2) + \frac{a^7b\pi \log(2)}{72 \times 2} \quad (190)$$

The alternative form of the expanded logarithmic form E. (193)

$$\frac{1}{288}a^6(-4+b)(-4 - a\pi + ab\pi + a\pi \log(4)) \quad (191)$$

with the root

$$a \neq 0, b = \frac{\pi a - 2\pi a \log(2) + 4}{\pi a}$$

$$a = 0, b = 0,$$

$$b = \frac{\pi a - \pi a \log(4) + 4}{\pi a} \quad (192)$$

The polynomial discriminant is $\Delta = 0$, and the derivative is

$$\frac{\partial}{\partial a} \left(\frac{(-4+b) \left(-a^3 + \frac{1}{4} a^4 \pi (-1+b+\log(4)) \right) \left(4\pi \left(\frac{a}{2} \right)^3 \right)}{(12\pi) \times 3} \right) \tag{193}$$

$$= \frac{1}{288} a^5 (-4+b) (7\pi a (b-1+\log(4)) - 24)$$

From the indefinite integral is

$$\min \left\{ \frac{\left((-4+b) \left(-a^3 + \frac{1}{4} a^4 \pi (-1+b+\log(4)) \right) \right) \left(4\pi \left(\frac{a}{2} \right)^3 \right)}{(12\pi) 3} \right\}$$

$$= \frac{1600000}{7411887\pi^6 (3+\log(4))^5}$$

at

$$(a,b) = \left(\frac{20}{7\pi(3+2\log(2))}, \frac{23}{5} + \frac{2\log(2)}{5} \right) + constant, \tag{194}$$

By dividing the integral Equation (183) with the integral Equation (194), we obtain the result

$$\frac{2\sqrt{2}}{\pi} \tag{195}$$

With the decimal approximation

$$0.9003163161571060695551991910067405826645741499552206255714374712 = \frac{2\sqrt{2}}{\pi}$$

(which is a DN Constant and also a transcendental number). It is also the reduced logarithmic form. The alternative representations are

$$\frac{a^7 (-4+b) (-32+7a\pi(-1+b+\log(4)))}{(a^7 (-4+b) (-32+7a\pi(-1+b+\log(4)))) (4032\sqrt{2}\pi)}$$

$$\frac{16128}{(-4+b) (-32+7a\pi(-1+b+\log_e(4))) a^7} \tag{196}$$

$$= \frac{(a^7 (-4+b) (-32+7a\pi(-1+b+\log(4)))) (4032\sqrt{2}\pi)}{16128}$$

$$\frac{a^7 (-4+b) (-32+7a\pi(-1+b+\log(4)))}{(a^7 (-4+b) (-32+7a\pi(-1+b+\log(4)))) (4032\sqrt{2}\pi)}$$

$$\frac{16128}{(-4+b) (-32+7a\pi(-1+b+\log(a)\log_a(4))) a^7} \tag{197}$$

$$= \frac{(a^7 (-4+b) (-32+7a\pi(-1+b+\log(4)))) (4032\sqrt{2}\pi)}{16128}$$

$$\frac{a^7(-4+b)(-32+7a\pi(-1+b+\log(4)))}{(a^7(-4+b)(-32+7a\pi(-1+b+\log(4))))(4032\sqrt{2}\pi)} \cdot \frac{16128}{16128} = \frac{(-4+b)(-32+7a\pi(-1+b-Li_1(-3)))a^7}{(a^7(-4+b)(-32+7a\pi(-1+b+Li_1(-3))))(4032\sqrt{2}\pi)} \cdot \frac{16128}{16128} \tag{198}$$

where $\log_b x$ is the base b logarithm, $Li_n(x)$ is the polylogarithm function

1) Series representations

$$\frac{a^7(-4+b)(-32+7a\pi(-1+b+\log(4)))}{(a^7(-4+b)(-32+7a\pi(-1+b+\log(4))))(4032\sqrt{2}\pi)} \cdot \frac{16128}{16128} = \frac{4}{\pi\sqrt{z_0}\sum_{k=0}^{\infty}\frac{(-1)^k\left(-\frac{1}{2}\right)_k(2-z_0)^k z_0^{-k}}{k!}} \tag{199}$$

for (not ($z_0 \in \mathbb{R}$ and $-\infty < z_0 \leq 0$))

$$\frac{a^7(-4+b)(-32+7a\pi(-1+b+\log(4)))}{(a^7(-4+b)(-32+7a\pi(-1+b+\log(4))))(4032\sqrt{2}\pi)} \cdot \frac{16128}{16128} = \frac{4}{\pi\sqrt{z_0}\sum_{k=0}^{\infty}\frac{(-1)^k\left(-\frac{1}{2}\right)_k(2-z_0)^k z_0^{-k}}{k!}} \tag{200}$$

for (not ($z_0 \in \mathbb{R}$ and $-\infty < z_0 \leq 0$))

$$\frac{a^7(-4+b)(-32+7a\pi(-1+b+\log(4)))}{(a^7(-4+b)(-32+7a\pi(-1+b+\log(4))))(4032\sqrt{2}\pi)} \cdot \frac{16128}{16128} = \frac{4}{\pi\exp\left(i\pi\left[\frac{\arg(2-x)}{2\pi}\right]\right)\sqrt{x}\sum_{k=0}^{\infty}\frac{(-1)^k(2-x)^k x^{-k}\left(-\frac{1}{2}\right)_k}{k!}} \tag{201}$$

for ($x \in \mathbb{R}$ and $x < 0$)

$$\frac{a^7(-4+b)(-32+7a\pi(-1+b+\log(4)))}{(a^7(-4+b)(-32+7a\pi(-1+b+\log(4))))(4032\sqrt{2}\pi)} \cdot \frac{16128}{16128} = \frac{4\left(\frac{1}{z_0}\right)^{-1/2\lceil\arg(2-z_0)/(2\pi)\rceil} z_0^{-1/2(1+\lceil\arg(2-z_0)/(2\pi)\rceil)}}{\pi\sum_{k=0}^{\infty}\frac{(-1)^k\left(-\frac{1}{2}\right)_k(2-z_0)^k z_0^{-k}}{k!}} \tag{202}$$

SECTION C: On the application of the formulas of the volumes of an octahedron and a sphere to quantum gravity

In this section we apply the number theoretic properties and the Ramanujan recurring number properties to the quantum geometry of the white hole. With regard to a sphere inscribed in an octahedron, we have the following formulas.

$$V_0 = \frac{1}{3}\sqrt{2}l^3, \quad V_s = \frac{4}{3}\pi r^3 \quad \text{where } r_s = \frac{l}{2} \tag{203}$$

We take the ratio between the two above formulas for the octahedron and sphere in Equation (203) as shown in **Figure 15**

$$\frac{\frac{1}{3}\sqrt{2}l^3}{\frac{4}{3}\pi\left(\frac{l}{2}\right)^3} = \frac{2\sqrt{2}}{\pi}, \quad (\text{for } l \neq 0) \tag{204}$$

with the decimal approximation,

$$0.9003163161571060695551991910067405826645741499552206255714374712\dots = \frac{2\sqrt{2}}{\pi} \tag{205}$$

(which is a DN Constant, and a transcendental number)

The series representations Equation (204)

$$\frac{\sqrt{2}l^3}{\frac{1}{3}\left(4\pi\left(\frac{l}{2}\right)^3\right)^3} = \frac{2\sqrt{z_0} \sum_{k=0}^{\infty} \frac{(-1)^k \left(-\frac{1}{2}\right)_k (2-z_0)^k z_0^{-k}}{k!}}{\pi} \tag{206}$$

for (not $(z_0 \in \mathbb{R} \text{ and } -\infty < z_0 \leq 0)$)

$$\frac{\sqrt{2}l^3}{\frac{1}{3}\left(4\pi\left(\frac{l}{2}\right)^3\right)^3} = \frac{2 \exp\left(i\pi \left\lfloor \frac{\arg(2-x)}{2\pi} \right\rfloor\right) \sqrt{x} \sum_{k=0}^{\infty} \frac{(-1)^k (2-x)^k x^{-k} \left(-\frac{1}{2}\right)_k}{k!}}{\pi} \tag{207}$$

for $(x \in \mathbb{R} \text{ and } x < 0)$

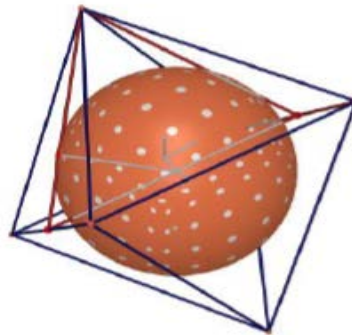


Figure 15. Sphere inscribed in an octahedron.

$$\frac{\sqrt{2}l^3}{\frac{1}{3}\left(4\pi\left(\frac{l}{2}\right)^3\right)^3} = \frac{2\left(\frac{1}{z_0}\right)^{1/2[\arg(2-z_0)/(2\pi)]} z_0^{1/2(1+[\arg(2-z_0)/(2\pi)])} \sum_{k=0}^{\infty} \frac{(-1)^k \left(-\frac{1}{2}\right)_k (2-z_0)^k z_0^{-k}}{k!}}{\pi} \quad (208)$$

from which we obtain

$$\left(\frac{\frac{1}{3} \frac{2}{\frac{1}{\sqrt{2}l^3}}}{\frac{4}{3}\pi\left(\frac{l}{2}\right)^3} \right)^2 = \frac{\pi^2}{6}, \quad (209)$$

with the decimal approximation

$$1.6449340668482264364724151666460251892189499012067984377355582293 = \zeta(2) = \pi^2/6 = 1.644934 \quad (210)$$

(which is the trace of the instanton shape and Ramanujan Recurring Number, and it is also a transcendental number).

The series representations of Equation (209) are

$$\left(\frac{\frac{1}{3} \frac{2}{\sqrt{2}l^3}}{\frac{3}{3}\left(4\pi\left(\frac{l}{2}\right)^3\right)} \right)^2 = \sum_{k=1}^{\infty} \frac{1}{k^2}, \quad (211)$$

$$\left(\frac{\frac{1}{3} \frac{2}{\sqrt{2}l^3}}{\frac{3}{3}\left(4\pi\left(\frac{l}{2}\right)^3\right)} \right)^2 = -2 \sum_{k=1}^{\infty} \frac{(-1)^k}{k^2} \quad (212)$$

$$\left(\frac{\frac{1}{3} \frac{2}{\sqrt{2}l^3}}{\frac{3}{3}\left(4\pi\left(\frac{l}{2}\right)^3\right)} \right)^2 = \frac{4}{3} \sum_{k=0}^{\infty} \frac{1}{(1+2k)^2}, \quad (213)$$

with the integral representations

$$\frac{1}{3} \frac{\left(\frac{2}{\sqrt{2}l^3} \right)^2}{\left(\frac{3}{3} \left(4\pi \left(\frac{l}{2} \right)^3 \right) \right)^2} = \frac{8}{3} \left(\int_0^1 \sqrt{1-t^2} dt \right)^2 \tag{214}$$

$$\frac{1}{3} \frac{\left(\frac{2}{\sqrt{2}l^3} \right)^2}{\left(\frac{3}{3} \left(4\pi \left(\frac{l}{2} \right)^3 \right) \right)^2} = \frac{2}{3} \left(\int_0^\infty \frac{1}{1+t^2} dt \right)^2 \tag{215}$$

$$\frac{1}{3} \frac{\left(\frac{2}{\sqrt{2}l^3} \right)^2}{\left(\frac{3}{3} \left(4\pi \left(\frac{l}{2} \right)^3 \right) \right)^2} = \frac{2}{3} \left(\int_0^1 \frac{1}{1+t^2} dt \right)^2 \tag{216}$$

We note that, from the sum of the first nine numbers excluding 0, *i.e.*, $1 + 2 + 3 + 4 + 5 + 6 + 7 + 8 + 9 = 45$ (these are the fundamental numbers, from which, through infinite combinations, all the other numbers are obtained), we obtain the following interesting formula:

$$1 + \frac{1}{\sqrt[3]{\left(\phi^2 + \frac{2\pi}{3} C_{MRB} \right) \left(\frac{1}{e} \sqrt[3]{1+2+3+4+5+6+7+8+9} \right)}} \tag{217}$$

where ϕ is the golden ratio, C_{MRB} is the *MRB* constant. The exact result of Equation (217) is then given by

$$3^{-2/(3\pi)} \times 5^{-1/(3\pi)} \sqrt[3]{\frac{e}{\frac{2\pi C_{MRB}}{3} + \phi^2}} + 1, \tag{218}$$

With the decimal approximation

$$1.6452973785207760327718962297937282004549534211102915708253939286 \approx \zeta(2) = \pi^2/6 = 1.644934 \tag{219}$$

(which is a trace of the instanton shape and Ramanujan Recurring Number)

The alternate forms for Equation (218) is

$$3^{1/3-2/(3\pi)} \times 5^{-1/(3\pi)} \sqrt[3]{\frac{e}{2\pi C_{MRB} + 3\phi^2}} + 1, \tag{220}$$

$$3^{-2/(3\pi)} \times 5^{-1/(3\pi)} \sqrt[3]{\frac{e}{\frac{2\pi C_{MRB}}{3} + \frac{1}{2}(3 + \sqrt{5})}} + 1, \tag{221}$$

$$2^{2/3} \times 3^{1/3-2/(3\pi)} \times 5^{-1/(3\pi)} \sqrt[3]{\frac{e}{8\pi C_{MRB} + 18 + 6\sqrt{5}}} + 1, \tag{222}$$

From which the expanded forms are

$$3^{-2/(3\pi)} \times 5^{-1/(3\pi)} \sqrt[3]{\frac{e}{\frac{2\pi C_{MRB}}{3} + \frac{1}{4}(1 + \sqrt{5})^2}} + 1, \tag{223}$$

$$3^{-2/(3\pi)} \times 5^{-1/(3\pi)} \sqrt[3]{\frac{e}{\frac{2\pi C_{MRB}}{3} + \frac{3}{2} + \frac{\sqrt{5}}{2}}} + 1, \tag{224}$$

and making input

$$\sqrt[6]{\left(1 + \frac{1}{\sqrt[3]{\left(\phi^2 + \frac{2\pi}{3} C_{MRB}\right) \left(\frac{1}{e} \sqrt[3]{1+2+3+4+5+6+7+8+9}\right)}}\right)}, \tag{225}$$

then we get exact results

$$\sqrt[6]{\left(3^{-2/(3\pi)} \times 5^{-1/(3\pi)} \sqrt[3]{\frac{e}{\frac{2\pi C_{MRB}}{3} + \phi^2}} + 1\right)} \tag{226}$$

with the decimal approximation

$$3.141939571526843089243307321961626326775133868116590446825417393 \approx \pi \tag{227}$$

(which is a Ramanujan Recurring Number)

The alternate form of Equation (226) is

$$\sqrt[6]{\left(3^{1/3-2/(3\pi)} \times 5^{-1/(3\pi)} \sqrt[3]{\frac{e}{2\pi C_{MRB} + 3\phi^2}} + 1\right)}, \tag{228}$$

$$3^{1/2-1/(3\pi)} \times 5^{-1/(6\pi)} \sqrt[2]{\left(\sqrt[3]{\frac{6e}{4\pi C_{MRB} + 9 + 3\sqrt{5}}} + 3^{2/(3\pi)} \sqrt[3]{5}\right)}, \tag{229}$$

from which the expanded forms are

$$\sqrt[6]{\left(3^{-2/(3\pi)} \times 5^{-1/(3\pi)} \sqrt[3]{\frac{e}{\frac{2\pi C_{MRB}}{3} + \frac{1}{4}(1 + \sqrt{5})^2}} + 1\right)}, \tag{230}$$

$$\sqrt[6]{\left(2 \times 3^{1-2/(3\pi)} \times 5^{-1/(3\pi)} \sqrt[3]{\frac{e}{\frac{2\pi C_{MRB}}{3} + \frac{3}{2} + \frac{\sqrt{5}}{2}}} + 6\right)}. \tag{231}$$

All 2nd roots of $6 \left(3^{-2/(3\pi)} 5^{-1/(3\pi)} \left(\frac{e}{\left(\frac{2\pi C_{MRB}}{3} + \phi^2 \right)^{1/3}} \right)^{1/3} + 1 \right)$ are

$$e^0 \sqrt[3]{6 \left(3^{-2/(3\pi)} \times 5^{-1/(3\pi)} \sqrt[3]{\frac{e}{\frac{2\pi C_{MRB}}{3} + \phi^2}} + 1 \right)} \approx 3.1419 \quad (232)$$

(real, principal root)

$$e^{i\pi} \sqrt[3]{6 \left(3^{-2/(3\pi)} \times 5^{-1/(3\pi)} \sqrt[3]{\frac{e}{\frac{2\pi C_{MRB}}{3} + \phi^2}} + 1 \right)} \approx -3.1419 \quad (233)$$

(real root).

Furthermore, form the input:

$$2\pi\sqrt{2} \times \frac{\frac{1}{3}\sqrt{2}l^3}{\frac{4}{3}\pi\left(\frac{l}{2}\right)^3} = 8, \quad (234)$$

where value 8 is linked to the “Ramanujan function” (an elliptic modular function that satisfies the need for “conformal symmetry”) that has 8 “modes” corresponding to the physical vibrations of a superstring.

The series representations Equation (234) are

$$\frac{(2\pi\sqrt{2})(\sqrt{2}l^3)}{\frac{1}{3}\left(4\pi\left(\frac{l}{2}\right)^3\right)^3} = 4\sqrt{z_0}^{-2} \left(\sum_{k=0}^{\infty} \frac{(-1)^k \left(-\frac{1}{2}\right)_k (2-z_0)^k z_0^{-k}}{k!} \right)^2 \quad (235)$$

for (not $(z_0 \in \mathbb{R}$ and $-\infty < z_0 \leq 0)$),

$$\begin{aligned} & \frac{(2\pi\sqrt{2})(\sqrt{2}l^3)}{\frac{1}{3}\left(4\pi\left(\frac{l}{2}\right)^3\right)^3} \\ &= 4 \exp^2 \left(i\pi \left[\frac{\arg(2-x)}{2\pi} \right] \right) \sqrt{x}^{-2} \left(\sum_{k=0}^{\infty} \frac{(-1)^k (2-x)^k x^{-k} \left(-\frac{1}{2}\right)_k}{k!} \right)^2 \end{aligned} \quad (236)$$

for $(x \in \mathbb{R}$ and $x < 0)$

$$\frac{(2\pi\sqrt{2})(\sqrt{2}l^3)}{\frac{1}{3}\left(4\pi\left(\frac{l}{2}\right)^3\right)^3} = 4 \left(\frac{1}{z_0} \right)^{\lfloor \frac{\arg(2-z_0)}{(2\pi)} \rfloor} z_0^{1+\lfloor \frac{\arg(2-z_0)}{(2\pi)} \rfloor} \left(\sum_{k=0}^{\infty} \frac{(-1)^k \left(-\frac{1}{2}\right)_k (2-z_0)^k z_0^{-k}}{k!} \right)^2 \quad (237)$$

And by the input

$$6\pi\sqrt{2} \times \frac{\frac{1}{3}\sqrt{2}l^2}{\frac{4}{3}\pi\left(\frac{l}{2}\right)^3} = 24 \tag{238}$$

The value 24 is linked to the ‘‘Ramanujan function’’ (an elliptic modular function that satisfies the need for ‘‘conformal symmetry’’) that has 24 ‘‘modes’’ corresponding to the physical vibrations of a bosonic string representing a bosons. From the analysis, we observe that there is no number theoretic connection with physical vibrations of fermionic strings at extremely low entropy. This fact is confirmed by the fact that the Higgs bosons at the moment of the big bang and infinitesimally shortly thereafter, facilitated the creation of fermions (matter and antimatter particles) [8]. Thus we note that the ingredients for the formation of electromagnetic radiation from photons (a Boson), and the formation of matter from the Higgs boson after the big bang, are intrinsic properties of the vacuum energy in pre big bang.

The series representations are

$$\frac{(6\pi\sqrt{2})(\sqrt{2}l^3)}{\frac{1}{3}\left(4\pi\left(\frac{l}{2}\right)^3\right)^3} = 12\sqrt{z_0}^{-2} \left(\sum_{k=0}^{\infty} \frac{(-1)^k \left(-\frac{1}{2}\right)_k (2-z_0)^k z_0^{-k}}{k!} \right)^2 \tag{239}$$

for (not $(z_0 \in \mathbb{R}$ and $-\infty < z_0 \leq 0)$),

$$\begin{aligned} & \frac{(6\pi\sqrt{2})(\sqrt{2}l^3)}{\frac{1}{3}\left(4\pi\left(\frac{l}{2}\right)^3\right)^3} \\ &= 12 \exp^2 \left(i\pi \left[\frac{\arg(2-x)}{2\pi} \right] \right) \sqrt{x}^{-2} \left(\sum_{k=0}^{\infty} \frac{(-1)^k (2-x)^k x^{-k} \left(-\frac{1}{2}\right)_k}{k!} \right)^2 \end{aligned} \tag{240}$$

for $(x \in \mathbb{R}$ and $x < 0)$,

$$\begin{aligned} & \frac{(6\pi\sqrt{2})(\sqrt{2}l^3)}{\frac{1}{3}\left(4\pi\left(\frac{l}{2}\right)^3\right)^3} \\ &= 12 \left(\frac{1}{z_0} \right)^{\lceil \arg(2-z_0)/(2\pi) \rceil} z_0^{1+\lceil \arg(2-z_0)/(2\pi) \rceil} \left(\sum_{k=0}^{\infty} \frac{(-1)^k \left(-\frac{1}{2}\right)_k (2-z_0)^k z_0^{-k}}{k!} \right)^2 \end{aligned} \tag{241}$$

By the input

$$\left(2\pi\sqrt{2} \times \frac{\frac{1}{3}\sqrt{2}l^3}{\frac{4}{3}\pi\left(\frac{l}{2}\right)^3} \right)^4 = 4096. \tag{242}$$

The number $4096 = 64^2$, is the Ramanujan Recurring Number, that when multiplied by 2 give 8192. The total amplitude vanishes for gauge group SO (8192) for bosonic string SO (8192), while the vacuum energy is negative and independent of the gauge group. The vacuum energy and dilaton tadpole to lowest non-trivial order for the open bosonic string. While the vacuum energy is non-zero and independent of the gauge group, the dilaton tadpole is zero for a unique choice of gauge group, SO (2^{13}) *i.e.* SO (8192), [9]. This could be the implications for a pre-big bang scenario where only self-perturbative bosonic strings lived when the enthalpy was extremely low as discussed above. This regime contains all the intrinsic properties of superstrings inherent in the bosonic strings that as observed by [10], (2006), would at the big bang give effect to the properties of matter (fermions) as Higgs Boson. This number theoretic connection to the gauge group SO (8192), gives a much more compelling relevance of the bosonic string theory SO (8192), to quantum gravity and places this string theory where it should appropriately be in the evolution of the universe from a quantum gravity perspective rather than it be neglected because it doesn't include fermionic strings to confirm to post big-bang reality. The vanishing of the bosonic string's amplitude could be explained by the effect of extreme low entropy on the quantum vacuum geometry as discussed in [4]. Thus, as the entropy increases infinitesimally as a result of the vacuum self-perturbation then also is the amplitude of the vibrating bosonic strings from zero. [9] was right to indicate that the "vanishing of the amplitude of the bosonic string could be the results of string theory itself", but here, we give a much more elaborate explanation of what could be happening.

We further proceed and make the input

$$27 \sqrt[4]{\left(2\pi\sqrt{2} \times \frac{\frac{1}{3}\sqrt{2}l^3}{\frac{4}{3}\pi\left(\frac{l}{2}\right)^3} \right)^4} + 1 = 1729 \quad (243)$$

This result is very near to the mass of candidate glueball $f_0(1710)$ scalar meson. Furthermore, 1728 occurs in the algebraic formula for the j-invariant of an elliptic curve $1728 = 8^2 \times 3^3$. The number 1728 is one less than the Hardy-Ramanujan number 1729 (taxicab number, as it can be expressed as the sum of two cubes in two different ways $10^3 + 9^3 = 12^3 + 1^3 = 1729$ and Ramanujan's recurring number). Since bosons are made of gauge bosons and scalar bosons (meson), then this number theoretic analysis perhaps confirm that the number 1729, confirm the fact that both the gauge and scalar bosons are actually different states of a single bosonic string, and that these states are isomorphic or that the states vibrations are synchronised with the state of the bosonic string. This also implies that each state lives inside a cubic or octahedron as a spherical cloud, and that the total sum of these two states is the state of the bosonic string. Taking the cross section of the bosonic string, we realise that it must be a rectangular, or a two shaped octahedron. As the string vibrates in difference

frequencies, so is the two spherical cloud states inside the string. That is, the string vibrations simply excites the gauge bosons *i.e.* Photon, gluon, W and Z inside one cube/octahedron, and the scalar boson *i.e.* Higgs inside the other cube/octahedron.

Furthermore, if we bring the picture of loop quantum gravity (LQG) with the property of a discontinuous quantum geometry, we can therefore, think of the graviton living on the vertices of the rectangles or the octahedrons. This graviton then acts a glue binding the bosonic strings lattice together forming a complete cross section of alternating states of between the gauge bosons and scalar bosons. This arrangement of states then gives a precise supersymmetric quantum picture of the vacuum geometry at low entropy.

But the geometry further reveal very important fact, that since the vacuum geometry is discontinues, then we observe that there is no relation whatsoever between the quantum vibrational frequencies of the strings, and that of the vertices of the vacuum geometry where the graviton lives. Ashtekar *et al.*, (2021) asserted that gravity is simply a manifestation of spacetime geometry. Thus, the graviton cannot be a string boson, however, there is a duality between gravity and strings [11]. Also, gauge bosons have spin-1, while the graviton has spin-2. Then lastly, because of the thermodynamic constraints we were able to arrive at the results we have, now this bring us to this fundamental question; that string theory and LQG theory are two intrinsic aspects of a complete quantum gravity theory we are after? That is, without the other no complete and compelling quantum geometry can be attained, as it is done here? This needs to be investigated further.

The series representations of Equation (243) are

$$27 \sqrt[4]{\left(\frac{(2\pi\sqrt{2})(\sqrt{2}l^3)}{\frac{1}{3}\left(4\pi\left(\frac{l}{2}\right)^3\right)3}\right)^4} + 1 = 1 + 27\sqrt{-1 + 256\sqrt{2}^8} \sum_{k=0}^{\infty} \left(\frac{1}{2}\right)_k \left(-1 + 256\sqrt{2}^8\right)^k, \quad (244)$$

$$27 \sqrt[4]{\left(\frac{(2\pi\sqrt{2})(\sqrt{2}l^3)}{\frac{1}{3}\left(4\pi\left(\frac{l}{2}\right)^3\right)3}\right)^4} + 1 = 1 + 27\sqrt{-1 + 256\sqrt{2}^8} \sum_{k=0}^{\infty} \frac{(-1)^k \left(-\frac{1}{2}\right)_k \left(-1 + 256\sqrt{2}^8\right)^{-k}}{k!}, \quad (245)$$

$$27 \sqrt[4]{\left(\frac{(2\pi\sqrt{2})(\sqrt{2}l^3)}{\frac{1}{3}\left(4\pi\left(\frac{l}{2}\right)^3\right)3}\right)^4} + 1 = 1 + 27\sqrt{z_0} \sum_{k=0}^{\infty} \frac{(-1)^k \left(-\frac{1}{2}\right)_k \left(256\sqrt{2}^8 - z_0\right)^k z_0^{-k}}{k!}. \quad (246)$$

$$\frac{\left(\frac{2(\sqrt{2}l^3)\pi\sqrt{2}}{\frac{3}{3}\left(4\pi\left(\frac{l}{2}\right)^3\right)}\right)^4 + \left(27\sqrt{\left(\frac{2(\sqrt{2}l^3)\pi\sqrt{2}}{\frac{3}{3}\left(4\pi\left(\frac{l}{2}\right)^3\right)} + 1\right)^4}\right)}{144 \times 25}$$

$$= \frac{1}{3600} \left[1 + 256 \left(\frac{1}{z_0}\right)^{4\lfloor \arg(2-z_0)/(2\pi) \rfloor} z_0^{4+4\lfloor \arg(2-z_0)/(2\pi) \rfloor} \sum_{k=0}^{\infty} \frac{(-1)^k \left(-\frac{1}{2}\right)_k (2-z_0)^k z_0^{-k}}{k!} \right] \quad (251)$$

$$+ 27 \left(\frac{1}{z_0}\right)^{1/2\lfloor \arg(256\sqrt{2}^8 - z_0)/(2\pi) \rfloor} z_0^{1/2+1/2\lfloor \arg(256\sqrt{2}^8 - z_0)/(2\pi) \rfloor} \sum_{k=0}^{\infty} \frac{(-1)^k \left(-\frac{1}{2}\right)_k (256\sqrt{2}^8 - z_0)^k z_0^{-k}}{k!} \right]$$

From inputting the transcendental number Equation (233), we obtain:

$$\sqrt{6 \left(\frac{1}{3} \left(\frac{2}{\frac{2\sqrt{2}}{\pi}} \right)^2 \right)}, \quad (252)$$

with the decimal approximation

$$3.1415926535897932384626433832795028841971693993751058209749445923\dots = \pi \quad (253)$$

(which is a transcendental number).

All 2nd roots of π^2 are $\pi e^0 \approx 3.1416$ (real, principal root), $\pi e^{i\pi} \approx -3.1416$ (real root). Thus the series representations of Equation (252) are

$$\sqrt{\frac{6}{3} \left(\frac{2}{\frac{2\sqrt{2}}{\pi}} \right)^2} = 4 \sum_{k=0}^{\infty} \frac{(-1)^k}{1+2k}, \quad (254)$$

$$\sqrt{\frac{6}{3} \left(\frac{2}{\frac{2\sqrt{2}}{\pi}} \right)^2} = \sum_{k=0}^{\infty} \frac{4(-1)^k 1195^{-1-2k} (5^{1+2k} - 4 \times 239^{1+2k})}{1+2k}, \quad (255)$$

$$\sqrt{\frac{6}{3} \left(\frac{2}{\frac{2\sqrt{2}}{\pi}} \right)^2} = \sum_{k=0}^{\infty} \left(-\frac{1}{4}\right)^k \left(\frac{1}{1+2k} + \frac{2}{1+4k} + \frac{1}{3+4k} \right). \quad (256)$$

The integral representations are

$$\sqrt{\frac{6}{3} \left(\frac{2}{\frac{2\sqrt{2}}{\pi}} \right)^2} = 4 \int_0^1 \sqrt{1-t^2} dt, \quad (257)$$

$$\sqrt{\frac{6}{3} \left(\frac{2}{2\sqrt{2}} \right)^2} = 2 \int_0^1 \frac{1}{\sqrt{1-t^2}} dt \tag{258}$$

$$\sqrt{\frac{6}{3} \left(\frac{2}{2\sqrt{2}} \right)^2} = 2 \int_0^\infty \frac{1}{1+t^2} dt \tag{259}$$

It is plausible to hypothesize that π and φ , in addition to being important mathematical constants, are constants that also have a fundamental relevance in the various sectors of Theoretical Physics and Cosmology

From $\frac{\pi^2}{6}$, we obtain:

$$\sqrt{\frac{1}{\frac{\pi^2}{6}} \times \frac{4}{3}} \tag{260}$$

With the decimal approximation

$$0.90031631615710606955519919100674058266457414995522062557714374713 = \frac{2\sqrt{2}}{\pi}$$

(which is the DN Constant, and a transcendental number).

All 2nd roots of $\frac{8}{\pi^2}$ are $\frac{2\sqrt{2}e^0}{\pi} \approx 0.9003$ (real, principal root), and

$\frac{2\sqrt{2}e^{i\pi}}{\pi} \approx 0.003$ (real root). The series representations of Equation (260) are

$$\sqrt{\frac{4}{3\pi^2}} = \sum_{k=0}^\infty \frac{(-1)^k \left(-1 + \frac{8}{\pi^2}\right)^k \left(-\frac{1}{2}\right)_k}{k!} \tag{261}$$

$$\sqrt{\frac{4}{3\pi^2}} = \sqrt{z_0} \sum_{k=0}^\infty \frac{(-1)^k \left(-\frac{1}{2}\right)_k \left(\frac{8}{\pi^2} - z_0\right)^k z_0^{-k}}{k!} \tag{262}$$

for (not ($z_0 \in \mathbb{R}$ and $-\infty < z_0 \leq 0$)),

$$\sqrt{\frac{4}{3\pi^2}} = \exp\left(i\pi \left[\frac{\arg\left(\frac{8}{\pi^2} - x\right)}{2\pi} \right]\right) \sqrt{x} \sum_{k=0}^\infty \frac{(-1)^k \left(\frac{8}{\pi^2} - x\right)^k x^{-k} \left(-\frac{1}{2}\right)_k}{k!} \tag{263}$$

for ($x \in \mathbb{R}$ and $x < 0$)

Section B: Number connections to the Planck multipole spectrum frequency and to the hypothetical Gluino mass

We note that, from the number 8, we obtain as follows:

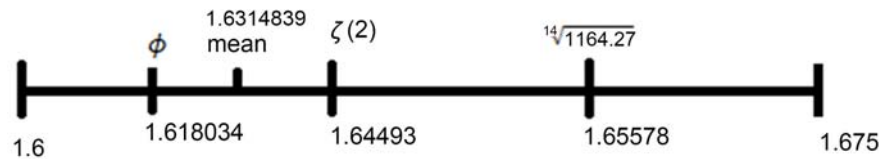


Figure 16. “Golden” Range number scale.

$$8^2 = 64, \quad 8^2 \times 2 \times 8 = 1024, \quad 8^4 = 8^2 \times 2^2, \quad (\text{True})$$

$$8^4 = 4096, \quad 8^2 \times 2^6 = 4096, \quad 2^{13} = 2 \times 8^4, \quad (\text{True})$$

$$2^{13} = 8192, \quad 2 \times 8^4 = 8192$$

From **Figure 16**, we notice how from the numbers 8 and 2 we get 64, 1024, 4096 and 8192, and that 8 is the fundamental number. In fact $8^2 = 64$, $8^3 = 512$, $8^4 = 4096$. We define it “fundamental number”, since 8 is a Fibonacci number, which by rule, divided by the previous one, which is 5, gives 1.6, a value that tends to the golden ratio, as for all numbers in the Fibonacci sequence

Finally we note how $8^2 = 64$, multiplied by 27, to which we add 1, is equal to 1729, the so-called “Hardy-Ramanujan number”. Then taking the 15th root of 1729, we obtain a value close to $\zeta(2)$ that 1.6438..., which, in turn, is included in the range of what we call “golden numbers”

Furthermore for all the results very near to 1728 or 1729, adding $64 = 8^2$, one obtains values about equal to 1792 or 1793. These are values almost equal to the Planck multiple spectrum frequency (Black Body Radiation) 1792.35 and to the hypothetical Gluino mass.

Acknowledgements

We would like to thank Professor **Augusto Sagnotti** theoretical physicist at Scuola Normale Superiore (Pisa-Italy) for his very useful explanations and his availability

Conflicts of Interest

The authors declare no conflicts of interest regarding the publication of this paper.

References

- [1] Rovelli, C. (1998) *Living Reviews in Relativity*, **1**, Article No. 1. <https://doi.org/10.12942/lrr-1998-1>
- [2] Becker, K., Becker, M. and Schwarz, J.H. (2006) *String Theory and M-Theory: A Modern Introduction*. Cambridge University Press, Cambridge. <https://doi.org/10.1017/CBO9780511816086>
- [3] Kubeka, A.S. and Amani A. (2022) *International Journal of Modern Physics A*, **37**, Article ID: 2250039. <https://doi.org/10.1142/S0217751X22500397>
- [4] Kubeka, A.S., Amani, A. and Lekala, M. (2023) *Journal of Modern Physics*, **14**, 1587-1599. <https://doi.org/10.4236/jmp.2023.1412092>
- [5] Ashtekar A. and Bianchi, E. (2021) *Reports on Progress in Physics*, **84**, Article ID:

042001. <https://doi.org/10.1088/1361-6633/abed91>
- [6] Redlich K. and Zalewski K. (2016) *Acta Physica Polonica B*, **47**, No. 7. <https://doi.org/10.5506/APhysPolB.47.1943>
- [7] Muller, H. (2019) *Progress in Physics*, **15**, 148-155.
- [8] Goulette, M. (2012) *What Should We Know about the Higgs Particle?* (blog). Atlas Experiment/CERN. <https://atlas.cern/updates/blog/what-should-we-know-about-higgs-particle>
- [9] Michael, R.D. and Grinstein B. (1986) *Physics Letters B*, **183**, 52-58. [https://doi.org/10.1016/0370-2693\(87\)91416-X](https://doi.org/10.1016/0370-2693(87)91416-X)
- [10] Trevors J.T. (2006) *Theory in Biosciences*, **124**, 403-412. <https://doi.org/10.1016/j.thbio.2005.04.002>
- [11] Ortin, T. (2015) *Gravity and Strings*. Cambridge University Press, Cambridge.

Correspondence Principle for Empirical Equations in Terms of the Cosmic Microwave Background Temperature with Solid-State Ionics

Tomofumi Miyashita

Miyashita Clinic, Osaka, Japan

Email: tom_miya@ballade.plala.or.jp

How to cite this paper: Miyashita, T. (2024) Correspondence Principle for Empirical Equations in Terms of the Cosmic Microwave Background Temperature with Solid-State Ionics. *Journal of Modern Physics*, 15, 51-63.

<https://doi.org/10.4236/jmp.2024.151002>

Received: December 4, 2023

Accepted: January 15, 2024

Published: January 18, 2024

Copyright © 2024 by author(s) and Scientific Research Publishing Inc.

This work is licensed under the Creative Commons Attribution International License (CC BY 4.0).

<http://creativecommons.org/licenses/by/4.0/>



Open Access

Abstract

Previously, we presented several empirical equations using the cosmic microwave background (CMB) temperature that were mathematically connected. Next, we proposed an empirical equation for the fine-structure constant. Considering the compatibility among these empirical equations, the CMB temperature (T_c) and gravitational constant (G) were calculated to be 2.726312 K and $6.673778 \times 10^{-11} \text{ m}^3 \cdot \text{kg}^{-1} \cdot \text{s}^{-2}$, respectively. Every equation can be explained in terms of the Compton length of an electron (λ_e), the Compton length of a proton (λ_p) and α . However, these equations are difficult to follow. Using the correspondence principle with the thermodynamic principles in solid-state ionics, we propose a canonical ensemble to explain these equations in this report. For this purpose, we show that every equation can be explained in terms of Avogadro's number and the number of electrons in 1 C.

Keywords

Temperature of the Cosmic Microwave Background

1. Introduction

The symbol list is shown in Section 2. We discovered Equations (1), (2) and (3) [1] [2] [3] expressed in terms of the cosmic microwave background (CMB) temperature. We then attempted to reduce their errors by modifying the values of 4.5 and π [4] [5].

$$\frac{Gm_p^2}{hc} = \frac{4.5}{2} \times \frac{kT_c}{1\text{kg} \times c^2} \quad (1)$$

$$\frac{Gm_p^2}{\left(\frac{e^2}{4\pi\epsilon_0}\right)} = \frac{4.5}{2\pi} \times \frac{m_e}{e} \times hc \quad (2)$$

$$\frac{m_e c^2}{e} \times \left(\frac{e^2}{4\pi\epsilon_0}\right) = \pi \times kT_c \quad (3)$$

Next, we discovered an empirical equation for the fine-structure constant [6].

$$137.0359991 = 136.0113077 + \frac{1}{3 \times 13.5} + 1 \quad (4)$$

$$13.5 \times 136.0113077 = 1836.152654 = \frac{m_p}{m_e} \quad (5)$$

Equations (4) and (5) may be related to the transference number [7] [8]. Next, we proposed the following values as deviations of the values of 9/2 and π [8] [9].

$$3.13201(\text{V} \cdot \text{m}) = \frac{\left(\frac{m_p}{m_e} + \frac{4}{3}\right) m_e c^2}{ec} \quad (6)$$

$$4.48852\left(\frac{1}{\text{A} \cdot \text{m}}\right) = \frac{q_m c}{\left(\frac{m_p}{m_e} + \frac{4}{3}\right) m_p c^2} \quad (7)$$

Then, $\left(\frac{m_p}{m_e} + \frac{4}{3}\right)$ has units of $\left(\frac{\text{m}^2}{\text{s}}\right)$. Using the redefinition of Avogadro's number and the Faraday constant, these values can be adjusted back to 9/2 and π [9].

$$\pi(\text{V} \cdot \text{m}) = \frac{\left(\frac{m_p}{m_e} + \frac{4}{3}\right) m_{e_new} c^2}{e_{new} c} \quad (8)$$

$$4.5\left(\frac{1}{\text{A} \cdot \text{m}}\right) = \frac{q_{m_new} c}{\left(\frac{m_p}{m_e} + \frac{4}{3}\right) m_{p_new} c^2} \quad (9)$$

Furthermore, every equation can be explained in terms of the Compton length of an electron (λ_e), the Compton length of a proton (λ_p) and α [10]. However, these equations are difficult to follow. Our purpose in this report is to consider the physical meanings. Using the correspondence principle with the thermodynamic principles in solid-state ionics, we propose a canonical ensemble to explain these equations. For this purpose, we show that every equation can be explained in terms of Avogadro's number and the number of electrons in 1 C. The remainder of this paper is organized as follows. In Section 2, we present the list of symbols used in our derivations. In Section 3, we discuss the purpose of this report. Using the correspondence principle with the thermodynamic principles in solid-state ionics, we try to show the canonical ensemble to explain these equations. In Section 4, we propose several equations that are functions of Avoga-

dro's number and the number of electrons in 1 C. In Section 5, using these equations, we explain our main equations. The remaining problems are discussed. In Section 6, our conclusions are described.

2. Symbol List

2.1. MKSA Units (These Values Were Obtained from Wikipedia)

G : gravitational constant: 6.6743×10^{-11} ($\text{m}^3 \cdot \text{kg}^{-1} \cdot \text{s}^{-2}$)

(we use the compensated value 6.673778×10^{-11} in this report)

T_c : CMB temperature: 2.72548 (K)

(we use the compensated value 2.726312 K in this report)

k : Boltzmann constant: 1.380649×10^{-23} ($\text{J} \cdot \text{K}^{-1}$)

c : speed of light: 299792458 (m/s)

h : Planck constant: $6.62607015 \times 10^{-34}$ (J s)

ϵ_0 : electric constant: $8.8541878128 \times 10^{-12}$ ($\text{N} \cdot \text{m}^2 \cdot \text{C}^{-2}$)

μ_0 : magnetic constant: $1.25663706212 \times 10^{-6}$ ($\text{N} \cdot \text{A}^{-2}$)

e : electric charge of one electron: $-1.602176634 \times 10^{-19}$ (C)

q_m : magnetic charge of one magnetic monopole: $4.13566770 \times 10^{-15}$ (Wb)

(this value is only a theoretical value, $q_m = h/e$)

m_p : rest mass of a proton: $1.6726219059 \times 10^{-27}$ (kg)

(we use the compensated value $1.672621923 \times 10^{-27}$ kg in this report)

m_e : rest mass of an electron: $9.1093837 \times 10^{-31}$ (kg)

Rk : von Klitzing constant: 25812.80745 (Ω)

Z_0 : wave impedance in free space: 376.730313668 (Ω)

α : fine-structure constant: 1/137.035999081

λ_p : Compton wavelength of a proton: 1.32141×10^{-15} (m)

λ_e : Compton wavelength of an electron: $2.4263102367 \times 10^{-12}$ (m)

2.2. Symbol List after Redefinition

$$e_{new} = e \times \frac{4.48852}{4.5} = 1.59809\text{E} - 19(\text{C}) \quad (10)$$

$$q_{m_new} = q_m \times \frac{\pi}{3.13201} = 4.14832\text{E} - 15(\text{Wb}) \quad (11)$$

$$h_{new} = e_{new} \times q_{m_new} = h \times \frac{4.48852}{4.5} \times \frac{\pi}{3.13201} = 6.62938\text{E} - 34(\text{J} \cdot \text{s}) \quad (12)$$

$$Rk_{new} = \frac{q_{m_new}}{e_{new}} = Rk \times \frac{4.5}{4.48852} \times \frac{\pi}{3.13201} = 25958.0(\Omega) \quad (13)$$

We observe that Equation (13) can be rewritten as follows.

$$Rk_{new} = 4.5 \left(\frac{1}{\text{A} \cdot \text{m}} \right) \times \pi(\text{V} \cdot \text{m}) \times \frac{m_p}{m_e} = 25957.9966027(\Omega) \quad (14)$$

$$Z_{0_new} = \alpha \times \frac{2h_{new}}{e_{new}^2} = 2\alpha \times Rk_{new} = Z_0 \times \frac{4.5}{4.48852} \times \frac{\pi}{3.13201} = 378.849(\Omega) \quad (15)$$

We observe that Equation (15) can be rewritten as follows.

$$Z_{0_new} = 4.5 \left(\frac{1}{\text{A} \cdot \text{m}} \right) \times \pi (\text{V} \cdot \text{m}) \times 2\alpha \times \frac{m_p}{m_e} = 378.8493064 (\Omega) \quad (16)$$

$$\mu_{0_new} = \frac{Z_{0_new}}{c} = \mu_0 \times \frac{4.5}{4.48852} \times \frac{\pi}{3.13201} = 1.26371\text{E} - 06 (\text{N} \cdot \text{A}^{-2}) \quad (17)$$

$$\varepsilon_{0_new} = \frac{1}{Z_{0_new} \times c} = \varepsilon_0 \times \frac{4.48852}{4.5} \times \frac{3.13201}{\pi} = 8.80466\text{E} - 12 (\text{F} \cdot \text{m}^{-1}) \quad (18)$$

$$c_{_new} = \frac{1}{\sqrt{\varepsilon_{0_new} \mu_{0_new}}} = \frac{1}{\sqrt{\varepsilon_0 \mu_0}} = c = 299792458 (\text{m} \cdot \text{s}^{-1}) \quad (19)$$

The Compton wavelength (λ) is as follows.

$$\lambda = \frac{h}{mc} \quad (20)$$

This value (λ) should be unchanged since the unit for 1 m is unchanged. However, in Equation (12), the Planck constant is changed. Therefore, the units for the masses of one electron and one proton should be redefined.

$$m_{e_new} = \frac{4.48852}{4.5} \times \frac{\pi}{3.13201} \times m_e = 9.11394\text{E} - 31 (\text{kg}) \quad (21)$$

$$m_{p_new} = \frac{4.48852}{4.5} \times \frac{\pi}{3.13201} \times m_p = 1.67346\text{E} - 27 (\text{kg}) \quad (22)$$

From the dimensional analysis in the previous report [9],

$$kT_{c_new} = \frac{4.48852}{4.5} \times \frac{\pi}{3.13201} \times kT_c = 3.7659625\text{E} - 23 (\text{J}) \quad (23)$$

Next, to simplify the calculation, G_N is defined as follows.

$$G_N = G \times 1 \text{ kg} (\text{m}^3 \cdot \text{s}^{-2}) = 6.673778\text{E} - 11 (\text{m}^3 \cdot \text{s}^{-2}) \quad (24)$$

Now, we hope that the value of G_N remains unchanged. However, G_N should change [9].

$$G_{N_new} = G_N \times \frac{4.5}{4.48852} (\text{m}^3 \cdot \text{s}^{-2}) = 6.69084770\text{E} - 11 (\text{m}^3 \cdot \text{s}^{-2}) \quad (25)$$

2.3. Symbol List in Terms of the Compton Length of an Electron (λ_e), the Compton Length of a Proton (λ_p) and α

The following equations were proposed in a previous report [10].

$$\begin{aligned} & m_{e_new} c^2 \times \left(\frac{m_p}{m_e} + \frac{4}{3} \right)^2 \left(\frac{\text{J} \cdot \text{m}^4}{\text{s}^2} \right) \\ &= \frac{\pi}{4.5} \left(\text{V} \cdot \text{m} \cdot \text{A} \cdot \text{m} = \frac{\text{J} \cdot \text{m}^2}{\text{s}} \right) \times \lambda_p c \left(\frac{\text{m}^2}{\text{s}} \right) = 2.76564\text{E} - 07 \left(\frac{\text{J} \cdot \text{m}^4}{\text{s}^2} \right) = \text{constant} \end{aligned} \quad (26)$$

$$\begin{aligned} & e_{new} c \times \left(\frac{m_p}{m_e} + \frac{4}{3} \right) \left(\frac{\text{A} \cdot \text{m}^3}{\text{s}} \right) \\ &= \frac{1}{4.5} (\text{A} \cdot \text{m}) \times \lambda_p c \left(\frac{\text{m}^2}{\text{s}} \right) = 8.80330\text{E} - 08 \left(\frac{\text{A} \cdot \text{m}^3}{\text{s}} \right) = \text{constant} \end{aligned} \quad (27)$$

$$\begin{aligned}
 & m_{p_new} c^2 \times \left(\frac{m_p}{m_e} + \frac{4}{3} \right)^2 \left(\frac{\text{J} \cdot \text{m}^4}{\text{s}^2} \right) \\
 &= \frac{\pi}{4.5} \left(\frac{\text{J} \cdot \text{m}^2}{\text{s}} \right) \times \lambda_e c \left(\frac{\text{m}^2}{\text{s}} \right) = 5.07814\text{E} - 04 \left(\frac{\text{J} \cdot \text{m}^4}{\text{s}^2} \right) = \text{constant}
 \end{aligned} \tag{28}$$

$$\begin{aligned}
 & q_{m_new} c \times \left(\frac{m_p}{m_e} + \frac{4}{3} \right) \left(\frac{\text{V} \cdot \text{m}^3}{\text{s}} \right) \\
 &= \pi (\text{V} \cdot \text{m}) \times \lambda_e c \left(\frac{\text{m}^2}{\text{s}} \right) = 2.28516\text{E} - 03 \left(\frac{\text{V} \cdot \text{m}^3}{\text{s}} \right) = \text{constant}
 \end{aligned} \tag{29}$$

$$\begin{aligned}
 & kT_{c_new} \times \frac{2\pi}{\alpha} \times \left(\frac{m_p}{m_e} + \frac{4}{3} \right)^3 \left(\frac{\text{J} \cdot \text{m}^6}{\text{s}^3} \right) \\
 &= \frac{\pi}{4.5} \left(\frac{\text{J} \cdot \text{m}^2}{\text{s}} \right) \times \lambda_p c \times \lambda_e c = 2.011697\text{E} - 10 \left(\frac{\text{J} \cdot \text{m}^6}{\text{s}^3} \right) = \text{constant}
 \end{aligned} \tag{30}$$

$$\begin{aligned}
 & G_{N_new} \left(\frac{\text{m}^3}{\text{s}^2} \right) \times \left(\frac{m_p}{m_e} + \frac{4}{3} \right) \left(\frac{\text{m}^2}{\text{s}} \right) \\
 &= (\lambda_p c)^2 \left(\frac{\text{m}^4}{\text{s}^2} \right) \times c \left(\frac{\text{m}}{\text{s}} \right) \times \frac{9\alpha}{8\pi} = 1.22943\text{E} - 07 \left(\frac{\text{m}^5}{\text{s}^3} \right) = \text{constant}
 \end{aligned} \tag{31}$$

3. Purpose

The purpose of this report is to explain the empirical equations through the correspondence principle with thermodynamic principles in solid-state ionics.

3.1. Introduction to the Thermodynamic Principles in Solid-State Ionics

A solid oxide fuel cell (SOFC) directly converts the chemical energy of a fuel gas, such as hydrogen or methane, into electrical energy. A solid oxide film is used as the electrolyte, where the main carriers are oxygen ions and the minor carriers are electrons. When samarium-doped ceria (SDC) electrolytes are used in SOFCs, the open-circuit voltage ($OCV = 0.80 \text{ V}$ at 1073 K) becomes lower than the Nernst voltage ($V_{th} = 1.15 \text{ V}$ at 1073 K), which is obtained when using yttria-stabilized zirconia (YSZ) electrolytes. The canonical ensemble is shown in **Figure 1**.

Then, we noticed the following equations, which can be explained by Jarzynski's equality [11] [12].

$$OCV = V_{th} - (1 - t_{ion}) \times \frac{E_a}{2e} \tag{32}$$

where t_{ion} is the transference number of ions near the anode. E_a is the activation energy for ions. When SDC electrolytes are used, t_{ion} near the anode is 0. E_a is 0.7 eV. Thus,

$$OCV = 1.15 \text{ V} - \frac{0.7 \text{ eV}}{2e} = 0.80 \text{ V} \tag{33}$$

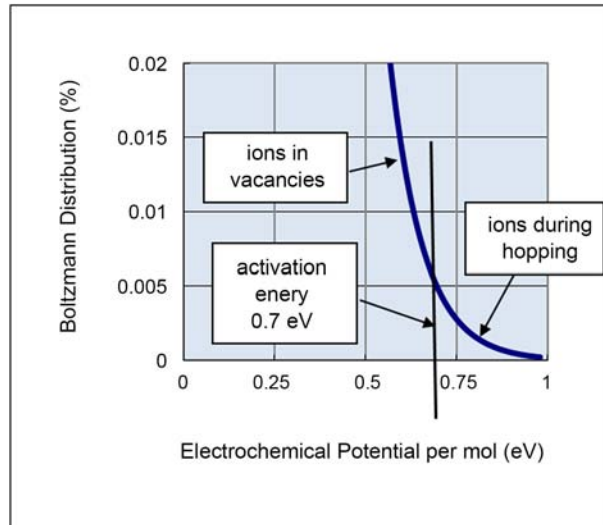


Figure 1. Canonical ensemble in SOFCs.

To explain Equation (32) by the electrochemical method, the following equations are proposed.

$$\eta_i = \mu_i + z_i F \varphi \tag{34}$$

$$\eta_{i_hopping} = \eta_{i_vacancies} \tag{35}$$

$$\mu_{i_hopping} = \mu_{i_vacancies} + N_A E_a \tag{36}$$

$$Z_i F \phi_{hopping} = Z_i F \phi_{vacancies} - N_A E_a \tag{37}$$

where η_i , μ_i , Z_i , F , φ and N_A are the electrochemical potential energy of ions, the chemical potential energy of ions, valence of species i , the Faraday constant, the electrical potential and Avogadro's number. $\eta_{i_hopping}$, $\eta_{i_vacancies}$, $\mu_{i_hopping}$, $\mu_{i_vacancies}$, $\phi_{hopping}$, and $\phi_{vacancies}$ are the electrochemical potential energy of hopping ions, electrochemical potential energy of ions in vacancies, chemical potential of hopping ions, chemical potential of ions in vacancies, electrical potential of hopping ions, and electrical potential of ions in vacancies, respectively.

From Equation (37),

$$\phi_{hopping} = \phi_{vacancies} + \frac{E_a}{2e} \tag{38}$$

This electrical potential is neutralized by free electrons and dissipated. Therefore, the energy loss due to dissipation ($E_{loss_dissipation}$) is

$$E_{loss_dissipation} = (1 - t_{ion}) \times E_a \tag{39}$$

3.2. Correspondence Principle with the Thermodynamic Principles in Solid-State Ionics

The fine structure constant is the interaction coefficient. Thus,

$$\alpha = 1 - t_{ion} \tag{40}$$

We thought that kT_c is related to the energy loss due to dissipation. From Equations (39) and (40),

$$E_{a_space} = \frac{E_{loss_dissipation}}{1 - t_{ion}} = \frac{kT_c}{\alpha} = 0.03219 \text{ (eV)} \quad (41)$$

where E_{a_space} is the activation energy of the space. The canonical ensemble from the correspondence principle is shown in **Figure 2**. From Equations (36) and (41),

$$\frac{\mu_{i_vacancies}}{N_A} = \frac{\mu_{i_hopping}}{N_A} - \frac{kT_{c_new}}{\alpha} > 0 \quad (42)$$

Therefore, the minimum mass (M_{min}), which may be related to our main Equation (2), is

$$M_{min} = \frac{E_{space}}{c^2} = \frac{kT_c}{\alpha \times c^2} = 5.739210E - 38 \text{ (kg)} \quad (43)$$

3.3. Our Image for the Proposed Canonical Ensemble from the Correspondence Principle

From the correspondence principle, there should be inevitable dissipations from the wave situation to the particle situations. In the area of solid-state ionics, the dissipations recover immediately after ion hopping.

Gravity is not directly related to the dissipation energy and is related to the activation energy (kT/α). In the area of solid-state ionics, the activation energy becomes small when the vacancies increase. From the correspondence principle, a large mass has a smaller activation energy due to the increase in the number of vacancies. Then, one large mass has a smaller dissipation energy than the sum of dissipation energies from the two separated masses.

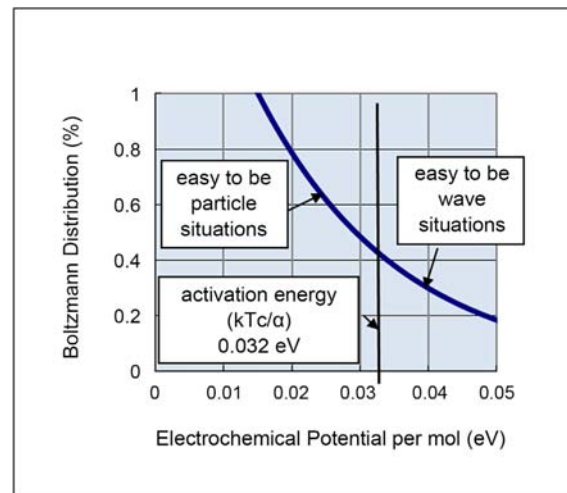


Figure 2. Canonical ensemble from the correspondence principle.

4. Methods

4.1. Introduction to Avogadro's Number and the Number of Electrons in 1 C

Avogadro's number is $6.02214076 \times 10^{23}$. This value is related to the following

value.

$$N_A = \frac{1g}{m_p} = 5.978637E + 23 \quad (44)$$

Using the redefined values, the new definition of Avogadro's number is

$$N_{A_new} = \frac{1kg_{new}}{m_{p_new}} = 5.975649E + 26 \quad (45)$$

From Equations (44) and (45),

$$N_{A_new} = N_A \times \frac{4.5}{4.488520} \times \frac{3.132011}{\pi} \times 1000 \quad (46)$$

The number of electrons in 1 C (N_e) is

$$N_e = \frac{1C}{e} = 6.241509E + 18 \quad (47)$$

Using the redefined values,

$$N_{e_new} = \frac{1C_{new}}{e_{new}} = 6.257473E + 18 \quad (48)$$

From Equations (47) and (48),

$$N_{e_new} = N_e \times \frac{4.5}{4.488520} \quad (49)$$

4.2. List of Important Equations

We propose the following 7 equations using N_{A_new} (5.975649.E+26), N_{e_new} (6.257473E+18), c and α .

$$m_{p_new} = \frac{1}{N_{A_new}} \quad (50)$$

$$m_{e_new} = \frac{m_e/m_p}{N_{A_new}} \quad (51)$$

Here, m_p/m_e (=1836.1526) is not changed after redefinition.

$$e_{new} = \frac{1}{N_{e_new}} \quad (52)$$

$$q_{m_new} = \frac{4.5\pi \times m_p/m_e}{N_{e_new}} = 4.148319E - 15 \quad (53)$$

$$h_{new} = \frac{4.5\pi \times m_p/m_e}{(N_{e_new})^2} = 6.62938382E - 34 \quad (54)$$

$$kT_{c_new} = \frac{4.5 \times c^3 \times \alpha}{2\pi \times N_{e_new} \times N_{A_new}} = 3.7659625E - 23 \quad (55)$$

$$G_{N_new} = \frac{4.5^3 \times m_p/m_e \times N_{A_new} \times c^2 \times \alpha}{4 \times N_{e_new}^3} = 6.6908477E - 11 \quad (56)$$

5. Results

From this section onward, the values used are those obtained after redefinition. Strictly speaking, m_e should therefore be written as m_{e_new} . However, we omit the subscript “new” to avoid unnecessarily notational complexity.

5.1. Explanation of Our First Equation

For convenience, Equation (1) is rewritten as follows.

$$\frac{Gm_p^2}{hc} = \frac{4.5}{2} \times \frac{kT_c}{1\text{kg} \times c^2} \quad (57)$$

So,

$$\frac{G_N m_p^2}{hc} = \frac{4.5}{2} \times \frac{kT_c}{c^2} \quad (58)$$

The left side in Equation (58) is rewritten as

$$\frac{G_N m_p^2}{hc} = \frac{4.5^3 \times m_p/m_e \times 5.975649\text{E} + 26 \times (299792458)^2 \times \alpha}{4 \times (6.257473\text{E} + 18)^3 \times (5.975649\text{E} + 26)^2} \quad (59)$$

$$\frac{4.5\pi \times m_p/m_e}{(6.257473\text{E} + 18)^2} \times 299792458$$

Therefore,

$$\frac{G_N m_p^2}{hc} = \frac{4.5^2 \times 299792458 \times \alpha}{4\pi \times 6.257473\text{E} + 18 \times 5.975649\text{E} + 26} \quad (60)$$

The right side in Equation (58) is

$$\frac{4.5}{2} \times \frac{kT_c}{c^2} = \frac{4.5}{2} \times \frac{4.5 \times (299792458)^3 \times \alpha}{2\pi \times 6.257473\text{E} + 18 \times 5.975649\text{E} + 26 \times (299792458)^2} \quad (61)$$

Therefore,

$$\frac{Gm_p^2}{hc} = \frac{4.5}{2} \times \frac{kT_c}{1\text{kg} \times c^2} \quad (62)$$

5.2. Explanation of Our Second Equation

For convenience, Equation (2) is rewritten as follows.

$$\frac{Gm_p^2}{\left(\frac{e^2}{4\pi\epsilon_0}\right)} = \frac{4.5}{2\pi} \times \frac{m_e}{e} \times hc \quad (63)$$

Therefore,

$$\frac{G_N m_p^2}{hc} = \frac{4.5}{2\pi} \times \frac{m_e}{e} \times \left(\frac{e^2}{4\pi\epsilon_0}\right) \quad (64)$$

According to Equation (60), the left side in Equation (63) is

$$\frac{G_N m_p^2}{hc} = \frac{4.5^2 \times 299792458 \times \alpha}{4\pi \times 6.257473\text{E} + 18 \times 5.975649\text{E} + 26} \quad (65)$$

Regarding the right side in Equation (63),

$$\frac{4.5}{2\pi} \times \frac{m_e}{e} \times \left(\frac{e^2}{4\pi\epsilon_0} \right) = \frac{4.5}{2\pi} \times m_e \times \frac{ec}{4\pi\epsilon_0 c} = \frac{4.5}{2\pi} \times m_e \times \frac{ec}{4\pi} \times Z_0 \quad (66)$$

For convenience, Equation (16) is rewritten as follows.

$$Z_0 = 9\pi \times \alpha \times \frac{m_p}{m_e} \quad (67)$$

Therefore,

$$\frac{4.5}{2\pi} \times \frac{m_e}{e} \times \left(\frac{e^2}{4\pi\epsilon_0} \right) = \frac{4.5}{2\pi} \times m_e \times \frac{ec}{4\pi} \times 9\pi \times \alpha \times \frac{m_p}{m_e} = \frac{4.5}{8\pi} \times 9m_p \times ec \times \alpha \quad (68)$$

Hence,

$$\frac{4.5}{8\pi} \times 9\alpha \times ec \times m_p = \frac{4.5^2}{4\pi} \times \alpha \times \frac{299792458}{6.257473E+18 \times 5.975649E+26} \quad (69)$$

From Equations (65) and (69), we obtain

$$\frac{G_N m_p^2}{hc} = \frac{4.5}{2\pi} \times \frac{m_e}{e} \times \left(\frac{e^2}{4\pi\epsilon_0} \right) \quad (70)$$

Therefore,

$$\frac{G m_p^2}{\left(\frac{e^2}{4\pi\epsilon_0} \right)} = \frac{4.5}{2\pi} \times \frac{m_e}{e} \times hc \quad (71)$$

5.3. Explanation of Our Third Equation

For convenience, Equation (3) is rewritten as follows.

$$\frac{m_e c^2}{e} \times \left(\frac{e^2}{4\pi\epsilon_0} \right) = \pi \times kT_c \quad (72)$$

The left side in Equation (72) is

$$m_e c^2 \times \frac{e}{4\pi\epsilon_0} = m_e c^2 \times \frac{ec}{4\pi\epsilon_0 c} = m_e c^2 \times \frac{ec}{4\pi} \times Z_0 \quad (73)$$

Therefore, using Equation (16), we obtain

$$m_e c^2 \times \frac{ec}{4\pi} \times Z_0 = m_e c^2 \times \frac{ec}{4\pi} \times 9\pi \times \alpha \times \frac{m_p}{m_e} = m_p c^2 \times ec \times \frac{9}{4} \alpha \quad (74)$$

Therefore,

$$m_p c^2 \times ec \times \frac{9}{4} \alpha = \frac{9}{4} \alpha \times \frac{(299792458)^3}{5.975649E+26 \times 6.257473E+18} \quad (75)$$

The right side in Equation (72) is

$$\pi \times kT_c = \frac{4.5 \times (299792458)^3 \times \alpha}{2 \times 6.257473E+18 \times 5.975649E+26} \quad (76)$$

From Equations (75) and (76), we obtain the following equation.

$$m_e c^2 \times \frac{e}{4\pi\epsilon_0} = \pi \times kT_c \quad (77)$$

5.4. Compatibility between Two Lists

The compatibility between the list shown in Section 2.3 and the list shown in Section 4.2 is explained in this section. The Faraday constant is

$$\begin{aligned} 1F_{new} &= e_{new} \times N_{A_new} \left(\frac{C}{mol} \right) = \frac{5.97564907E+26}{6.25747328E+18} \left(\frac{C}{mol} \right) \\ &= 9.5496198E+07 \left(\frac{C}{mol} \right) \end{aligned} \quad (78)$$

This value is rewritten as follows:

$$9.5496198E+07 = \frac{c}{\pi} \times \left(\frac{m_p}{m_e} + \frac{4}{3} \right) \times \frac{m_e}{m_p} = \frac{299792458 \times 1837.485988}{\pi \times 1836.152654} \quad (79)$$

Next,

$$\frac{\pi e c}{m_e c^2} = \frac{\pi \times 5.97564907E+26 + 26 \times 1836.152654}{6.25747328E+18 \times 299792458} = 1837.485988 = \left(\frac{m_p}{m_e} + \frac{4}{3} \right) \quad (80)$$

$$\frac{q_m c}{4.5 m_p c^2} = \frac{Rk \times 5.97564907E+26}{4.5 \times 6.25747328E+18 \times 299792458} = 1837.485988 = \left(\frac{m_p}{m_e} + \frac{4}{3} \right) \quad (81)$$

Consequently, Equation (82) is related to the Faraday constant.

$$\left(\frac{m_p}{m_e} + \frac{4}{3} \right) = \frac{q_m c}{4.5 m_p c^2} = \frac{\pi e c}{m_e c^2} \quad (82)$$

5.5. The Problem of the Number of Real Microstates

The canonical ensemble is related with Boltzmann's entropy formula as follows.

$$S = k \ln W$$

where S and W are the entropy and the number of real microstates, respectively. The main problem is that we cannot calculate W . Strictly speaking, we need years to do it. However, the hints are shown in this section.

5.5.1. More Suitable Expression for G and kT_c

Equations (30) and (55) for kT_c are very complex. Equations (31) and (56) for G are very complex, too. We discovered a more suitable expression. For kT_c , there are the following two equations.

$$kT_c = \frac{\alpha}{2\pi} \times \frac{1}{\pi} \left(\frac{1}{V \cdot m} \right) \times q_m c \times m_e c^2 = 3.76596254E-23 \quad (83)$$

$$kT_c = \frac{\alpha}{2\pi} \times 4.5 \left(\frac{1}{A \cdot m} \right) \times e c \times m_p c^2 = 3.76596254E-23 \quad (84)$$

In Equations (83) and (84), 2π is dimensionless. For G , there are the following two equations.

$$G_N = \frac{\alpha c}{4\pi} \times (4.5 \times e c)^2 \times \frac{q_m c}{m_p c^2} = 6.69084770E-11 \quad (85)$$

$$G_N = \frac{\alpha c}{4\pi} \times (4.5 \times ec)^3 \times \frac{\pi}{m_e c^2} = 6.69084770E - 11 \quad (86)$$

In Equations (85) and (86), 4π is dimensionless. In a previous report [10], there seemed to be two definitions for 1 kg. However, the definition of 1 kg is only one. The definition of G_N should be more complex.

5.5.2. Schwarzschild Radius of Electrons

We calculated the Schwarzschild radius of electrons (r_g) using redefined values.

$$r_g \text{ (m)} = \frac{2G_N \times m_e}{1kg \times c^2} = \frac{6.690848E - 11 \times 9.113939E - 31}{299792458^2} = 1.356988E - 57 \text{ (m)} \quad (87)$$

Then, using Equations (51) and (56),

$$r_g \text{ (m)} = \frac{2G_N \times m_e}{1kg \times c^2} = \frac{4.5^3 \times \alpha}{2 \times (6.257473E + 18)^3} = 1.356988E - 57 \text{ (m)} \quad (88)$$

So, using Equation 52,

$$r_g \text{ (m)} = \frac{\alpha}{2} \times (4.5 \times e)^3 = 1.356988E - 57 \quad (89)$$

We hope that these equations will be the solution for the black hole entropy.

5.5.3. Unexplained Issues

Regarding the protons, the positive charge and the mass ratio with the electrons are unexplained, which will be explained in a future report.

6. Conclusions

We tried to explain empirical equations by using the correspondence principle with the thermodynamic principles in solid-state ionics. We proposed a canonical ensemble from the correspondence principle. We proposed the existence of a minimum mass of $5.7420807E-38$ kg. Our images for kT_c and G are explained. We showed that every equation can be explained in terms of Avogadro's number (N_{A_new}) and the number (N_{e_new}) of electrons in 1 C.

$$m_{p_new} = \frac{1}{N_{A_new}} \quad (90)$$

$$m_{e_new} = \frac{m_e/m_p}{N_{A_new}} \quad (91)$$

$$e_{new} = \frac{1}{N_{e_new}} \quad (92)$$

$$q_{m_new} = \frac{4.5\pi \times m_p/m_e}{N_{e_new}} = 4.148319E - 15 \quad (93)$$

$$h_{new} = \frac{4.5\pi \times m_p/m_e}{(N_{e_new})^2} = 6.62938382E - 34 \quad (94)$$

$$kT_{c_new} = \frac{4.5 \times c^3 \times \alpha}{2\pi \times N_{e_new} \times N_{A_new}} = 3.7659625E - 23 \quad (95)$$

$$G_{N_new} = \frac{4.5^3 \times m_p / m_e \times N_{A_new} \times c^2 \times \alpha}{4 \times N_{e_new}^3} = 6.6908477E - 11 \quad (96)$$

Using these seven equations, we have proven our three main equations. The main problem in the proposed correspondence principle is that we cannot calculate W (the number of real microstates). Strictly speaking, we need years to do it. However, we tried to show the hints to calculate W . About the protons, the positive charge and the mass ratio with the electrons are unexplained, which will be explained in the future report.

Conflicts of Interest

The author declares no conflicts of interest regarding the publication of this paper.

References

- [1] Miyashita, T. (2020) *Journal of Modern Physics*, **11**, 1180-1192. <https://doi.org/10.4236/jmp.2020.118074>
- [2] Miyashita, T. (2021) *Journal of Modern Physics*, **12**, 623-634. <https://doi.org/10.4236/jmp.2021.125040>
- [3] Miyashita, T. (2021) *Journal of Modern Physics*, **12**, 859-869. <https://doi.org/10.4236/jmp.2021.127054>
- [4] Miyashita, T. (2020) *Journal of Modern Physics*, **11**, 1159-1560. <https://doi.org/10.4236/jmp.2020.1110096>
- [5] Miyashita, T. (2021) *Journal of Modern Physics*, **12**, 1160-1161. <https://doi.org/10.4236/jmp.2021.128069>
- [6] Miyashita, T. (2022) *Journal of Modern Physics*, **13**, 336-346. <https://doi.org/10.4236/jmp.2022.134024>
- [7] Miyashita, T. (2018) *Journal of Modern Physics*, **9**, 2346-2353. <https://doi.org/10.4236/jmp.2018.913149>
- [8] Miyashita, T. (2023) *Journal of Modern Physics*, **14**, 160-170. <https://doi.org/10.4236/jmp.2023.142011>
- [9] Miyashita, T. (2023) *Journal of Modern Physics*, **14**, 432-444. <https://doi.org/10.4236/jmp.2023.144024>
- [10] Miyashita, T. (2023) *Journal of Modern Physics*, **14**, 1217-1227. <https://doi.org/10.4236/jmp.2023.148068>
- [11] Miyashita, T. (2017) *Journal of The Electrochemical Society*, **164**, E3190-E3199. <https://doi.org/10.1149/2.0251711jes>
- [12] Jarzynski, C. (1997) *Physical Review Letters*, **78**, 2690-2693. <https://doi.org/10.1103/PhysRevLett.78.2690>

Calculation of the Standard Model Parameters and Particles Based on a SU(4) Preon Model

Jan Helm

Department of Electrical Engineering, Technical University, Berlin, Germany

Email: jan.helm@alumni.tu-berlin.de

How to cite this paper: Helm, J. (2024) Calculation of the Standard Model Parameters and Particles Based on a SU(4) Preon Model. *Journal of Modern Physics*, 15, 64-124.
<https://doi.org/10.4236/jmp.2024.151003>

Received: December 5, 2023

Accepted: January 27, 2024

Published: January 30, 2024

Copyright © 2024 by author(s) and Scientific Research Publishing Inc. This work is licensed under the Creative Commons Attribution International License (CC BY 4.0).

<http://creativecommons.org/licenses/by/4.0/>



Open Access

Abstract

This paper describes an extension and a new foundation of the Standard Model of particle physics based on a SU(4)-force called hyper-color, and on preon subparticles. The hyper-color force is a generalization of the SU(2)-based weak interaction and the SU(1)-based right-chiral self-interaction, in which the W- and the Z-bosons are Yukawa residual-field-carriers of the hyper-color force, in the same sense as the pions are the residual-field-carriers of the color SU(3) interaction. Using the method of numerical minimization of the SU(4)-action based on this model, the masses and the inner structure of leptons, quarks and weak bosons are calculated: the mass results are very close to the experimental values. We calculate also precisely the value of the Cabibbo angle, so the mixing matrices of the Standard model, CKM matrix for quarks and PMNS matrix for neutrinos can also be calculated. In total, we reduce the 29 parameters of the Standard Model to a total of 7 parameters.

Keywords

SU(4), Generalization of Weak Interaction, Extension of Standard Model, Numerical Minimization of Action, Hyper-Color, Preon

1. Introduction

The Standard Model of Particle Physics (SM) formulated in its final form in mid-seventies, is a very successful theory: in spite of repeated search for deviation from observation, after 50 years there is not a single experimental result contradicting it.

Still, it has several shortcomings, which make it hard to accept as a final theory, so it is generally considered to be incomplete.

SM has the following problems [1] [2] [3] [4]:

- SM does not fully explain baryon asymmetry (observed imbalance of matter

and antimatter)

- SM does not explain the left-right-chiral asymmetry of the electro-weak force (spontaneous symmetry breaking $SU(2)_L \times SU(1)_R$)
- SM does not explain the CP violation in kaons, it has to be introduced as a complex phase in the quark mixing Cabibbo-Kobayashi-Maskawa (CKM) matrix
- SM does not naturally incorporate neutrino oscillations and their non-zero masses, the masses are introduced by hand, and neutrino oscillations are inserted by introducing the purely experimental Pontecorvo-Maki-Nakagawa-Sakata (PMNS) matrix
- Pauli-SU(2) weak interaction is mediated by massive W- and Z-bosons, which is hard to accept from the relativistic point-of-view: all fundamental interactions should propagate with maximum velocity c , like gravitation, electromagnetism, and color interaction. Furthermore, this has remarkable parallels to the early interpretations of color interaction as a Yukawa force mediated by massive pions.
- SM does not contain any candidates for the dark matter particle required by observational cosmology
- SM has no explanation for the observed three generations of quarks and leptons
- SM has 29 parameters, which makes hard to accept as a complete theory

A starting point for an extended formulation of SM appears to be the fifth problem in the above list: Pauli-SU(2) weak interaction.

A plausible solution of the problem is the introduction of a SU(4) interaction with four charges and fifteen massless field bosons in analogy to the concept of the SU(3) color interaction with three charges (colors r g b), eight massless field-bosons (gluons) and eightfold symmetry introduced by Gell-Mann, Fritsch and Leutwyler in 1973.

SU(4) interaction, in the following called hypercolor, in analogy to the color interaction, yields a renormalizable quantum gauge field theory, with confinement and asymptotic freedom.

Pauli-SU(2) weak interaction becomes then the Yukawa weak force of the SU(4)-hypercolor interaction, and the mass of the Yukawa-bosons W and Z (~ 90 GeV) give the critical energy ($E_{hc} = 2m(Z) = 180$ GeV) in analogy to the Callan-Symanzik color critical energy $E_{col} = 220$ MeV.

So in reality the extended weak hypercolor force is roughly 1000 times stronger than the color force.

A plausible formulation of the four charges is $hc = (L-, L+, R-, R+)$, where (+, -) is the electric charge, and (L, R) is the (left, right) chirality. The chirality χ is a fundamental invariant for spinors (left-chiral and right-chiral Weyl-spinors are components of a Dirac-bispinor).

This hc-charge definition is the only possible, because it has to encompass the electric charge (because of the electro-weak interaction) and chirality (because of the chiral asymmetry in SM).

With this hc-charge definition, there is a spontaneous symmetry breaking of the SU(4)-hc-interaction $SU(4) = SU(2)_L \otimes SU(1) \otimes SU(1)_{em}$

A remaining task is to find a sub-structure (preons), which unifies the basic components of SM: the 6 leptons and the 6 quarks. The simplest ansatz is introducing preons r and q with hc-charges, plus color-charge for q , with the parameters:

wave function $\Psi = (u_{L-}, u_{L+}, u_{R-}, u_{R+})$

r-preons $(r_{L-}, r_{L+}, r_{R-}, r_{R+})$, $Q(r) = -1/2$, $m(r) \ll 1 \text{ MeV}$,

q-preons $(q_{L-}, q_{L+}, q_{R-}, q_{R+})$, $Q(q) = +1/6$, $m(q) \sim 1 \text{ MeV}$, $Q_{col}(q) = (r, g, b)$

At first, such an ansatz based purely on symmetry aspects, seems risky to say the least.

Substructure ansatzes based on preons were proposed before (e.g. Harari [5]), and ended in speculations without concrete results.

Here enters the third component of a successful SM-extension: a new powerful and numerically relatively simple calculation method: direct minimization of action [6] [7]. This calculation method was introduced in [4] [7] and applied successfully in QCD for calculation of hadrons.

With these three ansatzes it is possible, as shown in the rest of this paper:

- to calculate numerically the mass hierarchy spectrum of the basic leptons and quarks in SM
- to explain naturally the huge differences of scale in energy-mass in SM, in particular the minuscule neutrino masses
- to explain naturally the three generations (simply by symmetry-compatible hc-boson configurations)
- to calculate in principle the mixing matrices CKM for quarks and PMNS for neutrinos (which explains also the neutrino oscillations)
- to reduce the number of parameters in SM from 29 to 7 parameters

Furthermore, reproducing by pure numeric calculation correctly the energy-mass spectrum of SM is as good as a direct experimental verification for proving the observational correctness of the extended SU(4)-preon-model (SU4PM).

Taken all this into account, it appears extremely lucky that such an ad-hoc model proved to be so successful both theoretically and experimentally. On the other hand, it is another example of the extreme importance and fundamental significance of symmetry aspects in physics.

In the following, we introduce in chap.2 the SU(4) gauge theory with 15 generalized Gell-Mann 4×4 -matrices as generators of the SU(4) Lie group.

In chap.3 we extend the SM to SU4PM by the introduction of the SU(4)-hypercolor interaction, and the two preons (r , q) as sub-particles of leptons and quarks.

In chap.4 the ansatz for wavefunctions, and the numerical algorithm are described.

In chap.5 we present the calculation results for energy-mass of the SM: the six leptons, the six quarks, and the interaction bosons W, Z, H (higgs), and some

weakly interacting new particles, which arise from the ansatz.

In chap.6 we discuss some selected weak hadron decays.

2. SU(4) Gauge Theory

2.1. Gauge Theory

In the following, we consider the gauge theory QCD (quantum chromodynamics) based on SU(3) and the gauge theory QHCD (quantum hyper-color dynamics) based on SU(4) [8] [9].

The gauge invariant QCD Lagrangian is ($\hbar = c = 1$)

$$L = \bar{\psi}(i\gamma^\mu D_\mu - m)\psi - \frac{1}{4}F^a_{\mu\nu}F_a^{\mu\nu} \tag{1}$$

where $\psi_i(x)$ is the quark field, a dynamical function of spacetime, in the fundamental representation of the SU(3) gauge group, indexed by i, j ; $A^a_\mu(x)$ are the fields, also dynamical functions of spacetime, in the adjoint representation of the SU(3) or the SU(4) gauge group, indexed by a, b, \dots . The γ^μ are Dirac matrices connecting the spinor representation to the vector representation of the Lorentz group.

The total field is $A^a_\mu(x) \equiv A^a_\mu(x)\lambda_a$ and the Dirac-conjugate

$\bar{\psi}_i(x) = \psi_i^c(x)\gamma^0$, where ψ_i^c is the complex-conjugate.

D_μ is the gauge covariant derivative for calculation

$$D_\mu \equiv \partial_\mu - ig\tilde{A}_\mu^a\lambda_a \tag{2}$$

for simplicity, instead of $D_\mu \equiv \partial_\mu - igA^a_\mu T^a$, with rescaled field $\tilde{A}_\mu^a \equiv A^a_\mu/2$, and where g is the coupling constant and $T^a = \lambda_a/2$ are the generators of the gauge group/algebra.

For the QCD based on SU(3) ([10] [11] [12] [13]), $A^a_\mu(x)$ is the (color) gluon gauge field, for eight different gluons $a = 1, \dots, 8$, $\psi(x)$ is a four-component Dirac spinor, and λ_a is one of the eight Gell-Mann matrices,

$$a = 1, \dots, 8$$

$$\begin{aligned} \lambda_1 &= \begin{pmatrix} 0 & 1 & 0 \\ 1 & 0 & 0 \\ 0 & 0 & 0 \end{pmatrix} & \lambda_2 &= \begin{pmatrix} 0 & -i & 0 \\ i & 0 & 0 \\ 0 & 0 & 0 \end{pmatrix} & \lambda_3 &= \begin{pmatrix} 1 & 0 & 0 \\ 0 & -1 & 0 \\ 0 & 0 & 0 \end{pmatrix} \\ \lambda_4 &= \begin{pmatrix} 0 & 0 & 1 \\ 0 & 0 & 0 \\ 1 & 0 & 0 \end{pmatrix} & \lambda_5 &= \begin{pmatrix} 0 & 0 & -i \\ 0 & 0 & 0 \\ i & 0 & 0 \end{pmatrix} \\ \lambda_6 &= \begin{pmatrix} 0 & 0 & 0 \\ 0 & 0 & 1 \\ 0 & 1 & 0 \end{pmatrix} & \lambda_7 &= \begin{pmatrix} 0 & 0 & 0 \\ 0 & 0 & -i \\ 0 & i & 0 \end{pmatrix} & \lambda_8 &= \frac{1}{\sqrt{3}} \begin{pmatrix} 1 & 0 & 0 \\ 0 & 1 & 0 \\ 0 & 0 & -2 \end{pmatrix} \end{aligned} \tag{3}$$

These matrices are traceless $Tr(\lambda_a) = 0$, Hermitian, and obey the extra trace orthonormality relation

$$Tr(\lambda_a\lambda_b) = 2\delta_{ab}$$

and commutation relations

$$[\lambda_a, \lambda_b] = 2i \tilde{f}^{abc} \lambda_c, \quad \tilde{f}^{abc} = 2f^{abc} \tag{4}$$

For the QHCD based on SU(4) $A_\mu^a(x)$ is the hc-boson field, for 15 hc-bosons and λ_a are the 15 generators of the SU(4), $a = 1, \dots, 15$, the hc-matrices [14] [15] (in analogy to the 8 Gell-Mann matrices for the SU(3)):

$$\begin{aligned} \lambda_1 &= \begin{pmatrix} 0 & 1 & 0 & 0 \\ 1 & 0 & 0 & 0 \\ 0 & 0 & 0 & 0 \\ 0 & 0 & 0 & 0 \end{pmatrix} & \lambda_2 &= \begin{pmatrix} 0 & -i & 0 & 0 \\ i & 0 & 0 & 0 \\ 0 & 0 & 0 & 0 \\ 0 & 0 & 0 & 0 \end{pmatrix} & \lambda_3 &= \begin{pmatrix} 1 & 0 & 0 & 0 \\ 0 & -1 & 0 & 0 \\ 0 & 0 & 0 & 0 \\ 0 & 0 & 0 & 0 \end{pmatrix} \\ \lambda_4 &= \begin{pmatrix} 0 & 0 & 1 & 0 \\ 0 & 0 & 0 & 0 \\ 1 & 0 & 0 & 0 \\ 0 & 0 & 0 & 0 \end{pmatrix} & \lambda_5 &= \begin{pmatrix} 0 & 0 & -i & 0 \\ 0 & 0 & 0 & 0 \\ i & 0 & 0 & 0 \\ 0 & 0 & 0 & 0 \end{pmatrix} \\ \lambda_6 &= \begin{pmatrix} 0 & 0 & 0 & 0 \\ 0 & 0 & 1 & 0 \\ 0 & 1 & 0 & 0 \\ 0 & 0 & 0 & 0 \end{pmatrix} & \lambda_7 &= \begin{pmatrix} 0 & 0 & 0 & 0 \\ 0 & 0 & -i & 0 \\ 0 & i & 0 & 0 \\ 0 & 0 & 0 & 0 \end{pmatrix} & \lambda_8 &= \frac{1}{\sqrt{3}} \begin{pmatrix} 1 & 0 & 0 & 0 \\ 0 & 1 & 0 & 0 \\ 0 & 0 & -2 & 0 \\ 0 & 0 & 0 & 0 \end{pmatrix} \\ \lambda_9 &= \begin{pmatrix} 0 & 0 & 0 & 1 \\ 0 & 0 & 0 & 0 \\ 0 & 0 & 0 & 0 \\ 1 & 0 & 0 & 0 \end{pmatrix} & \lambda_{10} &= \begin{pmatrix} 0 & 0 & 0 & -i \\ 0 & 0 & 0 & 0 \\ 0 & 0 & 0 & 0 \\ i & 0 & 0 & 0 \end{pmatrix} \\ \lambda_{11} &= \begin{pmatrix} 0 & 0 & 0 & 0 \\ 0 & 0 & 0 & 1 \\ 0 & 0 & 0 & 0 \\ 0 & 1 & 0 & 0 \end{pmatrix} & \lambda_{12} &= \begin{pmatrix} 0 & 0 & 0 & 0 \\ 0 & 0 & 0 & -i \\ 0 & 0 & 0 & 0 \\ 0 & i & 0 & 0 \end{pmatrix} \\ \lambda_{13} &= \begin{pmatrix} 0 & 0 & 0 & 0 \\ 0 & 0 & 0 & 0 \\ 0 & 0 & 0 & 1 \\ 0 & 0 & 1 & 0 \end{pmatrix} & \lambda_{14} &= \begin{pmatrix} 0 & 0 & 0 & 0 \\ 0 & 0 & 0 & 0 \\ 0 & 0 & 0 & -i \\ 0 & 0 & i & 0 \end{pmatrix} & \lambda_{15} &= \frac{1}{\sqrt{6}} \begin{pmatrix} 1 & 0 & 0 & 0 \\ 0 & 1 & 0 & 0 \\ 0 & 0 & 1 & 0 \\ 0 & 0 & 0 & -3 \end{pmatrix} \end{aligned} \tag{5}$$

The symbol $F^a_{\mu\nu}$ the gauge invariant field strength tensor, analogous to the electromagnetic field strength tensor, $F^{\mu\nu}$, in quantum electrodynamics. It is given by

$$F^a_{\mu\nu} = \partial_\mu A^a_\nu - \partial_\nu A^a_\mu + g f^{abc} A^b_\mu A^c_\nu,$$

$$\text{rescaled } F^a_{\mu\nu} = \partial_\mu \tilde{A}^a_\nu - \partial_\nu \tilde{A}^a_\mu + g \tilde{f}^{abc} \tilde{A}^b_\mu \tilde{A}^c_\nu$$

where f^{abc} resp. \tilde{f}^{abc} are the structure constants of SU(3) or SU(4).

the generators $T^a = \lambda_a/2$ satisfy the commutator relations

$$[T^a, T^b] = i f^{abc} T^c, \text{ rescaled } [\lambda_a, \lambda_b] = i \tilde{f}^{abc} \lambda_c$$

General Yang-Mills theory

Yang-Mills theories are a special example of gauge theory with a non-commu-

tative symmetry group given by the Lagrangian [3]

$$L_{gf} = -\frac{1}{4} F^{a\mu\nu} F^a_{\mu\nu} \tag{6}$$

with the generators of the Lie algebra, indexed by a , corresponding to the F -quantities (the curvature or field-strength form) satisfying

$$Tr(T^a T^b) = \frac{1}{2} \delta^{ab} \quad [T^a, T^b] = i f^{abc} T^c,$$

where for SU(3) and SU(4) $T^a = \lambda_a/2$, and where the f^{abc} are structure constants of the Lie algebra, and the covariant derivative defined as

$D_\mu \equiv \partial_\mu - i g A^a_\mu T_a$ resp. $D_\mu \equiv \partial_\mu - i g \tilde{A}^a_\mu \lambda_a$, where A^a_μ is the field carrier, $\tilde{A}^a_\mu \equiv A^a_\mu/2$ is the rescaled field, and g is the coupling constant, and for a SU(N) group one has $N^2 - 1$ generators.

The relation for the field tensor

$$F^a_{\mu\nu} = \partial_\mu A^a_\nu - \partial_\nu A^a_\mu + g f^{abc} A^b_\mu A^c_\nu$$

$$\tilde{F}^a_{\mu\nu} = \partial_\mu \tilde{A}^a_\nu - \partial_\nu \tilde{A}^a_\mu + g \tilde{f}^{abc} \tilde{A}^b_\mu \tilde{A}^c_\nu$$

follows from the commutator for the covariant derivative D_μ

$$[D_\mu, D_\nu] = -i g T_a F^a_{\mu\nu}$$

The field has the property of being self-interacting and equations of motion that one obtains are said to be semilinear, as nonlinearities are both with and without derivatives. This means that one can manage this theory only by perturbation theory, with small nonlinearities.

From the given Lagrangian one can derive the equations of motion given by

$$\partial^\mu F^a_{\mu\nu} + g f^{abc} A^{b\mu} F^c_{\mu\nu} = 0 \quad (\text{Yang-Mills-equations}), \tag{7}$$

$$\text{resp. } \partial^\mu F^a_{\mu\nu} + g \tilde{f}^{abc} \tilde{A}^{b\mu} F^c_{\mu\nu} = 0$$

which correspond to the Maxwell equations in electrodynamics $\partial^\mu F^a_{\mu\nu} = 0$, where $f^{abc} = 0$

Putting $F_{\mu\nu} = T^a F^a_{\mu\nu}$, these can be rewritten as

$$(D^\mu F_{\mu\nu})^a = 0$$

The Bianchi identity holds

$$(D_\mu F_{\nu\kappa})^a + (D_\kappa F_{\mu\nu})^a + (D_\nu F_{\kappa\mu})^a = 0$$

which is equivalent to the Jacobi identity

$$[D_\mu, [D_\nu, D_\kappa]] + [D_\kappa, [D_\mu, D_\nu]] + [D_\nu, [D_\kappa, D_\mu]] = 0 \quad \text{for Lie-groups}$$

since $[D_\mu, F^a_{\nu\kappa}] = D_\mu F^a_{\nu\kappa}$.

Define the dual strength tensor $\tilde{F}^{\mu\nu} \equiv \frac{1}{2} \varepsilon^{\mu\nu\rho\sigma} F_{\rho\sigma}$, then the Bianchi identity can be rewritten as

$$D_\mu \tilde{F}^{\mu\nu} = 0$$

A source current J^a_ν enters into the equations of motion (eom) as

$$\partial^\mu F^a_{\mu\nu} + g f^{abc} A^{b\mu} F^c_{\mu\nu} = -J^a_\nu$$

The Dirac part of the Lagrangian is

$$L_D = \bar{\psi} (i\hbar D_\mu \gamma^\mu - mc) \psi$$

with the resulting eom = gauge Dirac equation

$$(i\hbar D_\mu \gamma^\mu - mc) \psi = 0$$

2.2. The Running Coupling Constant of the QCD

We introduce the qq-potential (Cornell potential)

$$V(R, \beta) \approx V_0 - \frac{4}{3} \frac{\alpha \hbar c}{R} + \frac{\sigma R}{\hbar c} \quad \text{potential} = \langle q\bar{q} \rangle, \quad \sqrt{\sigma} \approx 440 \text{ MeV}$$

its measured values are shown below.

R_0 is the characteristic scale $R_0 \approx 0.49 \text{ fm}$, the scaling β -function is defined below.

Measured values of for different values of β are shown in **Figure 1**.

The data at $\beta = 6.0, 6.2, 6.4$ and 6.8 has been scaled by R_0 , and normalized such that $V(R_0) = 0$. The collapse of the different sets of data on to a single curve after the rescaling by R_0 is evidence for scaling. The linear rise at large rR implies confinement [16] [17].

The color confinement results from $\lim(V(R), R \rightarrow \infty) = \infty$.

2.3. Callan-Symanzik Equation

The Callan-Symanzik equation describes the behavior of the transfer function of a Feynman diagram with n momentums [3]

$$G^{(n)}(x_1, x_2, \dots, x_n; m, M, g),$$

where M = renormalization (cut-off) energy, g = coupling constant. ϕ = field strength, m = energy, with original and renormalized field $\phi = Z\phi_0$, transfer function $G^{(n)} = Z^{n/2} G_0^{(n)}$, under scaling transformation

$$g \rightarrow g + \delta g \quad M \rightarrow M + \delta M \quad \phi = Z\phi_0 \rightarrow Z'\phi_0 M = (1 + \delta\eta)\phi$$

$$G^{(n)} \rightarrow (1 + n\delta\eta)G^{(n)}$$

From the cut-off independence

$$\frac{\partial}{\partial M} G_0^{(n)} = 0$$

we get the Callan-Symanzik equation

$$\left(M \frac{\partial}{\partial M} + \beta(g) \frac{\partial}{\partial g} + n\gamma + m\gamma_m \frac{\partial}{\partial m} \right) G^{(n)}(x_1, x_2, \dots, x_n; m, M, g) = 0,$$

where $\gamma = -M \frac{\partial \eta}{\partial M}$ $\beta = M \frac{\partial g}{\partial M}$ $\gamma_m = \frac{M}{m} \frac{\partial \eta}{\partial M}$

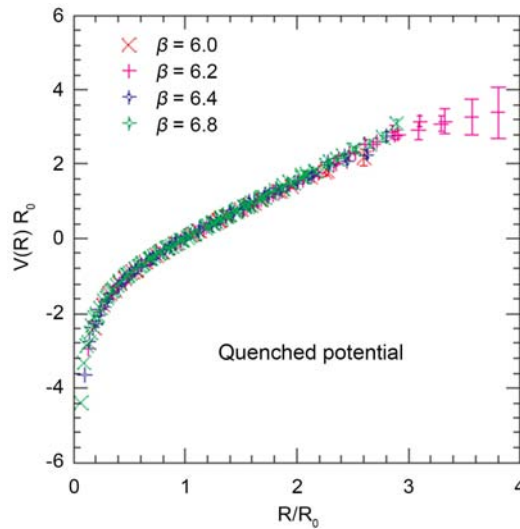


Figure 1. The static qq-potential in the quenched approximation obtained by the Wuppertal collaboration [16].

From the definition we get a differential equation for $g(M)$

$$M \frac{\partial g}{\partial M} + \beta(g) = 0 \tag{8}$$

The running coupling for QCD is characterized by the β -function with colors $N = 3$, flavors $n_f = 3$, $M =$ cut-off energy [16]

$$M \frac{\partial g}{\partial M} = -\beta(g) = -(\beta_0 g^3 + \beta_1 g^5 + \dots)$$

$$\beta_0 = \frac{1}{16\pi^2} \left(\frac{11}{3} N - \frac{2}{3} n_f \right)$$

$$\beta_1 = \frac{1}{(16\pi^2)^2} \left(\frac{34}{3} N^2 - \frac{10}{3} N n_f - \frac{n_f}{N} (N^2 - 1) \right)$$

resulting in first order in
$$g^2(m) = \frac{g^2(M)}{1 + g^2(M) \beta_0 \log\left(\frac{m^2}{M^2}\right)}$$

Which becomes for

$$m \rightarrow \infty \quad g(m) = \frac{1}{\sqrt{2\beta_0 \log\left(\frac{m}{M}\right)}} \tag{9a}$$

$$\alpha_s(m) = \frac{g^2(m)}{4\pi} = \frac{1}{8\pi\beta_0 \log\left(\frac{m}{\Lambda}\right)} = \frac{12\pi}{(11N - 2n_f) \log\left(\frac{m^2}{\Lambda^2}\right)} \tag{9b}$$

$\alpha_s =$ coupling constant

where

$M = \Lambda \approx 220$ MeV critical energy of QCD, $\Lambda \approx m(\text{pion})2 = 280$ MeV

$n_f = 3$: number of quark flavours

The corresponding critical length of QCD

$$r_{0c} = \frac{\hbar c}{\Lambda} = \frac{1.96 * 10^{-7} \text{ eV} \cdot \text{m}}{220 \text{ MeV}} = 0.89 * 10^{-15} \text{ m}$$

which is about the proton radius.

For energies $m \approx \Lambda$ we have the exact formula

$$g_c(m) = 4\pi \sqrt{\frac{3}{2(11N - 2n_f) \sqrt{\left(\log\left(\frac{m}{\Lambda}\right)\right)^2 + c_{GE0}^2}}}$$

$$= 4\pi \sqrt{\frac{1}{18 \sqrt{\left(\log\left(\frac{m}{\Lambda}\right)\right)^2 + c_{GE0}^2}}}$$

for the numerical calculation we set $c_{GE0} = \frac{1}{\log\left(\frac{m(p)}{\Lambda_{QCD}}\right)} = 0.683$, which is con-

sistent with the Callan-Symanzik relation for $m > 2\Lambda$, as shown in the plot **Figure 2** below.

2.4. The Running Coupling Constant of the QHCD

For the QHCD the Callan-Symanzik equation is still valid, as it is derived from the scale-independence of the theory.

The running coupling for QHCD with colors $N = 4$, flavors $n_f = 3$, $\Lambda =$ transfer energy becomes in analogy to (9b)

$$\alpha_{hc}(m) = \frac{g^2(m)}{4\pi} = \frac{12\pi}{(11N - 2n_f) \log\left(\frac{m^2}{\Lambda_{hc}^2}\right)} \tag{10a}$$

Again, it must be corrected to avoid a singularity for

$$m = \Lambda_{hc} \tag{10b}$$

$$g_{hc}(m) = 4\pi \sqrt{\frac{3}{2(11N - 2n_f) \sqrt{\left(\log\left(\frac{m}{\Lambda_{hc}}\right)\right)^2 + c_{GE1}^2}}}$$

$$= 4\pi \sqrt{\frac{3}{76 \sqrt{\left(\log\left(\frac{m}{\Lambda_{hc}}\right)\right)^2 + c_{GE1}^2}}}$$

we set $\Lambda_{hc} = 2m(Z_0) = 180 \text{ GeV}$ in analogy to the QCD, and $c_{GE1} = \frac{1}{\log\left(\frac{m(t)}{m(d)}\right)}$,

with the masses of the top- and the d-quark: this should assess the logarithmic scale of the generation energy ratio.

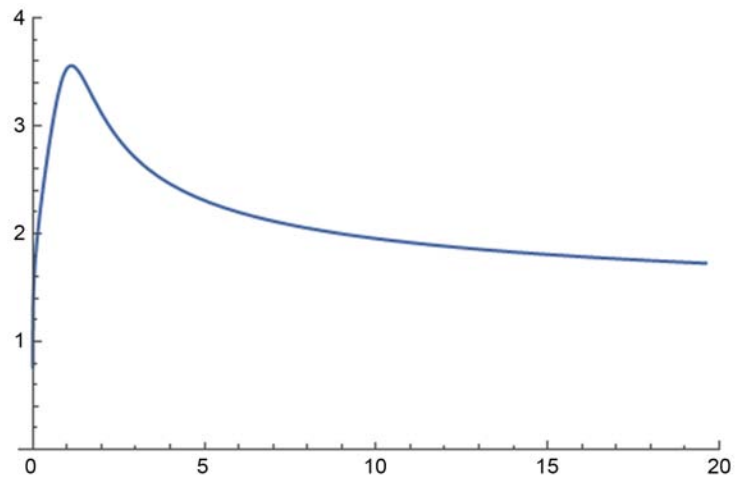


Figure 2. $g_c(m)$, m in E_0 -units, $E_0 = 196$ MeV [18].

Both settings are of course only a plausible guess, but these values work very well for the preon model, as we will see.

The coupling constant g_{hc} for the QHCD is shown in the plot **Figure 3** below.

The peak is much higher than in QCD, which reflects the enormous span of the mass scale in the Standard Model.

The corresponding critical length of QHCD

$$r_{0hc} = \frac{\hbar c}{\Lambda_{hc}} = \frac{1.96 * 10^{-7} \text{ eV} \cdot \text{m}}{180 \text{ GeV}} = 1.08 * 10^{-18} \text{ m}$$

which is about 1/1000 of the proton radius: the energy scale of the QHCD is by a factor 1000 larger, and consequently the length scale by a factor 1000 smaller than in QCD. This agrees with the experimental assessment of the quark radius being about 1/1000 of the proton radius.

3. The Standard Model and QCD, the SU(4)-Preon Model and QHCD

The Standard Model of particle physics (SM) emerged in the mid 1970s as the universal theory of high-energy physics encompassing the electromagnetic, weak Pauli and strong color interactions, and based on a particle model with 6 basic lepton and 6 basic quark spinors in 3 generations (=flavors), plus field carrier bosons: 1 photon, 8 color gluons, 2 weak Pauli massive W-Z bosons, and scalar higgs H ([2] [3] [14] [20] [21] [22]).

The interactions of SM are described by $SU(n)$ gauge theories: trivial $SU(1)$ electromagnetic, $SU(2)$ weak Pauli interaction, and $SU(3)$ strong color interaction. The gauge charges are: $n = 1$ electromagnetic charge q , $n = 2$ the weak isospin $I_3 = \pm 1$, $n = 3$ the color $c = (r, g, b)$.

The quarks form composite particles known as hadrons, among them the nucleons (p, n) which build the atomic nuclei, the leptons do not form composite particles.

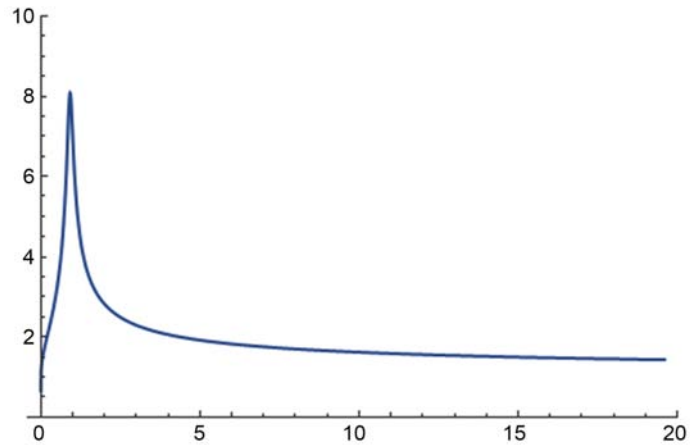


Figure 3. $g_{bc}(m)$, m in E_0 -units, $E_0 = 196$ GeV [19].

The weak Pauli interaction breaks the chiral symmetry and becomes $SU(2)_L \times SU(1)_R$ gauge interaction.

It combines via the Glashow-Weinberg mechanism with the electromagnetic interaction to become electroweak interaction $SU(2)_L(W) \times SU(1)(Z) \times SU(1)(\gamma)$ with W-boson, Z-boson, photon.

Finally, the masses of the basic particles are generated via the Higgs mechanism through $SU(n)$ symmetry breaking by the higgs H particle.

Based on this scaffold, the SM developed into a powerful theory, which describes all of particle physics correctly with no deviation from experiment until present.

3.1. Parameters of the Standard Model

Basic particles of the standard model [22]

The properties of the basic particles of the Standard Model are shown in **Table 1** below.

The quark radius: as of 2014, experimental evidence indicates they are no bigger than 10^{-4} times the size of a proton, *i.e.* less than 10^{-19} metres [23].

Field bosons

The following **Table 2** describes the basic bosons of the SM: 3 massive bosons W^\pm , Z, H and 2 massless field-carriers: photon γ and gluon g .

Parameters Standard Model

The model has 28 parameters + fine-structure constant α_{em} [2] [21], as described in **Table 3** below.

3.2. The Basics of the Preon Model

The preon model describes the basic particles of the Standard Model (leptons, quarks and exchange bosons) as composed of smaller particles (preons), which obey a super-strong hyper-color interaction.

Examples are the rishon model (Harari 1979 [5] [24]) and the primon model (de Souza 2002 [25]).

Table 1. Basic particles of the Standard Model.

Generation 1						
Fermion left-handed	Symbol	Electric charge	Weak isospin	Weak hyper-charge	Color charge	Mass
electron	e^-	-1	-1/2	-1	1	511 keV
positron	e^+	+1	0	2	1	511 keV
e-neutrino	ν_e	0	+1/2	-1	1	<0.22 eV
e-antineutrino	$\bar{\nu}_e$	0	0	0	1	<0.22 eV
up-quark	u	+2/3	+1/2	+1/3	3	2.3 MeV
up-antiquark	\bar{u}	-2/3	0	-4/3	$\bar{3}$	2.3 MeV
down-quark	d	-1/3	-1/2	+1/3	3	4.8 MeV
down-antiquark	\bar{d}	+1/3	0	-2/3	$\bar{3}$	4.8 MeV
Generation 2						
muon	μ^-	-1	-1/2	-1	1	105.6 MeV
antimuon	μ^+	+1	0	2	1	105.6 MeV
mu-neutrino	ν_μ	0	+1/2	-1	1	<0.22 eV
mu-antineutrino	$\bar{\nu}_\mu$	0	0	0	1	<0.22 eV
charm-quark	c	+2/3	+1/2	+1/3	3	1275 MeV
charm-antiquark	\bar{c}	-2/3	0	-4/3	$\bar{3}$	1275 MeV
strange-quark	s	-1/3	-1/2	+1/3	3	95 MeV
strange-antiquark	\bar{s}	+1/3	0	-2/3	$\bar{3}$	95 MeV
Generation 3						
tau	τ^-	-1	-1/2	-1	1	1776.8 MeV
antitau	τ^+	+1	0	2	1	1776.8 MeV
tau-neutrino	ν_τ	0	+1/2	-1	1	<0.22 eV
tau-antineutrino	$\bar{\nu}_\tau$	0	0	0	1	<0.22 eV
top-quark	t	+2/3	+1/2	+1/3	3	173,210 MeV
top-antiquark	\bar{t}	-2/3	0	-4/3	$\bar{3}$	173,210 MeV
bottom-quark	b	-1/3	-1/2	+1/3	3	4180 MeV
bottom-antiquark	\bar{b}	+1/3	0	-2/3	$\bar{3}$	4180 MeV

Table 2. Field bosons of the Standard Model.

Particle	Charge	w.Isospin T	w.hcharge Y	Spin	Color	Lifetime	Mass
W±	±1	±1	0	1	0	3×10^{-25} s	80.4 GeV
Z	0	0	0	1	0	3×10^{-25} s	91.2 GeV
γ photon	0	0	0	1	0		0
g gluon	0	0	0	1	3		0
H higgs	0	0	0	0	0	10^{-22} s	125.1 GeV

Table 3. Parameters of the Standard Model [16], where electromagnetic fine-structure constant $\alpha_{em} = \frac{e_0^2}{4\pi} = \frac{1}{137}$.

Parameters of the Standard Model			
Symbol	Description	Renormalization scheme (point)	Value
m_e	Electron mass		511 keV
m_μ	Muon mass		105.7 MeV
m_τ	Tau mass		1.78 GeV
m_u	Up quark mass	$\mu_{MS} = 2 \text{ GeV}$	1.9 MeV
m_d	Down quark mass	$\mu_{MS} = 2 \text{ GeV}$	4.4 MeV
m_s	Strange quark mass	$\mu_{MS} = 2 \text{ GeV}$	87 MeV
m_c	Charm quark mass	$\mu_{MS} = m_c$	1.32 GeV
m_b	Bottom quark mass	$\mu_{MS} = m_b$	4.24 GeV
m_t	Top quark mass	On-shell scheme	172.7 GeV
θ_{12}	CKM 12-mixing angle	q flavor mixing	13.1°
θ_{23}	CKM 23-mixing angle		2.4°
θ_{13}	CKM 13-mixing angle		0.2°
δ_{13}	CKM CP-violating Phase		0.995
θ_{12}	PMNS 12-mixing angle	ν flavor mixing	33.6° ± 0.8°
θ_{23}	PMNS 23-mixing angle		47.2° ± 4°
θ_{13}	PMNS 13-mixing angle		8.5° ± 0.15°
δ_{13}	PMNS CP-violating Phase		4.1 ± 0.75
g_1 or g'	U (1) gauge coupling	$\mu_{MS} = m_Z$	0.357
g_2 or g	SU (2) gauge coupling	$\mu_{MS} = m_Z$	0.652
g_3 or g_s	SU (3) gauge coupling	$\mu_{MS} = m_Z$	1.221
Λ	crit. energy in SU (3)		220 MeV
c_{gE0}	additional log in col-coupling		0.69
θ_{QCD}	QCD vacuum angle		~0
v	Higgs vacuum expectation value		246 GeV
m_H	Higgs mass		125.36 ± 0.41 GeV
$m_{\nu e}$	electron neutrino mass		≤0.12 eV
$m_{\nu \mu}$	mu neutrino mass		≤0.12 eV
$m_{\nu \tau}$	tau neutrino mass		≤0.12 eV
α_{em}	fine-structure constant		1/137

The rishon model

In the rishon model, there are two preons (called rishons) T (charge +1/3e) and V (charge 0). Leptons and quarks and exchange bosons are built of 3 rishons. They obey a hc-interaction based on SU(3), the 3-rishon combinations have the

(color)x(hyper-color) representation $SU(3)_c \times SU(3)_{hc}$

TTT = antielectron

VVV = electron neutrino

TTV, TVT, VTT = three colours of up quarks

TVV, VTV, VVT = three colours of down antiquarks

\overline{TTT} = electron

\overline{VVV} = electron antineutrino

$\overline{TTV}, \overline{TVT}, \overline{VTT}$ = three colours of up antiquarks

$\overline{TVV}, \overline{VTV}, \overline{VVT}$ = three colours of down quarks

W^+ boson = $TTTVVV$

Generations are explained as excited states of the first generations, mass is not explained.

The primon model

In the primon model there are four preons (called primons) (p_1, p_2, p_3, p_4), which carry charge $(+5/6, -1/6, -1/6, -1/6)$ and hc-charge, they obey a hc-interaction based on $SU(2)$.

Quarks are built of two primons:

u (p_1, p_2), c (p_1, p_3), t (p_1, p_4), d (p_2, p_3), s (p_2, p_4), b (p_3, p_4), leptons are non-composite, there are 3 non-composite Higgs-bosons.

Generations are explained as primon-configuration, the mass spectrum is only qualitatively explained

Requirements for the preon model

The two basic ideas of the preon model (PM) are

-the basic particles of the Standard Model (SM) are composed of a few fundamental fermions

-there is a super-strong hyper-color interaction, with massless field bosons

A successful PM should uphold the symmetries and invariances of the SM and solve its main problems:

-PM should encompass the preservation of the baryon and lepton number

-PM should explain and derive the generations (flavor) of the SM and their energy scales

-PM should explain the allowed and not-allowed decay modes and the flavor-mixing of the SM

-PM should correctly calculate the mass spectrum, and explain the huge difference in mass scale between leptons and quarks, and between the generations: $m(\text{neutrino } \nu_e) \sim 10^{-4} \text{ eV}$, $m(\text{top quark } t) = 170 \text{ GeV}$, which makes a factor of 10^{15}

-PM should describe the weak exchange bosons W, Z, and the higgs H as Yukawa-bosons of the hc-interaction,

as all other fundamental field bosons graviton $A^{\mu\nu}$, photon A^μ , gluon A_c^μ are massless waves; the field bosons A_{hc}^μ of hc should be also massless

-hc interaction should be stronger the $SU(3)$ -color interaction and should encompass the weak $SU(2)$, also it should reproduce the spontaneous symmetry breaking of the electroweak symmetry group

$SU(2)_{L, \text{ch-weak}} \otimes SU(1)_{n\text{-weak}} \otimes SU(1)_{\text{em}}$ with their exchange bosons $\{W^\mu\} \otimes \{Z^\mu\} \otimes \{A^\mu\}$ and corresponding currents {charged-weak} \otimes {neutral-weak} \otimes {electromagnetic}.

-PM should reduce the 28 parameters of the SM to very few fundamental parameters.

3.3. Realization of the SU(4) Preon Model

The SU(4) preon model (SU4PM) is based essentially on two assumptions

-The SU4PM postulates two basic Weyl-spinors $\{r, q\}$ as the fundamental particles and the SU(4) as the gauge group of the hc-interaction, with spin $S = 1/2$, with electrical charge $Q_e = \{-1/2, 1/6\}$ and color charge $Q_c = \{0, 1\}$

-The field-bosons are the 15 generators A_{hc}^μ of the SU(4), described by the 15 standard generator 4×4 matrices λ_i of the SU(4). The SU(4) has 4 hc-charges: {chirality L, chirality R, electrical charge +, electrical charge -} in analogy to the 3 color charges of the SU(3): {r, g, b}.

From these assumptions follow the basic particle families of

-leptons $L = r \otimes r$ being a hc-tetra-spinor of a doublet of two r-preons, fermions with total spin $S = 1/2$

-quarks $Q = r \otimes q$ being a hc-tetra-spinor of a doublet of an r- and a q-preon, colored fermions with color $Q_c = 1$ with total spin $S = 1/2$

-(hypothetical) strong neutrinos $N_c = q \otimes q$ being a hc-tetra-spinor of a doublet of two q-preons, colored fermions with color $Q_c = 0$ with total spin $S = 1/2$

-weak bosons $B_w = r \pm r$ being a linear combinations of two or more r-preons, with total spin $S = 0$ (scalar like higgs H) or $S = 1$ (vector like W and Z)

-(hypothetical) strong bosons $B_c = q \pm q$ being a linear combinations of two or more q-preons, with color $Q_c = 0$ and total spin $S = 0$ (scalar like higgs H_q) or $S = 1$ (vector like Z_q)

A a hc-tetra-spinor is a hc-quadruplet with the hc-charges $\{L-, L+, R-, R+\}$.

Both preons can carry all four charges of SU(4), *i.e.* there are $\{rL-, rL+, rR-, rR+\}$ and $\{qL-, qL+, qR-, qR+\}$, where the spinor-anti-spinor pairs are $\{rL-, rR+\}$ and $\{rL+, rR-\}$.

The r-q-doublets, *i.e.* the quarks, have one more degree of freedom, as they consist of different fermions, and are therefore chiral-neutral, which is energetically more favorable.

A hc-doublet occupies two positions in a hc-tetra-spinor with indices (i, j) , e.g. the e-neutrino with the configuration $\{rL-, rL+, 0, 0\}$ has the hc-indices $(1, \bar{2})$, the bar over 2 signifies the anti-spinor.

One can show, that for two hc-indices $\{i, j\}$ there are three field-boson configurations, which are compatible with the SU(4) symmetry: one boson A_{ij} (corresponding to the non-diagonal hc-matrix $\tilde{\lambda}_{ij}$ interchanging i with j , e.g. for $(i, j) = (1, 2)$ $\tilde{\lambda}_{ij} = \lambda_1$), four bosons $A_{ij}, \bar{A}_{ij}, A_{kl}, \bar{A}_{kl}$ (interchanging resp. $(i, j), (i, \bar{j}),$ and the dual index pairs $(k, l), (k, \bar{l})$), and all 15 bosons as the third configuration. These correspond to the three generations (flavors) of the

SM, as the calculation shows.

Basic parameters of SU4PM

We have 6 parameters for SU4PM: 2 preon masses, and hyper-color/SU4 interaction the critical energy Λ_{hc} and the peak height constant c_{GE1} . Furthermore, we still have the corresponding 2 parameters of the color/SU3 interaction: the critical energy Λ_c and the peak height constant c_{GE0} .

The 4 interaction parameters have been derived in chap. 2.

For the mass of the r-preon, we make a guess of $m(\text{e-neutrino})/3$: in the lightest lepton, the e-neutrino, there are two r-preons and one hc-boson, so $m(r)$ will be approximately 1/3 of the assessed $m(\text{e-neutrino})$: this is assumed to be 1/1000 (1000 = approximate factor for flavor 3) of the best upper limit for $m(\text{tau-neutrino}) = 0.1 \text{ eV}$.

For the mass of the q-preon, we take 1/3 of mass(u-quark) the lightest quark, in analogy to the r-preon.

preon data

r-preons $\{rL-, rL+, rR-, rR+\}$

$Q(r) = -1/2, m(r) = 0.033 \text{ meV}$

q-preons $\{qL-, qL+, qR-, qR+\}$

$Q(q) = +1/6, m(q) = 0.77 \text{ MeV}$

coupling constant of hc-interaction

The coupling from the Callan-Symanzik equation must be corrected to avoid a singularity for $\mu = \Lambda_{hc}$

$$g_{hc}(m) = 4\pi \sqrt{\frac{3}{76 \sqrt{\left(\log\left(\frac{m}{\Lambda_{hc}}\right)\right)^2 + c_{GE1}^2}}} \tag{11}$$

we set $\Lambda_{hc} = 2m(Z_0) = 180 \text{ GeV}$ in analogy to the QCD, and

$$c_{GE1} = \frac{1}{\log\left(\frac{m(t)}{m(d)}\right)} = 0.095$$

The configuration of the SM in the SU4PM

Every basic particle of the SM is assigned a preon and a hc-boson configuration.

The preon configuration of a fermion (leptons and quarks) occupies two of the 4 positions in a hc-quadruplet by a Dirac-bispinor, e.g. for electron with index pair (I, β) we have $\begin{pmatrix} rL- \\ 0 \end{pmatrix}$ in position 1 and $\begin{pmatrix} rR- \\ 0 \end{pmatrix}$ in position 3, according to the hc-charge. The hc-quadruplet has the hc-charges $(L-, L+, R-, R+)$.

There are 3 possible hc-boson configurations for an index-pair (i, j) , which are consistent with the SU(4)-symmetry: 1 hc-boson Aij corresponding to first generation of flavor = 1, 4 hc-bosons $Aij + \bar{A}ij + Akl + \bar{A}kl$ corresponding to flavor = 2 (the bar specifies the conjugate coupler, and (k, l) is the complementary in-

dex pair, e.g. for electron it is $(2, 4)$, and finally all 15 hc-bosons corresponding to flavor = 3.

The fermions (leptons and quarks) have two independent preon-components $u1$ and $u2$, they form a bispinor with spin $S = 1/2$.

The bosons (weak boson W, Z, H) have only one independent preon-component $u1$, which is a linear combination of two preons, the spins add up to $S = 1$ for W and Z, or to $S = 0$ for H, e.g. for $Z = Z0$ $u1 = ((rL -) + (rR -))/\sqrt{2}$ and

$$Z0 = \left(\left(\begin{matrix} u1 \\ 0 \end{matrix} \right), \left(\begin{matrix} 0 \\ u1 \end{matrix} \right), \left(\begin{matrix} u1 \\ 0 \end{matrix} \right), \left(\begin{matrix} 0 \\ u1 \end{matrix} \right) \right) / \sqrt{2} .$$

The weak bosons W and Z0 are carrier of the residual weak interaction, and the higgs H generates masses for all r-containing particles: leptons, quarks, weak bosons and the r-preon itself.

The SU4PM predicts the existence of hypothetical strong neutrinos, which consist of $q\bar{q}$ with electrical charge $Q = 0$ and color charge $Q_c = 0$. They are heavy ($m(qnu) = 23.2$ MeV) practically non-interacting particles: they interact only via very heavy q-boson Zq ($m(Zq) = 644$ GeV), *i.e.* they interact only at high resonance energies with small cross-sections. There is a new hypothetical model for Dark Matter called SIMP with mass around 100 MeV and interacting strongly at high resonance energies [26]. The strong-neutrinos do fit into this category.

Furthermore, the SU4PM predicts the existence of strong bosons Zq and Hq , in analogy to weak bosons Z0 and H, built of q-preons instead of r-preons. The strong neutrinos interact with themselves via Zq , and Hq generates masses for strong neutrinos and the q-preon.

The decay of neutron and pion requires (to safeguard the conservation of hc-charge) the existence of further weak neutrinos: the non-chiral (sterile) neutrinos with masses similar to lepton neutrinos. The nc-neutrinos are neutral, non-chiral, and interact with themselves and lepton neutrinos via the weak ZL-boson similar to the Z0, but left-chiral.

The SU4PM SU(4) symmetry is spontaneously broken into the electroweak symmetry group

$$SU(2)_{L, ch-weak} \otimes SU(1)_{n-weak} \otimes SU(1)_{em}$$

with their exchange bosons $\{W^\mu\} \otimes \{Z^\mu\} \otimes \{A^\mu\}$ and corresponding currents {charged-weak} \otimes {neutral-weak} \otimes {electromagnetic}.

The basic particle families in the SU4PM representation of the Standard Model are shown in the schematic **Table 4** below.

4. The Calculation Method of the SU(4)-Preon Model

We apply for the calculation of the parameters of SM particles the numerical minimization of action, using a Ritz-Galerkin expansion for the hc-bosons and a parameterized gaussian for the preons.

4.1. The Ansatz for the Wavefunction

Hc-boson wavefunction

Table 4. Particle configurations in the SU4PM representation of the Standard Model.

<p>charged leptons {e, mu, tau}</p> $x = \left(\begin{pmatrix} rL- \\ 0 \end{pmatrix}, 0, \begin{pmatrix} rR- \\ 0 \end{pmatrix}, 0 \right)$ <p>$e = x + A13$ flavor F=1 one boson $mu = x + A13 + \bar{A}13 + A24 + \bar{A}24$ F=2: four bosons $tau = x + A$ F=3: all bosons</p>	<p>lepton neutrinos {nue, num, nut}</p> $x = \left(\begin{pmatrix} rL- \\ 0 \end{pmatrix}, \begin{pmatrix} 0 \\ rL+ \end{pmatrix}, 0, 0 \right)$ <p>$nue = x + A12$ $num = x + A12 + \bar{A}12 + A34 + \bar{A}34$ $nut = x + A$</p>
<p>u-quarks {u,c,t}</p> $x = \left(0, \begin{pmatrix} (rL++qL+)/2 \\ (rL++qL+)/2 \end{pmatrix}, 0, \begin{pmatrix} (rR++qR+)/2 \\ (rR++qR+)/2 \end{pmatrix} \right) \begin{matrix} \sqrt{2} \\ \sqrt{2} \end{matrix}$ <p>$u = x + A24$ $c = x + A24 + \bar{A}24 + A13 + \bar{A}13$ $t = x + A$</p>	<p>sterile neutrinos {nus1,nus2,nus3}</p> $x = \left(\begin{pmatrix} rL- \\ 0 \end{pmatrix}, 0, 0, \begin{pmatrix} 0 \\ rR+ \end{pmatrix} \right)$ <p>$nus1 = x + A14$ $nus2 = x + A14 + \bar{A}14 + A23 + \bar{A}23$ $nus3 = x + A$</p>
<p>d-quarks {d, s, b}</p> $x = \left(\begin{pmatrix} (rL-+qL+)/2 \\ 0 \end{pmatrix}, 0, \begin{pmatrix} (rR-+qR+)/2 \\ 0 \end{pmatrix}, 0 \right) \begin{matrix} \sqrt{2} \\ \sqrt{2} \end{matrix}$ <p>$d = x + A13$ $s = x + A13 + \bar{A}13 + A24 + \bar{A}24$ $b = x + A$</p>	
<p>weak massive bosons {W, Z0, ZL, H}</p> <p>F=3, all A</p> $W = \left(0, 0, \begin{pmatrix} u1 \\ 0 \end{pmatrix}, 0 \right) \sqrt{2} \quad u1 = ((rR-) - (rR-)) / \sqrt{2}$ $Z0 = \left(\begin{pmatrix} u1 \\ 0 \end{pmatrix}, \begin{pmatrix} 0 \\ u1 \end{pmatrix}, \begin{pmatrix} u1 \\ 0 \end{pmatrix}, \begin{pmatrix} 0 \\ u1 \end{pmatrix} \right) / \sqrt{2} \quad u1 = ((rL-) + (rR-)) / \sqrt{2}$ $ZL = \left(\begin{pmatrix} u1 \\ u1 \end{pmatrix}, \begin{pmatrix} u1 \\ u1 \end{pmatrix}, 0, 0 \right) / \sqrt{2} \quad u1 = ((rL-) + (rL+)) / \sqrt{2}$ $H = \left(\begin{pmatrix} u1 \\ u1 \end{pmatrix}, \begin{pmatrix} u1 \\ u1 \end{pmatrix}, \begin{pmatrix} u1 \\ u1 \end{pmatrix}, \begin{pmatrix} u1 \\ u1 \end{pmatrix} \right) / 2 \quad u1 = ((rL-) + (rL+) + (rR-) + (rR+)) / 2$	
<p>strong neutrinos {qnue, qnum, qnut}</p> $x = \left(\begin{pmatrix} qL- \\ 0 \end{pmatrix}, 0, 0, \begin{pmatrix} 0 \\ qR+ \end{pmatrix} \right)$ <p>$qnue = x + A14$ $qnum = x + A14 + \bar{A}14 + A23 + \bar{A}23$ $qnut = x + A$</p>	
<p>strong massive bosons {Zq, Hq}</p> <p>F=3, all A</p> $Zq = \left(\begin{pmatrix} u1 \\ 0 \end{pmatrix}, \begin{pmatrix} 0 \\ u1 \end{pmatrix}, \begin{pmatrix} u1 \\ 0 \end{pmatrix}, \begin{pmatrix} 0 \\ u1 \end{pmatrix} \right) / \sqrt{2} \quad u1 = ((qL-) + (qR-)) / \sqrt{2}$ $Hq = \left(\begin{pmatrix} u1 \\ u1 \end{pmatrix}, \begin{pmatrix} u1 \\ u1 \end{pmatrix}, \begin{pmatrix} u1 \\ u1 \end{pmatrix}, \begin{pmatrix} u1 \\ u1 \end{pmatrix} \right) / 2 \quad u1 = ((qL-) + (qL+) + (qR-) + (qR+)) / 2$	

For the hc-boson wavefunction we apply here the full Ritz-Galerkin series on the function system

$$f_k(r, \theta) = \{ bfunc(r, r_0, dr_0) r^{k_1}, k_1 = 0, \dots, n_r \} \times \{ (\cos^{k_2} \theta, \cos^{k_2} \theta \sin \theta), k_2 = 0, \dots, n_\theta \}$$

with coefficients α_k , where $bfunc(r, r_0, dr_0) = \frac{1}{1 + \exp\left(\frac{r - r_0}{dr_0}\right)}$ is a Fermi-step-

function which limits the region $r \leq r_0$ of the preon with “smearing width” dr_0 .

$$Ag_i(t, r, \theta) = \left\{ \begin{array}{l} Ag_{i1}(t, r, \theta) \cos aA_i \\ Ag_{i2}(t, r, \theta) \cos aA_i \\ Ag_{i1}(t, r, \theta) \sin aA_i \\ Ag_{i2}(t, r, \theta) \sin aA_i \end{array} \right\}, i = 1, \dots, 15 \quad (12)$$

where aA_i is the phase angle between the particle and the anti-particle part of the hc-boson, and with the Ritz-Galerkin-expansion

$$Ag_{kl}(t, r, \theta) = \sum_j \alpha[k, l, j] f_j(r, \theta) \exp(-it EA_k), \quad k = 1, \dots, 15; l = 1, 2$$

with energies EA_k

Because of hc-symmetry, the active (non-zero) hc-bosons are

$Ag = \{Ag_1, \dots, Ag_{15}\}$ all hc-bosons: generation 3, flavor = 3

$Ag = \{Ag_{ij}, \bar{A}g_{ij}, Ag_{kl}, \bar{A}g_{kl}\}$ 4 hc-bosons: coupler and anti-coupler for hc-indices (i, j) and the corresponding 2 coupler-anti-coupler pair for the complementary indices (k, l) : generation 2, flavor = 2

$Ag = \{Ag_{ij}\}$ one hc-boson for the hc-indices (i, j) : generation 1, flavor = 1.

Preon wavefunction

The hc-quadruplet has 4 positions with the hc-charges $\{L-, L+, R-, R+\}$, and the particle wavefunction of a fermion (lepton or quark) has two positions occupied with indices (i, j)

$u = \{..(u_1)..(u_2)..\}$ u_1 and u_2 are preon Weyl spinors with 2 components.

For the preons we use here a model of a gaussian “blob”

$$u_k(t, r, \theta) = \left(\begin{array}{l} \exp(-it Eu_k) \exp\left(-\frac{(\vec{r} - \vec{r}_{u,k})^2}{2 dr_{u,k}}\right) \cos a_k \\ \exp(-it Eu_k) \exp\left(-\frac{(\vec{r} - \vec{r}_{u,k})^2}{2 dr_{u,k}}\right) \sin a_k \end{array} \right) \quad (13)$$

where Eu_k is the energy, $\vec{r}_{u,k} = (ru_k, \theta u_k)$ and $dr_{u,k}$ is the position (r, θ) and its width, a_k is a phase.

A basic particle of the Standard Model consists of 2 preons u_i and 1, 4, 15 hc-bosons Ag_i for generation 1, 2, 3 respectively. The hc-boson number i of Ag_i is equal to the general Gell-Mann matrix λ_4 .

For instance, the electron has one hc-boson $Ag_4 = A13$ corresponding Gell-Mann matrix λ_4 , and the preon configuration

electron $e = (rL-, rR-)$, occupied positions (1, 3)

$$\text{electron configuration: } u = \left(\left(\begin{array}{c} r_{L-} \\ 0 \end{array} \right), 0, \left(\begin{array}{c} r_{R-} \\ 0 \end{array} \right), 0 \right)$$

$$\text{Antiparticle positron configuration } \bar{u} = \left(0, \left(\begin{array}{c} 0 \\ r_{L+} \end{array} \right), 0, \left(\begin{array}{c} 0 \\ r_{R+} \end{array} \right) \right)$$

The SU(4) Lagrangian

From 2.1 we have for the SU(4) Lagrangian

$$L_{QCD} = \bar{u} \left(i \gamma^\mu D_\mu - m \right) u - \frac{1}{4} F_{\mu\nu}^a F_a^{\mu\nu},$$

where u is the particle (lepton or quark) wave function defined above, and the covariant derivative is $D_\mu = \partial_\mu - i g A g_\mu^a \lambda_a$ with SU(4) Gell-Mann 4×4 matrices λ_a ($a = 1, \dots, 15$) and the field tensor is

$$F_{a,\mu\nu} = \partial_\mu (A g_\nu^a) - \partial_\nu (A g_\mu^a) + g f^{abc} (A g_b)_\mu (A g_c)_\nu,$$

where $A g_a$ are the hc-boson wavefunctions ($a = 1, \dots, 15$).

The action is $S = \int L_{QCD} (x^\mu, u_i, A g_i) r^2 \sin \theta dt dr d\theta d\phi$, which is to be integrated over the particle volume V and minimized in the parameters of u and $A g^a$.

The parameters of the component preons and the hc-bosons within a particle are (see below):

$$par(u_i) = \{Eu_i, a_i, ru_i, \theta u_i, dru_i\}, \quad par(A g_i) = \{EA_i, aA_i\},$$

where Eu_i and EA_i are energies, a_i and aA_i are internal phases, $(ru_i, \theta u_i, dru_i)$ describe particle's location and smear-out.

The calculation method of minimization of SU(4) action is shown below for the electron in a schematic **Table 4(a)**.

4.2. The Numerical Algorithm

The energy, length, and time are made dimensionless by using the units: E ($E_0 = \frac{\hbar c}{1 am} = 0.196 \text{ TeV}$), $r(\text{fm})$, $t(am/c)$ $am = 10^{-18} \text{ m}$. We can assume axial symmetry, so we can set $\varphi = 0$ and use the spherical coordinates

$$(t, r, \theta).$$

We choose the equidistant lattice for the intervals $(t, r, \theta) \in [0, 1] \times [0, 1] \times [0, \pi]$ with $21 \times 21 \times 11$ points and, for the minimization $8x$ in parallel, 8 random sublattices [4] [19]:

$$l[ix, j] = \left\{ \left\{ (t_{i1}, r_{i2}, t_{i3}) \mid (i1, i2, i3) = \text{random}(\text{lattice}, j = 1, \dots, 100) \right\} \mid ix = 1, \dots, 8 \right\}.$$

For the Ritz-Galerkin expansion in (r, θ) we use the 12 functions

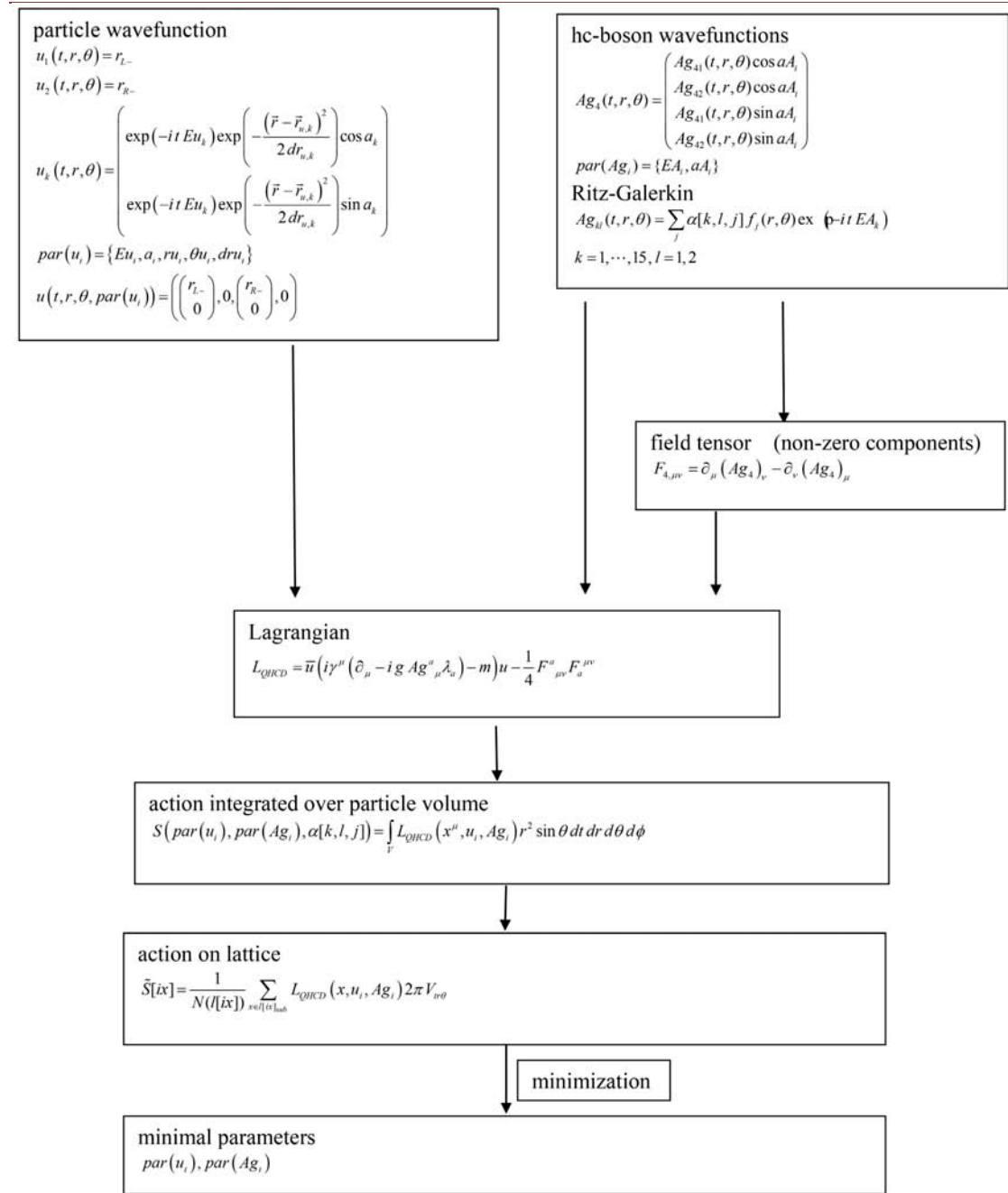
$$f_k(r, \theta) = \left\{ \text{bfunc}(r, r_0, dr_0) r^{k_1}, k_1 = 0, \dots, n_r \right\} \times \left\{ (\cos^{k_2} \theta, \cos^{k_2} \theta \sin \theta), k_2 = 0, \dots, n_\theta \right\}$$

The action $S = \int L_{QCD} (x^\mu, u_i, A g_i) r^2 \sin \theta dt dr d\theta d\phi$ becomes a mean-value on the sublattice $l[ix]$

$$\tilde{S}[ix] = \frac{1}{N(l[ix])} \sum_{x \in [ix]_{sub}} L_{QCD}(x, u_i, A g_i) 2\pi V_{r\theta},$$

where $V_{r\theta} = \pi$ the (t, r, θ) -volume and $N(l[ix])$ is the number of points. We set $N(l[ix]) = 100$ for generation 1 and 2, $N(l[ix]) = 25$ for generation 3.

Table 4(a). Minimization of SU (4) action for the electron.



We impose the boundary condition for $Ag_i(r = r_0) = 0$ via penalty-function (imposing exact conditions is possible, but slows down the minimization process enormously).

\tilde{S} is minimized 8x in parallel with the Mathematica-minimization method “simulated annealing”.

The proper parameters of the component preons and the hc-bosons within a particle are:

$$par(u_i) = \{Eu_i, a_i, ru_i, \theta u_i, dru_i\}, \quad par(Ag_i) = \{EA_i, aA_i\}$$

Eu_i is the energy-mass of the preon u_i
 a_i is $\sin(\text{phase})$ of the preon u_i , where phase is the phase between the two spinor components

$(ru_i, \theta u_i)$ is the location of the preon u_i

dru_i is the uncertainty (stdev) of ru_i

EA_i is the energy of the hc-boson Ag_i

aA_i is $\sin(\text{phase})$ of the hc-boson Ag_i , where phase is the phase between the two upper and the two lower components of the vector Ag_i

The complexities and execution times (on a 2.7 GHz Xeon E5 work-station) differ greatly for different generations.

For the generation 1 electron $e = \left(\left(\begin{matrix} rL- \\ 0 \end{matrix} \right), 0, \left(\begin{matrix} rR- \\ 0 \end{matrix} \right), 0 \right)$ with 1 hc boson A13:

complexity (Lagrangian) = 6.2×10^6 terms, minimization time t (minimization) = 37 s.

For the generation 3 tauon $\tau = \left(\left(\begin{matrix} rL- \\ 0 \end{matrix} \right), 0, \left(\begin{matrix} rR- \\ 0 \end{matrix} \right), 0 \right)$ with all 15 hc-bosons:

complexity (Lagrangian) = 283×10^6 terms, minimization time t (minimization) = 2500 s.

5. The Particles and Families of the SU(4)-Preon Model

Here we present the result of the calculation of the masses, inner structure, and some of the angles of the mixing matrices CKM and PMNS, using the minimization of the action described in chap.4.

5.1. Charged Leptons Electron, Muon, Tau

Spin $S = 1/2$, two free preons, occupying fixed positions in the hc-tetra-spinor

Preon configuration: $u = \left(\left(\begin{matrix} rL- \\ 0 \end{matrix} \right), 0, \left(\begin{matrix} rR- \\ 0 \end{matrix} \right), 0 \right)$

Boson configuration: flavor = 1: ($A13 = \lambda4$), flavor = 2:
 $(A13 = \lambda4, \bar{A}13 = \lambda5, A24 = \lambda11, \bar{A}24 = \lambda12)$

flavor = 3: all 15 bosons

The leptons are charged particles, they interact electromagnetically or weakly via Z and W bosons.

The leptons are spherically symmetric, and have therefore the gyromagnetic ratio $g = 2$ exactly, which is valid from the Dirac-equation for a point-like (or spherically symmetric) spin-1/2-particle.

The spherical symmetry arises from the fact, that all leptons consist of two r-preons, which differ only in the hc-charge, so it is plausible that their geometric parameters are equal (equal radius r_b , its uncertainty dr_b , equal phase angle a_b , and inter-preon-angle $\theta = 0$), as is shown in calculation.

In the energy distribution, the preons (shown in the first two values: $i = (1, 2)$) have considerably less energy than the hc-bosons in the case of the muon and

the tauon, for the electron the only hc-boson carries almost all of the energy.

The calculated and observed masses of the charged leptons are shown in **Table 5**.

The energy of component preons and field bosons are shown in **Figures 4-6**.

The structure, *i.e.* calculated average distances of components with smear-out are shown in **Figure 7**.

The parameters of the three generations (flavors) are shown in **Tables 6-8**.

Table 5. Charged lepton masses.

	$m(e)$	$m(\mu)$	$m(\tau)$
exp.	0.511 MeV	106 MeV	1.78 GeV
calc.	0.29 ± 0.23 MeV	228 ± 150 MeV	2.26 ± 0.7 GeV

Table 6. Parameters of the electron.

Eu_i (MeV)	EA_i	a_i	aA_i	dru_i	ru_i	$\sin(\theta_{u_i})$
0.0256, 0.0256	0.241	-0.27, -0.27	-0.017	0.104, 0.104	0.276, 0.276	0
ΔEu_i	ΔEA_i	Δa_i	ΔaA_i	Δdru_i	Δru_i	$\Delta \sin(\theta_{u_i})$
0.057, 0.044	0.121	.	.	0.058, 0.058	0.014, 0.014	.

Table 7. Parameters of the muon.

Eu_i (MeV)	EA_i	a_i	aA_i	dru_i	ru_i	$\sin(\theta_{u_i})$
24.06, 24.06	0.00036, 0.0013, 46.33, 133.75	-0.48, -0.48	0.24, 0.266, -0.55, -0.632	0.648, 0.648	0.68, 0.68	0
ΔEu_i	ΔEA_i	Δa_i	ΔaA_i	Δdru_i	Δru_i	$\Delta \sin(\theta_{u_i})$
18.32, 18.32	0.00045, 0.0011, 30.89, 87.17	.	.	0.045, 0.045	0.047, 0.047	.

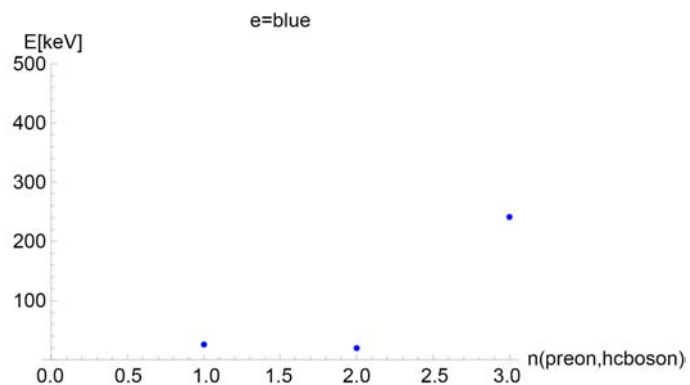


Figure 4. Energy distribution of electron: first preons (u_1, u_2), then bosons Ag_i .

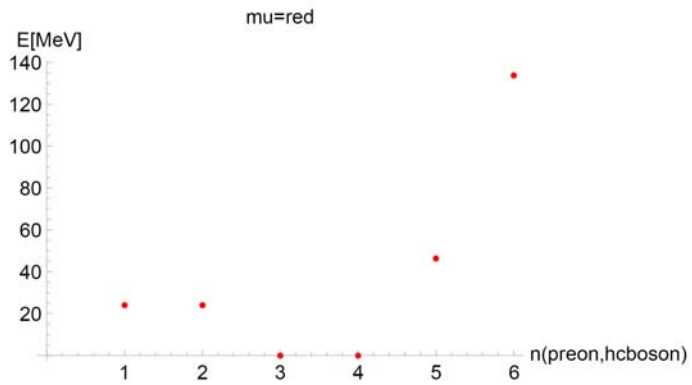


Figure 5. Energy distribution of muon: first preons (u_1, u_2), then bosons A_i .

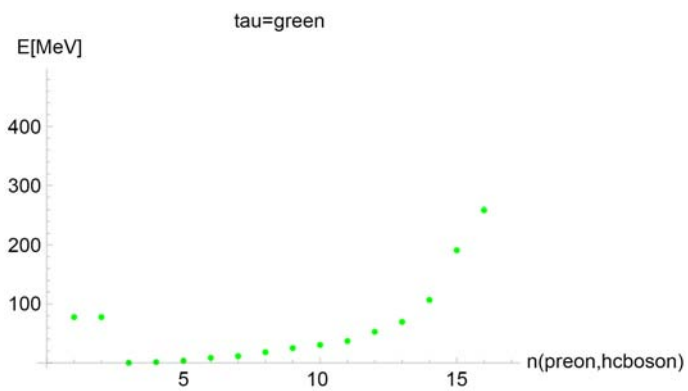


Figure 6. Energy distribution of tauon: first preons (u_1, u_2), then bosons A_i .

Table 8. Parameters of the tauon.

Eu_i MeV	EA_i	a_i	aA_i	dru_i	ru_i	$\sin(\theta_{u_i})$
			-0.33192, -0.0188942,			
	0.000258, 1.274,		-0.0449149, -0.325663,			
	3.51, 8.51, 11.45,		-0.0118209, \			
77.68,	18.12, 25.0369,	0.216842,	-0.0943335, -0.226005,	0.19,	0.36,	0
77.68	30.46, 37.057,	0.216842	-0.149676, 0.143007,	0.19	0.36	
	52.78, 69.55,		0.0745547,			
	106.83, 191.129,		0.102575, -0.154493,			
	259.009, 1297.48		-0.0987211, -0.161108,			
			-0.0258635			
ΔEu_i	ΔEA_i	Δa_i	ΔaA_i	Δdru_i	Δru_i	$\Delta \sin(\theta_{u_i})$
	0.00028103,					
	1.68893,					
	2.36353, 5.65246,					
77.66,	6.56911, 9.40924,			0.033,	0.076,	
77.66	11.9228, 11.9599,	.		0.033	0.077	
	15.7698,					
	30.2164, 34.4179,					
	17.5376, 107.57,					
	106.864, 180.17					

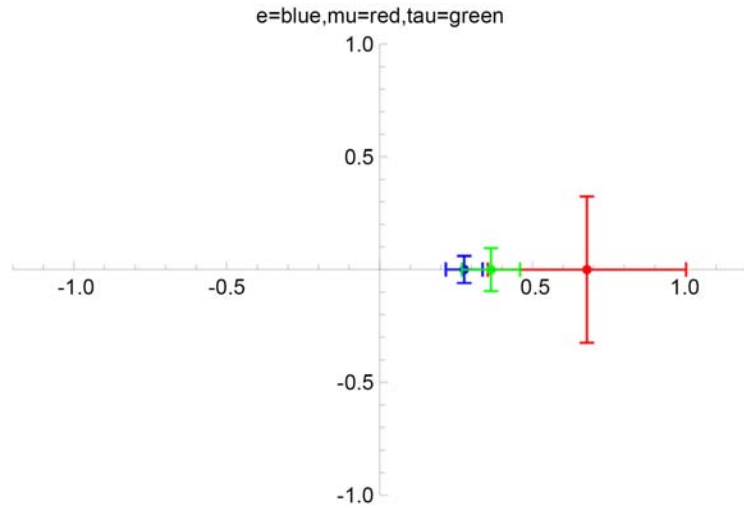


Figure 7. Structure of charged leptons: preons ($u1, u2$) radii r_i , uncertainty dr_i and angle θ_i .

electron e = (rL-, rR-)

$$\text{Preon configuration: } u = \left(\begin{pmatrix} rL- \\ 0 \end{pmatrix}, 0, \begin{pmatrix} rR- \\ 0 \end{pmatrix}, 0 \right)$$

$$\text{Antiparticle positron } \bar{u} = \left(0, \begin{pmatrix} 0 \\ rL+ \end{pmatrix}, 0, \begin{pmatrix} 0 \\ rR+ \end{pmatrix} \right)$$

hc-boson $Ag_4 \hat{=} \lambda_4$, as $A13 = \lambda_4$

$$E_{exp} = 0.511 \text{ MeV } Q = -1$$

$$E_{tot} = 0.29 \text{ MeV}, \Delta E_{tot} = 0.23 \text{ MeV}$$

muon mu = (rL-, rR-)

hc-bosons

$$Ag_4 = A13 \hat{=} \lambda_4, Ag_5 = \bar{A}13 \hat{=} \lambda_5, Ag_{11} = A24 \hat{=} \lambda_{11}, Ag_{12} = \bar{A}24 \hat{=} \lambda_{12}$$

$$E_{exp} = 106 \text{ MeV } Q = -1$$

$$E_{tot} = 228 \text{ MeV}, \Delta E_{tot} = 154$$

taupon tau = (rL-, rR-)

hc-bosons: all 15 Ag_1, \dots, Ag_{15}

$$E_{exp} = 1.78 \text{ GeV } Q = -1$$

$$E_{tot} = 2.26 \text{ GeV}, \Delta E_{tot} = 0.70.$$

5.2. Lepton Neutrinos $\nu_e, \nu_{mu}, \nu_{tau}$

Spin $S = 1/2$, two free preons, occupying fixed positions in the hc-tetra-spinor

$$\text{Preon configuration: } u = \left(\begin{pmatrix} rL- \\ 0 \end{pmatrix}, \begin{pmatrix} 0 \\ rL+ \end{pmatrix}, 0, 0 \right)$$

Boson configuration: flavor = 1: ($A12 = \lambda_1$), flavor = 2:

$$(A12 = \lambda_1, \bar{A}12 = \lambda_2, A34 = \lambda_{13}, \bar{A}34 = \lambda_{14})$$

flavor = 3: all 15 bosons

The lepton neutrinos [27] are spherically symmetric, as shown in the calculation, and have therefore zero magnetic momentum. The spherical symmetry

arises from the fact, that all leptons consist of two r-preons, which differ only in the hc-charge, so it is plausible that their geometric parameters are equal (equal radius r_b , its uncertainty dr_b , equal phase angle a_b , and inter-preon-angle $\theta = 0$).

The lepton neutrinos are neutral, interact only weak via Z and W bosons.

As for mass, the best upper limit from cosmological data is $m < 0.12$ eV.

The calculated masses of the lepton neutrinos are shown in **Table 9**.

The energy of component preons and field bosons are shown in **Figure 8**.

The structure, *i.e.* calculated average distances of components with smear-out are shown in **Figure 9**.

The parameters of the three generations (flavors) are shown in **Tables 10-12**.

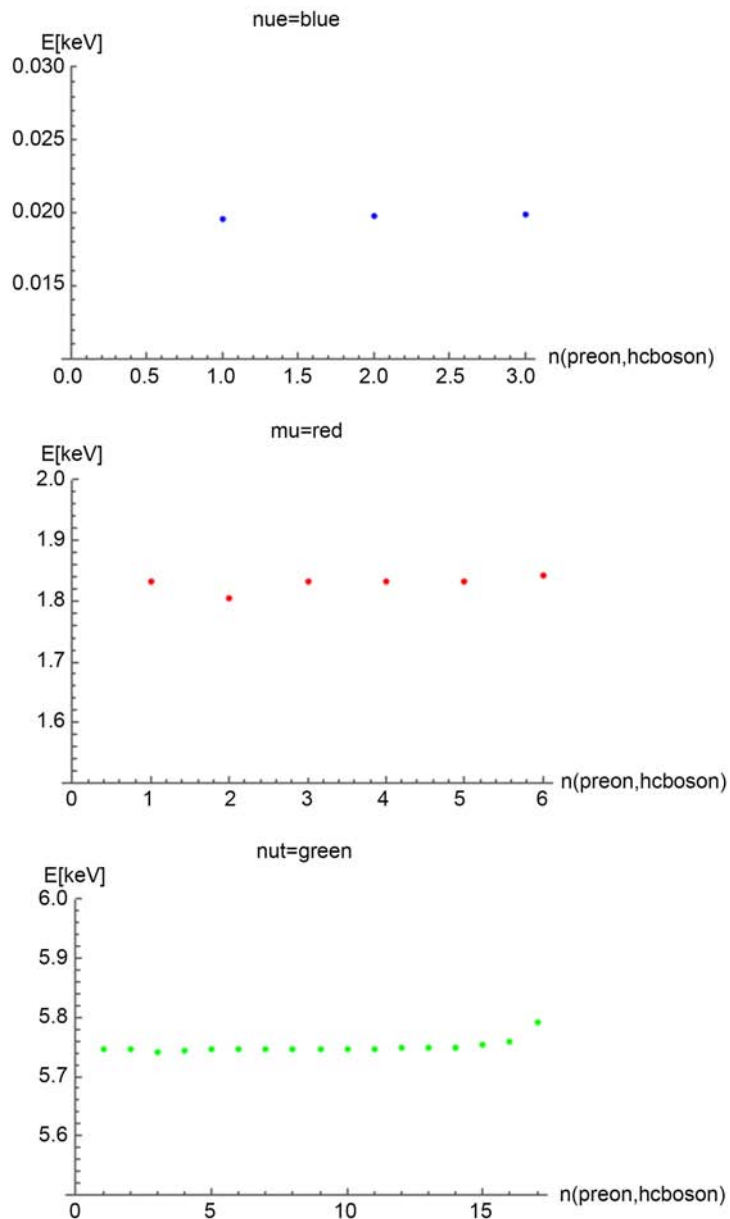


Figure 8. Energy distribution of lepton neutrinos: first preons ($u1, u2$), then bosons A_i .

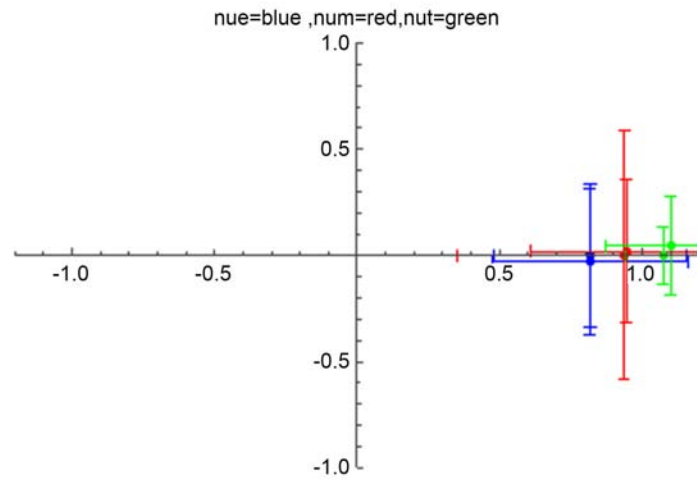


Figure 9. Structure of lepton neutrinos: preons ($u1, u2$) radii r_i , uncertainty dr_i and angle θ_i .

Table 9. Lepton neutrino masses.

	m (nue)	m (num)	m (nut)
exp.			
calc.	0.30 meV	11 meV	98 meV

Table 10. Parameters of the electron neutrino.

Eu_i (meV)	EA_i	a_i	aA_i	dru_i	ru_i	$\sin(\theta_{u_i})$
0.0195789, 0.0198162	0.0198727	-0.00159052, 0.00281348	0.000719502	0.672092, 0.672795	0.817591, 0.817365	-0.0362275
ΔEu_i	ΔEA_i	Δa_i	ΔaA_i	Δdru_i	Δru_i	$\Delta \sin(\theta_{u_i})$
0.000442384, 0.000217995	0.0000872723	.		0.0533686, 0.0533475	0.000416971, 0.00028167	

Table 11. Parameters of the muon neutrino.

Eu_i (meV)	EA_i	a_i	aA_i	dru_i	ru_i	$\sin(\theta_{u_i})$
1.83215, 1.80438	1.83322, 1.83333, 1.83335, 1.84298	0.00294051, 0.00304653	0.000719502	0.306423, 0.3312	0.943812, 0.936186	0.02
ΔEu_i	ΔEA_i	Δa_i	ΔaA_i	Δdru_i	Δru_i	$\Delta \sin(\theta_{u_i})$
0.00234254, 0.0359295	0.000209844, 2.8895×10^{-6} , 0.0000362216, 0.0162998	.		0.111082, 0.111082	0.126494, 0.179059	

e-neutrino nue = ($rL-, rL+$)

$$\text{Preon configuration: } u = \left(\begin{pmatrix} rL- \\ 0 \end{pmatrix}, \begin{pmatrix} 0 \\ rL+ \end{pmatrix}, 0, 0 \right)$$

Table 12. Parameters of the tauon neutrino.

E_{u_i} (meV)	EA_i	a_i	aA_i	dru_i	ru_i	$\sin(\theta_{u_i})$	
	5.74263,		0.0645884,				
	5.74519,		0.0321258,				
	5.74578,		0.0714192,				
	5.74647,		0.0356015,				
	5.74688,		0.0665154,				
	5.74707,		0.0652989,				
	5.74725,		0.060689,				
5.74691,	5.74761,	0.00216278,	0.0555585,	0.306423,	1.1011,	0.0414724	
5.74691	5.7479,	-0.0145027	0.0499117,	0.3312	1.07371		
	5.74861,		0.062275,				
	5.74951,		0.0407549,				
	5.75005,		0.0359398,				
	5.7531,		0.0666184,				
	5.7595,		0.0482816,				
	5.79127		0.031136				
ΔE_{u_i}	ΔEA_i	Δa_i	ΔaA_i	Δdru_i	Δru_i		$\Delta \sin(\theta_{u_i})$
	0.112495,						
	0.112474,						
	0.112249,						
	0.111351,						
	0.110999,						
	0.110905,						
	0.110818,						
0.110619,	0.110445,	.		0.207277,	0.0609252,		
0.110619	0.110137,			0.197369	0.06686		
	0.109776,						
	0.109065,						
	0.108836,						
	0.107668,						
	0.102724,						
	0.09513						

Antiparticle right-chiral antineutrino $\bar{u} = \left(0, 0, \begin{pmatrix} rR^- \\ 0 \end{pmatrix}, \begin{pmatrix} 0 \\ rR^+ \end{pmatrix} \right)$

$E_{exp} < 0.12$ eV $Q = 0$

$E_{tot} = 0.30$ meV, $\Delta E_{tot} = 0.038$

mu-neutrino num = (rL-, rL+)

$E_{exp} < 0.12$ eV $Q = 0$

$E_{tot} = 11.0$ meV, $\Delta E_{tot} = 0.055$

tau-neutrino nut = (rL-, rL+)

$E_{exp} < 0.12$ eV $Q = 0$

$E_{tot} = 98.0$ meV, $\Delta E_{tot} = 1.85$.

5.3. Non-Chiral Sterile (Hypothetical) Neutrinos vs1, vs2, vs3

Spin $S = 1/2$, two free preons, occupying fixed positions in the hc-tetra-spinor

$$\text{Preon configuration: } u = \left(\left(\begin{matrix} rL- \\ 0 \end{matrix} \right), 0, 0, \left(\begin{matrix} 0 \\ rR+ \end{matrix} \right) \right)$$

Boson configuration: flavor = 1: ($A_{14} = \lambda_9$), flavor = 2:
 ($A_{14} = \lambda_9, \bar{A}_{14} = \lambda_{10}, A_{23} = \lambda_6, \bar{A}_{23} = \lambda_7$)
 flavor = 3: all 15 bosons

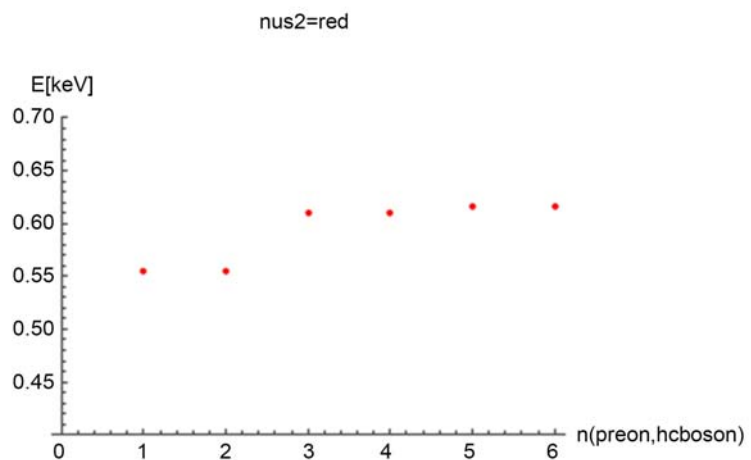
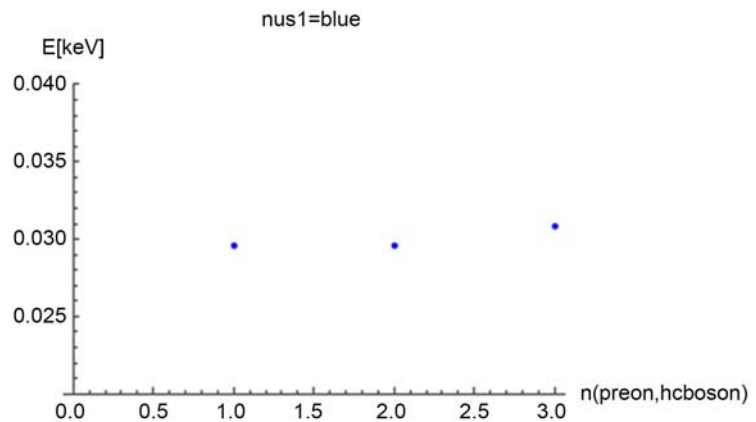
The hypothetical sterile neutrinos are involved in the neutron decay and interact only among themselves and with lepton neutrinos via the weak chiral boson ZL (see 4.1), so the denomination “sterile” is justified. They have similar masses as the lepton neutrinos, but they are Majorana particles: antiparticle = particle. Like lepton neutrinos, they are spherically symmetric and have zero magnetic momentum.

The calculated masses of the sterile neutrinos are shown in **Table 13**.

The energy of component preons and field bosons are shown in **Figure 10**.

The structure, *i.e.* calculated average distances of components with smear-out are shown in **Figure 11**.

The parameters of the three generations (flavors) are shown in **Tables 14-16**.



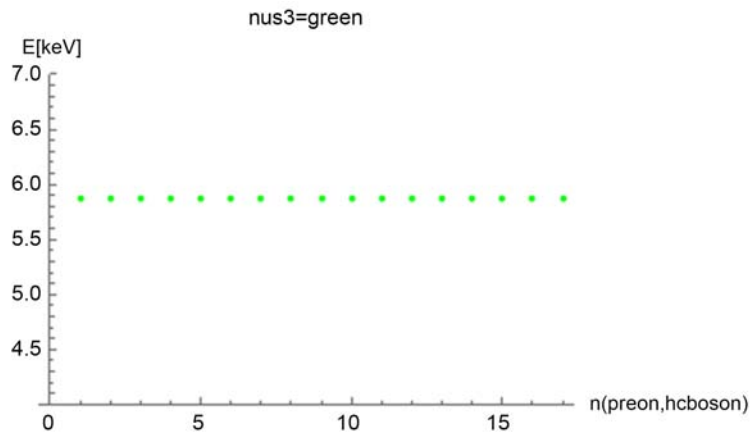


Figure 10. Energy distribution of sterile neutrinos: first preons ($u1, u2$), then bosons A_i .

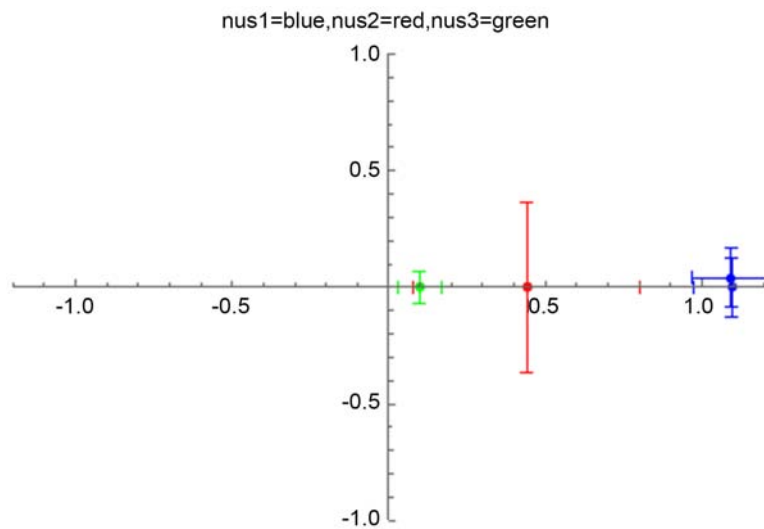


Figure 11. Structure of sterile neutrinos: preons ($u1, u2$) radii r_i , uncertainty dr_i and angle θ_i .

Table 13. Masses of sterile neutrinos.

	$m(\text{nus1})$	$m(\text{nus2})$	$m(\text{nus3})$
exp.			
calc.	0.09 meV	3.6 meV	100 meV

Table 14. Parameters of the sterile e-neutrino.

Eu_i (meV)	EA_i	a_i	aA_i	dru_i	ru_i	$\sin(\theta_{u_i})$
0.0295438, 0.0295438	0.03085	0.00981786, -0.00539754	0.000719502	0.247601, 0.245064	1.0941, 1.09465	0.0385823
ΔEu_i	ΔEA_i	Δa_i	ΔaA_i	Δdru_i	Δru_i	$\Delta \sin(\theta_{u_i})$
0.000714214, 0.000714214	0.000840173	.		0.00802575, 0.00776682	0.00348974, 0.00362492	

Table 15. Parameters of the sterile mu-neutrino.

E_{u_i} (meV)	EA_i	a_i	aA_i	dru_i	ru_i	$\sin(\theta_{u_i})$
	0.610776,		0.524038,			
0.555866,	0.610849,	0.0837203,	0.145884,	2.22087,	0.439613,	0.0
0.555866	0.616444,	0.0837203	0.584979,	2.22087	0.439613	
	0.616708		0.615694			
ΔE_{u_i}	ΔEA_i	Δa_i	ΔaA_i	Δdru_i	Δru_i	$\Delta \sin(\theta_{u_i})$
	0.029421,					
0.0579322,	0.0294231,			1.8611,	0.337827,	
0.0579322	0.0244551,			1.8611	0.337827	
	0.0243638					

Table 16. Parameters of the sterile tau-neutrino.

E_{u_i} (meV)	EA_i	a_i	aA_i	dru_i	ru_i	$\sin(\theta_{u_i})$	
	5.88029,		0.0517683,				
	5.88029,		0.0478681,				
	5.88029,		0.156694,				
	5.88029,		0.0480563,				
	5.88029,		0.0494643,				
	5.88029,		0.0577212,				
5.87822,	5.88029,	0.0997489,	0.0685586,	0.0261638,	0.0974364,	0.0	
5.87822	5.88029,	0.0997489	0.155112,	0.0261638	0.0974364		
	5.88029,		0.0500668,				
	5.88029,		0.050109,				
	5.88029,		0.0505401,				
	5.88029,		0.15493,				
	5.88029,		0.468362,				
	5.88029,		0.154732,				
	5.88029		0.155897				
ΔE_{u_i}	ΔEA_i	Δa_i	ΔaA_i	Δdru_i	Δru_i		$\Delta \sin(\theta_{u_i})$
	0.00339045,						
	0.00339045,						
	0.00339044,						
	0.00339043,						
	0.00339043,						
	0.00339043,						
	0.00339042,						
0.00678084,	0.00339042,			0.0738441,	0.0850158,		
0.00678084	0.00339042,			0.0738441	0.0850158		
	0.00339042,						
	0.00339042,						
	0.00339041,						
	0.00339011,						
	0.00338995,						
	0.00338953,						
	0.00338949						

nc-neutrino 1 nus1 = (rL-, rR+)

$$\text{Preon configuration: } u = \left(\left(\begin{matrix} rL- \\ 0 \end{matrix} \right), 0, 0, \left(\begin{matrix} 0 \\ rR+ \end{matrix} \right) \right)$$

Antiparticle $\bar{u} = u$ (Majorana neutrino)

$$E_{exp} = ? \quad Q = 0$$

$$E_{tot} = 0.090 \text{ meV}, \Delta E_{tot} = 0.023$$

nc-neutrino 2 nus2 = (rL-, rR+)

$$E_{exp} = ? \quad Q = 0$$

$$E_{tot} = 3.56 \text{ meV}, \Delta E_{tot} = 0.22$$

nc-neutrino 3 nus3 = (rL-, rR+)

$$E_{exp} = Q = 0$$

$$E_{tot} = 100 \text{ meV}, \Delta E_{tot} = 0.064.$$

5.4. U-Quarks u, c, t

Spin $S = 1/2$, two free preons, occupying fixed positions in the hc-tetra-spinor

$$\text{Preon configuration: } u = \left(0, \left(\frac{(rL++qL+)}{\sqrt{2}} \right), 0, \left(\frac{(rR++qR+)}{\sqrt{2}} \right) \right)$$

Boson configuration: flavor = 1: ($A_{24} = \lambda_{11}$), flavor = 2:

$$(A_{24} = \lambda_{11}, \bar{A}_{24} = \lambda_{12}, A_{13} = \lambda_{13}, \bar{A}_{13} = \lambda_{14})$$

flavor = 3: all 15 bosons

The U-quarks have the composition (r+, q+), and they are non-chiral, *i.e.* a superposition of (rL+, qR+) and (rR+, qL+). They are non-symmetric in r and q, so their internal structure is cylinder-symmetric or ring-symmetric, therefore there are corrections to the standard gyromagnetic factor 2, like for the nucleons. They carry the color charge, and do not appear separately, as the overall color must be zero (white).

The calculated and observed masses of the U-quarks are shown in **Table 17**.

The energy of component preons and field bosons are shown in **Figure 12**.

The structure, *i.e.* calculated average distances of components with smear-out are shown in **Figure 13**.

The parameters of the three generations (flavors) are shown in **Tables 18-20**.

Table 17. Masses of U-quarks.

	$m(u)$	$m(c)$	$m(t)$
exp.	2.3 MeV	1.34 GeV	171 GeV
calc.	$2.35 \pm 0.26 \text{ MeV}$	$3.2 \pm 1.87 \text{ GeV}$	$163 \pm 55 \text{ GeV}$

Table 18. Parameters of the up-quark.

$Eu_i \text{ (MeV)}$	EA_i	a_i	aA_i	dru_i	ru_i	$\sin(\theta u_i)$
0.00100815, 0.00100963	1.58472	0.0674651, 0.100981	-0.538922	0.209696, 0.253259	0.0263, -0.280785	0.318731
ΔEu_i	ΔEA_i	Δa_i	ΔaA_i	Δdru_i	Δru_i	$\Delta \sin(\theta u_i)$
0.000620367, 0.00057238	0.254744	.	.	0.0522386, 0.0483211	0.0472523, 0.0327625	.

Table 19. Parameters of the c-quark.

Eu_i (MeV)	EA_i	a_i	aA_i	dru_i	ru_i	$\sin(\theta u_i)$
	84.6596,		0.187462,			
207.62,	281.775,	-0.0473157,	0.228959,	0.157295,	0.0654933,	0.15086
158.774	304.222,	-0.196647	0.152956,	0.31158	0.259696	
	2180.43		-0.33979			
ΔEu_i	ΔEA_i	Δa_i	ΔaA_i	Δdru_i	Δru_i	$\Delta \sin(\theta u_i)$
	281.296,					
482.44,	312.201,			0.0332725,	0.00845404,	
296.717	159.539,			0.0300652	0.00406528	
	339.955					

Table 20. Parameters of the t-quark.

Eu_i (MeV)	EA_i	a_i	aA_i	dru_i	ru_i	$\sin(\theta u_i)$
	447.568,		0.0345205,			
	1324.51,		-0.0889711,			
	1905.22,		0.117581,			
	3572.08,		0.0804355,			
	4060.9,		0.0439144,			
	5512.97,		0.0473357,			
16169.4,	7201.35,	0.260102,	-0.10843,	2.30158,	0.661335,	0.381818
10963.2	8224.84,	-0.288355	0.016335,	2.56518	-0.588081	
	8756.76,		-0.129588,			
	9567.63,		-0.247394,			
	11233.9,		-0.0279795,			
	12195.9,		-0.18897,			
	14838.4,		-0.337228,			
	19649.7,		0.0823711,			
	27968.5		-0.174481			
ΔEu_i	ΔEA_i	Δa_i	ΔaA_i	Δdru_i	Δru_i	
	650.619,					
	827.92,					
	845.732,					
	723.36,					
	260.622,					
	1147.26,					
10545.1,	2692.84,			0.896934,	0.559172,	
7710.93	3336.08,			0.609087	0.505538	
	3111.95,					
	2532.61,					
	1738.6,					
	1466.69,					
	3647.34,					
	7499.15,					
	7115.09					

up-quark $u = (rL+ + qR+)/\sqrt{2}$

Preon configuration: $u = \left(0, \left(\frac{(rL++qL+)}{\sqrt{2}} \right), \left(\frac{(rL++qL+)}{\sqrt{2}} \right), 0, \left(\frac{(rR++qR+)}{\sqrt{2}} \right), \left(\frac{(rR++qR+)}{\sqrt{2}} \right) \right)$

$$\text{Antiparticle } \bar{u} = \left(\left(\frac{(rL - +qL -)}{\sqrt{2}} \right), 0, \left(\frac{(rR - +qR -)}{\sqrt{2}} \right), 0 \right)$$

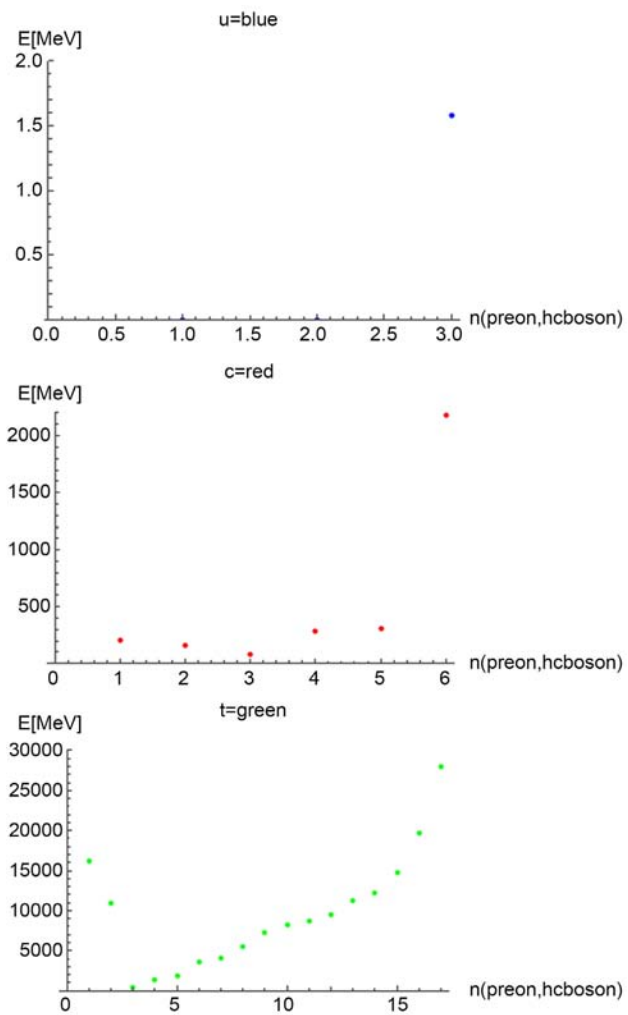


Figure 12. Energy distribution of U-quarks: first preons ($u1$, $u2$), then bosons A_i .

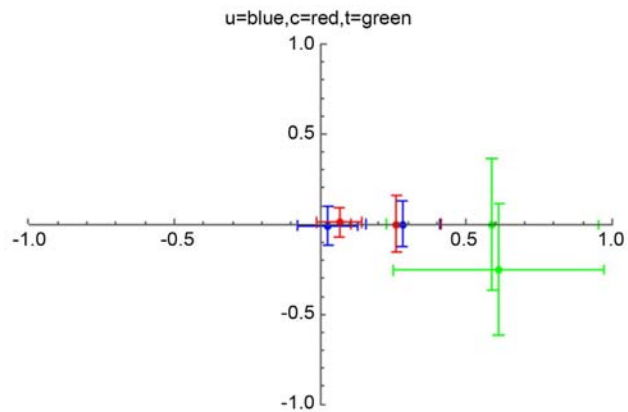


Figure 13. Structure of U-quarks: preons ($u1$, $u2$) radii r_i , uncertainty dr_i and angle θ_i .

hc-boson $Ag_{11} \hat{=} \lambda_{11}$

$E_{exp} = 2.3 \text{ MeV } Q = +2/3$

$E_{tot} = 2.35 \text{ MeV}, \Delta E_{tot} = 0.26$

c-quark $c = (rL+ + qR+)/\sqrt{2}$

hc-bosons

$Ag_{11} = A_{24} \hat{=} \lambda_{11}, Ag_{12} = \bar{A}_{24} \hat{=} \lambda_{12}, Ag_4 = A_{13} \hat{=} \lambda_4, Ag_5 = \bar{A}_{13} \hat{=} \lambda_5$

$E_{exp} = 1.34 \text{ GeV } Q = +2/3$

$E_{tot} = 3.2 \text{ GeV}, \Delta E_{tot} = 1.87$

t-quark $t = (rL+ + qR+)/\sqrt{2}$

hc-bosons: all 15 Ag_1, \dots, Ag_{15}

$E_{exp} = 171 \text{ GeV } Q = +2/3$

$E_{tot} = 163 \text{ GeV}, \Delta E_{tot} = 55.$

5.5. D-Quarks d, s, b

Spin $S = 1/2$, two free preons, occupying fixed positions in the hc-tetra-spinor

$$\text{Preon configuration: } u = \left(\left(\begin{matrix} (rL- + qL+)/\sqrt{2} \\ 0 \end{matrix} \right), 0, \left(\begin{matrix} (rR- + qR+)/\sqrt{2} \\ 0 \end{matrix} \right), 0 \right)$$

Boson configuration: flavor = 1: ($A_{13} = \lambda_4$), flavor = 2:

($A_{13} = \lambda_4, \bar{A}_{13} = \lambda_5, A_{24} = \lambda_{11}, \bar{A}_{24} = \lambda_{12}$)

flavor = 3: all 15 bosons

The D-quarks have the composition ($r-, q+$), and they are non-chiral, *i.e.* a superposition of ($rL-, qR+$) and ($rR-, qL+$). They are non-symmetric in r and q, so their internal structure is cylinder-symmetric or ring-symmetric, therefore there are corrections to the standard gyromagnetic factor 2, like for the nucleons.

Apparently, the breaking of spherical symmetry is caused by flavor-mixing, as demonstrated in the dC-quark.

They carry the color charge, and do not appear separately, as the overall color must be zero (white).

D-quark flavors intermix via the CKM-matrix, its angles can be calculated (see dC-quark) by making a linear combination with variable CKM-angles, inserting into the hc-Lagrangian and minimizing. The solution is the energetically optimal CKM-mixture and yields the observed CKM-angles.

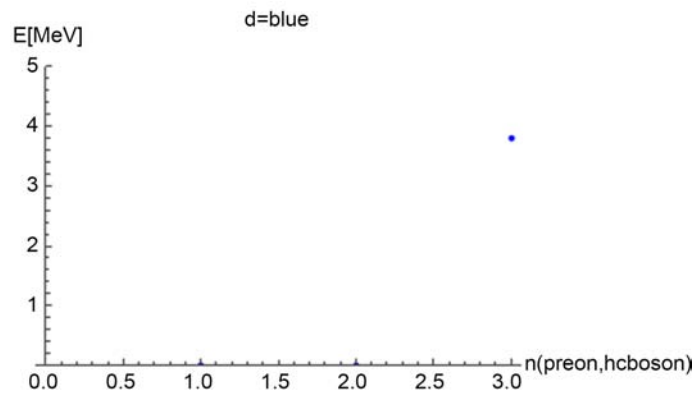
The calculated and observed masses of the D-quarks are shown in **Table 21**.

The energy of component preons and field bosons of the three flavors and Cabibbo-mixed quark (d, s) are shown in **Figure 14**.

The structure, *i.e.* calculated average distances of components with smear-out are shown in **Figure 15**.

Table 21. Masses of D-quarks.

	$m(d)$	$m(dC), \alpha(C)$	$m(s)$	$m(b)$
exp.	4.8 MeV	4.8 MeV, 13.04°	100 MeV	4.2 GeV
calc.	$4.58 \pm 0.3 \text{ MeV}$	4.74 MeV, 13.1°	$149 \pm 15 \text{ MeV}$	$6.1 \pm 2.9 \text{ GeV}$



dC = d-part of Cabibbo-mixed quark (d, s), calculated Cabibbo-angle $a_{C12} = 0.229 = 13.13^\circ$ (exp. $13.04^\circ \pm 0.05$)

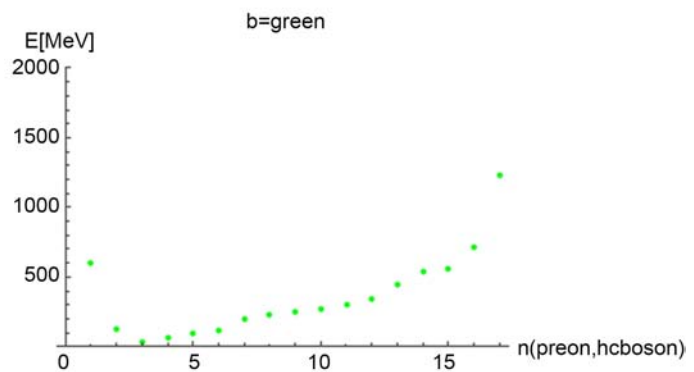
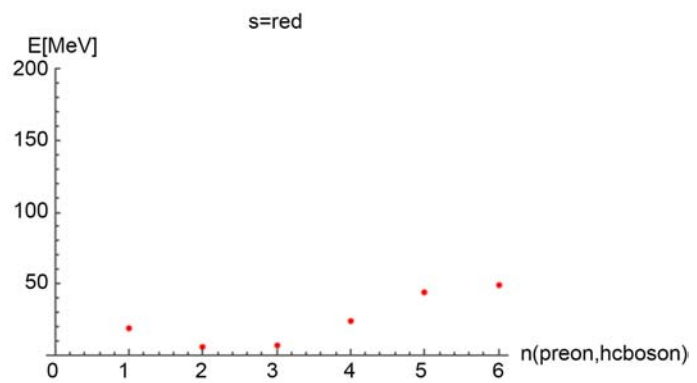
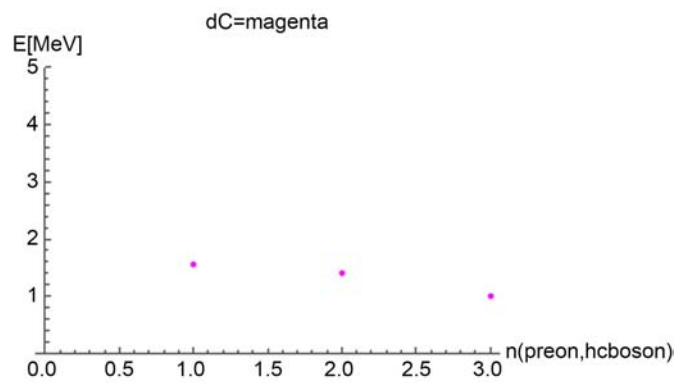


Figure 14. Energy distribution of D-quarks: first preons ($u1, u2$), then bosons A_i .

The parameters of the three of the three flavors and Cabibbo-mixed quark (d, s) are shown in **Tables 22-25**.

down-quark d = $(rL- + qR+)/\sqrt{2}$

Preon configuration: $u = \left(\left(\begin{matrix} (rL- + qL+)/\sqrt{2} \\ 0 \end{matrix} \right), 0, \left(\begin{matrix} (rR- + qR+)/\sqrt{2} \\ 0 \end{matrix} \right), 0 \right)$

Antiparticle $\bar{u} = \left(0, \left(\begin{matrix} 0 \\ (rL++ + qL-)/\sqrt{2} \end{matrix} \right), 0, \left(\begin{matrix} 0 \\ (rR++ + qR-)/\sqrt{2} \end{matrix} \right) \right)$

hc-boson: $Ag_4 \hat{=} \lambda_4$

$E_{exp} = 4.8 \text{ MeV } Q = -1/3$

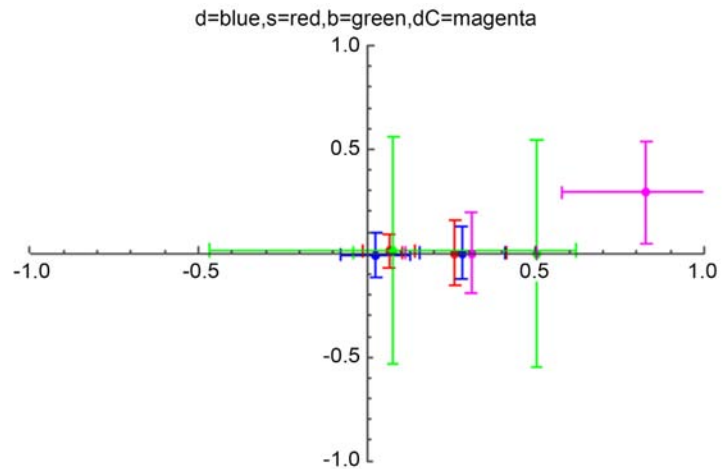


Figure 15. Structure of D-quarks: preons ($u1, u2$) radii r_i , uncertainty dr_i and angle θ .

Table 22. Parameters of the down-quark.

Eu_i (MeV)	EA_i	a_i	aA_i	dru_i	ru_i	$\sin(\theta_{u_i})$
0.0011901, 0.000620564	3.81209	0.067465, 0.100981	-0.538924	0.209696, 0.253259	0.0263002, -0.280785	0.318731
ΔEu_i	ΔEA_i	Δa_i	ΔaA_i	Δdru_i	Δru_i	$\Delta \sin(\theta_{u_i})$
0.000811471, 0.00070369	0.305601	.		0.0188066, 0.0900718	0.00476172, 0.00350625	

Table 23. Parameters of the s-quark.

Eu_i (MeV)	EA_i	a_i	aA_i	dru_i	ru_i	$\sin(\theta_{u_i})$
18.791, 5.99053	6.94284, 24.1632, 43.9623, 48.9406	-0.047311, -0.196639	-0.339778, 0.228951, 0.164457, 0.175962	0.157295, 0.311592	0.0654906, 0.259695	0.150859
ΔEu_i	ΔEA_i	Δa_i	ΔaA_i	Δdru_i	Δru_i	$\Delta \sin(\theta_{u_i})$
1.73863, 1.93842	2.1682, 1.88257, 6.34742, 1.22757			0.018, 0.0088	0.0183405, 0.08854	

Table 24. Parameters of the b-quark.

Eu_i (MeV)	EA_i	a_i	aA_i	dru_i	ru_i	$\sin(\theta_{u_i})$	
	35.4338,		-0.119199,				
	69.6218,		0.0701848,				
	92.0785,		0.0403467,				
	120.049,		0.2601,				
	193.853,		0.0412506,				
	224.967,		0.175386,				
601.532,	255.088,	-0.350658,	-0.0645038,	2.00585,	0.0775948,	0.186426	
130.4	266.136,	0.419618	0.196578,	1.73462	0.502463		
	297.881,		0.00791169,				
	348.389,		-0.0408362,				
	446.951,		-0.309195,				
	535.473,		0.147146,				
	559.583,		0.0139774,				
	713.301,		-0.126303,				
	1232.01		-0.178367				
ΔEu_i	ΔEA_i	Δa_i	ΔaA_i	Δdru_i	Δru_i		$\Delta \sin(\theta_{u_i})$
	20.0937,						
	39.4015,						
	39.3106,						
	70.0438,						
	171.994,						
	191.423,						
472.193,	173.845,			0.903552,	0.0546897,		
67.3475	173.003,			0.675784	0.235836		
	149.678,						
	106.309,						
	107.786,						
	107.91,						
	124.87,						
	228.263,						
	689.167						

Table 25. Parameters of the Cabibbo-mixed down-quark.

Eu_i (MeV)	EA_i	a_i	aA_i	dru_i	ru_i	$\sin(\theta_{u_i})$
1.55842,		-0.624805,		0.495338,	0.877748,	0.332405
1.40699	1.00898	0.263432	-0.649125	0.386903	0.308765	
ΔEu_i	ΔEA_i	Δa_i	ΔaA_i	Δdru_i	Δru_i	$\Delta \sin(\theta_{u_i})$
1.38348,		.		0.00188066,	0.122162,	
0.700002	0.373778			0.0900718	0.0502502	

$E_{tot} = 4.58$ MeV, $\Delta E_{tot} = 0.31$

s-quark $\mathbf{s} = (rL^- + qR+)/\sqrt{2}$

hc-bosons $Ag_4 = A13 \hat{=} \lambda_4, Ag_5 = \bar{A}13 \hat{=} \lambda_5, Ag_{11} = A24 \hat{=} \lambda_{11}, Ag_{12} = \bar{A}24 \hat{=} \lambda_{12}$

$E_{exp} = 100$ MeV $Q = -1/3$

$E_{tot} = 149$ MeV, $\Delta E_{tot} = 15$

b-quark $\mathbf{b} = (rL^- + qR+)/\sqrt{2}$

hc-bosons: all 15 Ag_1, \dots, Ag_{15}

$$\begin{aligned}
 E_{exp} &= 4.2 \text{ GeV} \quad Q = -1/3 \\
 E_{tot} &= 6.1 \text{ GeV}, \Delta E_{tot} = 2.9 \\
 \text{Cabibbo-mixed down-quark } dC &= (rL^- + qR+)/\sqrt{2} \\
 E_{exp} &= 4.8 \text{ MeV} \quad Q = -1/3 \\
 E_{tot} &= 4.74 \text{ MeV}, \Delta E_{tot} = 2.45.
 \end{aligned}$$

5.6. Weak Massive Bosons W, Z0, ZL, H

Spin $S = 1$ or $= 0$, one preon $u1$: combination of one, two or four spinors

Preon configuration:

$$u = \left(0, 0, \begin{pmatrix} u1 \\ 0 \end{pmatrix}, 0 \right) \text{ for weak exchange boson } W, S = 1$$

$$u = \left(\begin{pmatrix} u1 \\ 0 \end{pmatrix}, \begin{pmatrix} 0 \\ u1 \end{pmatrix}, \begin{pmatrix} u1 \\ 0 \end{pmatrix}, \begin{pmatrix} 0 \\ u1 \end{pmatrix} \right) \text{ for weak exchange boson } Z0, S = 1$$

$$u = \left(\begin{pmatrix} u1 \\ u1 \end{pmatrix}, \begin{pmatrix} u1 \\ u1 \end{pmatrix}, 0, 0 \right) \text{ for (hypothetical) left-chiral Z-boson } ZL, S = 1$$

$$u = \left(\begin{pmatrix} u1 \\ u1 \end{pmatrix}, \begin{pmatrix} u1 \\ u1 \end{pmatrix}, \begin{pmatrix} u1 \\ u1 \end{pmatrix}, \begin{pmatrix} u1 \\ u1 \end{pmatrix} \right) \text{ for higgs } H, S = 0$$

Boson configuration: only one flavor = 3: all 15 bosons

The weak massive bosons are the Yukawa bosons of the hc -interaction, *i.e.* they mediate the residual force of the hc -interaction in the form of a exponentially decreasing potential.

As shown below, they are spherically symmetric, the only preon is located approximately at radius $r \approx 1$ am.

The L-projections of leptons and quarks interact via $SU(2)$ and (W, Z0) bosons, the R-projections of leptons and quarks interact via $SU(1)$ and Z0.

This happens because of the $SU(4)$ -symmetry breaking $SU(4) = SU(2)_L \otimes SU(1)_R \otimes SU(1)_{em}$ with their exchange bosons $\{W\} \otimes \{Z0\} \otimes \{A_{em}\}$.

The higgs H is the only scalar among them, it generates mass for leptons and quarks, and also for the r-preon.

The sterile nc -neutrinos interact $SU(2)$ -weakly with neutrinos via the (hypothetical) ZL-boson.

The calculated and observed masses of the weak massive bosons are shown in **Table 26**.

The energy of component preons and field bosons are shown in **Figure 16**.

The structure, *i.e.* calculated average distances of components with smear-out are shown in **Figure 17**.

Table 26. Masses of weak massive bosons.

	$m(W)$	$m(Z0)$	$m(ZL)$	$m(H)$
exp.	80.4 GeV	91.2 GeV		125.1 GeV
calc.	89 GeV	97 GeV	91 GeV	125 GeV

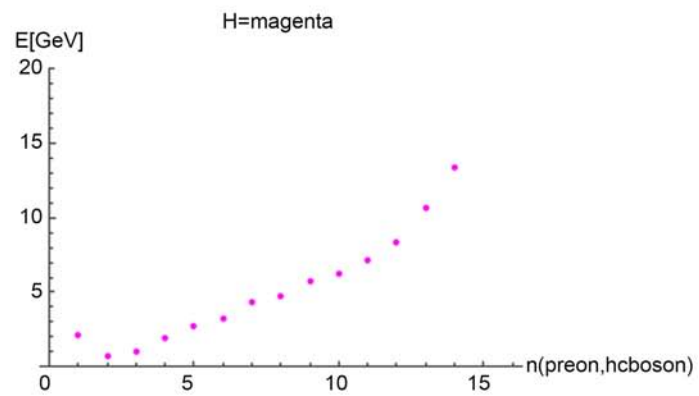
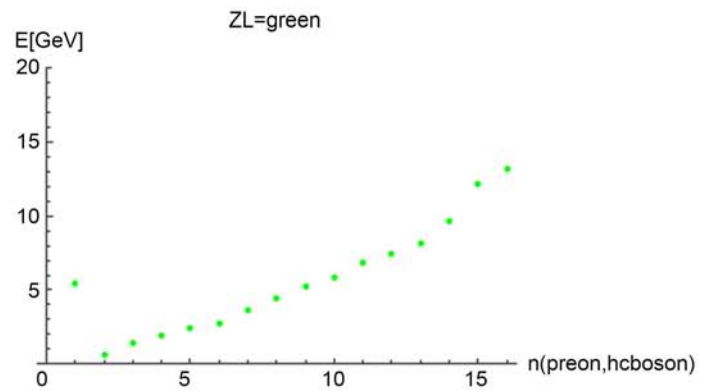
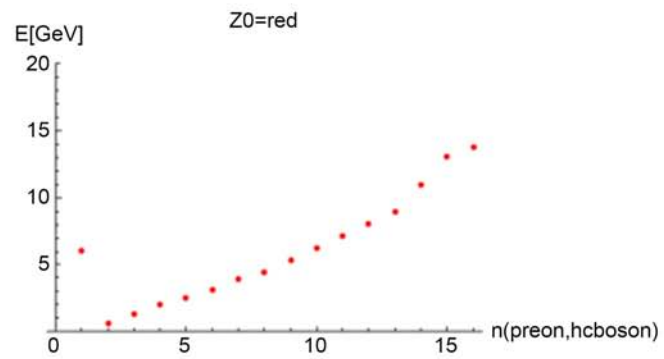
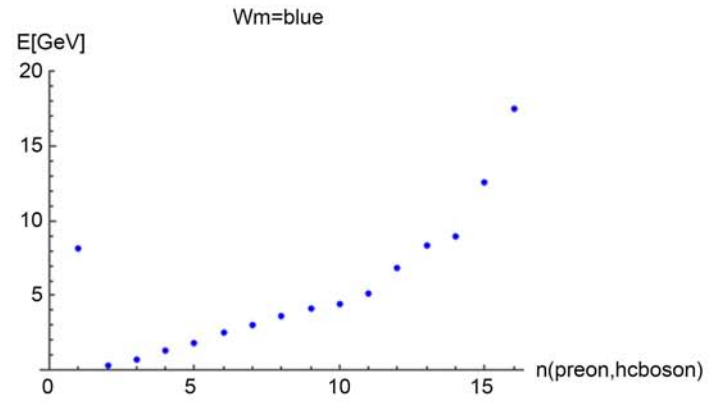


Figure 16. Energy distribution of weak massive bosons: first preons ($u1$), then bosons A_i .

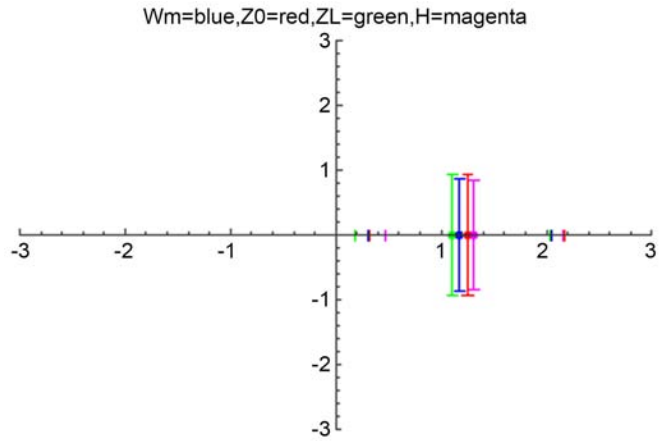


Figure 17. Structure of weak massive bosons: preons ($u1$) radii r_i , uncertainty dr_i and angle θ_i , the only preon is located approximately at radius $r \approx 1$ am.

The parameters of the individual bosons are shown in **Tables 27-30**.

weak right-handed exchange boson W^{--} $W^{--} = (rR^- - rR^-)/\sqrt{2}$, $S = 1$

Preon configuration: $u = \left(0, 0, \begin{pmatrix} u1 \\ 0 \end{pmatrix}, 0\right) \sqrt{2}$ $u1 = ((rR^-) - (rR^-))/\sqrt{2}$ antiparticle

$\bar{W} = W^+$ configuration $u = \left(0, \begin{pmatrix} 0 \\ u1 \end{pmatrix}, 0, 0\right)$ $u1 = ((rL^+) - (rL^+))/\sqrt{2}$ hypothetical chiral counterpart: left-handed W^* $u = \left(\begin{pmatrix} u1 \\ 0 \end{pmatrix}, 0, 0, 0\right)$

$u1 = ((rL^-) - (rL^-))/\sqrt{2}$

$$E_{exp} = 80.4 \text{ GeV } Q = -1$$

$$E_{tot} = 89 \text{ GeV}, \Delta E_{tot} = 26$$

neutral weak exchange boson Z_0 $Z_0 = (rL^- + rR^- + rL^+ + rR^+)/2$, $S = 1$

Preon configuration: $u = \left(\begin{pmatrix} u1 \\ 0 \end{pmatrix}, \begin{pmatrix} 0 \\ Cu1 \end{pmatrix}, \begin{pmatrix} u1 \\ 0 \end{pmatrix}, \begin{pmatrix} 0 \\ Cu1 \end{pmatrix}\right) \sqrt{2}$

$$u1 = ((rL^-) + (rR^-))/\sqrt{2} \quad Cu1 = ((rL^+) + (rR^+))/\sqrt{2}$$

antiparticle $\bar{Z}_0 = Z_0$

$$E_{exp} = 91.2 \text{ GeV } Q = 0$$

$$E_{tot} = 97 \text{ GeV}, \Delta E_{tot} = 30$$

neutral left-handed weak (hypothetical) Z_L $Z_L = (rL^- + rL^+)/\sqrt{2}$, $S = 1$

Preon configuration: $u = \left(\begin{pmatrix} u1 \\ u1 \end{pmatrix}, \begin{pmatrix} u1 \\ u1 \end{pmatrix}, 0, 0\right) \sqrt{2}$ $u1 = ((rL^-) + (rL^+))/\sqrt{2}$ antiparticle right-handed \bar{Z}_L $\bar{u} = \left(0, 0, \begin{pmatrix} u1 \\ u1 \end{pmatrix}, \begin{pmatrix} u1 \\ u1 \end{pmatrix}\right) \sqrt{2}$ $u1 = ((rR^-) + (rR^+))/\sqrt{2}$

$E_{exp} = ?$ $Q = 0$

$$E_{tot} = 91 \text{ GeV}, \Delta E_{tot} = 28$$

neutral mass-generating scalar higgs boson H $H = (rL^- + rL^+ + rR^- + rR^+)/2$, $S = 0$

Table 27. Parameters of the W-boson.

Eu_i (GeV)	EA_i	a_i	aA_i	dru_i	ru_i	$\sin(\theta_{u_i})$
8.20997	0.316331,	-0.294831	0.0551789,	2.6109	1.17267	0
	0.68873,		-0.362417,			
	1.31464,		-0.131927,			
	1.8232,		0.176835,			
	2.48807,		-0.207657,			
	3.07844,		0.0407577,			
	3.6289,		0.0430164,			
	4.09488,		0.042737,			
	4.45176,		-0.161912,			
	5.1892,		0.0364995,			
	6.90223,		0.056686,			
	8.4103,		0.0374209,			
	8.99396,		0.10742,			
	12.5852,		-0.0329776,			
17.5486	0.0255881					
ΔEu_i	ΔEA_i	Δa_i	ΔaA_i	Δdru_i	Δru_i	$\Delta \sin(\theta_{u_i})$
10.1252	0.188613,			0.81355	0.654887	
	0.334553,					
	0.70658,					
	0.801391,					
	0.626902,					
	0.823354,					
	0.876158,					
	1.0928,					
	0.869573,					
	0.559216,					
	2.0035,					
	2.08725,					
	1.95618,					
	1.91668,					
1.3873						

Table 28. Parameters of the Z0-boson.

Eu_i (GeV)	EA_i	a_i	aA_i	dru_i	ru_i	$\sin(\theta_{u_i})$
6.04329	0.601016,	-0.294831	0.0551789,	2.6109	1.17267	0
	1.31219,		-0.362417,			
	2.03588,		-0.131927,			
	2.57426,		0.176835,			
	3.10174,		-0.207657,			
	3.96319,		0.0407577,			
	4.46575,		0.0430164,			
	5.33916,		0.042737,			
	6.22519,		-0.161912,			
	7.11513,		0.0364995,			
	8.06896,		0.056686,			
	8.94095,		0.0374209,			
	10.9788,		0.10742,			
	13.0787,		-0.0329776,			
13.777	0.0255881					

Continued

$\Delta E u_i$	$\Delta E A_i$	Δa_i	$\Delta a A_i$	$\Delta d r u_i$	$\Delta r u_i$	$\Delta \sin (\theta u_i)$
	0.42354,					
	0.63418,					
	0.928717,					
	0.946956,					
	1.1372,					
	1.30358,					
	1.4114,					
4.21067	1.20844,			0.81355	0.654887	
	1.02434,					
	1.25918,					
	1.27045,					
	0.93689,					
	2.58041,					
	5.49091,					
	5.57065					

Table 29. Parameters of the ZL-boson.

$E u_i$ (GeV)	$E A_i$	a_i	$a A_i$	$d r u_i$	$r u_i$	$\sin (\theta u_i)$
	0.635455,		-0.0634903,			
	1.45762,		-0.0177523,			
	1.94515,		0.0393775,			
	2.40743,		-0.0141295,			
	2.76174,		0.238785,			
	3.62666,		0.06813,			
	4.40736,		-0.0828258,			
5.41018	5.29138,	-0.28215	-0.0566217,	4.20897	1.10542	0
	5.81184,		0.0147406,			
	6.81575,		-0.0549006,			
	7.50969,		-0.129071,			
	8.17982,		-0.193776,			
	9.70438,		0.0224101,			
	12.2009,		-0.196448,			
	13.1613		-0.0777609			
$\Delta E u_i$	$\Delta E A_i$	Δa_i	$\Delta a A_i$	$\Delta d r u_i$	$\Delta r u_i$	$\Delta \sin (\theta u_i)$
	0.361193,					
	0.294054,					
	0.542048,					
	0.685343,					
	0.734258,					
	1.14914,					
	1.37386,					
3.61896	1.86499,			0.896122	0.764349	
	2.16942,					
	2.02409,					
	1.91406,					
	1.31147,					
	1.01549,					
	4.24462,					
	4.70292					

Table 30. Parameters of the higgs H.

Eu_i (GeV)	EA_i	a_i	aA_i	dru_i	ru_i	$\sin(\theta u_i)$
2.12256	0.687867,		0.203185,			
	1.06114,		0.209845,			
	1.89688,		0.0797134,			
	2.72051,		0.249824,			
	3.1891,		0.098651,			
	4.31443,		-0.0453497,			
	4.70774,		0.111729,			
	5.75923,	0.242174	0.153663,	2.65352	1.31158	0
	6.2929,		0.156595,			
	7.21059,		0.261526,			
	8.37697,		-0.0971455,			
	10.7365,		-0.0358294,			
	13.3999,		0.0815874,			
	22.669,		0.0875567,			
30.1505		-0.0353346				
ΔEu_i	ΔEA_i	Δa_i	ΔaA_i	Δdru_i	Δru_i	$\Delta \sin(\theta u_i)$
0.963583	0.596931,					
	0.840909,					
	0.733675,					
	1.05086,					
	1.1562,					
	1.75893,					
	1.94705,					
	1.83638,				0.164707	0.599096
	2.30989,					
	2.54619,					
	2.87418,					
	4.01778,					
	2.02776,					
	10.3933,					
8.6628						

Preon configuration: $u = \left(\begin{pmatrix} u1 \\ u1 \end{pmatrix}, \begin{pmatrix} u1 \\ u1 \end{pmatrix}, \begin{pmatrix} u1 \\ u1 \end{pmatrix}, \begin{pmatrix} u1 \\ u1 \end{pmatrix} \right) / 2$
 $u1 = ((rL-) + (rL+) + (rR-) + (rR+)) / 2$
 antiparticle: itself $\bar{H} = H$
 $E_{exp} = 125.1 \text{ GeV } Q = 0$
 $E_{tot} = 125 \text{ GeV}, \Delta E_{tot} = 44.$

5.7. Strong Neutrinos (Hypothetical) qve qvm qvt

Spin S = 1/2, two free preons, occupying fixed positions in the hc-tetra-spinor

Preon configuration: $u = \left(\begin{pmatrix} qL- \\ 0 \end{pmatrix}, \begin{pmatrix} 0 \\ qL+ \end{pmatrix}, 0, 0 \right)$

Boson configuration: flavor = 1: $(A12 = \lambda_1)$, flavor = 2:
 $(A12 = \lambda_1, \bar{A}12 = \lambda_2, A34 = \lambda_{13}, \bar{A}34 = \lambda_{14})$

flavor = 3: all 15 bosons

The strong neutrinos are neutral spherically symmetric particles with composition (q^+ , q^-) and have masses starting with 23 MeV. They can hc-interact via Zq strong bosons, but only for high energies

($E \sim m(Zq) = 644 \text{ GeV}$), they are colorless and do not interact strongly.

The strong neutrinos are spherically symmetric, the two preons are located approximately at radius $r \approx 1 \text{ am}$, as shown in the structure plot below.

They are candidates for dark matter, as they are in the appropriate mass range (around 100 MeV, according to the new SIMP-scheme for dark matter), and they interact with themselves at high energies, as was observed for dark matter in certain galaxies.

The calculated masses of the strong neutrinos are shown in **Table 31**.

The energy of component preons and field bosons are shown in **Figure 18**.

The structure, *i.e.* calculated average distances of components with smear-out are shown in **Figure 19**.

The parameters of the three generations (flavors) are shown in **Tables 32-34**.

Table 31. Masses of strong neutrinos.

	$m(\text{qnue})$	$m(\text{qnum})$	$m(\text{qnut})$
exp.			
calc.	23.2 MeV	205 MeV	2.4 GeV

Table 32. Parameters of the qe-neutrino.

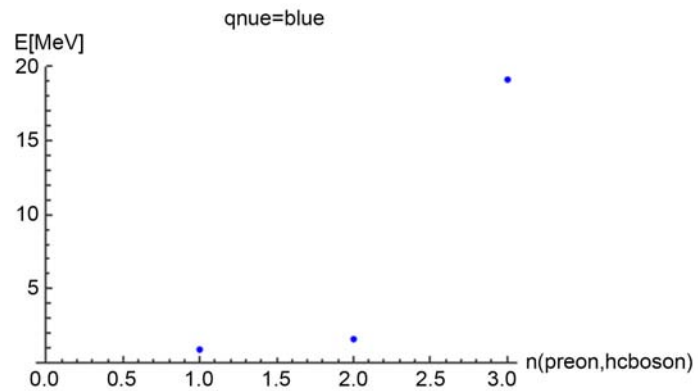
$Eu_i \text{ (MeV)}$	EA_i	a_i	aA_i	dru_i	ru_i	$\sin(\theta u_i)$
0.916713, 1.57978	19.1558	0.0499768, 0.0499806	0.0499709	0.218706, 0.217761	1.08906, 1.08886	0.0495826
ΔEu_i	ΔEA_i	Δa_i	ΔaA_i	Δdru_i	Δru_i	$\Delta \sin(\theta u_i)$
2.59139, 4.46489	6.42353			0.00260392, 0.0000482519	0.000467796, 0.0000799548	

Table 33. Parameters of the qm-neutrino.

$Eu_i \text{ (MeV)}$	EA_i	a_i	aA_i	dru_i	ru_i	$\sin(\theta u_i)$
	3.2139,		0.0499795,			
2.31669, 2.10932	27.2516, 36.8587,	0.049974, 0.0499723	0.0499777, 0.0499851,	0.218962, 0.217768	1.08916, 1.08885	0.0494963
	131.637		0.0499601			
ΔEu_i	ΔEA_i	Δa_i	ΔaA_i	Δdru_i	Δru_i	$\Delta \sin(\theta u_i)$
4.18504, 4.14824	16.4507, 20.6083,			0.00272481, 0.0000218384	0.000633244, 0.0000799629	
	43.8355					

Table 34. Parameters of the qt-neutrino.

Eu_i (MeV)	EA_i	a_i	aA_i	dru_i	ru_i	$\sin(\theta u_i)$	
	6.27604,		0.0499212,				
	9.78005,		0.0499565,				
	14.0006,		0.0499232,				
	17.2518,		0.0499843,				
	26.4587,		0.0500119,				
	32.2502,		0.0499806,				
	44.8203,		0.0499806,				
62.9487,	62.4957,	0.0498284,	0.0500343,	0.250849,	1.09488,	0.0362321	
61.5266	71.6555,	0.0496889	0.0499183,	0.21778	1.08809		
	88.2316,		0.0495368,				
	105.198,		0.0499496,				
	154.92,		0.0501089,				
	251.417,		0.0500246,				
	406.445,		0.0500326,				
	980.267		0.0499384				
ΔEu_i	ΔEA_i	Δa_i	ΔaA_i	Δdru_i	Δru_i		$\Delta \sin(\theta u_i)$
	7.47768,						
	7.63514,						
	11.768,						
	12.944,						
	23.1368,						
	23.3382,						
	31.1644,						
80.6687,	43.8489,			0.0345065,	0.00516914,		
82.6461	52.4387,			0.000493132	0.000793051		
	59.1117,						
	70.624,						
	56.9479,						
	109.749,						
	231.239,						
	579.301						



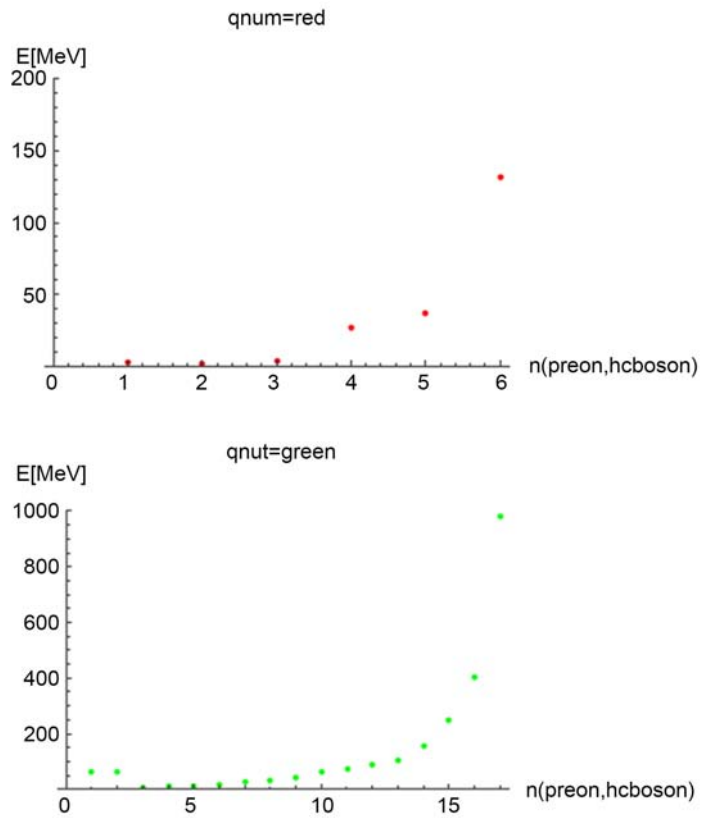


Figure 18. Energy distribution of strong neutrinos: first preons ($u1, u2$), then bosons A_i .

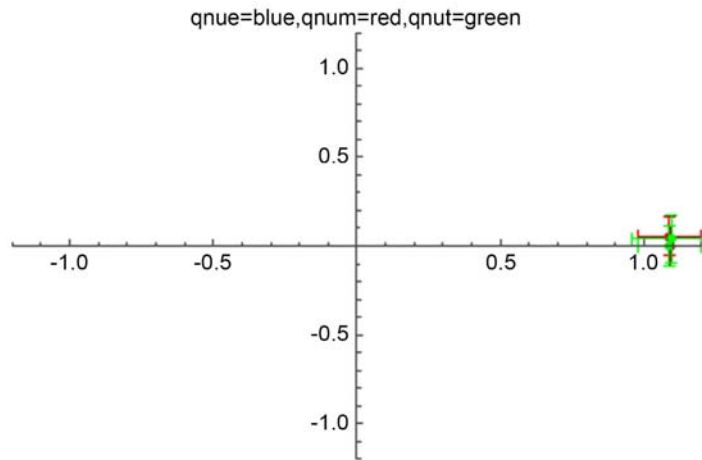


Figure 19. Structure of strong neutrinos: preons ($u1, u2$) radii r_i , uncertainty dr_i and angle θ .

qe-neutrino $qne = (qL-, qL+)$

Preon configuration: left-handed q-neutrino $u = \left(\left(\begin{matrix} 0 \\ qL- \end{matrix} \right), \left(\begin{matrix} qL+ \\ 0 \end{matrix} \right), 0, 0 \right)$

Antiparticle right-handed anti-q-neutrino $\bar{u} = \left(0, 0, \left(\begin{matrix} 0 \\ qR- \end{matrix} \right), \left(\begin{matrix} qR+ \\ 0 \end{matrix} \right) \right)$

$$E_{exp} = ? \quad Q = 0$$

$$E_{tot} = 23 \text{ MeV}, \Delta E_{tot} = 13.5$$

qm-neutrino qnum = (qL-, qL+)

$$E_{exp} = ? \quad Q = 0$$

$$E_{tot} = 205 \text{ MeV}, \Delta E_{tot} = 93$$

qt-neutrino qnut = (qL-, qL+)

$$E_{exp} = ? \quad Q = 0$$

$$E_{tot} = 2.40 \text{ GeV}, \Delta E_{tot} = 1.48.$$

5.8. Strong Bosons (Hypothetical) Zq, Hq

Spin $S = 1$ or 0 , one free preon u1: combination of four spinors

Preon configuration:

$$u = \left(\begin{pmatrix} u1 \\ 0 \end{pmatrix}, \begin{pmatrix} 0 \\ u1 \end{pmatrix}, \begin{pmatrix} u1 \\ 0 \end{pmatrix}, \begin{pmatrix} 0 \\ u1 \end{pmatrix} \right) \text{ for strong exchange boson } Zq$$

$$u = \left(\begin{pmatrix} u1 \\ u1 \end{pmatrix}, \begin{pmatrix} u1 \\ u1 \end{pmatrix}, \begin{pmatrix} u1 \\ u1 \end{pmatrix}, \begin{pmatrix} u1 \\ u1 \end{pmatrix} \right) \text{ for q-higgs } Hq$$

Boson configuration; all hc-bosons active flavor = 3

The strong bosons are color-neutral and do not interact by color.

They are spherically symmetric, the only preon is located approximately at radius $r \approx 1 \text{ am}$, as shown in the structure plot below.

The strong boson Zq is the Yukawa-boson for the hc-interaction of q-neutrinos.

The strong higgs Hq generates masses for the q-neutrinos and for the q-preons.

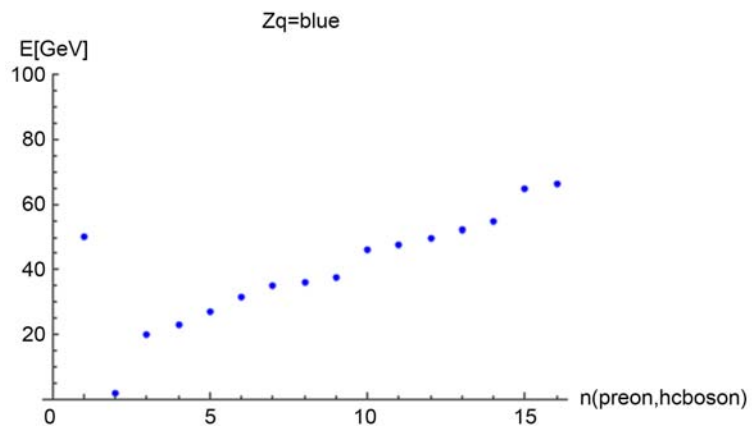
The q-neutrinos interact very weakly, because the masses of the strong bosons are very large.

The calculated masses of the strong bosons are shown in **Table 35**.

The energy of component preons and field bosons are shown in **Figure 20**.

The structure, *i.e.* calculated average distances of components with smear-out are shown in **Figure 21**.

The parameters of the individual bosons are shown in **Table 36**, **Table 37**.



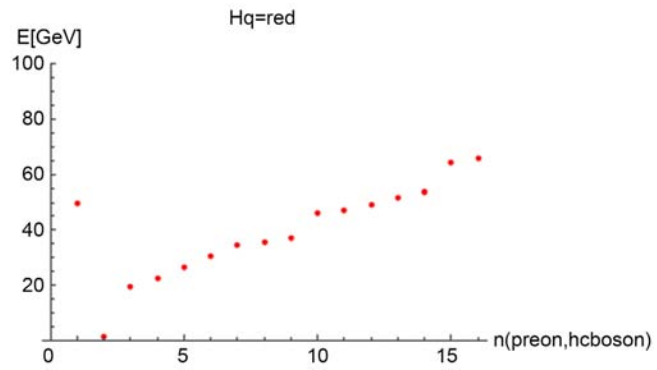


Figure 20. Energy distribution of strong bosons: first preon ($u1$), then bosons A_i .

Table 35. Masses of strong bosons.

	$m(Zq)$	$m(Hq)$
exp.		
calc.	644 GeV	637 GeV

Table 36. Parameters of the strong boson Zq .

Eu_i (GeV)	EA_i	a_i	aA_i	dru_i	ru_i	$\sin(\theta_{u_i})$
	1.75913,		0.231796,			
	20.0747,		-0.207073,			
	22.9369,		0.131049,			
	27.0332,		-0.253369,			
	31.3827,		0.15414,			
	35.2293,		0.199737,			
	36.2947,		0.161236,			
50.1031	37.6842,	0.242169	0.266433,	2.90034	0.953641	0
	46.383,		-0.269026,			
	47.6871,		0.131364,			
	49.7122,		0.155354,			
	52.4871,		0.203886,			
	54.6914,		0.235986,			
	64.7501,		0.226728,			
	66.1951		0.056805			
ΔEu_i	ΔEA_i	Δa_i	ΔaA_i	Δdru_i	Δru_i	$\Delta \sin(\theta_{u_i})$
	1.40428,					
	2.2256,					
	2.1451,					
	4.24188,					
	3.13026,					
	1.44886,					
	1.19789,					
0.501804	1.53643,			0.0598953	0.243724	
	1.07209,					
	0.567924,					
	0.839207,					
	1.81534,					
	1.76197,					
	1.38173,					
	1.23064					

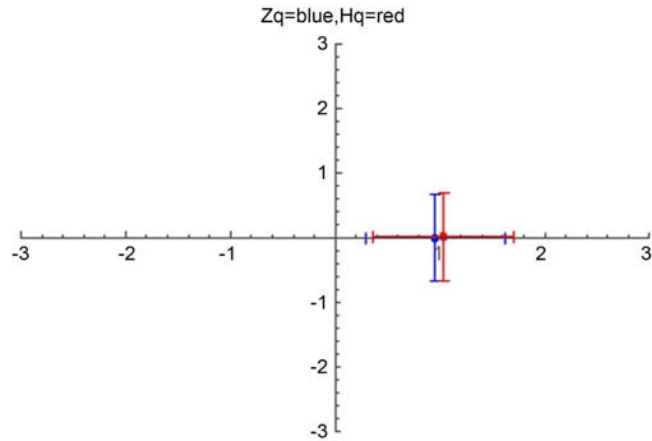


Figure 21. Structure of strong bosons: preon ($u1$) radii r_i , uncertainty dr_i and angle θ_i , the only preon is located approximately at radius $r \approx 1$ am.

Table 37. Parameters of the strong higgs Hq.

Eu_i (GeV)	EA_i	a_i	aA_i	dru_i	ru_i	$\sin(\theta_{u_i})$
	66.1951},					
	{49.8974,		0.207549,			
	1.49444,		-0.304129,			
	19.6994,		0.131516,			
	22.5362,		-0.254004,			
	26.3583,		0.253908,			
	30.6179,		0.206301,			
	34.632,		0.161453,			
49.8974	35.8439,	0.242181	0.252253,	2.97112	1.03787	0
	37.1908,		-0.272395,			
	46.1384,		0.131765,			
	47.4992,		0.163953,			
	49.4017,		0.204921,			
	51.9202,		0.242696,			
	54.0522,		0.221589,			
	64.3069,		0.0809426			
	65.783					
ΔEu_i	ΔEA_i	Δa_i	ΔaA_i	Δdru_i	Δru_i	$\Delta \sin(\theta_{u_i})$
	0.958115,					
	1.67958,					
	1.65813,					
	3.0444,					
	1.70715,					
	0.281763,					
	0.812278,					
0.0563816	0.540787,			0.071377	0.253642	
	0.748368,					
	0.324524,					
	0.292485,					
	2.08406,					
	0.685153,					
	0.707936,					
	1.09514					

strong exchange boson Z_q $Z_q = (qL^- + qR^- + qL^+ + qR^+)/2$

Preon configuration: $u = \left(\begin{pmatrix} u1 \\ 0 \end{pmatrix}, \begin{pmatrix} 0 \\ Cu1 \end{pmatrix}, \begin{pmatrix} u1 \\ 0 \end{pmatrix}, \begin{pmatrix} 0 \\ Cu1 \end{pmatrix} \right) / \sqrt{2}$

$Cu1 = ((qL^-) + (qR^-)) / \sqrt{2}$ $u1 = ((qL^+) + (qR^+)) / \sqrt{2}$

antiparticle itself $\bar{Z}_q = Z_q$

$E_{exp} = ?$ $Q = 0, S = 1$

$E_{tot} = 644$ GeV, $\Delta E_{tot} = 26$

strong higgs scalar boson (hypothetical) H_q , $H_q = (qL^- + qL^+ + qR^- + qR^+)/2$

Preon configuration: $u = \left(\begin{pmatrix} u1 \\ u1 \end{pmatrix}, \begin{pmatrix} u1 \\ u1 \end{pmatrix}, \begin{pmatrix} u1 \\ u1 \end{pmatrix}, \begin{pmatrix} u1 \\ u1 \end{pmatrix} \right) / 2$

$u1 = ((qL^-) + (qL^+) + (qR^-) + (qR^+)) / 2$

antiparticle: itself $\bar{H}_q = H_q$

$E_{exp} = ?$ $Q = 0, S = 0$

$E_{tot} = 637$ GeV, $\Delta E_{tot} = 17$.

5.9. Mass Hierarchy and the Koide Formula

In 1982 Koide set up a formula for the 3 generations of charged lepton masses [28]

$$m_1 + m_2 + m_3 = \frac{2}{3} (\sqrt{m_1} + \sqrt{m_2} + \sqrt{m_3})^2, \text{ where } m_1 = m_e, m_2 = m_\mu, m_3 = m_\tau \text{ or}$$

for the Koide function $k(m_1, m_2, m_3) = \frac{2 (\sqrt{m_1} + \sqrt{m_2} + \sqrt{m_3})^2}{3 (m_1 + m_2 + m_3)}$ we get

$$k(e) = k(m_e, m_\mu, m_\tau) = 1 \text{ for charged leptons } = l_e = (e, \mu, \tau).$$

Calculation with observed values for basic particles yields [6] for the Koide value for charged leptons, U-quarks, and D-quarks

$$k(e) = 0.9998, k(u) = 1.0001, k(d) = 1.0891$$

and for neutrinos with SU4PM calculated values

$$k(\nu) = 0.8654$$

The masses of the 3 generations of the basic particles of the Standard Model are given in **Table 38** below, where the neutrino masses are taken from the SU(4)-preon calculation above, the remaining values are measured.

Table 38. Masses of the 3 generations of the basic particles of the Standard Model.

	m_1	m_2	m_3
neutrino (ν_e, ν_μ, ν_τ)	0.30 meV	11 meV	98 meV
ch.lepton (e, μ , τ)	0.511 MeV	106 MeV	1.78 GeV
u-quark (u, c, t)	2.3 MeV	1.34 GeV	171 GeV
d-quark (d, s, b)	4.8 MeV	100 MeV	4.2 GeV

Nan Li [28] gives the assessment for $k(\nu)$: $0.50 < k(\nu) < 0.85$, which is roughly in agreement with the above value for $k(\nu)$.

The Koide formula is approximately $k \approx 1$ for all basic particles, with a deviation of about 20% for neutrinos and u-quark generations.

In the SU(4)-preon model, the generations are due to the 3 configuration of hc-bosons (hcb) $N_i = (1, 4, 15)$ which are compatible with the symmetry of SU(4) (are invariant under an automorphism subgroup).

We make an ansatz for the mass-energy of generations u_i :

$M(u_i) = E_{ui} + m_{ui} N_i^{a_{ui}}$, where E_{ui} is the non-hcb energy contribution, m_{ui} is the first-generation-energy, a_{ui} is the hcb-exponent, and $N_i = (1, 4, 15)$ is the number of hcb's in a generation i .

Fitting the mass table with this ansatz gives

$$E_{u_1} = -28.18 \quad E_{u_2} = -139.84 \quad E_{u_3} = -550.62 \quad E_{u_4} = -61.19$$

$$m_{u_1} = 5.06 \quad m_{u_2} = 10.79 \quad m_{u_3} = 19.16 \quad m_{u_4} = 6.99$$

$$a_{u_1} = 1.11 \quad a_{u_2} = 1.20 \quad a_{u_3} = 1.50 \quad a_{u_4} = 1.34$$

The resulting exponents a_{ui} vary from $a_{u1} = 1.11$ for neutrinos to $a_{u3} = 1.50$ for u-quark generations with a mean

$$E(a_{ui}) = 1.292 \text{ and standard deviation } Std(a_{ui}) = 0.1720.$$

If we approximate the mass formula $\hat{M}(u_i) = m_{ui} N_i^{a_{ui}}$ neglecting the non-hcb energy E_{uib} then the scale factor cancels out, and the Koide function depends only on the exponent a_{ui} of the family (u_i).

We get the following approximate values k' for the Koide value k of the 4 families:

$$k(\nu) = 0.8106, \quad k(e) = 0.9177, \quad k(\mu) = 0.9242, \quad k(d) = 1.091$$

which is a good approximation.

So we can conclude:

the **approximate validity of the Koide formula $k \approx 1$** for the 4 families is the result of the power law of the generation mass hierarchy with the **exponent $a_{ui} \approx 1.3$ approximately constant** across the 4 families.

5.10. Assessment of the Quark and Lepton Mixing

It is possible to assess roughly the values of the CKM matrix for quark mixing and the PMNS matrix for neutrino mixing based on the SU(4) preon model.

Quark mixing

In 4.5 we calculated the CKM 12-element for the $d \rightarrow u$ decay (Cabibbo angle) as $a_{C12} = 0.229$, which agrees well with the experimental value. The calculation for the other elements of the CKM matrix can be carried out correspondingly. However, one can assess these elements roughly, based on the number of hc-bosons per generation.

The particle configuration for the generations (=flavors) is

flavor 1: 1 hc-boson+2 preons e.g. $A13, rL-, rR-$ for electron e^-

flavor 2: 4 complementary hc-bosons with conjugates +2 preons e.g.

$A13, \bar{A}13, A24, \bar{A}24, rL-, rR-$ for electron e^-

flavor 3: all 15 hc-boson +2 preons

We expect naively that the coupling between generations scales roughly with the Boltzmann factor ($k_B = 1$)

$$c_{i,j} = C_1 \exp\left(\frac{E_0 N(i)}{T}\right) = C_1 \beta^{N(i)}$$

where $N(i)$ = number of particles in i -th generation T the temperature and C_1, β constants.

With $\beta = 1.34$ and $C_1 = 0.5$ we get $c_{1,2} = 0.206$ $c_{2,3} = 0.019$ $c_{1,3} = 0.0080$ in comparison with CKM values (0.22, 0.041, 0.0035)

Lepton mixing

With quarks, quark transformations run according to the scheme $q_1 \rightarrow q_2 + W$, with a W -boson, which consists of r -preons.

With electrons and neutrinos, transformations $e \rightarrow \nu + X$ or $\nu \rightarrow e + X$ are impossible because of preon conservation.

Transformations between neutrino flavors $\nu_i \rightarrow \nu_j$ are described by the PMNS matrix, according to the above formula $c_{i,j} = C_1 \exp\left(\frac{E_0 N(i)}{T}\right)$. Normally neutrinos have kinetic energies much higher than their rest mass, e.g. solar neutrinos in MeV range, and $m(\nu) \approx E_0 N(i) \ll T$, so the exponent is around zero, and we expect the $c_{i,j}$ to be in the same range, which is the case.

Transformation between charged leptons with different flavors, e.g. $\mu \rightarrow e + X$ run with flavor conservation

$$\mu \rightarrow e + \bar{\nu}_e + \nu_\mu + \Delta E \text{ or in preon formulation}$$

$$(A13, \bar{A}13, A24, \bar{A}24, rL-, rR-) \rightarrow (A13, rL-, rR-) + (\bar{A}13, rR-, rR+) \text{ here}$$

$$+ (A13, \bar{A}13, A24, \bar{A}24, rL-, rL+) + \Delta E$$

two hcb's $A13$ $\bar{A}13$ are emitted, $rR-, rR+, rL-, rL+$ are created as pairs, and $A13, \bar{A}13, A24, \bar{A}24$ are simply "passed".

The flavor-violating transformation $\mu \rightarrow e + \bar{\nu}_e + \nu_e + \Delta E$ is not forbidden by conservation laws, but strongly suppressed in comparison to the flavor-conserving transformation because of the very small neutrino mass.

In preon formulation

$$(A13, \bar{A}13, A24, \bar{A}24, rL-, rR-)$$

$$\rightarrow (A13, rL-, rR-) + (\bar{A}13, rR-, rR+) + (A13, rL-, rL+) + \Delta E$$

In the inverse transformation, which is equivalent, the hcb quartet $A13, \bar{A}13, A24, \bar{A}24$ with muon energies has to be emitted in the neutrino ν_e . If we assume the temperature of the neutrinos to be about in the order of the electron mass, the process will be suppressed by the Boltzmann factor

$$f(\mu \rightarrow e + \bar{\nu}_e + \nu_e) = \exp\left(-\frac{4E(Aij, \mu)}{m(e)}\right) \approx \exp\left(-\frac{m(\mu)}{m(e)}\right)$$

$$= \exp\left(-\frac{100 \text{ MeV}}{0.511 \text{ MeV}}\right) = 1.0 \times 10^{-85}$$

5.11. Deviations from the Standard Model

We can assess the deviation of the SU(4) hypercolor model from the standard model by the energy ratio

$$f_{dev} = \left(\frac{mc^2}{E_{hc}} \right),$$

where m is the mass of the corresponding particle, and $E_{hc} = 180 \text{ GeV}$ is the hypercolor energy scale. As an example, let us consider the magnetic moment of the muon, where we measure a deviation from the Standard model result [29].

Assessed deviation of the muon and electron magnetic moment

The muon mass is $m_\mu = 105.6 \text{ MeV}$, the measured relative deviation

$$\frac{\Delta a_\mu}{a_\mu} = \frac{2.3}{1855900} = 1.2 \times 10^{-6} \quad [29],$$

the assessed deviation of the muon magnetic moment $\frac{\Delta a}{a} \sim \left(\frac{\Delta r}{r} \right)^2 \sim \left(\frac{\Delta E}{E} \right)^2$, so $\frac{\Delta a_\mu}{a_\mu} \approx \left(\frac{m_\mu c^2}{E_{hc}} \right)^2 = 0.34 \times 10^{-6}$, which is in the scale of the measured deviation.

For the electron we get the assessment $\frac{\Delta a_e}{a_e} \approx \left(\frac{m_e c^2}{E_{hc}} \right)^2 = 8 \times 10^{-12}$, where the current measurement precision is $\frac{\delta a_e}{a_e} = 3 \times 10^{-10}$, well above the assessed deviation.

6. Weak Hadron Decays in the SU(4)-Preon Model

6.1. Neutron Decay

The neutron decay obeys the scheme $dd \rightarrow ud + e^- + \bar{\nu}_e$, i.e. for free neutrons

$$n \rightarrow p + e^- + \bar{\nu}_e \quad (14)$$

with the mean lifetime of $\tau = 881.5 \pm 1.5 \text{ s}$ and energy $\Delta E = 0.782343 \text{ MeV}$

In the SM it is described by the interaction of a virtual W-boson

$$n \rightarrow p + W^- \rightarrow p + e^- + \bar{\nu}_e \quad (14a)$$

With the probability of about $p = 0.001$, an additional photon is emitted

$$n \rightarrow p + W^- \rightarrow p + e^- + \bar{\nu}_e + \gamma$$

Currently, there is a “neutron lifetime puzzle”: the lifetime measured by proton-counting (beam-method lifetime τ_1) yields $\tau_2 = \tau_1 + 8 \text{ s}$, compared to the bottle-method (lifetime τ_2) of counting the remaining neutrons.

A possible explanation is the possibility of other decay channels for n .

In the SU4PM the decay proceeds as follows

$$d(rR-, qL+) \rightarrow u(rL+, qR+) + W^-(rR-, rR-) + Z_q(qL-, qL+) \quad (15)$$

$$d(rL-, qR+) \rightarrow d(rR-, qL+) + Z_L(rL-, rL+) + \bar{Z}_q(qR-, qR+)$$

with the immediate decay $W^-(rR-, rR-) \rightarrow e^-(rL-, rR-) + \bar{\nu}_e(rR-, rR+)$ and the decay $Z_L(rL-, rL+) \rightarrow \nu_e(rL-, rL+) + \nu_{s1}(rL+, rR-)$, i.e. the total reaction

is $n \rightarrow p + e^- + \bar{\nu}_e + \nu_e + \nu_{s1}$, with the additional emission of a neutrino and a sterile neutrino, which are undetectable and carry away a small fraction of the total energy, ascribed to the antineutrino.

The neutrino and the antineutrino annihilate in a small fraction of events, producing an additional photon.

The virtual Z_q and \bar{Z}_q annihilate immediately and carry no energy away.

6.2. Transitions of Quarks

A quark can make a transformation, which swaps the chirality of its components. This is seen at the example of a d-quark transition (16)

$$\begin{aligned} d(rR-, qL+) &\rightarrow d(rL-, qR+) + \bar{Z}_L(rR-, rR+) + Z_q(qL-, qL+) \\ &\rightarrow d(rL-, qR+) + \bar{\nu}_e(rR-, rR+) + \nu_q(qL-, qL+) \\ d(rR-, qL+) &\rightarrow d(rL-, qR+) + \bar{Z}_L(rR-, rR+) + Z_q(qL-, qL+) \\ &\rightarrow d(rL-, qR+) + \bar{\nu}_e(rR-, rR+) + \nu_q(qL-, qL+) \end{aligned}$$

Both transitions take at least the energy $\Delta E = 23$ MeV for the mass of ν_q .

This transition can serve as an additional channel for the neutron decay:

$n \rightarrow n + \bar{\nu}_e + \nu_e + \bar{\nu}_q + \nu_q$, which takes away $\Delta E = 2 \times 23$ MeV and makes fast neutrons slow, making them undetectable by the usual scintillation method. This would explain the “neutron lifetime puzzle”.

6.3. Pion Decay

The pion decay is the other major source of weak hadron decays, in the SM it is described as

$$u\bar{d} \rightarrow e^+ + \nu_e \tag{17}$$

In the SU4PM the decay proceeds as follows

$$\begin{aligned} u(rR+, qL+) &\rightarrow u(rL+, qR+) + \bar{Z}_L(rR-, rR+) + \nu_q(qL-, qL+) \\ \bar{d}(rL+, qR-) &\rightarrow \bar{u}(rR-, qL-) + W^+(rL+, rL+) + \bar{\nu}_q(qR-, qR+) \end{aligned} \tag{18}$$

the virtual W-boson and ZL-boson decay into electron and neutrinos

$$\begin{aligned} W^+(rL+, rL+) &\rightarrow e^+(rL+, rR+) + \nu_e(rL-, rL+) \\ \bar{Z}_L(rR-, rR+) &\rightarrow \bar{\nu}_e(rR-, rR+) + \nu_{s1}(rL-, rR+) \end{aligned}$$

so the overall reaction is (19)

$$\begin{aligned} u(rR+, qL+) + \bar{d}(rL+, qR-) &\rightarrow u(rL+, qR+) + \bar{u}(rR-, qL-) \\ &+ e^+(rL+, rR+) + \nu_e(rL-, rL+) + \bar{\nu}_e(rR-, rR+) + \nu_{s1}(rL-, rR+) \end{aligned}, \text{ i.e.}$$

$u\bar{d} \rightarrow e^+ + \nu_e + \bar{\nu}_e + \nu_{s1}$, the pion decays into an electron and antineutrino plus the (undetectable) neutrino and sterile neutrino.

7. Conclusions

Formulation of the extended model

In the first three chapters we describe SU4PM, the extended SM.

The extension happens in four steps:

-in chap.2: extending the Pauli-SU(2) weak interaction to SU(4)-hypercolor interaction, which is renormalizable quantum gauge field theory, with confinement and asymptotic freedom, with charges $hc = (L-, L+, R-, R+)$.

Pauli-SU(2) weak interaction becomes then the Yukawa weak force of the SU(4)-hypercolor interaction, after a spontaneous symmetry breaking of the SU(4)-hc-interaction $SU(4) = SU(2)_L \otimes SU(1)_R \otimes SU(1)_{em}$.

-in chap.3: introducing sub-particles as constituents of basic particles of SM: preons r and q with hc-charges, plus color-charge for q , with the parameters:

wave function $\Psi = (u_{L-}, u_{L+}, u_{R-}, u_{R+})$
 r-preons $(r_{L-}, r_{L+}, r_{R-}, r_{R+})$, $Q(r) = -1/2$, $m(r) \ll 1 \text{ MeV}$,
 q-preons $(q_{L-}, q_{L+}, q_{R-}, q_{R+})$, $Q(q) = +1/6$, $m(q) \sim 1 \text{ MeV}$,
 $Q_{col}(q) = (r, g, b)$

-in chap.4: adding a new powerful calculation method: direct minimization of action. This calculation method was introduced in [4] [7] and applied successfully in QCD for calculation of hadrons.

-in chap.5: formulating the ansatz for wavefunctions.

The calculated results for energy-mass of basic particles are presented in chap.5.

Systematics

The systematics is described at the example of charged leptons.

For each particle family (generations), are presented:

-preon configuration and hc-boson configuration

Preon configuration: $u = \left(\begin{pmatrix} rL- \\ 0 \end{pmatrix}, 0, \begin{pmatrix} rR- \\ 0 \end{pmatrix}, 0 \right)$

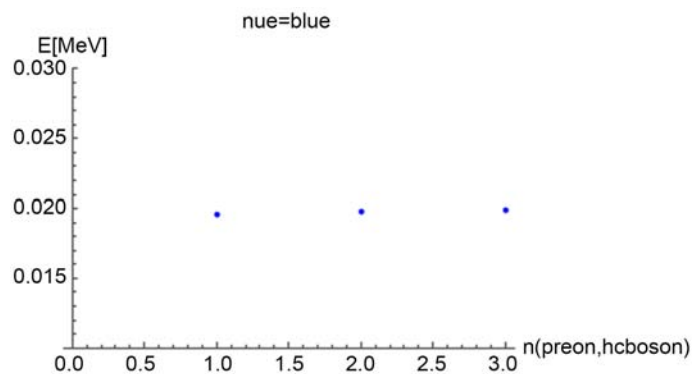
Boson configuration: flavor = 1: ($A13 = \lambda4$), flavor = 2:
 ($A13 = \lambda4, \bar{A}13 = \lambda5, A24 = \lambda11, \bar{A}24 = \lambda12$)

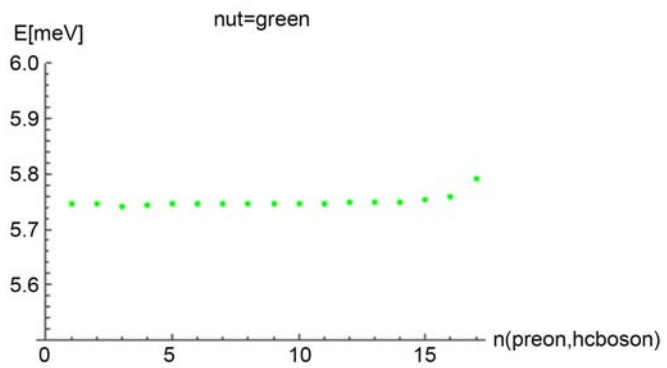
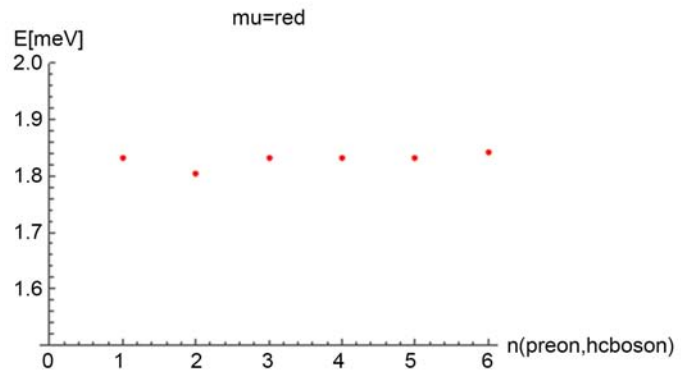
flavor = 3: all 15 bosons

-calculated and observed mass

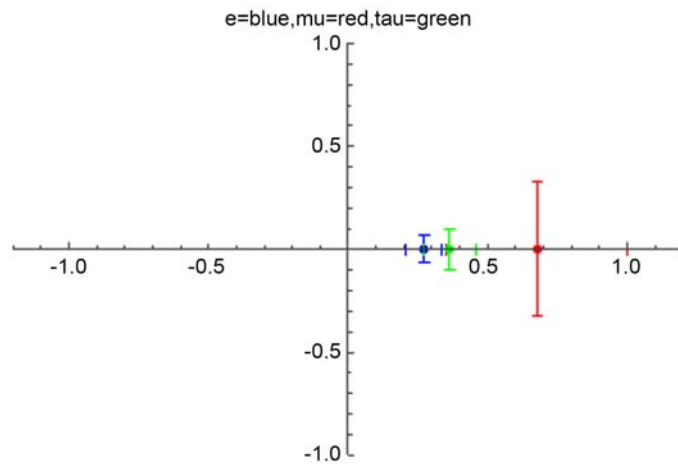
	$m(e)$	$m(\mu)$	$m(\tau)$
exp.	0.511 MeV	106 MeV	1.78 GeV
calc.	$0.293 \pm 0.22 \text{ MeV}$	$228 \pm 150 \text{ MeV}$	$2.26 \pm 0.7 \text{ GeV}$

-energy distribution for three generations





-spatial preon configuration in (r, θ) :



Mass hierarchy and the Koide formula

If we take for the neutrinos the calculated values, and for the rest the observed values, we get the following mass table for leptons and quarks

	m_1	m_2	m_3
neutrino (ν_e, ν_μ, ν_τ)	0.30 meV	11 meV	98 meV
electron (e, μ , τ)	0.511 MeV	106 MeV	1.78 GeV
u-quark (u, c, t)	2.3 MeV	1.34 GeV	171 GeV
d-quark (d, s, b)	4.8 MeV	100 MeV	4.2 GeV

The Koide formula [28] is approximately valid for the generations (1, 2, 3) of basic particles. The precise values are $k(\nu) = 0.8654$, $k(e) = 0.9998$, $k(u) = 1.2673$, $k(d) = 1.0891$ for the four basic families neutral leptons, charged leptons, u-quarks, d-quarks.

There is an approximate scaling law for the generation mass scale.

We make an ansatz for the mass-energy of generations u_i

, where E_{ui} is the non-hcb energy contribution, m_{ui} is the first-generation-energy, a_{ui} is the hcb-exponent, and $N_i = (1, 4, 15)$ is the number of hcb's in a generation i .

Fitting the formula yields the exponents

, so .

We have the result: the approximate validity of the Koide formula $k \approx 1$ for the 4 families is the result of the power law of the generation mass hierarchy with the exponent $a_{ui} \approx 1.3$ approximately constant across the 4 families.

Calculated and observed masses of basic SM particles

Leptons and pure quarks

	$m(e)$	$m(\mu)$	$m(\tau)$
exp.	0.511 MeV	106 MeV	1.78 GeV
calc.	0.293 ± 0.22 MeV	228 ± 150 MeV	2.26 ± 0.7 GeV
	$m(\nu_e)$	$m(\nu_\mu)$	$m(\nu_\tau)$
exp.			
calc.	0.30 meV	11 meV	98 meV
	$m(u)$	$m(c)$	$m(t)$
exp.	2.3 MeV	1.34 GeV	171 GeV
calc.	2.35 ± 0.26 MeV	3.2 ± 1.87 GeV	163 ± 55 GeV
	$m(d)$	$m(s)$	$m(b)$
exp.	4.8 MeV	100 MeV	4.2 GeV
calc.	4.58 ± 0.3 MeV	149 ± 15 MeV	6.1 ± 2.9 GeV

dC = Cabibbo-mixed d-quark

	$m(dC), \alpha(C)$
exp.	4.8 MeV, 13.04°
calc.	4.74 MeV, 13.1°

Weak massive bosons W, Z0, H (higgs), ZL (weakly interacting left-chiral Z-boson)

	$m(W)$	$m(Z0)$	$m(ZL)$	$m(H)$
exp.	80.4 GeV	91.2 GeV		125.1 GeV
calc.	89 GeV	97 GeV	91 GeV	125 GeV

new weakly interacting particles
sterile neutrinos $\nu s1, \nu s2, \nu s3$;
strong neutrinos $\nu qe \nu qm \nu qt$
strong bosons $Zq Hq$

	$m(\nu s1)$	$m(\nu s2)$	$m(\nu s3)$
exp.			
calc.	0.09 meV	3.6 meV	100 meV
	$m(\nu qe)$	$m(\nu qm)$	$m(\nu qt)$
exp.			
calc.	23.2 MeV	205 MeV	2.4 GeV
	$m(Zq)$	$m(Hq)$	
exp.			
calc.	644 GeV	637 GeV	

Structure of basic SM particles

Symmetry and inner structure of particles is determined by the spatial distribution of preons.

Length is specified in units $r0 = 0.2 \times 10^{-18}$ m

Mean location ($r(gi), \theta(gi)$) of preons in generation $i = 1, 2, 3$

	$r(g1)$	$r(g2)$	$r(g3)$	$\theta(g1)$	$\theta(g2)$	$\theta(g3)$
e	0.25	0.35	0.5			
ν	0.9	1.	1.1			
u	0, 0.3	0.1, 0.3	0.6, 0.6			0, $\pi/6$
d	0, 0.3	0, 0.3	0.1, 0.5			
dC	0.3, 0.8			0, $\pi/8$		

Structure characteristics

We have the following structure characteristics:

-charged leptons (e, μ, τ) are spherically symmetric, with increasing radii (0.25, 0.35, 0.5)

-neutral leptons ($\nu e, \nu \mu, \nu \tau$) are spherically symmetric, with roughly equal radius ≈ 1

-pure u-quarks (u, c, t) have double-peaked structure with increasing radii ((0, 0.3), (0.1, 0.3), (0.6, 0.6)), the first two are spherically symmetric, and only the t-quark is slightly axial $\theta = (0, \pi/6)$

-pure d-quarks (d, s, b) have double-peaked structure with increasing radii ((0, 0.3), (0, 0.3), (0.1, 0.5)), and are spherically symmetric

-Cabibbo-mixed d-quark dC has double-peaked structure (0.3, 0.8) and is slightly axial $\theta = (0, \pi/8)$

Consequences from the calculated structure

-Cabibbo-mixing breaks the spherical symmetry

The observed first generation quarks (uC, dC) are Cabibbo-mixed with the CKM matrix, the higher generation quarks can be considered as approximately pure.

Cabibbo-mixing breaks the spherical symmetry, as shown for dC, and makes both first-generation quarks (uC, dC) axial.

-neutrino-mixing with large angles

Neutrino generations are one-peaked spherically symmetric, with approximately equal radius. Therefore it is plausible that mixing by PMNS matrix is easy, *i.e.* with large angles (neutrino oscillations).

-comparison of PMNS and CKM matrix

Quark mixing by CKM matrix is of type V_{CKM} , where the first list labels the rows and the second list labels the columns, *i.e.* it is “partner-oriented” mixing.

Neutrino mixing by PMNS matrix is of type V_{PMNS} , *i.e.* it is “self-oriented” mixing.

Partner-oriented mixing of leptons according to the CKM scheme is not allowed (or energetically unfavorable), because neutrinos are chiral, and electrons are not.

Self-oriented mixing of quarks is allowed, but energetically unfavorable, which could be shown numerically by calculating a combination of both mixing schemes.

Conflicts of Interest

The author declares no conflicts of interest regarding the publication of this paper.

References

- [1] Greiner, W., Schramm S. and Stein, E. (2007) Quantum Chromodynamics. Springer, Berlin.
- [2] Casalderrey, J. (2017) Lecture Notes on the Standard Model. University of Oxford, Oxford.
<https://www2.physics.ox.ac.uk/system/files/profiles/casalderreysolana/tsm-jcs-41346.pdf>
- [3] Kaku, M. (1993) Quantum Field Theory. Oxford University Press, Oxford.
- [4] Helm, J. (2021) Standard Model of Particle Physics I Concise Review and New Methods with New Results.
https://www.researchgate.net/publication/335715929_Standard_model_of_particle_physics_I_concise_review_and_new_methods_with_new_results
- [5] Harari, H. (1979) *Physics Letters B*, **86**, 83-86.
[https://doi.org/10.1016/0370-2693\(79\)90626-9](https://doi.org/10.1016/0370-2693(79)90626-9)
- [6] https://www.researchgate.net/publication/377636035_Koide_mass_formula
- [7] Helm, J. (2019) Quantum Chromodynamics on-Lattice.
https://www.researchgate.net/publication/333356589_Quantum_chromodynamics_on-lattice

- [8] Hooft, G. (2008) *Scholarpedia*, **3**, 7443.
<https://doi.org/10.4249/scholarpedia.7443>
- [9] Cheng, T.P. and Li, L.F. (2006) *Gauge Theory of Elementary Particle Physics*. Oxford University Press, Oxford.
- [10] Salam, G. (2015) *Basics of QCD: Jets & Jet Substructure*. ICTP-SAIFR School on QCD and LHC Physics, São Paulo.
<http://gsalam.web.cern.ch/gsalam/repository/talks/2015-SaoPaulo-lecture4.pdf>
- [11] Salam, G. (2011) *Elements of QCD for Hadron Colliders*. [arXiv hep-th/1011.5131]
- [12] Skands, P.Z. (2018) *Introduction to QCD*. [arXiv hep-ph/1207.2389]
- [13] Schwinn, C. (2015) *Modern Methods of Quantum Chromodynamics*. Universität Freiburg, Freiburg.
- [14] Lee, Y.Y. and Chen-Tsai, C.T. (1965) *Chinese Journal of Physics*, **3**, 45-68.
- [15] Sbaïh, M.A., *et al.* (2013) *Electronic Journal of Theoretical Physics*, **10**, 9.
- [16] Gupta, R. (1998) *Introduction to Lattice QCD*. [arXiv hep-lat/9807.028]
- [17] Petreczky, P. (2014) *Basics of Lattice QCD*. Columbia University, New York.
<https://www.icts.res.in/sites/default/files/extremeqandg2019-2019-04-02-Peter-Petreczky.pdf>
- [18] Helm, J. (2022) *Quantum Chromodynamics on Lattice*.
https://www.researchgate.net/publication/358270905_Quantum_chromodynamics_on_lattice
- [19] Helm, J. (2022) *Standard Model Masses*.
https://www.researchgate.net/publication/358271143_Standard_Model_masses
- [20] Quarks (2018) <https://www.hyperphysics.phy-astr.gsu.edu/>
- [21] Ho-Kim, Q. and Xuan-Yem, P. (1998) *Elementary Particles and Their Interactions*. Springer, Berlin. <https://doi.org/10.1007/978-3-662-03712-6>
- [22] Yao, W.-M., *et al.* (2006) *Journal of Physics G*, **33**, 1.
<https://doi.org/10.1088/0954-3899/33/1/001>
- [23] Harari, H. (1975) *Physics Letters B*, **57**, 265-269.
[https://doi.org/10.1016/0370-2693\(75\)90072-6](https://doi.org/10.1016/0370-2693(75)90072-6)
- [24] Koike, H. (2006) *Proton Decay and Sub-Structure*. [arXiv:hep-ph/0601153v1]
- [25] de Souza, M. (2002) *General Structure of Matter*. [arXiv:hep-ph/0207301v1]
- [26] Mohanty, S. (2019) *MeV Scale Model of SIMP Dark Matter*. [arXiv: hep-ph/1908.00909]
- [27] *Leptonic Mixing Matrix and Neutrino Masses* (2018) <http://www.nu-fit.org/>
- [28] Li, N. and Ma, B.-Q. (2005) *Estimate of Neutrino Masses from Koide's Relation*. [arXiv:hep-ph/0505028]
- [29] Aoyama, T., *et al.* (2020) *Physics Reports*, **887**, 1-166.

The 111-Year-Old Cosmic Ray Puzzle Has Been Solved?

Shlomo Dado, Arnon Dar

Physics Department, Technion, Haifa, Israel

Email: dado@phep3.technion.ac.il

How to cite this paper: Dado, S. and Dar, A. (2024) The 111-Years-Old Cosmic Ray Puzzle Has Been Solved? *Journal of Modern Physics*, 15, 125-131.

<https://doi.org/10.4236/jmp.2024.151004>

Received: November 27, 2023

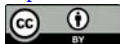
Accepted: January 27, 2024

Published: January 30, 2024

Copyright © 2024 by author(s) and Scientific Research Publishing Inc.

This work is licensed under the Creative Commons Attribution International License (CC BY 4.0).

<http://creativecommons.org/licenses/by/4.0/>



Open Access

Abstract

We show that recently multi-messenger astronomy has provided compelling evidence that the bulk of high energy cosmic rays (CRs) are produced by highly relativistic narrow jets of plasmoids launched in core collapse of stripped-envelope massive stars to neutron stars and stellar mass black holes. Such events produce also a visible GRB if the jet happens to point in our direction. This has been long advocated by the cannon ball (CB) model of high energy CRs and GRBs, but the evidence has been provided only recently by what were widely believed to be unrelated discoveries. They include the very recent discovery of a knee around TeV in the energy spectrum of high energy CR electrons, the peak photon energy in the “brightest of all time” GRB221009A, and the failure of IceCube to detect high energy neutrinos from GRBs, including GRB221009A. They were all predicted by the cannon-ball (CB) model of high energy CRs and GRBs long before they were discovered in observations, despite a negligible probability to occur by chance.

Keywords

Cosmic Rays, Gamma Ray Bursts, Neutrino Bursts

1. Introduction

Cosmic rays (CRs) are mostly high energy, stable, charged particles (protons, nuclei and electrons) which reside in the interstellar and intergalactic space. They were discovered in 1912 by Victor Hess [1]. Their scattering by interstellar and intergalactic magnetic fields so far has prevented identification of their main sources, and the origin of their high energies is still debated. In 1949 Fermi suggested [2] that their high energies are acquired by being reflected from interstellar “magnetic mirrors”—magnetized clouds, which move slowly in random directions in the interstellar medium. However, CR particles may lose energy by

synchrotron radiation faster than they gain by repeated magnetic reflections. Consequently, the original Fermi acceleration mechanism has been replaced by the so called Fermi shock acceleration [3]-[9]. In this model charged particles are assumed to gain energy by being scattered repeatedly between the upstream and downstream regions of strong shocks produced, e.g., by supernova shells expanding into the interstellar medium. This shock acceleration mechanism is widely believed to be the main origin of galactic and extragalactic cosmic rays.

An alternative model of CR acceleration [10]-[15], later called the cannonball (CB) model, unified the production of cosmic ray bursts (CRBs) and gamma ray bursts (GRBs). In this cannonball model, highly relativistic jets of plasmoids (CBs) of ordinary stellar matter are launched by fall back matter on a newly born neutron star or a stellar black hole in core collapse explosion of stripped envelope massive stars. GRBs are produced by inverse Compton scattering (ICS) of light photons on the path of the jet by the electrons in the plasmoids [16] [17], while magnetic reflection of the charged particles by the plasmoids produces the high energy cosmic rays [10]-[15]. In the CB model, the CR knee is the maximum energy that CR particles of a given type (electrons, protons or nuclei) acquire in a single magnetic reflection. These knee energies depend only on the largest Lorentz factor of the plasmoids in such jets and on the mass of the CR particles. In the CB model, CRs with energy above their knee are CRs which were reflected backward from slower CBs or supernova shells which were ejected earlier. This interpretation is different from that adopted in the Fermi/shock acceleration models, where the CR knee depends on their rigidity $R = pc/Z$, namely on the momentum of the CR particle multiplied by the speed of light per unit charge.

2. The Knee Energy of Cosmic Rays

The energy spectrum of high energy CR nuclei from well below to well above the CR knee is shown in **Figure 1** adopted from [18].

Until recently the measured knee energies of individual cosmic ray nuclei were not accurate enough to conclude whether they depend on their masses, as expected in the CB model [13], or on their rigidities as expected in the Fermi/shock acceleration models. However, while the rigidities of high energy electrons and protons are practically equal, their masses are very different; $m_p/m_e \approx 1836$. In the CB model, that implies knee energies of high energy CR electrons which satisfy [13] [14] [15],

$$E_{knee}(e) \approx (m_e/m_p) E_{knee}(p) \approx 1 \text{ TeV}. \quad (1)$$

Fortunately, during the past decade, precise enough measurements of the energy spectrum of CR electrons were extended into the TeV range, in particular by the H.E.S.S [19] [20], AMS [21], Fermi-LAT [22], DAMPE [23] and CALET [24] collaborations. As shown in **Figure 2**, they have confirmed the existence of a knee around ~ 1 TeV in the energy spectrum of high energy cosmic ray electrons, which was predicted by the CB model [13] [14] [15] using the observed knee around 2 PeV [18] in the energy spectrum of cosmic ray protons.

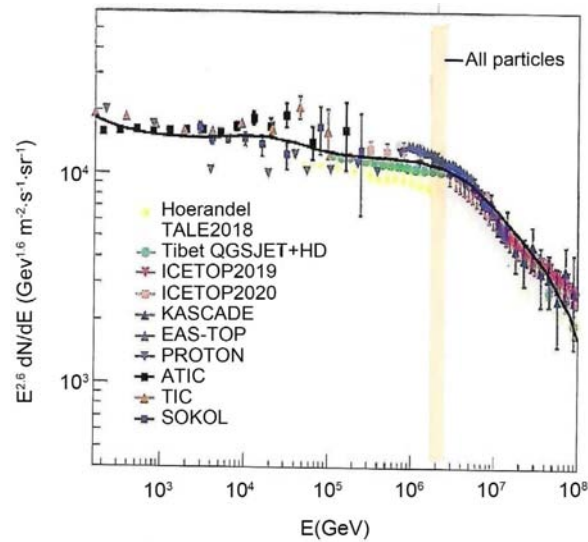


Figure 1. The energy spectrum of cosmic ray nuclei around the cosmic ray knee reported in [18]. The knee energy of cosmic ray protons is indicated by the wide band around 2 PeV.

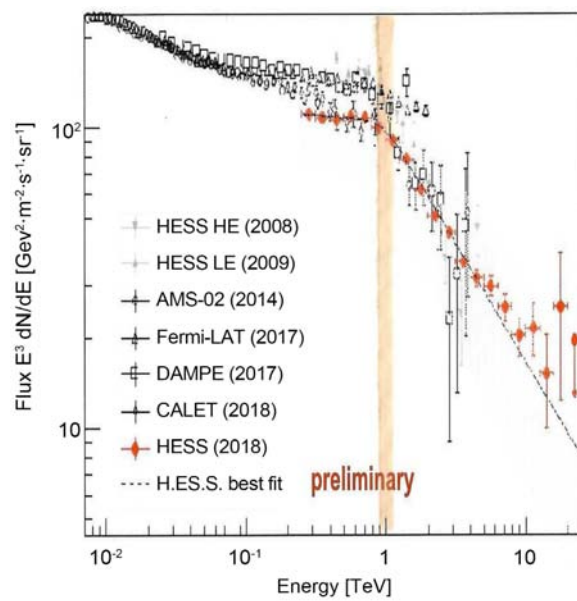


Figure 2. The high energy spectrum of cosmic ray electrons compiled in [19]. The electron knee energy predicted by the CB model is indicated by the vertical band around 1 TeV.

Moreover, the observed knees in the energy spectra of cosmic ray nuclei [18] and electrons [19]-[24] imply that the largest Lorentz factor of CBs fired ($t = 0$) by the main source of high energy CRs, is roughly,

$$\gamma_{max}(0) \approx \sqrt{E_{knee}(CR)/2m_{CR}c^2} \approx 1000. \tag{2}$$

In the CB model, this value of $\gamma_{max}(0)$ of CBs at launch is common to both the electrons and protons nearly at rest in the CBs. It allows the following critical tests of the common origin of CRs and GRBs.

3. Evidence from GRB 221009A

In the CB model, the peak energy E_p of the time integrated distribution of the prompt emission photons of a GRB, which is produced by inverse Compton scattering (ICS) of optical photons ($\varepsilon \approx 1.65$ eV, *i.e.*, $\nu = 4 \times 10^{14}$ Hz) by CB electrons having $\gamma_{max} \approx 1000$, is given by

$$\max[(1+z)E_p] \approx 2(\gamma_{max})^2 \varepsilon \approx 3.3 \text{ MeV}. \quad (3)$$

Indeed, this value is consistent with the measured $(1+z)E_p = 3503 \pm 133$ keV, [25] of the “brightest of all time” GRB 221009A at redshift $z = 0.151$.

Moreover, the time averaged peak photon energy $E_p \approx 2.912$ MeV and the isotropic equivalent energy release, $E_{iso} \approx (1.2 \pm 0.1) \times 10^{55}$ erg measured in GRB 221009A [25] are the record high values measured so far in a GRB. Such high values are estimated to be observed once in 10,000 years. They were shown [25] to be consistent with the best fit Amati correlation [26],

$$(1+z)E_p \propto [E_{iso}]^{0.42}, \quad (4)$$

in a sample of 315 Konus-Wind GRBs, which is shown in **Figure 3**.

In the CB model [17 for a review], far off axis GRBs, *i.e.*, those which are viewed from angles that satisfy, $\theta^2 \gamma^2 \gg 1$, have relatively low $(1+z)E_p$ and E_{iso} values which satisfy,

$$(1+z)E_p \propto [E_{iso}]^{1/3}. \quad (5)$$

Near axis GRBs, *i.e.*, those with viewing angles that satisfy, $\theta^2 \gamma^2 \leq 1$, have relatively large $(1+z)E_p$ and E_{iso} values and satisfy the correlation [26],

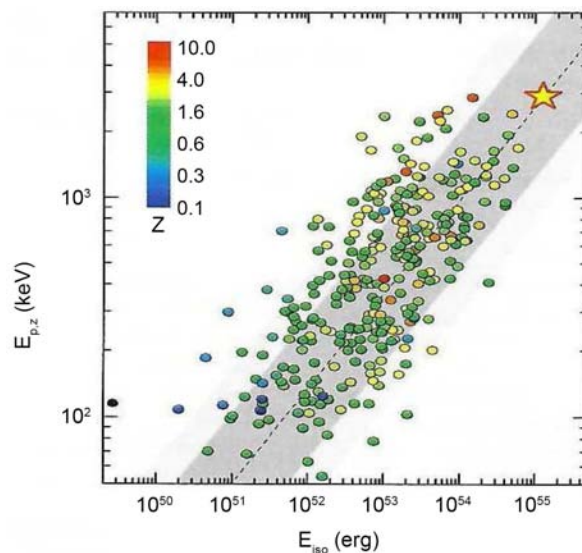


Figure 3. The best fit Amati correlation reported in [25] for 315 long GRBs with known redshift observed by Konus-Wind. GRBs are represented by circles; the color of each data point represents the GRB redshift. The error bars are not shown for reasons of clarity. GRB221009A is indicated by a red star. The best fit Amati relation is plotted as a dashed line.

$$(1+z)E_p \propto [E_{iso}]^{1/2}. \quad (6)$$

Consequently, a mixed population of near axis and far off axis GRBs is expected to satisfy the Amati correlation [26] with an average power-law index $(1/2 + 1/3)/2 \approx 0.42$. Indeed it is that reported in [25], and is shown in **Figure 3**. Moreover, a sum of two power laws corresponding to low and high values of $(1+z)E_p$,

$$(1+z)E_p = aE_{iso}^{1/3} + bE_{iso}^{1/2} \quad (7)$$

also describes well the mixed population of far off axis GRBs and near axis GRBs.

4. The Missing GRB Neutrinos

The jet of highly relativistic CBs, which produces a GRB, propagates through the interstellar medium and/or stellar shells ejected earlier. Its nucleons produce a narrow conical beam of short lived high energy pions and kaons along the axis of the much wider GRB cone [13]. Their decay produces a narrow conical beam of high energy gamma rays, electron and muon neutrinos. Since the transverse momentum of their parent π and K mesons is of the order of their masses [27], their produced high energy neutrinos and gamma rays (in the source rest frame) are mainly within a cone of an opening angle $\approx m_\pi/\gamma m_p$. The high energy gamma rays from GRBs are attenuated by pair production on background photons [28], while the high energy neutrinos are not attenuated. Both are emitted into a cone much narrower than that of the MeV gamma rays from a GRB. But, the small cross section of neutrinos and the CB model estimate [13] of the flux of GRB neutrinos imply that the chances to detect on Earth the narrow burst of high energy (TeV) neutrinos from a GRB are rather small. That is consistent with the reported failure by the IceCube collaboration [29] to detect high energy neutrinos from GRBs, including GRB 221009A.

5. Conclusion

Multi-messenger astronomy has recently provided compelling evidence in support of the CB model solution of the 111-years-old cosmic ray puzzle. Namely, the bulk of high energy cosmic rays (CRs) are produced by the highly relativistic narrow jets of plasmoids of ordinary stellar matter launched in core collapse of stripped-envelope massive stars to neutron stars and stellar mass black holes. Such events produce also visible GRBs only when the jet happens to point near our direction, but very rarely a detectable narrower neutrino burst. The maximal peak energy of GRBs, as measured in “the brightest of all time” GRB 221009A [30] correctly predicts the observed knee energies of CR protons, nuclei and electrons. The chances to detect the expected very narrow burst of neutrinos from a GRB by detectors such as IceCube are very small, even for record bright events like GRB 221009A. Despite the above, a complete understanding of how such highly relativistic jets of plasmoids are formed and why the maximum bulk

motion Lorentz factor of their plasmoids is ≈ 1000 is still lacking.

Acknowledgements

We thank M. Moshe for a useful comment.

Conflicts of Interest

The authors declare no conflicts of interest regarding the publication of this paper.

References

- [1] Hess, V.F. (1912) *Physikalische Zeitschrift*, **13**, 1084-1091.
- [2] Fermi, E. (1949) *Physical Review*, **75**, 1169-1174.
<https://doi.org/10.1103/PhysRev.75.1169>
- [3] Ginzburg, V.L. and Syrovatskii, S.I. (1964) *The Origin of Cosmic Rays*. Pergamon Press, Oxford. <https://doi.org/10.1016/B978-0-08-013526-7.50011-6>
- [4] Krymskii, G.F. (1977) *Akademiia Nauk SSSR Doklady Soviet Physics Doklady*, **22**, 327.
- [5] Bell, A.R. (1978) *MNRAS*, **182**, 147-156. <https://doi.org/10.1093/mnras/182.2.147>
- [6] Blandford, R.D. and Eichler, D. (1987) *Physics Reports*, **154**, 1-75.
[https://doi.org/10.1016/0370-1573\(87\)90134-7](https://doi.org/10.1016/0370-1573(87)90134-7)
- [7] Berezhko, E.G. and Krymskii, G.F. (1988) *Soviet Physics Uspekhi*, **31**, 27-51.
<https://doi.org/10.1070/PU1988v031n01ABEH002534>
- [8] Reynolds, S.P. (2008) *Annual Review of Astronomy and Astrophysics*, **46**, 89-126.
<https://doi.org/10.1146/annurev.astro.46.060407.145237>
- [9] Sinitsyna, V.G. and Sinitsyna, V.Y. (2023) *Universe*, **9**, Article No. 98.
<https://doi.org/10.3390/universe9020098>
- [10] Dar, A., Kozlovsky, B.Z., Nussinov, S. and Ramaty, R. (1992) *ApJ*, **363**, 118.
<https://doi.org/10.1086/171138>
- [11] Dar, A. (1998) *ApJ*, **500**, L93. <https://doi.org/10.1086/311401>
- [12] Dar, A. and Plaga, R. (1999) *Astronomy and Astrophysics*, **349**, 259-266.
- [13] Dar, A. and De Rújula, A. (2008) *Physics Reports*, **466**, 179-241.
<https://doi.org/10.1016/j.physrep.2008.05.004>
- [14] Dado, S. and Dar, A. (2015) *ApJ*, **812**, 38.
- [15] De Rújula, A. (2019) *Physics Letters B*, **790**, 444-452.
<https://doi.org/10.1016/j.physletb.2019.01.059>
- [16] Shaviv, N.J. and Dar, A. (1995) *ApJ*, **447**, 863. <https://doi.org/10.1086/175923>
- [17] Dado, S., Dar, A. and De Rújula, A. (2022) *Universe*, **8**, Article No. 350.
<https://doi.org/10.3390/universe8070350>
- [18] Zhang, P.-P., Guo, Y.-Q., Qiao, B.-Q. and Liu, W. (2012) Constraining the Position of the Knee in the Galactic Cosmic Ray Spectrum with Ultra-High-Energy Diffuse γ -Rays.
- [19] Kerszberg, D. (2017) Contributions of the High Energy Stereoscopic System (H.E.S.S.) to the 35th International Cosmic Ray Conference (ICRC), Busan, Korea 2017.
- [20] Aharonian, F., *et al.* (2008) *PRL*, **101**, Article ID: 261104.

- [21] Aguilar, M., *et al.* (2014) *PRL*, **13**, 21102.
- [22] Abdollahi, S., *et al.* (2017) *Physical Review D*, **95**, Article ID: 082007.
- [23] Chang, J., *et al.* (2017) *Astroparticle Physics*, **95**, 6-24.
- [24] Adriani, O., *et al.* (2018) *PRL*, **120**, Article ID: 261102.
- [25] Frederiks, D., Svinkin, D., Lysenko, A.L., Molkov, S., *et al.* (2023) *The Astrophysical Journal Letters*, **949**, L7. <https://doi.org/10.3847/2041-8213/acd1eb>
- [26] Amati, L. (2006) *Monthly Notices of the Royal Astronomical Society*, **372**, 233-245. <https://doi.org/10.1111/j.1365-2966.2006.10840.x>
- [27] Sirunyan, A.M., *et al.* (2017) *Physical Review D*, **96**, Article ID: 112003.
- [28] Gould, R.J. and Schrer, G. (1966) *Physical Review Letters*, **16**, 252-254.
- [29] Abbasi, R., *et al.* (2022) Searches for Neutrinos from Gamma-Ray Bursts Using the IceCube Neutrino Observatory.
- [30] Burns, E., Svinkin, D.S., Fenimore, E., *et al.* (2023) *The Astrophysical Journal Letters*, **946**, L31. <https://doi.org/10.3847/2041-8213/acc39c>

Calabi-Yau Topology of Primordial Fermions

Edwin Eugene Klingman 

Cybernetic Micro Systems, Inc., San Gregorio, CA, USA

Email: klingman@geneman.com

How to cite this paper: Klingman, E.E. (2024) Calabi-Yau Topology of Primordial Fermions. *Journal of Modern Physics*, 15, 132-158.

<https://doi.org/10.4236/jmp.2024.151005>

Received: December 21, 2023

Accepted: January 28, 2024

Published: January 31, 2024

Copyright © 2024 by author(s) and Scientific Research Publishing Inc.

This work is licensed under the Creative Commons Attribution International License (CC BY 4.0).

<http://creativecommons.org/licenses/by/4.0/>



Open Access

Abstract

Quantum field theory creates fermions via abstract operators exciting abstract fields, with a specific field for each type of specific particle. This operator algebra lends itself well to quantum statistics, nevertheless, our physical understanding of this process is nonintuitive at best. In this paper we analyze the creation of fermions from primordial gauge field quantum gravity loops in the context of Calabi-Yau manifold theory. I extend a prior mass-gap treatment based on Yang-Mills gauge theory of higher order self-interaction to include the half-integral spin of fermions.

Keywords

Calabi-Yau Topology, Fermion Spin, Particle Genesis, Primordial Field, Self-Interaction Equations, Yang-Mills Gravity

1. Introduction

Fermions, generally identified as the matter in our Universe, are characterized by a finite mass-gap above the vacuum and by $\frac{1}{2}$ -integer spin. There is currently no understanding of the creation of matter, meaning fermions with *mass*, *spin*, and *charge*. The *Millennium \$1,000,000 Mass gap Prize* asks for an explanation of why particle masses don't decay to vacuum energy. The lowest stable particle energy over the vacuum is the mass gap in question. The Standard Model of Particle Physics does not know how to compute particle masses; they are put in by hand. Mass is tricky in quantum field theory, which is based on the concept of a specific field distributed throughout space for each type of particle. Stimulating the field is considered to bring the particle into existence. How mass evolved is a mystery. Quantum fields cannot be measured, and their physical nature is unknown; both *epistemic* and *ontological* interpretations exist.

Sbitnev [1], using quaternions for translation in 4D space and spin rotation on 3D spheres, deals with a space densely filled by an incompressible quantum su-

perfluid; a Bose-Einstein condensate. Computations on this fluid lead to gravitomagnetic equations similar to Maxwell's equations for electromagnetic fields: "Schrödinger, vorticity, and wave equations follow from these equations as a natural outcome." Sbitnev's approach differs from primordial theory based primarily on ontological assumptions. For example, $\rho(\mathbf{r}, t)$ is the density distribution of "sub-quantum particles, carriers of masses"; no such sub-quantum particles exist in primordial theory. Also, "Physical vacuum is a special super fluid medium populated by enormous amounts of virtual particle-antiparticle pairs", while virtual pairs do not exist in primordial theory. Further, Sbitnev introduces a torus with a string twisting two times around the torus tube, then maps this (in a physically impossible way) into a 3D sphere and draws conclusions about spin. "The frequency ω is that of rotation about the center of the torus, the toroidal vortex wall can be filled by helicoidal strings." Strings do not exist in primordial theory. Rather than zero viscosity, Sbitnev considers dynamical "viscosity that fluctuates about zero in time. ... we believe that it is zero in the average in time, but its variance is not zero." He further believes that this viscosity μ avoids a singularity at the vortex core and supports infinite lifetime of the vortex. Based on $\Omega = c\rho_m\omega$, he observes that the vorticity equation $\rho_m \frac{\partial \omega}{\partial t} = \mu(t)\nabla^2 \omega$ describes vortex motion in a local reference frame sliding along an optimal trajectory guided by the wave function that is solution of Schrödinger's equation, ideally simulating the particle moving along the Bohm trajectory. In summary, Sbitnev treats gravito magnetism with *quantum fields per particle* and with *vacuum as virtual particle-antiparticle pairs*. Finally, Sbitnev assumes the "weak field approximation", a crucial mistake made by physicists for over a century.

Quantum field theory is well defined, so it is relatively easy to compare to primordial field theory, which is explicitly based on an ontological model of the *physically real* primordial field (that all modern theories assume that all forces converge to.) Quantum interactions occur between fields/particles and the system evolves through these interactions; primordial field evolution is possible only through *self-interaction; nothing else exists to interact with*. Quite simply, the change in state of the system, represented by ∇ acting on the system, is equal to the system acting on itself, hence:

$$\nabla \psi = \psi \psi \Rightarrow \psi(\xi) = -\xi^{-1}, \psi(\xi) = \xi^{-1} \quad (1)$$

with $\nabla_\xi = \partial_\xi$. Solutions to the self-interacting equations include inverse scalar and inverse vector; interpreted as time and space, these yield duration and distance, both applicable to fields. Primordial theory considers only one field to exist, with aspects based on space $\psi(\xi) = \frac{1}{\mathbf{r}}$ and time $\psi(\xi) = -\frac{1}{t}$, and dynamics based on turbulence of the ultra-dense field. Via Hestenes' *Geometric Calculus* operating on $\psi = \mathbf{G} + i\mathbf{C}$ we derive Heaviside's gravitomagnetic dual of Maxwell's electromagnetics. The important self-interactions are those of a given momentum density interacting with field circulations induced by the momentum den-

sity, formulated on a fractional lattice [2].

Primordial field theory has no undefined entities such as the quantum fields and wave functions of quantum field theory; there is only the reality of the gravitomagnetic field. Sbitnev neglects charge in his treatment of spin; we will derive electromagnetic charge in primordial field theory. First, we examine the issue of fermion spin.

In primordial field theory the primordial field is the real physical gravitomagnetic force field that interacts with moving mass density. In the beginning the density of mass-energy was essentially as high as we wish it to be. Since particle creation occurs at LHC energy densities, we already know the relevant range of energies; consider the *collision-event-resulting-jets* simply to be a case of the primordial field in action, induced via mind boggling instrumentation. In 2006, as I began primordial field theory, the LHC was in process of reassessing their expected “quark gas” in the collisions to be instead a *perfect fluid*. This very real particle phenomena is derived in primordial field theory through the self-interaction process. Self-linking turbulence involves varying energy distribution, and momentum density induces circulation in the local C-field. The key equation is $\nabla \times C = -\rho v + \frac{\partial G}{\partial t}$ with $g = c = \hbar = 1$. The field energy density ρ moving through local gravity G (the ether) induces circulation $\nabla \times C$. This circulation induces a higher order circulation, as the field interacts with itself. My quantum loop gravity fractional lattice treatment of this interlinked torus system has been shown to produce a stability zone in which collapse to a primal torus is energetically favored. I formulate this as a mass gap “existence proof”, analyzing mass-gap in terms of higher-order self-interactions of the primordial field by reinterpreting the non-Abelian term of Yang-Mills gauge theory as follows: $[A_\mu, A_\nu] \Rightarrow [A_\mu^{(i)}, A_\mu^{(i+2)}]$ adapting it to higher-order self-interaction. In this paper we assume this mass-gap existence proof establishes the fundamental requirement and we analyze the fermion spin in the context of Calabi-Yau theory.

A quantum theorist may wonder, “*why introduce Calabi-Yau?*” The answer is subtle, but for the most part it means that I do not have to *prove* my statements. Calabi-Yau provides a framework of proof and defines the limits and constraints of the framework: as long as I remain in the framework, my statements are true. For example, Sbitnev introduces a torus with a “string”, which he claims twists two times around the torus tube, then he proceeds to map this into a physically impossible 3D sphere. But as there is ever-more reason to doubt the efficacy of string theory, I prefer to have a specific mathematico-logical framework in mind and Calabi-Yau theory provides exactly that framework. The decision to remain within the bounds of a compact Kahler manifold, with a vanishing first Chern class, allows one to assume a Ricci-flat metric. Hestenes’ *Geometric Calculus* applies on a Ricci-flat metric, as well as Wolfram’s *Mathematica*-based 3D perspectives.

In short, *Primordial field theory* differs significantly from *Quantum field*

theory, which assigns an individual quantum field existing at every point in space-time for each class of elementary particle. Specific particles are invoked via particle creation operator and viewed as excitations in a specific field; when Feynman developed his quantum field theory of gravity, he began by assuming “*gravity as the 31st field*” [3]. Creation of such particles is nonintuitive; operator algebra enables physics in which the total number of particles changes based on harmonic oscillators and provides an *abstract* means of creating and annihilating *specific* particles, based on specific fields. Elsewhere I develop an intuitive understanding of particle creation from the primordial field of the universe, involving new concepts of physics. Many physicists, comfortable with complex, albeit nonintuitive, theories, tend to dismiss intuitive approaches to any complex problem they are familiar with, so I formulate the theory in terms of Einstein’s field equations, Yang-Mills gauge theory, and now Calabi-Yau topology, these being familiar approaches that have failed to deliver the goods but are felt to be generally valid approaches to the problem. The structure of this Letter is as follows:

Sec. 2 The ontology of time and space is introduced. We ask if there could be gravity in a universe devoid of matter (no particles)?

Sec. 3 The theory of the primordial field of our Universe, prior to the creation of matter.

Sec. 4 The *Calabi conjecture* is framed in terms of a metric, the geometry of a space, and such a metric, derived in 1921 by Kasner, yields an exact solution to Einstein’s field equations, interpreted herein in terms of the dynamical primordial field.

Sec. 5 Review of primordial field equation in the Kasner metric and higher order self-interaction physics. Re-interpreting the Yang-Mills nonabelian terms yields a mass-gap existence proof.

Sec. 6 Topological aspects of the Calabi-Yau manifold, including Kahler geometry, first class Chern, complex manifolds, and Ricci curvature.

Sec. 7 Primordial flow analyzed in Calabi terms.

Sec. 8 Ontological flow on a torus.

Sec. 9 Separation of $U(1) \times U(1)$ flow symmetry.

Sec. 10 Derivation of Quantum Spin.

Sec. 11 Parallel vector transport around a closed path shows $\frac{1}{2}$ -integral character of this flow.

Sec. 12 Measurements on a dynamic model.

Sec. 13 Summary.

Sec. 14 Conclusions.

2. The Ontology of Time and Space

Laurent Field states [4]: “*Spacetime is just an abstraction.... I believed all my life that spacetime exists, but I no longer do so.*” Einstein early concluded that space and time are abstractions; “*there is no vacuum [aka ‘empty space’] absent field.*”

[5]. He later concluded that the field is effectively the ether through which waves propagate but did not, however, go back and fix special relativity; he instead introduced *curved space*, which dominated physics for a century. In curved space local gravitational energy density is undefined; instead, we have variations of “*quasi-local-mass*”. I treat these conflicting concepts in terms of Heaviside’s gravitational equations derived from *the primordial field self-interaction principle* [6].

Relevant to these concepts is *Ricci curvature*, which corresponds to a space with no matter. Calabi, a geometer, asked if there could be gravity in our universe even if space is a vacuum totally devoid of matter [7]. If so, he saw that curvature makes gravity without matter possible. In the following we review the geometer’s approach to this (essentially physics) problem and attempt to clarify problematic areas of this conjecture: we identify “matter” with “particles”, specifically fermions, while we identify “the vacuum” as the primordial field.

3. The Primordial Field of the Universe

The standard model of particle physics assumes all forces merge into one at the big bang, though this has not been demonstrated. Our fundamental assumption is that the primordial field, and *nothing but the primordial field*, existed at the Creation. If interaction is to occur (as it must, to evolve to our current Universe) the field must interact with itself; nothing else exists to interact with. This *Self-Interaction Principle* is represented by the Self-Interaction equation

$\nabla\psi = \psi\psi$ where ψ represents the primordial field and ∇ represents the change operator. If the field depends upon some parameter ξ , the change operator becomes $\nabla \rightarrow \partial_\xi$, which leads to two formal solutions: a scalar solution $\psi(\xi) = -\xi^{-1}$ and a vector solution $\psi(\xi) = \xi^{-1}$, associated respectively with time t and position \mathbf{r} . Defining primordial field $\psi = \mathbf{G}(\mathbf{r}, t) + i\mathbf{C}(\mathbf{r}, t)$ with corresponding operator $\nabla = \nabla + \partial_t$, Equation (1) becomes

$$(\nabla + \partial_t)(\mathbf{G} + i\mathbf{C}) = (\mathbf{G} + i\mathbf{C})(\mathbf{G} + i\mathbf{C}) \tag{2}$$

A Hestenes’ Geometric Calculus expansion of this equation immediately leads to the following:

Self-Interaction equations	Heaviside equations	
$\nabla \cdot \mathbf{G} = \mathbf{G} \cdot \mathbf{G} - \mathbf{C} \cdot \mathbf{C}$	$\nabla \cdot \mathbf{G} = -\rho$	(3)
$i\nabla \cdot \mathbf{C} = i2\mathbf{G} \cdot \mathbf{C}$	$\nabla \cdot \mathbf{C} = 0$	
$\partial_t \mathbf{G} - \nabla \times \mathbf{C} = \mathbf{G} \times \mathbf{C} \pm \mathbf{C} \times \mathbf{G}$	$\nabla \times \mathbf{C} = -\rho\mathbf{v} + \partial_t \mathbf{G}$	
$i\nabla \times \mathbf{G} + i\partial_t \mathbf{C} = 0$	$\nabla \times \mathbf{G} = -\partial_t \mathbf{C}$	

The terms on the left are given *field energy density* interpretation leading to Heaviside’s 1893 formulation [8] of the right side of (3) with $\hbar = g = c = 1$. These equations are identical (under iteration) to Einstein’s non-linear field equations. Self-interaction Equations (3) derive from (2) in straightforward fashion. To obtain the right-hand side physical meaning is attached to field ψ , with \mathbf{G} gravity and \mathbf{C} the gravitomagnetic field. The concept of *field strength* is absent

in the derivation, other than the implicit assumption of strong fields existing at the big bang. When Heaviside's equations are derived by linearizing Einstein's equations (discarding higher order terms) the resultant equations are erroneously labeled the *weak field approximation* to Einstein's equations, leading physicists to regard Einstein's geometric equations as the "true" physics with Heaviside believed to hold only for *weak fields*. Since our Heaviside formulation is equivalent to Einstein at all field strengths; these equations of gravity hold at all scales, including the particle scale, *geometry-based* concepts of gravity are abstract and unnecessary for a theory of gravity; despite the common assumption that gravity depends on mass, Heaviside's equations clearly show that the actual dependence is on mass density ρ . The equations of gravity (3) are based on gravitational fields $G(\mathbf{r},t)$ and $C(\mathbf{r},t)$ while Yang-Mills is based on gauge fields. Field equation $\nabla \cdot C = 0$ implies we can make use of vector identity $\nabla \cdot \nabla \times A = 0$ to replace C with vector $\nabla \times A$. Compatible with Equations (3) are gauge field equations:

$$C = \nabla \times A, \quad G = -\nabla \phi - \partial_t A, \quad \partial_t \phi + \nabla \cdot A = 0 \quad (4)$$

The first two Equations in (4) define the fields in terms of the four-potential A , while the last eqn specifies the Lorenz gauge condition, $\partial_\mu A^\mu = 0$. The scalar potential $\phi = -m/r$, and vector potential $A = \mathbf{v}$; gauge field A is seen to be a velocity field \mathbf{v} . Expansion of the gauge field equation allows us to interpret the Abelian form of the field strength: $F_{\mu\nu} = \partial_\mu A_\nu - \partial_\nu A_\mu$. The field strength tensor constructed from the above is shown [9]:

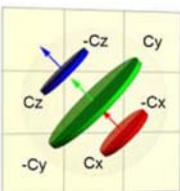
$$F_{\mu\nu} = \begin{bmatrix} 0 & G_x & G_y & G_z \\ G_x & 0 & -C_z & C_y \\ G_y & C_z & 0 & -C_x \\ G_z & -C_y & C_x & 0 \end{bmatrix} \Rightarrow \begin{array}{c} \text{Cz} \quad \text{Cy} \\ \text{-Cx} \quad \text{Cx} \\ \text{-Cy} \end{array} = n\hbar \quad (5)$$


Figure 1. The C-field momentum-energy density matrix.

Ten coefficients are needed to describe how metric coefficients change from point to point in the manifold. In **Figure 1**, the Heaviside field tensor is symmetrical about the 4×4 diagonal, with two sets of six numbers on either side of the diagonal. Gravitomagnetic terms $C_y = C_{xz}$ and $-C_y = C_{zx}$ represent bivectors rotating in the xz -plane equivalent to the rotation about the axial vector on the y -axis. If $g=c=1$ the C-field is described by $C = \mathbf{r} \times \mathbf{p}$ where \mathbf{p} is the momentum density inducing circulation equivalent to angular momentum density ($\mathbf{L} = \mathbf{r} \times \mathbf{p}$). In the Einstein-deHaas sense, gravitomagnetic field C essentially is angular momentum. At particle scale we expect this inherent spin density field to be quantized, as implied in **Figure 1**. Were this not the case, a C-field vortex, like a skater pulling in her arms to zero, would spin up to infinite density at a point. Thus, we anticipate an extended object, not the point particles of quantum field theory.

The formulation $F^{\mu\nu} = \partial^\mu A^\nu - \partial^\nu A^\mu$ separates radial field $G(\mathbf{r})$ and gra-

vitomagnetic field $C(\mathbf{r})$, with gravitomagnetic terms representing angular momentum. Planck's constant has dimensions of angular momentum $\hbar = ml^2/t = mvr$, so this is a feasible underlying degree of freedom to be quantized. If gravity does not interact with itself in a static situation, one must ask what Yang-Mills non-Abelian term $[A_\mu, A_\nu]$ represents. It has not been interpreted in any useful fashion dynamically, so our mass-gap existence proof attempts a new interpretation of *self-interaction* in Yang-Mills. This is justified by the fact that almost seventy years of work in this field has failed to solve the critical problems. This is perhaps hinted at with a quote from Taubes:

“Once upon a time a Martian arrived, gave us the Yang-Mills equations, and left.”

Jaffe and Witten define the mass gap problem [10] and note: *“Some results are known for Yang-Mills theory on a 4-torus T^4 approximating R^4 and, while the construction is not complete, there is ample indication that known methods could be extended to construct Yang-Mills on T^4 .”* The existence proof approach for a solution to the mass-gap problem [11] will now be used to explore the issue of $\frac{1}{2}$ integral spin.

4. The Calabi Conjecture

Yau observes that Einstein's equations tie curvature to gravity. This century old concept has been accompanied by century old paradoxes, of the type associated with the concept of “quasi-local-mass” [12]. How physical energy density can *be encoded as geometry* is explained in [13]. Our goal here is to employ topology and geometry on the primordial field ontology.

Calabi's conjecture is concerned with spaces that have a specific type of curvature known as *Ricci curvature*, relating to the distribution of matter within the space. *A space is Ricci-flat if space holds no matter.* Eugenio Calabi, a geometer, viewed the problem as “strictly geometry” and therefore framed the problem in terms of a *metric*, *i.e.*, the geometry of a space, defining the length of every path, in terms of distance between points in space. However, a given topological space can have many possible shapes and many possible metrics, so Yau concludes that Calabi's conjecture concerning what kind of metric a space can “support” is equivalent to asking, *“For a given topology, what kind of geometry is possible?”*

We are now dealing with ontological concepts of physics such as vacuum, field, matter, energy density, and abstract concepts of geometry such as metric, topology, curvature, and manifold. We begin with a specific physics problem, the universe defined by the Kasner metric, then analyze it in terms of topological concepts.

5. The Dynamic Universe Defined by the Re-Interpreted Kasner Theory

We assume that the primordial field was present at the moment of Creation and expanded as the *big bang*. Perhaps initially only spherical symmetry applied, G ,

but at some point, this symmetry broke, and the field became ultra-turbulent, with vortices and tori representing C-field angular momentum density distributions. Physically real turbulent loops twist in 3D and intersect themselves; such reconnection events realign forces—both energy and momentum proceed in opposite directions along the reconnection axis. Such an event has been used to initiate analysis of the Kasner metric, an exact solution to the Einstein field equation. In [14] I construct the physics of h_{ij} for a dynamic spatially homogenous anisotropic Bianchi vacuum model that solves Einstein's equations in terms of the physically real primordial field, otherwise devoid of matter. Kasner derived the solution to $R^{\mu\nu} = 0$ in 1921. Narlikar and Karmarkar's later formulation is:

$$ds^2 = c^2 dt^2 - \sum_{j=1}^{D-1} (1 + nt)^{2p_j} dx_j^2. \quad (6)$$

While Equation (6) is subject to constraints on p_j , the meaning of parameter n has been obscure. I interpret n to be primordial field $C(t)$ induced by momentum p_j , assumed to exist because of a reconnection event. In **Figure 2(a)** $r(x, y, z)$ is the point in space where the induced C-field is measured, while **Figure 2(b)** displays a C-field energy-density histogram based on axial symmetry associated with an arbitrary slice through the energy density history at $r(t)$. An arbitrary slice of the field shows self-induced field behavior, with first and second order induction diagrammed in **Figure 2(c)**.

The higher-order self-interaction shown in **Figure 2(c)** is treated elsewhere, but the matter-free field has energy density distribution that is turbulently dynamic. This contrasts with the static metrics of the one-body theory of general relativity such as Schwarzschild and Kerr. The Schwarzschild metric is $ds^2 = g_{\mu\nu} dx^\mu dx^\nu = (1 + 2\phi) dt^2 - (1 - 2\phi)(dx^2 + dy^2 + dz^2)$ where $\phi \sim m/r$ is a function only of position. In other words, the *static* metric is not a function of time; distribution of the field is fixed in space over all time. The *dynamic* metric (Equation (6)) is best understood as dynamically describing the distribution of the field over time, when $n \neq 0$, due to the effect of the momentum density \mathbf{p} of the field. When $n = 0$ the Kasner metric reduces to Euclidean space since $(1)^{2p} = 1$ is always unity. However, if we assume that momentum density \mathbf{p} is non-zero, then our interpretation of the n term as the value of the local C-field induced by \mathbf{p} implies that n cannot be zero.

Kasner is a spherical topology in the sense that the boundary of the field can be deformed to a sphere. The constraints on the Kasner metric include a geometry in which the distributed field lengthens in one direction while shrinking in the other two directions, and vice versa. Momentum constraints $\sum_{j=1}^{D-1} p_j = 1$ and $\sum_{j=1}^{D-1} p_j^2 = 1$ determine the specific shape. Kasner topology of a primordial field universe is not sufficient for creation of a fermion; the mass-gap existence proof relies upon local ultra-high-density field turbulence (found at the big bang or in atom-atom collisions at LHC) to assume evolution of a vortex-to-helix-to-torus topology, hence we next investigate topological concepts applicable to Calabi-Yau.

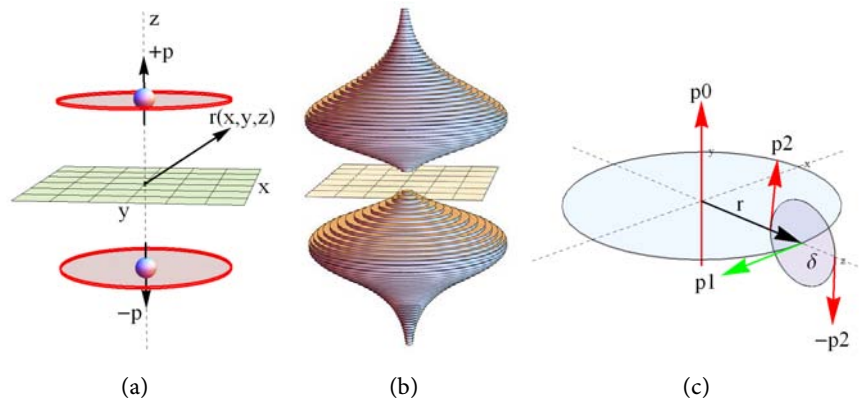


Figure 2. (a) C-field energy is calculated at position \mathbf{r} with respect to a reconnection event in an anisotropic open universe described by the Kasner metric. (b) An energy history of two such induced C-field circulations. The time axis is mapped onto the reconnection axis corresponding to the z -axis, and cylindrical symmetry is applied. (c) An arbitrary slice through the momentum axis reveals second and third order induced C-field flows.

6. The Topology of Calabi-Yau

A manifold is a space or surface of any dimension n ; the number of two-dimensional spaces is restricted to two basis types: either a sphere or a donut. The dynamic Kasner solution developed above represents a universe composed of nothing but a primordial field. Unlike the Schwarzschild solution, the cosmological Kasner solution does not have an “outside”; the surface or boundary of this universe is such that all the primordial field is “inside” the boundary, deformable into a sphere. In the Kasner solution the field is such that the distribution of field energy expands or contracts anisotropically; as noted, two dimensions increase in length, while one decreases, or vice versa. Conversely, the mass-gap solution has donut topology, specifically a one-hole torus. The Kasner *spherical* topology of the primordial universe differs from the local *toroidal* topology of the fermion, so relevant topological concepts are examined. Per Yau:

“Calabi wanted to know if a certain kind of complex manifold—a space that was compact and ‘Kahler’—that satisfied specific topological conditions (vanishing first Chern class) could have a Ricci-flat metric.”

Kahler: Manifolds resemble Euclidean space on a local scale but can be very different on a global scale. Calabi’s conjecture pertains strictly to *complex* manifolds—surfaces that are expressed in terms of complex numbers, *i.e.*, two-dimensional local surfaces. Riemann surfaces are complex and automatically qualify as Kahler; space looks Euclidean at a single point and stays close to Euclidean when one moves away from the point. Such spaces are even-dimensional as only complex manifolds can have Kahler geometry, which provides an indication of how close a space comes to being Euclidean based on criteria that are not strictly related to curvature. Whether a particular metric is Kahler is a function of how the metric changes as one moves from point to point. Kahler manifolds are a subclass of complex manifolds known as Hermitian manifolds, “on which

you can put the origin of a complex coordinate system at any point, such that the metric will look like a standard Euclidean metric at that point.” Kahler manifolds have a rotational symmetry such that vectors $(a,b) = a + ib$ on the manifold are rotated 90° via multiplication by the imaginary unit, i , with the length of the vector preserved. This “internal” symmetry supports parallel transport, as we will see in a following section. This internal symmetry, *which in many ways defines Kahler manifolds*, is restricted to the space tangent to the manifolds.

Internal symmetry: The “*internal symmetry*” of Kahler geometry is unrelated to the *internal symmetry* discussed in our Yang-Mills-based *existence proof* of the mass-gap. That internal symmetry refers to “iso-spin symmetry” which Heisenberg invented to allow use of Pauli’s SU(2) spin matrix algebra. *Abstract* iso-spin space differs from *physical* spin space, hence the qualification “internal space”. In Calabi-Yau space theory, “internal space” is instead associated with the six “hidden dimensions” (of a ten-dimensional string-theory formulation), assumed on the order of 10^{-30} cm, modelled after Kaluza-Klein’s treatment of the 5th dimension in their attempt to unify gravity and electromagnetics.

For the primordial field we choose 4-D constructions, rather than the 10-D or 11-D of string theory, which has been a center of interest in Calabi-Yau theory. Some string theorists make strong claims: “*All of the numbers we measure in nature—all of the things we consider fundamental, such as the mass of quarks and electrons—all of these derive from the geometry of Calabi-Yau.*” In this context, Calabi proposed an internal symmetry related to supersymmetry. Operation of LHC for over a decade has failed to show the slightest sign of supersymmetry, and Yau points out that, “*...without supersymmetry, string theory makes little sense.*” Our use of Calabi-Yau has nothing to do with supersymmetry.

Chern class: The next topological concept is *Chern class*, developed to mathematically characterize the difference between two manifolds. We are interested only in the simplest aspects dealing with complex manifolds. Specifically, we are interested in places where the flow in a vector field shuts down. For example, a spherical topology such as the earth supports the flow of wind currents at every point on the globe except two: there is zero net flow at the North pole and the South pole. These dead spots are places where nothing flows at all. The donut topology, on the other hand has no dead spots; flows around the surface of a torus can flow forever. Maxwell marveled at Helmholtz’s proof that “*in a perfect fluid such as a whirling ring, if once generated, would go on whirling forever.*” Clearly, we wish for our fermion flows to last forever—a topology in which this is the case is called a “*vanishing Chern class*” or “*first Chern class of zero*”.

Ricci curvature: Ricci curvature is essential to understanding what the Calabi conjecture is all about. It is a kind of average of a more detailed type of curvature known as *sectional curvature*. To find the Ricci curvature, pick a point on the manifold, find a vector tangent to that point, then look at all 2D tangent planes

that contain that vector, each of which has a sectional (Gauss) curvature associated with the plane. The Ricci curvature is the average of these sectional curvatures. “A Ricci-flat manifold means that for each vector one picks, the average sectional curvatures of all the tangent planes containing that vector equals zero.” This, although the sectional curvature of any individual plane may not be zero. In higher dimensions a manifold can be Ricci-flat without being flat overall. Einstein’s formulation equates the flow of matter density and momenta at a point to the Ricci tensor. This is its key relevance for our theory of fermions so with these topological concepts in hand, we state the Calabi conjecture: “A compact Kahler manifold with a vanishing first Chern class will admit a metric that is Ricci-flat.”

Before using these geometer’s concepts to formulate a theory of spin, we review the physics of the same problem.

7. Analysis of Primordial Field in Calabi Terms

Having just reviewed the relevant Calabi-Yau topological concepts, we now relate these to the physics of the Ricci tensor. Einstein’s field theory equation

$$R^{\mu\nu} = T^{\mu\nu} \quad (7)$$

is unique in that the stress-energy tensor $T^{\mu\nu}$ is expressed in Euclidean space, whereas the Ricci tensor $R^{\mu\nu}$ represents curved space coordinates. Despite its endurance for over a century, this formulation makes no sense. No one knows how to solve an equation in which each side is formulated in a different coordinate system, one of which is unknown. One might ask, why not just express $T^{\mu\nu}$ in curved space? The problem is that the curvature is not known until after the problem has been solved. Feynman hints at this:

“In general, it is not possible to write down any kind of consistent $T^{\mu\nu}$ (...) unless one has already solved the complete, tangled problem.” (...) “Even for very simple problems, we have no idea how to go about writing down a proper $T^{\mu\nu}$.”

Note that there is only one point common to both $T^{\mu\nu}$ and $R^{\mu\nu}$ —the point at the origin: (0, 0, 0). If we place a mass at this common point, the equation makes sense, and we can derive a solution, the Schwarzschild metric, based on the singularity at the origin. The field equation cannot be solved at the singularity, but does apply *outside* of the singularity, where $T^{\mu\nu} = 0$. Vishwakarma [15], concluding that curvature of $R^{\mu\nu}$ is derived from the gravitation field *outside* the mass point, proposed that $T^{\mu\nu}$ is superfluous, and can simply be deleted from Einstein’s equation, leaving

$$R^{\mu\nu} = 0. \quad (8)$$

That is, the stress-energy tensor representing energy density distributed over space, $T^{\mu\nu}$, is nonsensical and has never been solved for or tested against general relativity experiments. In agreement with Vishwakarma’s conclusion that $R^{\mu\nu}$ curvature is based on the gravitational field, I have shown how the gravita-

tional field energy density can be encoded as geometry (*i.e.*, curvature), however, a proper energy-stress tensor of the gravitational field does not exist. This century-old paradox has led to such erroneous concepts as “quasi-local-mass”.

We consider next the left-hand-side of the field equation; starting with a Riemannian tensor, R_{abcd} , we can obtain Ricci tensor $R^{\mu\nu}$ from the contraction $R_{ac} = g^{bd} R_{abcd}$, where the sum over repeated indices is a bit like taking a scalar product of two vectors. In this case the shape of spacetime is defined by the metric tensor g_{ab} with inverse such that $g^{ab} g_{ab} = [1]$. The Ricci *scalar* is given by $R = R_{ac} g^{ac}$. These are quantified expressions of spacetime curvature.

Consider a spherical region of closely spaced points around point P, moving with velocity v . As the points flow through curved space the sphere can rotate, twist, or distort. The Ricci tensor R_{ab} keeps track of the change in *volume* of the region. An associated Weyl tensor keeps track of the changes in *shape* of the region of points.

The fields of topology and physics converged when Yau realized that the Calabi-Yau conjecture need not be presented in purely geometric terms but can be written as a partial differential equation, whereas I start with differential equations and derive geometry (encoding energy density as geometry.) The differential equation he tried to solve in the Calabi-Yau conjecture is literally Einstein’s equation of empty space, ($T^{\mu\nu} = 0$), that is, Calabi-Yau manifolds are regarded as solutions to Einstein’s field equations.

Summarizing: Yau proved that a Ricci-flat metric can be found for compact Kahler space with a vanishing first Chern class; he could *not* produce a precise formulation of the metric itself. One is thus left, not with a solution, but merely an existence proof that a solution exists.

The simplest possible Calabi-Yau space is a two-dimensional torus or donut, compatible with the existence proof of the mass-gap, a torus derived from the use of Heaviside equations in turbulent media. Here we close with a simple topological “derivation” of the torus. (**Figure 3**)

Calabi’s conjecture is formulated in terms of complex manifold, Kahler geometry, metric, Chern class, Ricci curvature. Yau claims spaces satisfying the complicated set of topological demands are like rare diamonds, but the conjecture offers a general rule telling us that they are there.

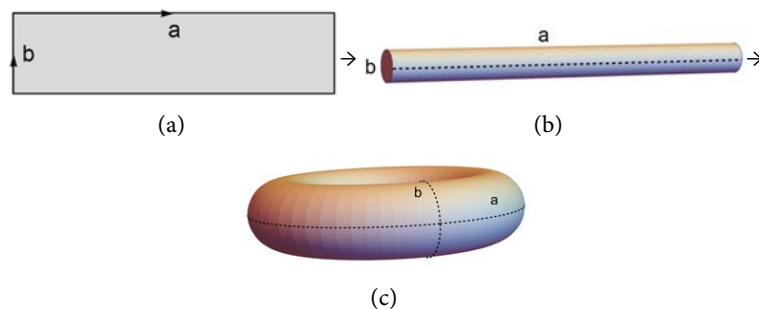


Figure 3. A toric surface can be entire “flat” (zero Gauss curvature) because it can be made, in principle, by rolling up a sheet of paper into a tube and then joining the ends of the tube to each other.

8. Ontological Flow on a Torus

The above treatment has provided topological context and introduced existence proofs. I now analyze fermion topology in a 4D Calabi-Yau, modified Yang-Mills context, by focusing on the relevant ontological flow. Ignoring *tangent bundles* of differential geometry, we focus on the fact that the tangent space on the manifold can be defined as the set of all velocity vectors.

The solution to Maxwell's field wave equations has $U(1)$ symmetry, $e^{i\theta} \sim \cos(\theta) + i \sin(\theta)$. In other words, the propagating field has helical structure. The physical regimes of interest are ultra-high-density gravitational fields, exemplified by big bang and atom-atom collisions at CERN. Both such regimes are extremely turbulent such that collisions of helices, including self-intersection occurs, potentially forming tori. In such cases the symmetry is $U(1) \times U(1)$.

Our mass-gap existence proof analyzes the self-interaction of a newly formed torus, concluding that beyond a certain stage of relaxation, the torus is self-stabilizing and self-healing against external interference and disturbances up to a limit. A key point on which we will construct our analysis is that Kahler manifolds are a subset of complex manifolds known as Hermitian manifolds, “*on which you can put the origin of the complex coordinate system at any point, such that the metric will look like a standard Euclidean metric $\eta_{\mu\nu}$ at that point.*” By implication, we could do so at any neighboring point, as well.

Consider the torus that is formed by “joining” the ends of a helical flow structure; the $U(1) \times U(1)$ structure is like circles surrounding every point on the torus “core” which is itself a circle. The surface of the donut represents the *flow* of the gravitomagnetic field energy density, described by the velocity vector, regarded as a vector being transported around a closed path. Topologically, this vector has the same direction as the tangent to the path at a given point. The tangent at any point on one of the $U(1)$ circles is given as follows: For a curve with radius $r(t)$ the unit tangent vector $\hat{T}(t)$ is defined by $\hat{T}(t) = \dot{\mathbf{r}}/|\dot{\mathbf{r}}|$. If we relabel this as $\dot{\mathbf{r}}/s$ where s is the arc length, then the tangent vector is given by $\frac{d\mathbf{r}}{ds}$, the change in the vector $\mathbf{r}(t)$ as it moves along arc length.

Our $U(1) \times U(1)$ conceptual model shows every circle disconnected from every other circle; *not* a helix, (Figure 4). To reflect the physical ontology of the torus, we desire helical flow lines. The tangent, and hence flow velocity, has the same definition, and since the radius is constant around the $U(1)$ circle, the velocity is constant. The parametric helix is $\mathbf{r} = |\mathbf{r}| \{ \cos(t), \sin(t), t \}$. This is easy to see, but for comparison with the torus we display it in Figure 5(b), according to the following:

```
x[t_]:=Cos[t]; y[t_]:=Sin[t]; z[t_]:=t;
velocities=Table[{{x'[t], y'[t], z'[t]}, {t, 0, 4π, π/180}}//N
ListPlot[Table[velocities[[n]][[1]], n], {n, 361}]]//N
```

Figure 5(b) shows the value of the velocity squared, $|\mathbf{v} \cdot \mathbf{v}| = 2$. Observe that the velocity of any point of a helix on a cylindrical surface has constant magnitude (speed). From the Kahler property we know that the velocity of a neigh-

boring point on a neighboring helix behaves the same. It is key that these neighboring helices do not intersect; since their tangents are parallel, as seen in **Figure 5(a)**.

We elaborate on simple helical flow because it is easy to grasp and yet differs from toroidal flow, despite that we constructed a torus from a helix, by curving the helix until its ends join; this joining changes the $U(1)$ helix symmetry to the $U(1) \times U(1)$ symmetry of the torus. We show the difference in **Figure 6** by plotting the velocity of the “helical” flow around the torus.

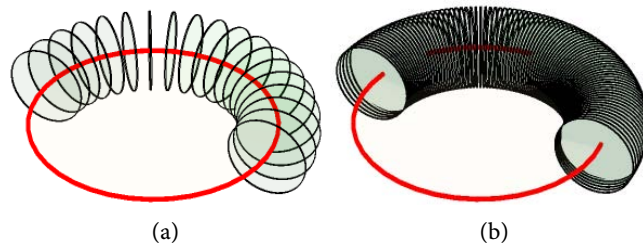


Figure 4. (a) $U(1)$ (circles) centered on red $U(1)$ circle yield; (b) Torus with $U(1) \times U(1)$ symmetry.

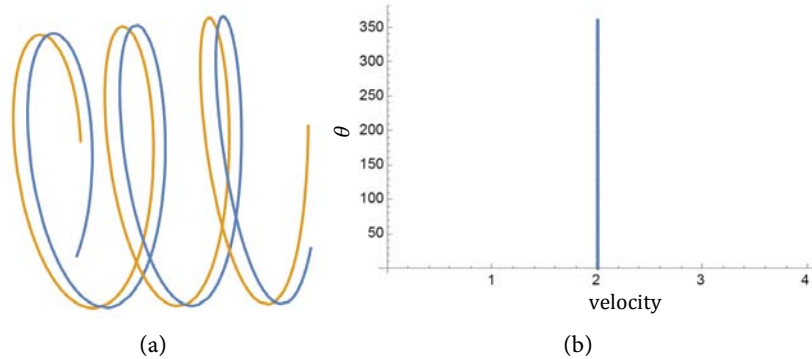


Figure 5. (a) Illustrating that neighboring helices [induced by the same momentum] do not intersect; neighboring vectors that are parallel are transported in parallel fashion. (b) The speed at any point, anywhere in either helix, is constant.

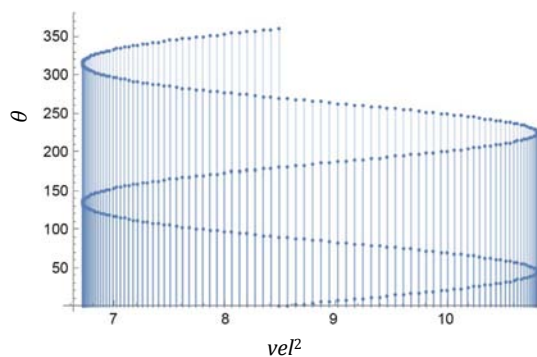


Figure 6. Unlike the constant velocity of helical flow, the [squared] velocity of toroidal flow is smoothly distributed between minimum and maximum velocities. The velocities range from ~ 6.5 to ~ 11 as the parametric path is followed from zero to 360 degrees. This differs from the velocity of the helix because the size of the torus has changed, nevertheless, this distribution of velocities represents any size torus.

If the donut retains a circular cross section, we might initially guess that the flow velocity would have constant magnitude like the helix. We investigate why this is not the case.

Calabi required Kahler manifolds, with the property that we can put the origin of a local coordinate system at any point, such that the metric will look like a standard Euclidean metric at that point. For simplicity, pick a point on the outer equator and choose a path that loops through the “hole” in the donut and eventually returns to the starting point. Such a path is closed. But we could have chosen a point on the equator infinitesimally close to the point we did choose, and created a new closed path in which every point on the new path is infinitesimally close to the equivalent point on the original path. One can show by construction (**Figure 5(a)**) that the two paths do not cross each other or intersect. The process of adding new paths infinitesimally displaced from the last path effectively builds a “sheet” of flow with surface energy density σ . Every point on the torus can be considered part of a sheet flowing *up* across the outer equator and *down* across the inner equator.

Ontologically, if we build the donut with smaller circles centered on a large circle in the plane of the donut, the tangent of the smaller circles is constant in magnitude; the flow velocity around the small circle is constant. But we cannot construct a physical torus from adjacent circles, so we must have a helical structure such that the flow is not only around the small “circle”, but also flows around the donut hole. Toroidal flow as an idealized helix leads to constant velocity, yet, ontologically, the topology is based on “surface flow”. If the surface flow along the outer equator is “up”—then continuous flow must be “down” along the inner equator of the torus. Consider a segment of arbitrary length Δx_o and arbitrary height Δy_o at the outer equator with flow velocity v_o as seen in **Figure 7(a)** with the segment between the two dashed radial lines shown as a green overlay on the torus. In **Figure 7(b)** we show the outer segment and corresponding inner segment, extracted from the torus.

In **Figure 7(a)** the green segment on the outer equator of the torus is labeled with arc length Δx_o and height Δy_o , yielding segmental area $\Delta a_o = \Delta x_o \Delta y_o$, through which the surface density of field energy flows with (upward) velocity v_{oz} . **Figure 7(b)** shows both segments labeled, with the inner segment described by arc length Δx_i and height Δy_i yielding segmental area $\Delta a_i = \Delta x_i \Delta y_i$ with inner velocity v_{iz} , flowing down across the inner equator. A U(1) slice through the torus perpendicular to both equators has two half circles, inner and outer, so we set segment heights equal, such that $\Delta y_o = \Delta y_i$. The toroidal velocity plot, **Figure 6**, shows that the velocity varies from minimum to maximum, so we assume that $v_o \neq v_i$. It is obvious that the length Δx_i of the inner subtended arc is less than that of the outer subtended arc Δx_o so that $\Delta x_o > \Delta x_i$. (Similarly, lengths Δy_j could be that of arc subtended by $\Delta \phi$ so that $\Delta y_o > \Delta y_i$). With the topology and geometry of the surface flow described, we next analyze the physical ontology.

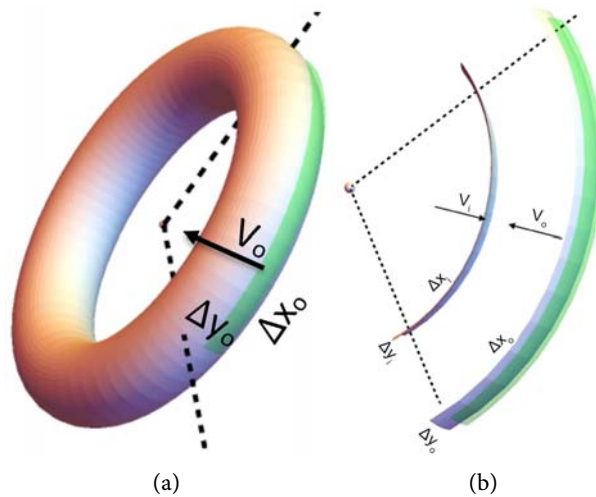


Figure 7. (a) Two arbitrary radii establish two arc segments subtended by the angle between the dashed lines. A green segment of height Δy_o spans the arc between these dashed lines. (b) The corresponding segment on the inner equator is shown from a different perspective. Surface energy density is assumed to flow through both segments. The labelled inner and outer segments are shown with respective vertical velocities v_{iz} and v_{oz} .

The circulating field energy density is proportional to $C \cdot C$, where $\nabla \times C = -p$. Although we envision the vortex surface as two dimensional, let us assume a finite wall thickness Δr_j so that we can write the field density as volume energy density $\rho \sim C \cdot C$ and mass flow (momentum P_j) through a segment with volume $\Delta x_j \Delta y_j \Delta r_j$ proportional to

$$P_j = (\Delta x_j \Delta y_j \Delta r_j) \rho_j v_j = \text{mass flow of field through wall segment } j \quad (9)$$

This momentum induces more C-field circulation, as analyzed in the mass-gap existence proof; the stable final state of the topological ontological structure is assumed to represent a fermion.

A stable continuous mass flow (momentum) *up* through the outer segment is assumed to equal the mass flow (momentum) *down* through the corresponding inner segment through conservation of momentum, thus all vertical mass flow across the outer equator equals vertical mass flow across the inner equator. If we turn the torus upside down, inner flow is up and the outer down, while the meaning of inner and outer equators will not change; therefore we use equator indices $\{i, o\}$:

$$v_{oz} = -v_{iz} \Rightarrow \Delta V_o \rho_o v_{oz} = -\Delta V_i \rho_i v_{iz} \Rightarrow P_{oz} = -P_{iz} \quad (10)$$

The negative sign denotes oppositely directed vertical velocities of vertical mass flows across outer and inner equators. Assume that vertical parameters Δy_j and wall thicknesses Δr_j are equal, then

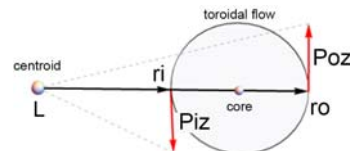
$$\frac{|v_{iz}|}{|v_{oz}|} = \frac{\rho_o \Delta V_o}{\rho_i \Delta V_i} \Rightarrow \frac{\rho_o \Delta x_o}{\rho_i \Delta x_i} \quad (11)$$

We group the energy/mass density ρ_j with the relevant velocity v_j , cancel

the product of vertical parameters and wall thickness $\Delta y_i \Delta r_i = \Delta y_o \Delta r_o$ and convert horizontal parameters, the segment lengths, to arc lengths for angle $\Delta\theta$ between the dashed lines, where $0 < \Delta\theta \leq 2\pi$ and arc length subtended by the angle is $\Delta x_j = r_j \Delta\theta$. Since $\Delta\theta$ cancels for all values of the angle, reduce (11) to vertical *momentum density* (mass density flows) p_{iz} and p_{oz} such that

$$\frac{\rho_i |v_{iz}|}{\rho_o |v_{oz}|} = \frac{r_o}{r_i} \Rightarrow r_i p_{iz} = r_o p_{oz} = \text{constant} \tag{12}$$

and expand the geometric product: $\mathbf{r}_j \mathbf{p}_{jz} = \mathbf{r}_j \cdot \mathbf{p}_{jz} + \mathbf{r}_j \wedge \mathbf{p}_{jz}$. Both $j=i$ and $j=o$ radius vectors are perpendicular to the vertical momentum vectors, **Figure 8**, hence scalar products $\mathbf{r}_j \cdot \mathbf{p}_j \equiv 0$ and, converting to cross products, we have

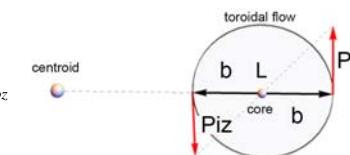


$$\mathbf{r}_i \times \mathbf{p}_{iz} = -\mathbf{r}_o \times \mathbf{p}_{oz} \tag{13}$$

Thus, we have coupled the density flow parameters \mathbf{p}_{jz} to the topology parameters \mathbf{r}_j . For an arbitrary slice through the torus the centroid angular momentum (point at center of hole) is:

$$\mathbf{L}_{\text{centroid}} = r_i p_{iz} + r_o p_{oz} \equiv 0 \tag{14}$$

The angular momentum of the centroid is shown to have a specific direction in the xy -plane for *arbitrary* θ (slice) therefore the value of \mathbf{L} must be zero. The bivector relation is $\mathbf{r}_i \mathbf{p}_{iz} = -\mathbf{r}_o \mathbf{p}_{oz}$ since vertical velocities have opposite directions with respect to the centroid, hence we have $\mathbf{r}_i \times \mathbf{p}_{iz} = -\mathbf{r}_o \times \mathbf{p}_{oz}$. With angular momentum density of the slice measured at the centroid zero; we calculate the angular momentum density at the torus core:

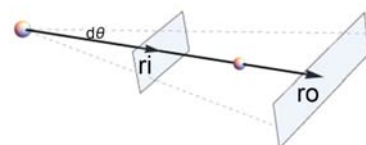


$$\mathbf{L}_{\text{core}} = \mathbf{b} \times \mathbf{p}_{iz} + \mathbf{b} \times \mathbf{p}_{oz} \tag{15}$$

Since $r_i p_{iz} = -r_o p_{oz}$ and $\mathbf{P}_{jz} = (\rho_j \Delta V_j) \mathbf{v}_{jz}$ where $\Delta V_j = \Delta x_j \Delta y_j \Delta r_j$ and $\Delta x_j = r_j \Delta\theta$ with Δy_j and Δr_j the height and thickness of the j^{th} equatorial segment specified as $\Delta y_i = \Delta y_o$ and $\Delta r_i = \Delta r_o$ so that $m_j = \rho_j (r_j \Delta\theta \Delta y \Delta r)$ under the assumption that the same mass flows across the inner and outer equatorial segments: $m_i = m_o$. From the above:

$$\frac{|\mathbf{p}_{iz}|}{|\mathbf{p}_{oz}|} = \frac{r_o}{r_i} = \frac{\rho_i v_{iz}}{\rho_o v_{oz}} \tag{16}$$

Based on the helical velocity the vertical velocity components are equal $v_{iz} \equiv v_{oz}$, despite that we have shown that $v_o > v_i$. If so, then we have



$$\frac{\rho_i}{\rho_o} = \frac{r_o}{r_i} \Rightarrow \rho_i = \left(\frac{r_o}{r_i}\right) \rho_o \tag{17}$$

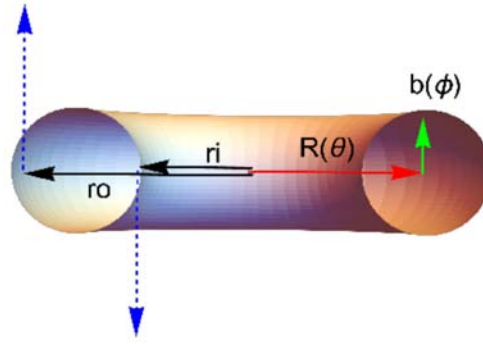


Figure 8. Cartoon depicting relevant vectors of the torus model of the fermion. The radii r_i , r_o , and R used in measurements in **Table 1**.

Thus, mass density of the inner equatorial segment is greater than the outer by ratio (r_o/r_i) and we have arrived at a relation between the topology and the (vertical) field momentum density. We rewrite angular momentum at the core, $\mathbf{L}_{core} = \mathbf{b} \times \mathbf{P}_{iz} + \mathbf{b} \times \mathbf{P}_{oz}$, as

$$\mathbf{L}_{core} = \mathbf{b}(\rho_i \Delta V_i \mathbf{v}_{iz} + \rho_o \Delta V_o \mathbf{v}_{oz}) \sim b(m_i \mathbf{v}_{iz} + m_o \mathbf{v}_{oz}) \tag{18}$$

Note that $b = \frac{r_o - r_i}{2}$ and that we have specified that the same mass must flow across the inner and outer equators, hence $\mathbf{L}_{core} = \frac{r_o - r_i}{2} [m_i \mathbf{v}_{iz} + m_o \mathbf{v}_{oz}]$. Since $m_i = m_o$ and $v_{iz} = v_{oz}$ the angular momentum at the core is

$$\mathbf{L}_{core} = \left(\frac{r_o - r_i}{2} \right) 2m_i v_{iz} \text{ or} \tag{19}$$

$$\mathbf{L}_{core} = (r_o - r_i) m_j v_{jz},$$

where

$$m_j \sim \underbrace{\mathbf{C} \cdot \mathbf{C}}_{\text{local energy density}} \underbrace{\Delta V_j}_{\text{local segment volume}} \tag{20}$$

and v_{jz} is the vertical velocity at equator j . Angular momentum at the toroidal core is induced by energy flowing at the toroidal surface. The energy flowing at the toroidal surface is equivalently induced/sustained by the core “current”, that is, we again arrive at a relation between the topology and the field momentum density, related to the motion of the field energy density.

We conclude this section on ontological flow by observing that the velocity variations seen in **Figure 6** imply that toroidal flow velocity varies and thus *cannot be* the constant speed of light. In other words, variations in energy density of the vector field flow through space, but NOT at the speed of light. The speed of light describes the propagation of a *stress wave* in the field across space.

9. Separation of $U(1) \times U(1)$ Flow Symmetry

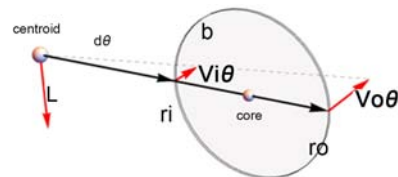
The relevant symmetry is $U(1) \times U(1)$ and we have up to this point focused on the $U(1)$ circulation about the torus *through* the donut hole and have required a

constant mass flow through the hole: $\mathbf{p}_{iz} = -\mathbf{p}_{oz}$. Next, we focus on the *other* U(1) circulation, that *around* the hole in the donut. In other words, the U(1) \times U(1) symmetry is resolved into two orthogonal flows $\mathbf{p} = \mathbf{p}_z + \mathbf{p}_\theta$ where \mathbf{p}_z is the momentum *through* the hole and \mathbf{p}_θ is the momentum *around* the hole. Referring to **Figure 8** we have three well defined radii, r_i , r_o and R , defining respectively the radius of the inner equator, the outer equator, and the core of the torus. Each of these distances is associated with a velocity: $|\mathbf{v}_\theta| = \sqrt{v_x^2 + v_y^2}$. Whereas the vertical velocity v_{jz} is constant, independent of r or θ , the mass flow through any given segment is proportional to the arc subtended by $\Delta\theta$, and the mass of each segment, by construction, is equal to that of the other segment, independent of $\Delta\theta$ and of $\Delta y \Delta r$, therefore the mass flow associated with each segment is proportional to $v_{j\theta}$, *i.e.*, $\mathbf{p}_{j\theta} = m_j(r_j)\mathbf{v}_{j\theta}$. Since $v_{o\theta} > v_{i\theta}$ we have $\mathbf{p}_{o\theta} > \mathbf{p}_{i\theta}$. Angular momentum \mathbf{L} at the centroid and at any point on the core are due to equatorial vertical velocities $v_{iz} = v_{oz}$ while $v_o > v_i$. Next consider angular momentum due to corresponding horizontal components $v_{o\theta} > v_{i\theta}$ with

$$\mathbf{v}_o = \mathbf{v}_{oz} + \mathbf{v}_{o\theta} \quad \text{and} \quad \mathbf{v}_i = \mathbf{v}_{iz} + \mathbf{v}_{i\theta}. \tag{21}$$

Angular momentum at the centroid due to equatorial momentum in the xy -plane is:

$$\mathbf{L} \sim \mathbf{r}_i \times m_i \mathbf{v}_{i\theta} + \mathbf{r}_o \times m_o \mathbf{v}_{o\theta}$$



$$\tag{22}$$

with $r_o > r_i$ and $v_{o\theta} > v_{i\theta}$ where $v_{i\theta} = \sqrt{(v_{ix})^2 + (v_{iy})^2}$ and $v_{o\theta} = \sqrt{(v_{ox})^2 + (v_{oy})^2}$. We thus resolve ontological flow on the torus into two components; vertical components rotate around the core (and through the hole) and induce angular momentum in the xy -plane at the core. Horizontal components flow around the hole in the θ direction and induce angular momentum (C-field) in the z -direction at the centroid. Vertical velocities are the same value at inner and outer equators, while horizontal velocity at the outer equator is greater than that at the inner equator. Conservation of mass flow in both directions is achieved via compensating changes in local field density, with the greater density appearing at the inner equator.

However, unlike the vertical momentum, which is constant around the torus, the horizontal momentum around the hole varies with the distance from the centroid and applies to mass that is off the equatorial plane, requiring integration over all radii from r_i to r_o complicating the issue. For that reason, we take a different approach to the problem. Rather than attempting to calculate the horizontal momentum associated with every point on the torus, we study the third Heaviside Equation in Equation (3): $\nabla \times \mathbf{C} = -\rho \mathbf{v}$ derived from the primordial self-interaction Equation (1). We ignore the time change in gravity field \mathbf{G} . The $\nabla \times \mathbf{C}$ represents the circulation of the field induced by momentum

density and $\rho = \frac{\text{mass}}{\text{volume}} = \frac{m}{\int d^3x}$ with \mathbf{v} the velocity of the U(1) mass density circulation in the equatorial plane, $\sim \mathbf{C}_\theta \cdot \mathbf{C}_\theta$. If \mathbf{P} is the momentum of this U(1) circulating field, then the U(1) circulation in the vertical plane is

$$\nabla \times \mathbf{C} = -\mathbf{P} / \int d^3x \sim \left(\frac{\mathbf{C}_\theta \cdot \mathbf{C}_\theta}{c^2} \right) \mathbf{v}_\theta \quad (23)$$

In this case the mass density ρ moving with velocity \mathbf{v} is the mass of the horizontal C-field circulation induced by the helical solenoid divided by the relevant volume, $V = \int d^3x$, that is

$$\rho \mathbf{v} = \mathbf{p} = \mathbf{P} / \int d^3x \quad (24)$$

Here momentum \mathbf{P} will be identified with the core of the torus, and volume with the inside of the torus. Recall that the minus sign in Heaviside's equation is associated with the direction of flow of the induced C-field circulation, we will drop it in our calculations of magnitude. We follow Arfken [16] and set an infinitesimal volume to be $\int d^3x = dx dy dz$ (cube) and specialize to the cylindrical volume corresponding to the U(1)-based e^{iCt} helix, in which case we redefine the volume in cylindrical coordinates as

$$\iiint d^3x = \iint dx dy \int dz \Rightarrow \iint_S r dr d\phi \int dz \quad (\text{cylinder}) \quad (25)$$

If we integrate z from 0 to 1 the result is the unit normal $\int_0^1 dz = \hat{n} = \frac{\mathbf{n}}{|\mathbf{n}|}$ to the vertical plane of circulation. We next use these results to invoke quantum half-integral spin.

10. Derivation of Quantum Spin

From the above, applying Stokes's theorem to Heaviside's equation

$$\nabla \times \mathbf{C} = -\left(\frac{g}{c^2} \right) \rho \mathbf{v} :$$

$$\iint_S da \hat{n} \cdot (\nabla \times \mathbf{C}) = \oint_{\partial S} \mathbf{C} \cdot d\mathbf{l} \quad (26)$$

we obtain the line integral around the closed (vertical) path. For a given momentum (in the z -direction) the circulation in the vertical plane is fixed and $\hat{n} \cdot (\nabla \times \mathbf{C})$ must not depend on the coordinate system. In the following we make use of the dimensional relations:

$$[da] = l^2, \quad \left[\frac{g}{c^2} \right] = \frac{l}{m}, \quad [\rho] = \frac{m}{l^3}, \quad [\hat{n}] = 1, \quad [v] = \frac{l}{t}, \quad [C] = \frac{1}{t}, \quad [\lambda] = l. \quad (27)$$

To obtain

$$da \hat{n} \cdot (\nabla \times \mathbf{C}) = l^2 \left(\frac{l}{m} \right) \left(\frac{m}{l^3} \right) \mathbf{v} \quad (28)$$

where velocity \mathbf{v} is perpendicular to the plane of the C-field circulation.

The results in Equation (28) allow us to modify equation (26) as follows:

$$m \iint_S da \hat{n} \cdot (\nabla \times \mathbf{C}) = m \mathbf{v} = \mathbf{P} = m \oint_{\partial S} \mathbf{C} \cdot d\mathbf{l} \quad (29)$$

At this point recall that our goal is to derive a fermion from a theory of quantum gravity, so we invoke deBroglie's fundamental basis of quantum theory, $P = \frac{h}{\lambda}$. Substituting this into Equation (29) and multiplying both sides by λ we obtain for $\lambda = \lambda \hat{n}$ and unit mass, $m = 1$:

$$\iint_S \lambda \cdot \nabla \times C da = h \quad (30)$$

This is a novel quantum relation, relating the wavelength of the core momentum to the circulation induced by this momentum and finding the quantized results in terms of Planck's constant. Since $\int d^3x = \lambda \cdot \int d^2x$ so λ is the length of the helical cylinder. From Equation (29) we further obtain

$$m\lambda \oint_{\partial S} C \cdot d\mathbf{l} = h, \quad \oint_{\partial S} C \cdot d\mathbf{l} = \left(\frac{1}{m}\right) \frac{h}{\lambda} = |\mathbf{v}| \quad (31)$$

which implies that the circulation around a closed loop is quantized, and that it is the gauge field vector. Of course, the helix is not closed, but the torus induced by momentum \mathbf{P} is closed, and that is the focus of our next development. We have calculated the vertical contributions of the field energy density momentum to the core of the torus and the centroid of the torus. We here identify the horizontal contribution to the angular momentum as related to Planck's constant.

11. Vector Transport around a Closed Path

Many are familiar with vector transport on the surface of a sphere—begin at the north pole and follow any longitude line to the equator, maintaining the vector as tangent to the curve at every point along the curve. When the equator is reached, the vector points south, and motion along the equator retains this direction of the vector. After reaching an arbitrary longitude begin moving the vector toward the north pole, maintaining its tangent nature at every point. When the north pole is reached, the final tangent vector is not parallel to the original vector at the same pole. The pole is used for simplicity, but this concept applies at any point and in any coordinate system. The concept of “holonomy” is a measure of how tangent vectors on a particular surface get twisted up in such parallel transport over a loop around the surface. In fact, to tie Calabi-Yau to string theory, supersymmetry was used as the bridge to holonomy; holonomy was used as the bridge to Calabi-Yau.

To analyze vector transport on the torus we arbitrarily choose the starting point on the vertical axis at R (red arrow in **Figure 8**). The green arrow of length b ends on the starting point. As this is at the top of the torus, the vertical coordinate is not changing at this point, hence $\dot{v}_z = 0$. As we move off the starting point toward an equator, the vertical component of velocity becomes nonzero, finally reaching v_{iz} (or v_{0z}) at the equator, then proceeding toward the bottom of the torus where again $\dot{v}_z = 0$. Continuing this U(1)-symmetry vertical motion the point of interest is transported around the torus through the “donut hole”. But the ontological flow has $U(1) \times U(1)$ symmetry and flows around the donut hole as parameter θ increases. Therefore, when the flow crosses the in-

ner equator the velocity at r_i is $\mathbf{v}_i = \mathbf{v}_z + \mathbf{v}_\theta$ where \mathbf{v}_θ is the rotational velocity of the flow in the xy -plane. The flow of the field is left-handed with respect to the core flow. The z -component of velocity v_{iz} is maximum at the equator, then diminishes until it vanishes at the bottom-most parts of the torus.

A 360° θ -rotation effects one complete circle around the torus, but only half a rotation about the hole in the torus; the final point on the path does not overlay the starting point. In every case, regardless of starting point, a further 2π rotation will return to the starting point, thus requiring a total 4π -rotation to close the path, as required for fermions. Once we determine that one circulation around the donut hole corresponds to two circulations around the “helical” torus, we invoke Equation (31) to conclude that $2 \oint_{\partial S} \mathbf{C} \cdot d\mathbf{l} = h$. This implies that the relevant wavelength is 2λ and thus, compatible with Equation (29), we have:

$$\iint_S \boldsymbol{\lambda} \cdot \nabla \times \mathbf{C} da = \frac{h}{2}. \quad (32)$$

That is, the quantum gravity-based spin of the fermion is $\frac{h}{2}$. This implies, correctly as we have seen, that the C-field must wind about the torus twice to return to its starting state.

12. Measurements on a Dynamic Model

Rather than complicating the visual dynamic flow further, by dividing it into two components as it flows around the torus, I decided to also dynamically display the values of the horizontal and vertical components of velocity as it flows through every point. I typically employ 360 points for each U(1) path, and so can, via *Mathematica* controls, determine the speed of simulation, as it is quite simple to walk my way around the path, slowing down at each of the critical points (the red and green arrow heads in **Figure 9(c)**) examining the velocity components, equatorial vertical velocities $v_{iz} = v_{oz}$ with $v_o > v_i$ and corresponding horizontal components $v_{o\theta} > v_{i\theta}$ with

$$\mathbf{v}_o = \mathbf{v}_{oz} + \mathbf{v}_{o\theta} \quad \text{and} \quad \mathbf{v}_i = \mathbf{v}_{iz} + \mathbf{v}_{i\theta}. \quad (33)$$

thereby building a table as seen in **Table 1**. The radii are defined in **Figure 8**, with r_i the inner radius, r_o the outer radius, and R the radius to the core of the torus.

At any point on the manifold the velocity $\mathbf{v} = \mathbf{v}_\theta + \mathbf{v}_z$. If we square both sides, term $\mathbf{v}_\theta \cdot \mathbf{v}_z = 0$ since \mathbf{v}_θ and \mathbf{v}_z are orthogonal, hence

$$v = \sqrt{v_\theta^2 + v_z^2} \quad (34)$$

Table 1. Measurement of velocity components.

deg	0	30	60	90	120	150	180	210
\mathbf{v}_θ	10.8	9	10.8	3	10.8	9	10.8	3
\mathbf{v}_z	0	9	0	9	0	9	0	9
\mathbf{v}	10.8	12.7279	10.8	9.48	10.8	12.72	10.8	9.48
radi	R	r_o	$-R$	$-r_i$	R	r_o	$-R$	r_i

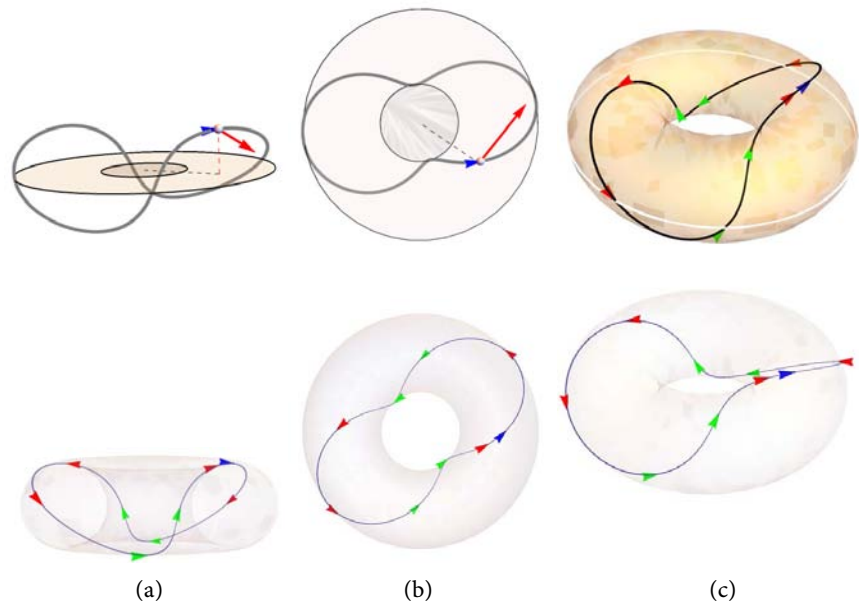


Figure 9. Based on equation 29 we draw a closed path around the torus, with the area of the enclosed xy -plane defining the horizontal boundaries of the torus. (a) shows a perspective angle on the path, while (b) shows an overhead perspective of the same path, and (c) depicts a semi-opaque torus with white outer equator shown and the closed path traversing the torus shown in black with colored arrows indicating direction of flow.

For example, at 30° the velocity is $\sqrt{9^2 + 9^2} = 12.7279220$ while at 90° $v = \sqrt{3^2 + 9^2} = 9.48$. We see from the table that the measurements confirm the intuitively derived relations based on the reasoning about *conservation of momentum*. In short, the dynamic visualization of the field behavior intuitively confirms the correctness of the model/theory, while the measurement access to arbitrary parameters can serve as proof of the flow model worked out by conservation equations and the $U(1) \times U(1)$ -symmetry. When these measurements on the model agree in detail with intuitively and/or analytically derived behavior, the feeling is as if one has “struck gold”. One can only sincerely thank David Hestenes and Steven Wolfram for their contributions to this task.

13. Summary

There are a lot of details in this paper, and my focus has been primarily on getting the details right. An anonymous reviewer asked for more context, and this has improved the presentation of the information, for which I am grateful.

The key to fermion spin is its half-integral nature. This was first interpreted from spectral statistics, and then projected onto Stern-Gerlach beam-splitting experimental results seen in the infamous Bohr-postcard. The formulation fits the expected data, but *no physical basis of half-integer spin is known*. Explained succinctly, half-integral spin is *not* mapped into itself in one revolution, but requires a 4π -rotation, a decidedly nonclassical result. The simplest math analog is the *mobius strip*, but no one takes that seriously. The complete lack of ontological theory of half-integral spin has led to such explanations as Feynman’s “belt

trick” wherein unobservable “tethers” are “tangled” such that a single rotation does not allow untangling to occur, while a 4π rotation untangles the system, restoring it to its initial state. Interestingly, Schiller has issued a preprint [17] based on a formalization of the belt trick.

The half-integral spin that flows from primordial field theory is not based on a belt trick; it is based on Heaviside’s gravitomagnetic *dual* to electromagnetism. The issue of computation of flow on the surface of the torus is one that is best addressed by constraining all calculations to the manifold defined by Calabi-Yau. This avoids any use of strings, while allowing use of Hestenes’ Geometric Calculus—instantiated in Wolfram’s *Mathematica 13*. The flow of C-field energy density around the surface of the torus is complicated; the vector being transferred around the path is always changing. Even the use of magnitude-adjusted, color-coded vectors is dynamically complex. A dynamically stable model of this complexity is a very strong argument for the integrity of the mathematical design. The ability to make measurements on the dynamic model which can then be compared to the predicted measurement results is rather convincing.

An Internet search for Calabi-Yau topology returns images of the type shown in **Figure 10**. They’re often viewed as “compactified”, meaning that the local topology exists at every point in 3D space. This is the “trick” that allows string theorists to claim that 10D and 11D theories are meaningful. A decade of operation of the LHC has failed to find any signs of supersymmetry, and string theory makes no sense without supersymmetry; nevertheless, support from the string theory community kept Calabi-Yau alive during its critical period.

Of course, in the context of today’s mysteries in physics, and ready belief in higher dimensionality at fundamental levels, such images are always enjoyed by physicists and the artistically inclined; but even if higher dimensional models turn out to be physically inappropriate, the Calabi-Yau manifolds retain supreme importance for (3D + 1)-space-time physics: they allow the use of Euclidean space tools locally in a global non-Euclidean ontology. In other words, we are allowed to compute flows on toroidal surfaces confidently.

In summary, a new theory of physics based on the existence of a primordial field at the creation of the universe resolves a number of paradoxes [logical contradictions] associated with 20th century physics. It contrasts with quantum field theory, which has one field per particle, and with general relativity, which equates the world to geometry.

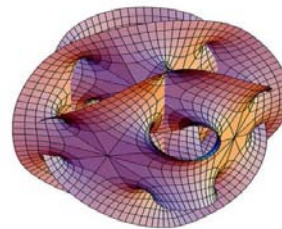


Figure 10. A 10D Calabi-Yau manifold image designed by Stewart Dickson at redbubble.com.

The new theory leads almost immediately to Heaviside's equations of gravity, dual to Maxwell's equations of electromagnetism. While these are generally recognized as iteratively equivalent to Einstein's field equations, physicists have been ultimately confused by the label "*weak field approximation*". Primordial field equations are *density-based* and *hold at all field strengths*.

In "*Self-linking Field Formalism*" [18] we note that the gravitomagnetic field, induced by and inter-acting with mass flow, is significantly different from the electromagnetic field induced by and interacting with charge flow, in that the electromagnetic field is uncharged and hence cannot interact with itself. The gravitomagnetic field has energy density, hence mass density, and can therefore interact with and induce itself.

The $U(1) \times U(1)$ symmetry described herein supports two orthogonal circulations, vertical and horizontal. It seems reasonable that these self-sustaining interactions have equal angular momenta, that is, each mode supports $\frac{h}{2}$. The vertical momenta induce the flow at the core, whereas the horizontal momentum produces the half-integral spin at the centroid. Only this spin is measurable.

Based on analogy with electromagnetism, we show that gravitomagnetism supports field structures that are self-induced; these structures include vortices in turbulent fluid, and we have shown that higher order self-interactions lead to toroidal structures that are self-stabilizing, thus bringing Calabi-Yau theory into the picture. The key contribution of Calabi-Yau to primordial field theory is found in the definition of Kahler manifold, vanishing Chern class, and Ricci-flat geometry. These establish a topological geometry framework subject to existence proofs. String theory has focused on 10D and 11D structures, for reasons to be examined elsewhere. Primordial field theory deals with $(3D + 1)$ of space and time. We consider the torus structure to be effectively described by $U(1) \times U(1)$ symmetry, in which a 4π rotation is required to transform any point in the flow into itself via vector transport over a path on the surface of the torus. This correlates perfectly with the half-integral spin that characterizes fermions.

Analysis of the flow of the gravitomagnetic field energy density on the toroidal surface leads to formulating flow relations through the donut hole and around the donut hole, with the velocity at any point resolved into v_z velocity and v_θ velocity.

Because primordial field theory is ontologically well defined, and the fermion is topologically well defined, we create a model fermion based in the mass-gap existence proof, now augmented by the half-integral spin existence proof. We then make measurements on this well-defined model and prove that our ontological analysis has yielded dynamical equations that match the measurements at well-defined points. This is considered an existence proof of the half-integral fermion spin.

The above theory is classical in nature, as is relativity. The quantum is introduced by invoking the key quantum relation underlying all quantum mechanics: deBroglie theorem: $p = h/\lambda$.

14. Conclusions

The above summary reviewed the fact that our primordial field theory is now adorned with two key proofs for toroidal fermions:

- Mass-gap existence proof
- half-integral spin existence proof

Note that the *standard model of particle physics* has no explanation of particle mass nor any explanation for half-integral spin. Nor can it calculate the mass of any particle. Of course, at this point, primordial field theory cannot calculate fermion mass either. It is known that the C-field circulation energy has mass density, and it is also known that *rotational energy is mass* [19]. What has not yet been proved is the nature of electric charge in primordial field theory. We cannot nail down the mass and size of the fermion until we include the charge and associated fields, which are not assumed present at the Creation. The goal is to show that this follows from the principles of the primordial field theory.

Conflicts of Interest

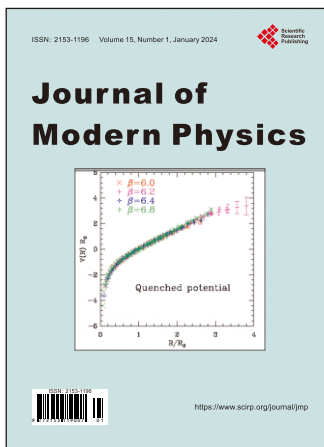
The author declares no conflicts of interest regarding the publication of this paper.

References

- [1] Sbitnev, V. (2019) *Foundations of Physics*, **49**, 107-143.
<https://doi.org/10.1007/s10701-019-00236-4>
- [2] Klingman, E. (2022) *Journal of Modern Physics*, **13**, 1128-1145.
<https://doi.org/10.4236/jmp.2022.137065>
- [3] Feynman, R. (1995) *Feynman Lectures on Gravitation*. Westview Press, Boulder.
- [4] Armas, J. (2021) *Conversations on Quantum Gravity*. Cambridge University Press, Cambridge. <https://doi.org/10.1017/9781316717639>
- [5] Einstein, A. (1952) *Relativity*. Crown Publishing, New York.
- [6] Klingman, E. (2020) *Journal of Modern Physics*, **12**, 65-81.
<https://doi.org/10.4236/jmp.2021.122007>
- [7] Yau, S. (2010) *The Shape of Inner Space*. Basic Books, New York.
- [8] Heaviside, O. (1893) *The Electrician*, **31**, 81-82.
- [9] Klingman, E. (2022) *Journal of Applied Mathematics and Physics*, **10**, 2292-2302.
<https://doi.org/10.4236/jamp.2022.107156>
- [10] Jaffe, A. and Witten, E. (2022) *Quantum Yang-Mills Theory*.
<https://www.claymath.org/wp-content/uploads/2022/06/yangmills.pdf>
- [11] Douglas, M. (2004) Yang-Mills Existence and Mass Gap: Prove That for Any Compact Simple Gauge Group G, Quantum Yang-Mills Theory of R4.
<https://www.researchgate.net/publication/237610692>
- [12] Klingman, E. (2022) *Journal of Modern Physics*, **13**, 347-367.
<https://doi.org/10.4236/jmp.2022.134025>
- [13] Klingman, E. (2021) *Journal of Modern Physics*, **12**, 1190-1209.
<https://doi.org/10.4236/jmp.2021.129073>
- [14] Klingman, E. (2019) *Prespacetime Journal*, **10**, No. 6.

<https://prespacetime.com/index.php/pst/article/view/1602>

- [15] Vishwakarma, R. (2013) Gravity of $R^{\mu\nu} = 0$: A New Paradigm in GR. arXiv:1206.2795v2
- [16] Arfken, G. (1966) *Mathematical Methods for Physicists*. Academic Press, New York.
- [17] Schiller, C. (2023) Testing a Model for Emergent Spinor Wave Functions Explaining Gauge Interactions and Elementary Particles.
https://www.researchgate.net/publication/361866270_Testing_a_model_for_emergent_spinor_wave_functions_explaining_gauge_interactions_and_elementary_particles
- [18] Klingman, E. (2021) *Journal of Modern Physics*, **12**, 440-452.
<https://doi.org/10.4236/jmp.2021.124031>
- [19] Smith, J. (2018) *Physical Review Letters*, **120**, Article ID: 143002.



Call for Papers

Journal of Modern Physics

ISSN: 2153-1196 (Print) ISSN: 2153-120X (Online)
<https://www.scirp.org/journal/jmp>

Journal of Modern Physics (JMP) is an international journal dedicated to the latest advancement of modern physics. The goal of this journal is to provide a platform for scientists and academicians all over the world to promote, share, and discuss various new issues and developments in different areas of modern physics.

Subject Coverage

Journal of Modern Physics publishes original papers including but not limited to the following fields:

Biophysics and Medical Physics	New Materials: Micro and Nano-Mechanics and Homogeneization
Complex Systems Physics	Non-Equilibrium Thermodynamics and Statistical Mechanics
Computational Physics	Nuclear Science and Engineering
Condensed Matter Physics	Optics
Cosmology and Early Universe	Physics of Nanostructures
Earth and Planetary Sciences	Plasma Physics
General Relativity	Quantum Mechanical Developments
High Energy Astrophysics	Quantum Theory
High Energy/Accelerator Physics	Relativistic Astrophysics
Instrumentation and Measurement	String Theory
Interdisciplinary Physics	Superconducting Physics
Materials Sciences and Technology	Theoretical High Energy Physics
Mathematical Physics	Thermology
Mechanical Response of Solids and Structures	

We are also interested in: 1) Short Reports—2-5 page papers where an author can either present an idea with theoretical background but has not yet completed the research needed for a complete paper or preliminary data; 2) Book Reviews—Comments and critiques.

Notes for Intending Authors

Submitted papers should not have been previously published nor be currently under consideration for publication elsewhere. Paper submission will be handled electronically through the website. All papers are refereed through a peer review process. For more details about the submissions, please access the website.

Website and E-Mail

<https://www.scirp.org/journal/jmp> E-mail: jmp@scirp.org

What is SCIRP?

Scientific Research Publishing (SCIRP) is one of the largest Open Access journal publishers. It is currently publishing more than 200 open access, online, peer-reviewed journals covering a wide range of academic disciplines. SCIRP serves the worldwide academic communities and contributes to the progress and application of science with its publication.

What is Open Access?

All original research papers published by SCIRP are made freely and permanently accessible online immediately upon publication. To be able to provide open access journals, SCIRP defrays operation costs from authors and subscription charges only for its printed version. Open access publishing allows an immediate, worldwide, barrier-free, open access to the full text of research papers, which is in the best interests of the scientific community.

- High visibility for maximum global exposure with open access publishing model
- Rigorous peer review of research papers
- Prompt faster publication with less cost
- Guaranteed targeted, multidisciplinary audience



**Scientific
Research
Publishing**

Website: <https://www.scirp.org>

Subscription: sub@scirp.org

Advertisement: service@scirp.org